ANALYSIS OF AC/DC SYSTEM DISTURBANCES

A thesis

presented for the degree of

Doctor of Philosophy in Electrical Engineering

in the

University of Canterbury,

Christchurch, New Zealand

by

M.D. HEFFERNAN B.E.(HONS), M.E.

1980

CONTENTS

LIST OF ILLUSTRATIONS

LIST OF TABLES

LIST OF PRINCIPAL SYMBOLS

The majority of symbols are defined as they appear in the text, and a comprehensive system of scripting is used for clarity. For convenience the principal symbols are redefined below.

A	:	ampere
ABS	:	absolute magnitude
a,b,c	:	a.c. phases
a.c., AC	:	alternating current
AVR	:	automatic voltage regulator
B	:	susceptance (matrix)
c	:	number of capacitive branches in a network
C	:	capacitance matrix
cos	:	cosine
CCC	:	constant current control
d1, d2	:	d.c. terminals of convertor bridge
d.c., DC	:	direct current
d/dt	:	rate of change with respect to time t
d/dθ	:	rate of change with respect to rotating angle vector θ
E	:	(vector of) e.m.f. sources
E_i	:	generator internal e.m.f.
EHVAC	:	extra high voltage alternating current
e	:	instantaneous values of Thevenin (source) voltages
e.m.f.	:	electromotive force
exp	:	exponential
EAC	:	extinction angle control

f( ), g( )	:	functional notation
F_i	:	firing instant for valve i
G	:	torque matrix
H	:	Henry
h	:	integration step length
HVDC	:	high voltage direct current
Hz	:	hertz
i	:	number of iterations in iterative procedure
I	:	branch current (vector)
ISC	:	invertor safety control
IOC	:	invertor optimisation control
IEE	:	Institution of Electrical Engineers
IEEE	:	Institute of Electrical and Electronics Engineers
j	:	$j^2 = -1$
J	:	nodal current (vector)
km	:	kilometre
k	:	number of convertor inductive branches
K	:	(node-branch) incidence/connection matrix
$K_1 - K_4$	:	convertor control system constants
$K_5 - K_6$	:	convertor line fault detection unit constants
l	:	number of inductive branches in a network
L	:	inductance matrix
msec	:	millisecond (10^{-3} second)
MIT	:	Massachusetts Institute of Technology
MW	:	megawatt
n	:	total number of nodes in a network
N.Z.	:	New Zealand
N.I.	:	North Island
P,Q,S	:	active, reactive and apparent power

ΔP_i	:	firing instant correction	
p	:	differential operator	
p.f.	:	power factor	
p.u.	:	per unit	
Q	:	electric charge (vector)	
r	:	number of resistive branches in a network	
R, r	:	resistance (matrix)	
r.m.s.	:	root mean square	
S.I.	:	South Island	
S.C.R.	:	short circuit ratio	
sin	:	sine	
t	:	time	
U	:	unit matrix	
UMIST	:	University of Manchester Institute of Science and Technology	
V	:	volt or voltage (vector)	
VA	:	volt-ampere	
VAR	:	volt-ampere reactive	
v1	:	valve 1	
X	:	reactance	
X_c	:	commutation reactance	
Y	:	admittance	
Z	:	impedance	
$\alpha,\beta,\gamma,\delta$	:	node types and numbers	
α	:	firing delay angle	in HVDC convertors
γ	:	commutation (overlap) angle	in HVDC convertors
δ	:	extinction angle	in HVDC convertors
θ	:	rotor angle relative to axis of phase 'a'	in synchronous machines
δ	:	rotor angle relative to external a.c. system	in synchronous machines

β	:	generator transformer phase shift)	
ϕ	:	generator terminal voltage phase angle (lagging)	in synchronous machines
'abc'	:	phase variable representation	
'dq0'	:	Park's representation based on Blondel's 2 axis reaction theory	
Ω	:	ohm	
$\sqrt{\ }$	:	square root	
o	:	degree	
Δ	:	increment	
%	:	per cent	
$\simeq$	:	approximately equal	
$\neq$	:	not equal	
$<(\leq)$	:	less than (or equal to)	
ε	:	an element of the set	
ε	:	convergence tolerance	
η	:	detection level	
μF	:	microfarad (10^{-6} farad)	
π	:	3.14159	
Σ	:	algebraic sum	
ψ	:	flux linkage (vector	
ω	:	angular frequency	
θ, ϕ	:	phase angles associated with voltage or current (vectors)	

Subscripts and Superscipts

X^{-1}	:	inverse of matrix X
X^{t}	:	transpose of matrix X
X^{sp}	:	specified value of X
$\dot{X}$	:	time derivative of X
X_t	:	value of X at time t

X_{ij}	:	general element of matrix X
X^o	:	initial estimate of X
X^j	:	j^{th} estimate of X
X'	:	modified or auxiliary value of X
X^f	:	fault values
X^{max}	:	maximum value of X
X^{min}	:	minimum value of X
$X_{f.l.}$	:	full load value of X
d,q	:	rotor direct and quadrature axis values respectively
fd	:	rotor field winding
kd	:	d-axis damper winding
kq	:	q-axis damper winding
s	:	synchronous
r,s	:	rotor, stator
g	:	generator (terminal)
B	:	base quantities
e	:	exciter quantities
o	:	optimum or nominal
1,...n	:	n harmonics
la	:	leakage
t	:	transformer
1,2	:	primary and secondary values
m	:	transformer magnetizing quantities
c,l,k,r	:	capacitive, inductive, convertor and resistive branches
$\alpha,\beta,\gamma,\delta$	:	node types
NC	:	non-commutating
a,b,c	:	a.c. phase quantities
d	:	d.c. quantities

r,i	:	rectifier, invertor
m,n,p	:	rectifier, invertor and fault a.c. buses
f	:	filter
m,t,b	:	middle, top, bottom node

Symbols Used In Diagrams

ew	:	earth wire
F	:	filters
I_r, I_i	:	rectifier and invertor direct currents
P_r, P_i	:	rectifier and invertor direct powers
V_r, V_i	:	rectifier and invertor output voltages
V_{lr}, V_{li}	:	rectifier and invertor line-side d.c. voltages
5 7 9 11 13 HP	:	harmonic filters

Graphical Symbols


: source of electromotive force


: resistor

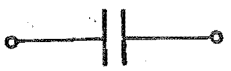
: capacitor


: inductor


: earth


: star transformer connection


: delta transformer connection

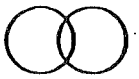 : three-phase two-winding transformer

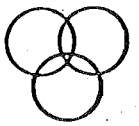 : parallel three-phase convertor transformers for 12 pulse operation

 : non conducting valve

 : conducting valve

 : uncontrolled (diode) rectifier bridge

 : controlled convertor bridge

 : matrix or vector quantity

ABSTRACT

This thesis describes the development of accurate transient equivalents for the efficient modelling of disturbances in interconnected a.c./d.c. power systems.

A survey of existing techniques for the dynamic analysis of such transients is made, and their major limitations are outlined. The most recent utilize diakoptical techniques with state space formulation, which allows detailed representation of all system plant, albeit at the expense of high computation costs.

Means of reducing such costs to a level which permits digital simulation to complement/replace physical simulators in the analysis of a.c./d.c. network transients are investigated, and an interactive algorithm is proposed which uses a multimachine a.c./d.c. transient stability programme and a small step dynamic analysis to achieve this purpose.

Typical disturbances in both a.c. and d.c. networks are investigated to show the potential of the new technique, and its ability to include accurate representation of the full system throughout the study period.

The dynamic analysis programme is also used in preliminary investigations of unit type generator-convertor schemes; the developed model provides a rigorous means of testing the practicalities of such schemes.

ACKNOWLEDGEMENTS

I am especially grateful to my supervisor, Professor J. Arrillaga, for his enthusiasm and advice throughout this research.

Also the value of the many discussions with my postgraduate colleagues, and in particular Keith Turner, is acknowledged.

I wish to thank New Zealand Electricity for their financial assistance and granting of study leave to enable this project to be completed. The Christchurch District Draughting Section of New Zealand Electricity is also thanked for the preparation of the many diagrams in this thesis. I also wish to thank the staff of the Computer Centre of the University of Canterbury for their invaluable help.

Last, but certainly not least, I wish to express my gratitude to Sue, not only for her assistance in preparing this thesis, but also for her encouragement and patience through the course of my work.

CHAPTER 1

INTRODUCTION

1.1 HVDC APPLICATIONS

The many unique characteristics of high voltage direct current (HVDC) transmission are well documented in the literature (Adamson and Hingorani 1960, Cory 1965, Kimbark 1971, Uhlmann 1975, and bibliographies B1 - B6).

In the last two decades, HVDC schemes have proved economically competitive with conventional extra high voltage alternating current (EHVAC) transmission under specific conditions. Systems requiring asynchronous ties (e.g. Sakuma, Japan), long distance bulk power transmission either overhead from generation to load centre (e.g. Volgograd - Donbass, USSR), or involving underground or submarine cables (e.g. Kingsnorth, UK and New Zealand respectively), were specific cases where HVDC proved desirable. The performances of these and other existing schemes have been regularly surveyed (Last and Middleton 1970 and 1972, Jarrett and Middleton 1974, Rumpf and Jarrett 1976), and these surveys have conclusively demonstrated the technical and economic feasibility, and reliability associated with the use of the HVDC attributes to meet the particular system requirements.

Until 1972, mercury arc valves were used exclusively in the a.c./d.c. conversion process. Technological developments saw the mercury arc valve superseded by the thyristor.

Consequential upgrading of thyristor ratings has pushed the practical power ratings of HVDC schemes dramatically upwards (Fotin *et al.* 1976), whilst in general the size and cost of convertor stations has dropped relatively, due to innovations in design concepts (Ellert and Hingorani 1976).

Also in the last decade, the ability of HVDC links to increase system reliability (Ellert and Hingorani 1976) and to improve a.c. system stability (Eel River, Canada, reference Haywood and Patterson 1976) and/or damp oscillations (Pacific Intertie, USA, reference Cresap *et al.* 1976) by rapid control of active power flow, has been a major factor in determining further applications. These and other potential applications have seen the development of a new level of sophistication in HVDC control systems and of additional overall system control policies (Jötten *et al.* 1978). As a result of these developments, considerable emphasis is now being placed on modelling of power systems which involve HVDC convertor plant, either by small scale analogue simulators or by analogue or digital computer simulation using mathematical models.

Ideally the use of all three techniques gives a basis for comparison of realism and consistency. In addition the benefits of each may be used to their best economic effect. In evaluating the way these techniques are best utilized the following bases must be used:

(i) degree of complexity and accuracy required;

(ii) availability of facilities possessing the necessary characteristics; and

(iii) associated cost and time involvement.

The limited capability and complexity available with analogue computer models, coupled with their inherent flexibility for changing system parameters and control methods, means it is an ideal tool for preliminary investigations and parameter optimization at little cost. Once a particular design concept has been established, simulation on a more complex physical model may be performed to obtain results with greater accuracy. The use of actual control systems on a physical simulator allows optimization of control circuits to be performed at little extra cost. The time and economic limits to the available size, range and complexity of the physical model installation, limits its total system representation, and demands the use of a digital computer which can model the entire system economically and accurately. The *a priori* knowledge of the control systems gained by analogue simulators or computation, allows derivation of accurate mathematical models for them, which may be used in the digital simulation.

The major limiting factor in digital computation is cost. The type of study required, i.e. load flow, stability, etc., will determine the mathematical model necessary, and then inherently, the associated cost. Therefore the mode of utilization of digital computation, which also has the benefits of both the other methods, will be determined largely by the type of study required.

The particular studies to be carried out will determine the required representation of the system and the control policy. Experience gained from other types of investigations, and real system behaviour, must be used in

exercising engineering judgement as to how best to simulate the conditions to be studied on a digital computer.

1.2 APPLICATIONS OF DIGITAL COMPUTER STUDIES

The prospective incorporation of new plant with special characteristics, such as HVDC schemes, into a power system, generally requires new types of digital computer simulation. As the level of sophistication of the special plant and any associated control grows, the level of the analysis methods used to investigate the feasibility of these developments must also become higher. Without this higher level of analysis, confident application of the new plant to its full potential is restricted.

In this process a variety of studies must be conducted, their complexity dependent on the particular aspects being investigated. However, no one study can be considered independent, and a degree of engineering judgement is necessary when considering possible interaction between various studies. This is also required when deciding on the level of plant representation in any particular study.

The behaviour of HVDC schemes is largely governed by the action of the convertor control schemes in response to terminal condition changes on either the a.c. or d.c. sides. The subsequent interaction of each convertor with its a.c. system, and/or the interaction between convertors, which will be modulated by the d.c. link itself, will then determine the transient behaviour of the inter-connected a.c./d.c. power system.

This behaviour can often be analysed by a quasi-steady state approach such as in determining the influence of the link on a.c. system transient stability (Arrillaga, Arnold *et al.* 1977). This approach will be valid only if the assumptions made in the analysis are satisfied by the responses of the convertors and their control systems. Under disturbed conditions however, it may not be possible to describe the behaviour of the convertors and the link by a set of equations based on quasi-steady state analysis, due to the presence of harmonic currents and the resulting waveform distortion. The predictability of valve firing sequences may be upset and valve maloperations, such as commutation failure, may occur. To analyse the overall system behaviour under such conditions requires a study which considers the transient behaviour of the convertors in greater detail.

1.3 HVDC DYNAMIC ANALYSIS

The study of the transient behaviour of HVDC schemes must consider the conditions in both the a.c. and d.c. systems, as well as the action of the firing control systems and the individual convertor valve switchings. The various types of a.c. system components offer different impedances to the harmonic and sequence currents produced by the HVDC link. As a result, these currents tend to follow different paths in the a.c. system, producing voltage drops and causing distortion in the voltages at convertor terminals. This waveform distortion may give rise to harmonic instabilities and convertor maloperations. It is therefore inappropriate

to represent the a.c. system by a single impedance element. The influence of a.c. harmonic filters on convertor operation is substantial and thus the need for their adequate representation is obvious. In addition, other significant plant at or near the convertor terminals may influence the convertor operation, and allowance must be made for their inclusion if assessment of their influence is required.

Conditions on the d.c. side of a converter have a less direct effect on convertor operation, but they do directly influence actions taken by the firing control systems, therefore necessitating adequate d.c. side representation.

The duration of a dynamic analysis simulation will be largely determined by the type of disturbance being investigated. After a disturbance, initial control response will be established quickly, and then the system will generally oscillate for some time before attaining the new steady state. However the dynamic analysis need only extend until the general behavioural tendencies are apparent. Normally study durations may therefore be confined to approximately 100-300 msec, even in the case of severe d.c. line faults.

1.4 REVIEW OF DIGITAL COMPUTER DYNAMIC ANALYSIS

Convertor operation consists of repeated waveform dependent topological changes which in general can neither be specified in advance, nor predicted with quasi-steady state models. The literature detailed below contains

descriptions of the early convertor models, covering both normal and abnormal convertor behaviour. However, the computer implementation of the models and analytical techniques developed around the convertor units were very restricted in their applicability to real power systems. The work of Hingorani *et al.* (1966(2), 1967, 1968), Hay *et al.* (1969(2), 1971(2)), Peterson *et al.* (1969), Reeve and Kapoor (1971) and Kapoor and Reeve (1973) was characterized by the use of an idealistic three phase source e.m.f. in series with an impedance to represent the a.c. system(s) (including the a.c. harmonic filters), with a simple leakage reactance model for the convertor transformers. The earlier simplistic control representations, derived by a quasi-steady state approach, were gradually replaced by more elaborate representations as highlighted by Reeve and Carr (1974). The importance of explicit representation of a.c. harmonic filters was recognised by O'Regan and Dillon (1970). This in turn necessitated a representation for the a.c. system which was applicable at other than fundamental frequencies, and Hingorani and Burberry (1970), Bowles (1970) and Giesner (1971) proposed models for a.c. systems using parallel-series impedance combinations which were applicable over such a range of harmonic frequencies.

These models for a.c. systems were used by Reeve and Kapoor (1972) to perform dynamic d.c. fault analyses using restricted control representations. Groschupf *et al.* (1973) performed dynamic a.c. fault analyses with apparently more detailed control representation.

The limitations of existing control schemes were

highlighted by Ainsworth (1967, 1968) and he proposed a new method of convertor control. An adaptation of this was used by Arrillaga and Giesner (1970, 1972) and Giesner and Arrillaga (1971, 1972(2)), in conjunction with proper a.c. system, d.c. link and explicit a.c. harmonic filter representations, to investigate the transient performance of convertors during a.c. faults and convertor maloperations.

The computer implementation of the existing analytical techniques (mesh or nodal) was restricted in versatility, since it was based on a digital computer programme containing many subroutines, each of which solved the specific set of differential equations relating to a particular convertor topology. All the subroutines were processed by the main programme, hence 'The Central Process Method'. However, this method could only be applied if the convertors were connected to infinite buses. When the a.c. system impedance was significant, many different sets of equations were necessary to describe the network, and the approach became cumbersome and computationally wasteful. By applying Kron's tensor analysis techniques (1959 and 1965) to the varying topology of convertor bridges, Williams and Smith (1973) developed a computer based analysis which was superior in generality and ease of programming, and more logical in automatic assembly and solution of network equations, for both normal and abnormal conditions.

This use of Kron's techniques was applied to a mesh analysis but it was equally applicable to a nodal analysis. Mesh analysis formed the basis of the work done by Milias-Argitis *et al.* (1976, 1977(2), 1978), and nodal analysis the

basis for the work done at UMIST (Arrillaga *et al.* 1977(2), 1978).

The work by Milias-Argitis *et al.* was an extension of the theoretical basis proposed by Smith and Williams (1973), and studied an HVDC link under transient conditions. Inclusion of a.c. filters and other auxiliary equipment that influences system response was reported to be possible, along with the simulation of various control schemes. However the results did not show this inclusion of filters, and the convertor transformer was still represented by a simple leakage reactance model. The d.c. line model used was a simple resistive drop, although an earlier analysis provided for the use of a single T element model.

The aim of Arrillaga *et al.* was to provide a more accurate and general model for the d.c. line, convertor transformers, synchronous generators, and various other a.c. plant, whilst maintaining a precise model for the HVDC convertor and its associated control system.

The result was a general dynamic model, formulated in terms of state space theory, which used a nodal analysis and utilised diakoptical tearing techniques (Kron 1963, Brameller *et al.* 1969) to segregate convertor branches and nodes from the rest of the network to avoid involving the whole network in the topological changes resulting from convertor valve switchings. Diakoptics were also used by Milias-Argitis *et al.* on a small scale, but Al-Khashali's application (1976, Arrillaga *et al.* 1977) resulted in an extensive reduction in computational burden. In a large power system representation, the portion of the network

actually involved in topological changes associated with HVDC convertor valve switchings is relatively small. If the subnetwork directly involved can be segregated and the topological operations be performed on it alone, the computational savings are obvious.

The model developed at UMIST accepted varying degrees of a.c. system representation to meet the requirements of any particular study. In each case the individual units of greater relevance could be emphasised, with the rest of the power system synthesized into a simpler equivalent circuit. Realistic representations for convertor transformers and synchronous machines (Campos Barros 1976) were developed and used in conjunction with the earlier representations for a.c. networks, harmonic filters, transmission lines (a.c. or d.c.) and other convertor plant. The controllers modelled were based on a direct digital control system developed by Arrillaga and Galanos (1969, 1970(3)), which was similar in principle to the phase locked oscillator of Ainsworth (1968), to simulate equidistant pulse firing. However, simple programme parameter changes permitted the simulation of the earlier method of individual phase control.

The UMIST model allowed these system components to be interconnected in any feasible way with either 6 or 12 pulse operation in a multibridge configuration possible.

As is normal in power systems, the network matrices were sparse. This sparsity was retained by the diakoptical treatment, and was manifested in the coefficient and incidence matrices. To obtain efficient solution processes for the network equations, which are performed many times in

a single study, particular attention was paid to utilisation of this sparsity.

1.5 PRESENT WORK

A major limitation to the work outlined in Section 1.4 is experienced in representing the a.c. system. Although the UMIST model allowed detailed, accurate representation of every network component, computer simulations of practical power systems would be overburdened in terms of storage and running cost, due to the size and complexity of the network. This may be overcome by using equivalent forms for (parts of) the a.c. network. However, accurate equivalents have not been readily available in the past, and in general have not incorporated the a.c. system's time response.

A means of obtaining accurate time variant network equivalents has been developed, utilising an interactive facility with a multi-machine a.c./d.c. transient stability programme. The network equivalents obtained from the stability programme accurately indicate the time response of the a.c. system by virtue of the synchronous machine models used in the transient stability analysis. By this interactive technique, equivalents may be obtained for various parts of the network, whilst still retaining explicit representation of the components of major interest. For example, in studies of interconnected a.c./d.c. systems, explicit modelling of the d.c. system, convertor transformers and harmonic filters is necessary.

Therefore the developed dynamic analysis programme

can not only accurately simulate the time varying convertor topology and its effect on the a.c. system(s), but also, by virtue of the interactive facility of a transient stability programme, can accurately represent the time response of the a.c. system(s), even though a much reduced representation is used.

In Chapter 2, the basic mathematical models for digital computer representation of each type of system component, e.g. transmission lines, transformers, synchronous generators, filters and HVDC convertors, as well as the representation of network equivalents, are detailed. The reasons for selecting the particular method of analysis used are explained, with emphasis on the need for network and parameter flexibility, as well as computational efficiency. The network equations are developed using a state space formulation with diakoptical segregation of the network for computer efficiency. Two formulations are presented. The second more efficient formulation which further segregates the a.c./d.c. network is later shown to have some limits to its practical application. The numerical integration process used to solve the network equations is indicated, and the per unit system used to simplify analysis and improve computational accuracy is explained.

Chapter 3 describes the basic digital computer programme used to implement the developed mathematical model. The programme has been written in a modular form so that flexibility for extensions or modifications is enhanced. The data input and initial value specification stage is detailed with particular attention paid to the effect

convertor and synchronous machine models have on the accuracy of the initial values. Since these values are usually determined by an analysis based on balanced sinusoidal waveforms, it is shown that short dynamic simulations of the steady state conditions are necessary to achieve the desired operating point dynamically. Various tools for shortening the period necessary for this are detailed. The implementation of the basic convertor functions (control action, valve firings and extinctions) is also described, and the numerical integration technique is outlined, along with the methods of optimisation for storage and repeated matrix operations. The types of disturbances/faults which can be catered for are indicated and a description of an efficient method of data output, storage and retrieval, which allows selective examination of results at a time other than the actual simulation time, is included. Finally the means for checking the validity of the programme is described.

Programme developments, such as circuit breaker modelling, necessary to use the programme to simulate various a.c. faults in interconnected a.c./d.c. systems are described in detail in Chapter 4, along with test results from studies of balanced and unbalanced faults in both the rectifier and invertor end a.c. systems. An interactive facility used to obtain network equivalents is described in detail, and some results are included to indicate the need for a time variant representation of the a.c. system when investigating these faults. A model which allows representation of transformer saturation is included in this chapter and some test results to indicate its use,

especially in relation to recovery from a.c. faults in a.c./d.c. networks, are presented.

Chapter 5 is dedicated to the simulation of d.c. line faults, and again necessary programme development work, such as in representing the fault characteristics and the coordination of protection associated with fault detection, extinction and recovery, is detailed. A particular fault is investigated in detail to illustrate the applicability of the interactive dynamic analysis - transient stability programmes in simulating such faults.

In Chapter 6 a new method for representing excitation systems is developed to cater for systems which use thyristor bridges. This is necessary since the fast changes in excitation available with such systems require accurate modelling of the topology of the excitation circuit. A dynamic model which can represent both normal and abnormal bridge behaviour is used. Its application in a.c. systems is used as a preliminary investigation of the model's validity and the exciter's performance. The importance of isolated generator plant connected to HVDC links for bulk power transmission has resulted in the suggested use of fast thyristor excitation of synchronous machines to replace the conventional rectifier mode of d.c. link control. This would allow replacement of the controlled rectifier by a diode rectifier with obvious advantages in both economics and reliability. A model is developed which can be used to accurately represent such schemes during disturbed conditions. This is of particular importance in assessing the ability of the excitation circuit to perform the control

and protection aspects normally associated with rectifier control. A preliminary study of a d.c. line fault is included to illustrate the developed model's use.

CHAPTER 2

MATHEMATICAL MODEL

2.1 INTRODUCTION

Development of a suitable dynamic model, and a method of computer analysis for a.c./d.c. power systems, has evolved from the work described in Section 1.4. The possible existence of uncharacteristic harmonics and imbalances in the a.c. system has ruled out the use of symmetrical transformation methods. The frequent topology changes on the d.c. side reduce the effectiveness of multiple frequency methods such as Fourier transform analysis. The application of travelling wave techniques to solving problems involving both distributed and lumped parameter components is also limited for the systems under consideration.

The most suitable approach, practised by the majority of researchers in this area, is a state space formulation which can be used in conjunction with the usual methods of (electric) circuit analysis to treat both linear and non-linear circuits. Any power system can be represented by a network of inductive, capacitive and resistive elements, where each network component has a particular circuit model defined in terms of these elements. The state space formulation will then provide a set of non-linear differential equations, in which the state variables relate to the energy storing components. Therefore linear capacitors, whose terminal voltage is related to the energy

stored in the electric field i.e. the electric charge, and inductances, whose current or flux linkage is related to the magnetic field energy storage, will determine the state elements. Resistors are non-state elements and their voltages and currents can be determined from the state variables.

2.2 REPRESENTATION OF COMPONENTS

When defining component models, one must apply restrictions pertinent to the major area of interest. Outside of this region will be the concern of a related study, although if necessary any interaction will need to be accounted for. In a dynamic analysis study the highest frequency of interest will be around 1 kHz so that higher frequency effects are neglected. This will considerably simplify convertor models, and allow the neglect of surge phenomena. Similarly at the other end of the frequency scale, representation of generator-rotor mechanical transients as a result of rotor-angle swings (approx. 1 Hz) can generally be neglected since this action is too slow to have an effect on the convertor or its controller's behaviour. In this case, source e.m.f.s are assumed to have constant frequency.

2.2.1 Static Convertors

The three phase convertor which has found universal acceptance in HVDC schemes is the Graetz bridge. The operation of these convertors is well documented (Adamson and Hingorani 1960, Cory 1965, Kimbark 1971, Uhlmann 1975).

For complete generality it is necessary to provide modelling facilities for both six and twelve pulse operation of these bridges. This may be done by assuming the convertor transformers to be star connected on the a.c. side with earthed neutral, while the bridge side may be either star or delta connected. The latter connection provides the 30^{o} phase shift necessary for 12 pulse operation. A convertor may operate as a rectifier or invertor, and multibridge configurations connected in either series or parallel on the d.c. side are catered for. The convertor bridge will contain the three transformer secondary winding terminals and two d.c. terminals, one of which is earth or the d.c. terminal of a further bridge.

Considerable simplification may be achieved by assuming the forward voltage drop of a conducting valve to be negligible so that the valve acts as an ideal switch. This is justifiable since the actual drop is largely independent of current and is only a fraction of the normal operating voltage. The auxiliary circuits and voltage grading devices draw very little power and have time constants so short as to not affect the convertor's transient behaviour.

In cases where it is deemed not necessary to represent a particular convertor in a multi-convertor system, provision has been made to model it by a d.c. source which has a constant e.m.f. behind an impedance.

2.2.1.1 Modes of Operation. Referring to a single six-pulse bridge, the topology of the convertor subnetwork is entirely dependent on the number and positions of

conducting valves. For the convertor to be in a conducting state at least two valves must provide a closed current path as viewed from the two d.c. terminals. Conducting states, both normal and abnormal, may be categorised by the following modes.

A - (Non-commutating mode): two valves on different sides and arms of the bridge are ON.

B - (Normal commutation): three valves, one on each arm, two commutating and at least one conducting on each side of the bridge.

C - (Non-commutating arm short-circuit): both valves on one of the arms are ON, with no other valves conducting.

D - (Commutating arm short-circuit): as in C with one or both valves on another arm being ON. With one valve on the second arm conducting (D1), there is a single commutation process. When both valves on the second arm conduct (D2), commutations are simultaneously taking place on both sides of the bridge.

E - (a.c. short-circuit): this is the case when the three secondary terminals of the convertor transformer are short-circuited by the conducting valves. This occurs when four or more conducting valves involve all three arms of the bridge. With four conducting valves (E1), two commutations occur simultaneously which may be on the same side of the bridge. When five valves conduct (E2), commutations take place on both sides and with six valves conducting (E3), multiple commutations take place on both sides of the bridge.

The bypass valve used in many existing schemes may be left out of the analysis, with considerable simplification in bridge representation, since its effect can be implicitly represented by modes C, D and E.

2.2.2 Convertor Control Systems

2.2.2.1 Introduction. The operations of the control system for HVDC schemes are, in general, different for each particular application. However, their basic principle is well documented (Adamson and Hingorani 1960, Cory 1965, Kimbark 1971, Uhlmann 1975, Jotten *et al.* 1978). The following is a résumé of their operation.

In the steady state the grid (or gate) pulse firing control system provides fast control of convertor valve firings to obtain optimum utilization of the link whilst maintaining the desired power transmission. To minimize losses a high link voltage is required, and to minimize reactive power demands the control angles (α_r and δ_i) are kept at their lowest practical values, with δ_i large enough to prevent commutation failures on the occurrence of minor disturbances.

When firing control can not perform these functions, convertor transformer tap changing is used to alter the level of the effective a.c. supply voltage. This is a relatively slow type of control.

The initial response of a link to sudden changes in system conditions or requirements is dependent on the firing control response which can produce substantial changes in d.c. voltages six times (for a 6 pulse bridge) within a cycle of fundamental frequency. Dynamic analysis studies

do not include tap changer representation, since it would be ineffective over the duration of the study.

The usual form of HVDC link control is for the rectifier to control link current by operating in a constant current mode (CCC) and for the invertor to determine the link voltages by operating with (minimum) extinction angle control (EAC). The invertor is also provided with CCC, set to operate during transient or abnormal conditions. In each case the current control settings are determined from d.c. power transmission requirements or auxiliary control functions such as a.c. frequency control.

2.2.2.2 Types of Control Systems. The timing of the firing instants is controlled by the types of system used:-

(i) Analogue methods of predictive control issue valve firing pulses individually, relative to valve (or a.c.) voltage zero crossings, and dependent on the link voltages and currents. Usually invertor EAC is based on a predictive inverse cosine process, with the rectifier on a fixed firing angle (α) control derived from CCC.

Although these systems were the norm in the majority of early HVDC schemes, they reflect any unbalance or distortion in a.c. supply voltages, a common phenomena with weak a.c. systems, by producing variations in valve conduction periods. These in turn produce further distortion and unbalance, with the result that uncharacteristic harmonics appear in the a.c. system, which may result in harmonic instability (Ainsworth 1968). Installation of a.c. harmonic and/or control

filters may reduce this problem but not remove it. The predictive approach to EAC means that some disturbances leading to convertor faults can be anticipated, and a measure of corrective action performed before the fault develops.

(ii) Uniform firing control in the steady state produces a train of equidistant pulses related to the supply frequency. This pulse train will be advanced or retarded in accordance with the normal control quantities. Absolute values of delay angle are only relevant if the system tries to violate a preset maximum or minimum limit. Invertor EAC uses an iterative closed loop process in measuring the extinction angle (δ) for each valve. Because this system is independent of the a.c. voltage waveforms, uncharacteristic harmonics and harmonic instability do not occur since equal conduction periods are assured. However, whereas predictive schemes may take action to avoid commutation failures, this system can only detect the condition after it has occurred. Most uniform firing schemes are variations of the phase locked oscillator techniques developed by Ainsworth (1967, 1968). The principle has been used recently (e.g. Kingsnorth) to cater for applications where the large rating of the HVDC scheme renders the a.c. system(s) relatively weak at the convertor stations, and thus susceptible to harmonic instability. More recently, proposals have been made to implement this type of valve firing control by digital techniques (Arrillaga

and Galanos 1969, 1970(3) and Arrillaga and Baldwin 1974).

The speed and accuracy of existing control and protection schemes which use analogue techniques does not utilize the inherent advantages of d.c. links sufficiently. Convertor operation which is based on discrete grid control pulses can theoretically achieve instantaneous control by using direct digital control including fast protective action. This requires the fast, accurate monitoring and telecommunication facilities described by Erinmez (1971) and Arrillaga and Galanos (1970(3)). The control scheme to be used in the dynamic analysis studies is a development of their proposals, and is described briefly below. However, any particular control system may be simulated by simple programme modifications since all control quantities are present.

A valve is switched to the conducting state when there is adequate positive voltage (anode - cathode) and a firing pulse has been applied to the grid (gate). The next valve (i) to fire is then set by a ring counter sequence and its firing instant is given by

$$F_i = F_{i-1} + 60^o + \Delta P_i \qquad \ldots (2.1)$$

where ΔP_i is the corrective action produced by the controllers, which in the steady state will be zero. This correction is dependent on the particular controller used. A simple algebraic relation is used to simulate what is in practice a complex circuit, with elements to simulate damping, and delay functions to match the controller response

to that of the d.c. link. The time scale and purpose of these studies justifies this simplification. With rectifier operation in the CCC mode

$$\Delta P_i = K_1 (I_d - I_d^{sp}) + K_2 \, dI_d/dt \qquad \ldots (2.2)$$

where, as explained above, K_1 and K_2 have been reduced to simple gain constants.

The direct digital control system is ideally suited to computer simulation since it is possible to sample the relevant variables at each integration step to form these corrections. To closely resemble the real life conditions, the following algorithm is used in which the instantaneous values of I_d and its derivative are accumulated over a 60^o period. At the instant of firing correction (when the valve voltage goes positive), these quantities are averaged and used in equation (2.2). The accumulators are then reset to zero to sample the next 60^o period.

Sophistications may be added to include constant power order or d.c. power modulation for a.c. system damping (Ainsworth and Martin 1966, Cresap *et al.* 1978) or a.c. frequency control (Uhlmann 1970, Haywood and Patterson 1976). However the controlled variable is still I_d and thus the basic current control proposed by Arrillaga and Baldwin (1974) is used. Excursions of firing instant are limited to prevent operation outside the normal range for the convertor. Therefore firing does not occur before a minimum delay angle (α^{min}) to ensure correct valve turn on, and a valve is triggered prematurely if α^{max} is reached before F_i, to avoid commutation failures during severe transients, e.g.

when a rectifier bridge is suddenly driven into inversion to reduce d.c. overcurrents as a result of a d.c. line fault. This requires measurement of the delay angle α_r. Under these circumstances the whole pulse train is advanced or retarded by the same amount.

Invertor extinction angle control is manifested by two mutually exclusive controls, viz. inverter optimisation control (IOC) and invertor safety control (ISC). Extinction of mercury-arc valves usually requires a short deionization time for the arc to deionize before a positive voltage applied across the valve will not cause the arc to restrike. Therefore a margin δ_f must be allowed to prevent such a commutation failure. A larger margin δ_o is usually allowed to prevent commutation failures arising from small disturbances, and this is the usual angle of operation. Unlike conventional predictive methods, this control is performed by a detective - corrective iterative process. IOC compares the smallest of the six most recent extinction angles (δ^{min}) with δ_o and applies a correction according to

$$\Delta P_i = K_3 (\delta^{min} - \delta_o) \quad \ldots (2.3)$$

where K_3 must be less than unity since commutation angles will increase with retardation of F_i. To prevent excessive encroachment on δ_f, ISC is performed immediately a valve i is detected to have an extinction angle (δ_i) less than δ_o, by the following action

$$\Delta P_i = K_4 (\delta_i - \delta_o) \quad \ldots (2.4)$$

in which case K_4 may be greater than unity to ensure safe operation.

Current control at the invertor usually has a setting less than that at the rectifier by some 10-15%, so that it is only invoked under transient conditions, e.g. when the two convertors' currents are different or when the rectifier is unable to increase I_d beyond the invertor's setting. The invertor is normally provided with a minimum delay angle of more than 90^o for CCC, to prevent it from reversing the link voltage polarity i.e. to prevent it operating as a rectifier.

2.2.3 Synchronous Machines

The majority of early dynamic analysis work did not include models for rotating machines. However in cases where the a.c. system in the vicinity of a convertor is dominated by synchronous machines, these machines must be modelled in detail.

Early digital computation work used the classical approach of transformation to eliminate time varying coefficients. Blondel's two-axes theory was perfected by Doherty and Nickle (1926), Park (1929) and others, eventually culminating in Kron's unified linear theory for rotating machines (Kron 1938). Before the advent of digital computers the solution required many assumptions, such as uniform speed, to avoid a system of non-linear differential equations. The analytical power of the digital computer allowed many of these assumptions to be removed. Several authors (Carter *et al.* 1961, Barton and Dunfield 1966, Dunfield and Barton 1967, Jones 1967, Smith and Snider 1972) investigated the basic simplifying assumptions inherent to the development of the two-axes model and concluded they

were least applicable to salient pole machines.

Individual phase identification is necessary when a convertor is in close proximity since there is a need to define details of the commutation process, and also because the machine's terminal voltage may not be sinusoidal or symmetric due to harmonic current flow from the convertor. Therefore a phase-variable representation has been proposed (Arrillaga *et al.* 1977, El Serafi and Shehata 1976). Since most manufacturer data is in the two-axes d - q - 0 form, this must be transformed (Concordia 1951, Fitzgerald and Kingsley 1961, Kimbark 1968) to yield the direct phase quantities (a,b,c).

The extra computation introduced by the time varying inductances associated with a phase-variable model is counterbalanced by the necessity of three phase representation which is achieved without the need of transformations at each step. By using a phase-variable model, asymmetries, non-linearities, and distortion effects can easily be handled, either implicitly, or by direct parameter modifications e.g. for saturation. A d-q axis representation is retained for the rotor circuit since it fits the actual geometry and winding arrangements. The model used includes the main field winding in the d axis with two damper windings. The rotor position θ is specified relative to the axis of phase 'a' in the positive direction of rotation. The machine is treated as a motor in writing its differential equations so that positive current flows into the positive terminal of a circuit branch. The terminal voltage may then be expressed in matrix form as

$$V_g = p\,(L_g \cdot I_g) + R_g \cdot I_g \qquad \ldots (2.5)$$

$$= L_g \cdot \frac{d}{dt} I_g + \omega \cdot \frac{d}{d\theta} L_g \cdot I_g + R_g \cdot I_g \qquad \ldots (2.6)$$

where $\omega = d\theta/dt$ is the angular velocity.

The elements of the time variant inductance matrix L_g, which is a 6 x 6 matrix, are illustrated in Appendix A1. The stator values can accommodate fourth harmonic terms if available, as these can be of significance in convertor-generator units (Campos Barros 1976).

The effect of excitation and governor controls will not normally be included in short duration transients due to their relatively long time constants. They may be approximated by constrained algebraic relations using field voltage and rotor speed as the interface variables. In the case of fast thyristor controlled excitation it is possible, and desirable, to explicitly represent the thyristor bridge exciter to monitor its dynamic behaviour (see Chapter 6).

2.2.4 Transmission Lines

The response of a transmission line to its terminal conditions can be analysed by wave propagation techniques. The modal components used in the wave equations require a sampling interval chosen so that travel times are integral multiples of this sampling time. When there are multiple a.c. and d.c. lines of varying lengths, the travel times may be very different. The problem of different velocities of propagation, associated with the different modes of a multiconductor line, compounds this so that a satisfactory

sampling interval which will coincide with the convertor switching operations will be too small for efficient computation.

A network approach is therefore adopted whereby the line is segmented into an appropriate number of short line pi- segments, according to the highest frequency of interest. The equivalent circuit of a transmission line is formed from the series impedances and shunt admittances per unit length. An example is given in Appendix A2.

2.2.5 Transformers

The traditional transformer equivalent circuit (Say 1958) involving a series impedance is not suitable for a full three phase dynamic analysis because different magnetic circuits offer different impedances to the current components, and the phase shifts inherent in the different connections need to be represented, especially when static convertors are present.

A single phase transformer may be denoted as two coils magnetically coupled by the iron core as in Fig. 2.1.

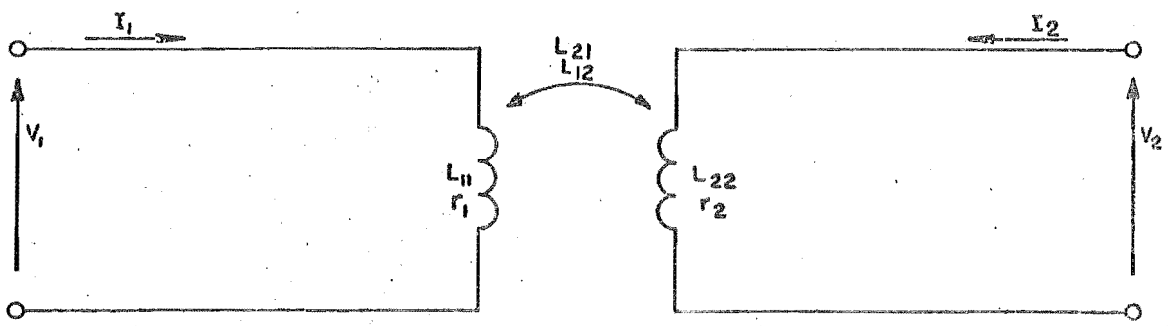

Fig. 2.1 Transformer Equivalent Circuit

Neglecting iron losses, the transformer can be represented by the coupled circuit model (MIT 1943) in terms of self (L_{11}, L_{22}) and mutual (L_{12}, L_{21}) inductances.

$$\begin{bmatrix} V_1 \\ V_2 \end{bmatrix} = \begin{bmatrix} L_{11} & L_{12} \\ L_{21} & L_{22} \end{bmatrix} p \begin{bmatrix} I_1 \\ I_2 \end{bmatrix} + \begin{bmatrix} R_1 & 0 \\ 0 & R_2 \end{bmatrix} \cdot \begin{bmatrix} I_1 \\ I_2 \end{bmatrix} \quad \ldots (2.7)$$

Numerically (in p.u.) the selfs are equal, as are the mutuals. Their interrelationship is given approximately by

$$L_{12} = L_{21} \approx \sqrt{L_{11}\,(L_{11} - x_{1a})} \quad \ldots (2.8)$$

where x_{1a} is the total leakage reactance of the transformer. This data must be determined accurately from the standard open and short circuit tests. In the case of a modern power transformer, the value of the self term is very high (e.g. 1% magnetizing current) and the leakage reactance is very small (e.g. 5%) so that in p.u.

$$L_{11} = L_{22} = 100 \text{ p.u.}$$

and thus $$L_{12} = L_{21} = 99.975 \text{ p.u.}$$

The numerical value of the off-diagonal terms is therefore close to that of the diagonal terms. Since the formulation requires inversion of the branch matrix L_t, numerical instabilities could be created by the use of inaccurate data.

Three winding transformers may be modelled by extending the dimension of equation (2.7) by one. Similarly three phase transformers may be modelled, although data for

interphase mutuals is often difficult to obtain (Duke 1979). Phase shifts, zero sequence circulating currents, neutral earthing etc., are all taken care of automatically. Modification of the tap side winding inductances can be used to represent off-nominal taps, although tap changing will not be a feature of dynamic analyses.

The coupled circuit model produces a magnetising current which is based on the assumption of linear core magnetization. Non-linearities in core magnetization (e.g. saturation) may be catered for if the relationship between the equivalent circuit and the magnetizing characteristic is established. This is done by continuously updating the elements of the matrix L_t in equation (2.7) to correspond to the instantaneous values of currents and flux linkages or voltages. This procedure is indicated in more detail in Section 4.7.

2.2.6 Static Shunt Elements

Apart from HVDC schemes which have an isolated (unit) rectifier, a.c. harmonic filters tuned to the main characteristic harmonics of the convertor are necessary. They are usually installed somewhere on the a.c. side of the convertor transformers and because of their capacitive appearance at fundamental frequency, will provide some reactive power compensation for the convertor. Due to their large time constants, these filters have a major influence on convertor waveforms following a disturbance and hence the need to accurately represent them in dynamic analyses. DC side harmonic filters and line dampers are often included depending on the actual scheme, particularly the type and

length of the d.c. line (Giesner 1971).

Various shunt elements (circuits) can be used to represent the above plant (e.g. Figs 2.2a,b,c). Local load representation and fault modelling is provided by the circuits in Figs 2.2d and e. Static capacitor compensation is provided by Fig. 2.2f which can also be used for modelling d.c. cables which have negligible series impedance.

All three phase a.c. components are assumed to be star connected with the neutral point earthed.

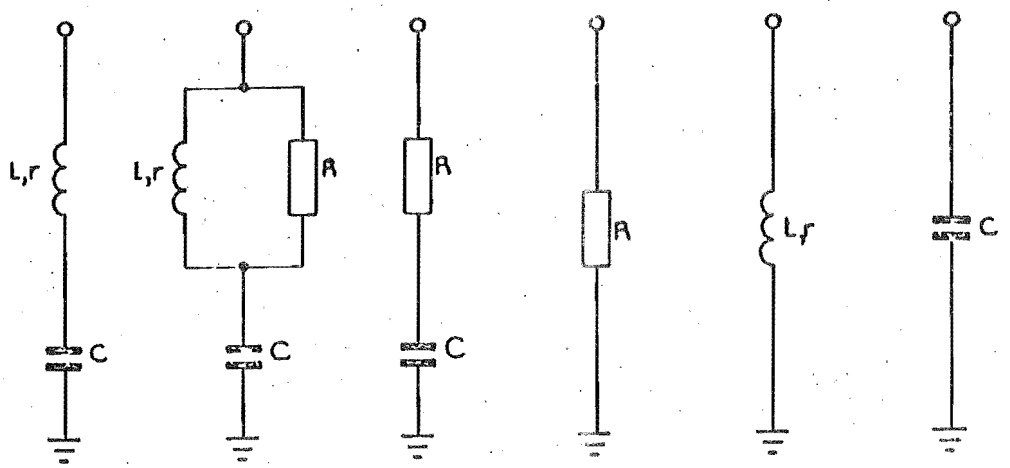

Fig. 2.2 Static Shunt Elements

2.2.7 AC System

Modelling of each component in an a.c. power system comprising many generators, transmission lines etc., is possible, but for a large system this becomes computationally uneconomic due to the size and complexity of the system.

Inevitably some assumptions must be made to obtain a less complex, yet sufficiently accurate, model for the system. System components of particular interest must be represented in detail; e.g. when a synchronous generator

dominates an a.c. system, the machine may be represented by its full transient equations as in Section 2.2.3. With static convertor plant, it is necessary to explicitly model a.c. harmonic filters (see Section 2.2.6) and the convertor transformers (see Section 2.2.5). The combined effects of other components may be treated by a form of network reduction. Various problems occur on reduction of (parts of) an a.c. system to an equivalent form. Not the least of these is establishing a model accurate for all harmonics of the power frequency. Use of a simple fundamental frequency model in general gives inaccurate and conservative results.

The a.c. system forms an oscillatory system with the a.c. harmonic filters which may have one or more natural resonant frequencies of a low order. Disturbances may excite these natural frequencies and subsequent waveform distortion, with possible overvoltages, may occur in the a.c. system. These in turn will interact with the convertors' controllers and affect their responses.

Correct a.c. system representation on a reduced basis would require knowledge of the impedance - frequency locus of the a.c. network. From this information an a.c. system representation such as proposed by Hingorani and Burberry (1970) and depicted in Fig. 2.3(a), may be used by the dynamic analysis programme. However, this information is subject to operational changes, such as line switching, which can alter the shape of the locus quite drastically. As a result, the availability of a locus for a particular system operating point is somewhat suspect. To avoid this problem some assumptions must be made which allow for the use of a less complex model.

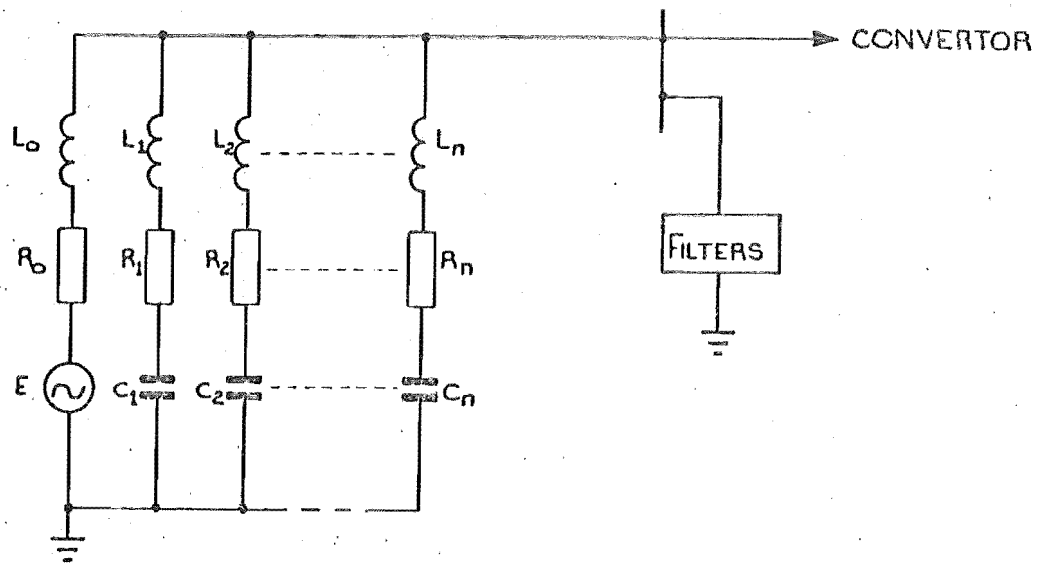

Fig. 2.3(a) nth order Network Equivalent - to represent the Harmonic Impedances of n Resonant Frequencies

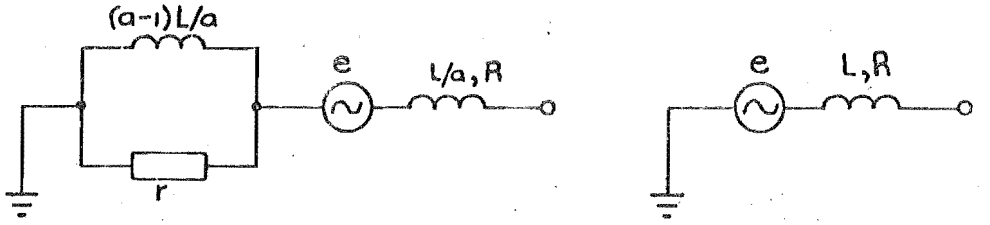

Fig. 2.3(b) (Modified) Thevenin Equivalents of Network

r chosen s.t. impedance angle gives correct damping.
R+jwL = source impedance.

Usually a locus would show a tendency for the system to be inductive for the important lower harmonics (up to 5th). The a.c. filters will be capacitive below the 5th harmonic and so a parallel resonant condition may exist around the 3rd or 4th harmonic, depending on the strength of the a.c. system. The stronger the system the higher the resonant frequency will be in general. An equivalent circuit which maintains a constant impedance angle over the lower frequency

range and provides realistic damping of harmonic voltages has been proposed by Bowles (1970). Giesner (1971) proposed an adapted version of this (Fig. 2.3(b)) in which the source impedance (which may be calculated from the short circuit level at the convertor transformer busbars) is split so that there are two, not necessarily equal, reactive elements with the resistive elements designed to give the required impedance angle. The representation of a simple e.m.f. behind a series (source) impedance is also provided for, although as explained, this will only be accurate at a single frequency. The impedance angle varies markedly from system to system. Its correct representation is important as its effect on damping of resonant conditions such as overvoltages is critical. Typical values of 75^{o} and 85^{o} for receiving and sending end a.c. systems respectively have been suggested (Bowles 1970). For frequencies at or above the high pass filter's resonance, the a.c. system impedance will be swamped. Thus the only assumption made is in the mid-range of frequencies where the likelihood of a resonant condition in realistic strength systems is small.

The use of an equivalent representation for an a.c. system therefore assumes there are no network resonances yet gives an adequate treatment to possible a.c. filter - system resonances. The possibility of associated over-voltages and waveform distortion and their effects on the convertors' controllers is then adequately catered for. Explicit busbar information would not be available at all busbars, but the extremely efficient simulation achieved in comparison with full a.c. system representation justifies the use of such a model in certain instances.

To determine an adequate equivalent network for the studies to be carried out, the areas of specific interest must first be identified. For a.c. fault studies in a.c./d.c. networks, the major area of interest may be at the convertor terminals and at the fault location. For d.c. fault studies the convertor terminals alone may be of particular importance in the absence of any major plant influence.

2.3 METHOD OF ANALYSIS

The behaviour of the electric network formed by the interconnection of the system component models is determined by two factors

- algebraic constraints, involving basic electric network laws such as Ohm's Law and Kirchhoff's Laws, which will relate the currents and voltages in individual branches, and branch, mesh and node quantities in accordance with
- topological constraints which are defined by the branch interconnections as per the branch list. For analytical convenience this list is translated into well known topological matrices.

Provided these constraints are obeyed, a solution is attainable irrespective of the analysis method used, i.e. nodal, branch, mesh, etc. The following factors will determine the most appropriate method for a particular study

- practicality and feasibility of solution, e.g. storage requirements and computational efficiency. A further

problem associated with numerical integration of differential equations is convergence of the solution process. As has been found in load flow work, the wrong form of algebraic manipulation i.e. network analysis method, choice of state variables, or numerical integration method, may lead to a divergent process, whereas a different combination will lead to a solution.

- convenience, e.g. ease of programming and the relation between input and output variables and programme variables.

Much of the early dynamic analysis work (Hingorani *et al.* 1966(2), 1967, 1968, Hay *et al.* 1969(2), 1971(2), O'Regan and Dillon 1970, and Milias Argitis *et al.* 1976, 1977(2), 1978) used a mesh analysis on the basis that for the particular system models used, fewer differential equations were required. These studies were of linear circuits which contained relatively few transmission lines, or used simple representations of them. However when the system contains many multiconductor transmission lines with mutual inductive effects and a high degree of capacitive branch interconnection, as is experienced in real power systems, a nodal approach becomes more efficient if sparsity of coefficient matrices is to be used in improving computational efficiency. This is so because mesh formulations of power systems tend to produce highly interconnected sets of meshes so that the corresponding coefficient matrices have low sparsity. The currents are expressed by branch relations which give the following flexibility to the analysis. The individual elements are

directly accessible which allows representation of non-linearities such as saturation to be directly accounted for. This is not possible using mesh analysis.

The majority of the early works did not include rotating machine models. El Serafi and Shehata (1976) and Campos Barros (1976) formulated dynamic analysis programmes based on direct phase representations for synchronous machines. Compared to a dqo axes representation, this presented the problem of time varying coefficients. However the many inherent advantages of the direct phase model (see Section 2.2.3) far outweigh this problem, which can be minimized computationally as follows. When a time varying representation is not used, the only time variance in the circuit is in the topological structure. In the mesh formulation this allows for direct modification of the inverse mesh inductance matrix without repeated explicit inversions. The time varying nature of a rotating machine model would affect the whole matrix so that direct modification of the inverse would no longer be practical. Conversely the branch matrix is sparse with a block diagonal structure leading to easy access for direct modifications of the inverse, since this will involve inversion of the relevant blocks only.

Therefore the use of a direct phase machine model and full transmission line representations in association with a node-branch formulation will allow easy accessing of individual elements, as well as minimizing the computational burden associated with inversion by retaining sparsity in block diagonal matrices. These advantages clearly outweigh

the fewer (by 10%-15%) number of differential equations associated with mesh analysis of a general a.c./d.c. power system.

The formulation derived here for the network equations therefore uses a branch frame of reference, solving for the currents in the individual inductive and resistive branches (Al-Khashali 1976).

The frequent valve switchings associated with HVDC convertors make it attractive to use a topological approach, with diakoptical tearing techniques applied to the sub-networks resulting from the interconnection of the various elements. This process enables segregation of subnetworks so that only the relevant portion of the network need be operated on to cater for any changes - either in elemental value (e.g. non-linearities) or in topology (e.g. valve switching or network faults).

The analysis assumes a general system configuration in which the system components may be interconnected in any way. To increase computing efficiency however, certain topological limitations are imposed e.g. filter representation, although this does not restrict the representation of system configurations.

2.4 NETWORK EQUATIONS

2.4.1 Definitions

Let the network contain n nodes interconnecting l inductive branches, r resistive branches, and c capacitive branches subject to the following restrictions:

(i) At least one end of each capacitive branch (or subnetwork) is the common reference point of the system.

(ii) At least one end of each resistive branch (or subnetwork) is the common reference point of the system or a node also having a capacitive connection.

(iii) There are no restrictions on inductive branches which may include inductive and resistive elements and be part of an inductive subnetwork, or connected to a node with resistive or capacitive connections.

These branch definitions in turn define a set of node types according to their branch connections.

α nodes : which have at least one capacitive connection

β nodes : which have at least one resistive, but no capacitive connections

γ nodes : which have only inductive connections.

Using the above definitions one can further define the topological matrices K_{ln}^t, K_{rn}^t, K_{cn}^t, which are the branch-node incidence matrices of the l, r, and c branches respectively, by their general elements viz.

K_{pi}^t = 1 if node i is the sending end of branch p

= -1 if node i is the receiving end of branch p

= 0 otherwise.

Partitioning according to node type, and applying the branch-node definitions above, yields

$$K_{ln}^t = [\, K_{l\alpha}^t \quad K_{l\beta}^t \quad K_{l\gamma}^t \,]$$

$$K_{rn}^t = [\, K_{r\alpha}^t \quad K_{r\beta}^t \quad 0 \,] \qquad \ldots (2.9)$$

$$K_{cn}^t = [\, K_{c\alpha}^t \quad 0 \quad 0 \,]$$

2.4.2 Assumptions

(i) For the purpose of this analysis, branch e.m.f. sources are defined as positive in the direction of positive current flow and generally are associated with inductive type branches.

(ii) Whereas in practice filters are connected between line and earth in a star configuration with the capacitors normally connected on the line side, in order to obey the topological constraints of Section 2.4.1 it is convenient to assume the opposite. For the purposes of this study this is not significant and does not affect the results.

(iii) No current sources exist.

(iv) Although linear capacitors are assumed, time variant inductances are allowed, i.e. $dL/dt \neq 0$, but $dC/dt = 0$.

2.4.3 Voltage and Current Relations

(i) In the absence of current sources, the following nodal equation applies

$$K_{nl} I_l + K_{nr} I_r + K_{nc} I_c = 0 \qquad \ldots (2.10)$$

where I are the branch current vectors. Applying diakoptics from equation (2.9), this can be rewritten as

$$K_{\gamma l} I_l = 0$$

or

$$K_{\gamma l} pI_l = 0 \qquad \ldots (2.11)$$

$$K_{\beta r} I_r + K_{\beta l} I_l = 0 \qquad \ldots (2.12)$$

$$K_{\alpha c} I_c + K_{\alpha r} I_r + K_{\alpha l} I_l = 0 \qquad \ldots (2.13)$$

(ii) The following branch equations written in diakoptical form can be written as matrix expressions for each branch type.

(a) inductive branches

$$E_l - p(L_l I_l) - R_l I_l + K_{l\alpha}{}^t V_\alpha + K_{l\beta}{}^t V_\beta + K_{l\gamma}{}^t V_\gamma = 0 \quad \ldots (2.14)$$

or $$pI_l = L_l^{-1} (E_l - pL_l \cdot I_l - R_l I_l + K_{l\alpha}{}^t V_\alpha + K_{l\beta}{}^t V_\beta + K_{l\gamma}{}^t V_\gamma) \quad \ldots (2.15)$$

(b) resistive branches

$$- R_r I_r + K_{r\alpha}{}^t V_\alpha + K_{r\beta}{}^t V_\beta = 0 \quad \ldots (2.16)$$

or $$I_r = R_r^{-1} (K_{r\alpha}{}^t V_\alpha + K_{r\beta}{}^t V_\beta) \quad \ldots (2.17)$$

(c) capacitive branches

$$C_c \, p(K_{c\alpha}{}^t V_\alpha) = I_c \quad \ldots (2.18)$$

Premultiplying by $K_{\alpha c}$ and substituting equation (2.13) yields

$$K_{\alpha c} C_c K_{c\alpha}{}^t \, pV_\alpha = - K_{\alpha l} I_l - K_{\alpha r} I_r \quad \ldots (2.19)$$

or $$pV_\alpha = C_\alpha^{-1} J_\alpha \quad \ldots (2.20)$$

where $$C_\alpha^{-1} = (K_{\alpha c} C_c K_{c\alpha}{}^t)^{-1} \quad \ldots (2.21)$$

and $$J_\alpha = - K_{\alpha l} I_l - K_{\alpha r} I_r = K_{\alpha c} I_c \quad \ldots (2.22)$$

The dependent variable vectors V_β and V_γ can be evaluated explicitly as below. Premultiplying equation (2.17) by $K_{\beta r}$ yields (and using 2.12 also)

$$V_\beta = - R_\beta \, (K_{\beta 1} I_1 + K_{\beta r} \, R_r^{-1} \, K_{r\alpha}^{\,t} \, V_\alpha) \qquad \ldots (2.23)$$

where $$R_\beta = (K_{\beta r} \, R_r^{-1} \, K_{r\beta}^{\,t})^{-1} \qquad \ldots (2.24)$$

Premultiplying equation (2.15) by $K_{\gamma 1}$ and substituting equation (2.11) yields

$$V_\gamma = - L_\gamma \, K_{\gamma 1} \, L_1^{-1} \, (E_1 - pL_1 \cdot I_1 - R_1 I_1 + K_{1\alpha}^{\,t} V_\alpha + K_{1\beta}^{\,t} \, V_\beta) \qquad \ldots (2.25)$$

where $$L_\gamma = (K_{\gamma 1} \, L_1^{-1} \, K_{1\gamma}^{\,t})^{-1} \qquad \ldots (2.26)$$

Equations (2.15) and (2.20) can now be integrated by numerical techniques to assess the system behaviour. The vectors V_β (equation (2.23)), V_γ (equation (2.25)) and I_r (equation (2.17)) may be eliminated entirely from the solution so that only I_1, V_α and the input vectors are explicit in the equations to be integrated. However, although this elimination (Al-Khashali 1976, Duke 1979) reduces the overall number of equations, it has the following computational disadvantages.

- some of the original matrix sparsity is sacrificed
- the modified incidence matrices now contain non-integer elements, thereby requiring actual multiplications rather than simple additions and subtractions when performing connection matrix-by-vector products
- in addition to modifying L_γ and $K_{\gamma 1}$ at every convertor

topological alteration, the auxiliary branch matrix L_1', created in the elimination process, will need reforming at these times.

Therefore it was decided to retain the equations in the above form and to evaluate the dependent variables V_β, V_γ and I_r at each step. This formulation has the advantage of providing useful output information directly.

2.4.4 Numerical Integration

Various integration methods are suited to the solution of linear first order ordinary differential equations, such as equations (2.15) and (2.20), starting from given initial conditions. However, the frequency of discontinuities occurring in the convertor bridges limits the choice to the self-starting single step methods. Multi-step methods would require frequent restarting at each discontinuity and, as a single step procedure is required for restarting, the frequent additional computation necessary would be prohibitive.

An implicit integration procedure, based on trapezoidal approximation, and a fourth-order Runge Kutta method have been used (Al-Khashali 1976) for the same type of dynamic analysis. These methods were originally developed for the solution of linear differential equations and therefore the step length used must be consistent with the assumption of constant coefficients within the integration interval. In order to cater for convertor generated harmonics, a sampling rate which gives six integration steps per cycle at the highest frequency of interest is necessary for accurate results. We have limited

our studies to effects below 1 kHz thus giving a maximum step length of approximately 2.5^{o} of fundamental (0.15 msec). With such small step lengths the integration methods have proved stable and sufficiently accurate, requiring only a few iterations to converge.

However a problem associated with the Runge Kutta method is its sensitivity to imperfect initial conditions (Campos Barros 1976). The impossibility of obtaining exact initial conditions for a dynamic analysis from the steady state analysis of a system including harmonic filters, convertor transformers, and rotor dampers ruled out the use of this method for such systems. This problem did not occur with the trapezoidal algorithm.

2.4.4.1 Implicit Trapezoidal Approximation. This integration procedure is defined by

$$\dot{X} = f(t,X) \qquad \ldots (2.27)$$

where $$X_{t+h} = X_t + \frac{h}{2}(\dot{X}_{t+h} + \dot{X}_t) \qquad \ldots (2.28)$$

or $$X_{t+h} - \frac{h}{2}\dot{X}_{t+h} = X_t + \frac{h}{2}\dot{X}_t \qquad \ldots (2.29)$$

which is a non-linear equation in X_{t+h}. It can be solved by direct or iterative methods depending on the characteristics of the problem. Duke (1976) used a direct method for a particular application of dynamic analysis, but here a very simple iterative procedure is used in which the calculations of the state variables (X) are segregated from the non-state variables as follows:

(i) as an initial estimate, assume $\dot{X}_{t+h} = \dot{X}_t$ so that

$$X^{o}_{t+h} = X_t + h\dot{X}_t \qquad \ldots (2.30)$$

(ii) iterate for better values, i.e.

$$\dot{X}^{j}_{t+h} = f\,(t+h,\ X^{j-1}_{t+h}) \qquad \ldots (2.31)$$

and

$$X^{j+1}_{t+h} = X_t + \frac{h}{2}\,(\dot{X}^{j}_{t+h} + \dot{X}_t) \qquad \ldots (2.32)$$

(iii) when all the state variables satisfy

$$\varepsilon \geq \text{ABS}\left(X^{j+1}_{t+h} - X^{j}_{t+h}\right) \qquad \ldots (2.33)$$

where ε is a given convergence tolerance, stop iterating, and thence

$$X_{t+h} = X^{j+1}_{t+h} \qquad \ldots (2.34)$$

and

$$\dot{X}_{t+h} = f\,(t+h,\ X_{t+h}) \text{ as required} \qquad \ldots (2.35)$$

Convergence is usually attained within 3 or 4 iterations with a suitable step length. The non-state variables are then calculated using the values in equations (2.34) and (2.35).

2.4.5 Choice of State Variables

2.4.5.1 For Integration Procedure. If the variables I_1 and V_α are used as integrands in the above process, the order of magnitude of the derivatives, which are dependent on the matrices L_1^{-1} and C_α^{-1}, may be such that a reduction in step length is necessary to achieve convergence within a few iterations. However by defining flux linkage ψ_1 and capacitor charge Q_α as

$$\psi_1 = L_1\, I_1 \qquad \ldots (2.36)$$

and

$$Q_\alpha = C_\alpha\, V_\alpha \qquad \ldots (2.37)$$

and using ψ_1 and Q_α as the state variables, the magnitudes of the derivatives are of the same order as the voltages and currents in the network. In addition it has been found that this allows the use of a variable integration step length without increasing computation burden.

2.4.5.2 Per Unit System. Normal steady state power system analyses use a per unit (p.u.) representation of voltages, currents and impedances in which these quantities are scaled to the same relative order, thereby treating each quantity to the same degree of accuracy. In dynamic analyses, instantaneous phase quantities are used in both a.c. and d.c networks and at the same time derivatives of relatively fast changing variables are evaluated.

The usual cosinusoidal relation between a state variable and its derivative indicates that the relative difference in magnitude is ω, which may be high, so that the degree of accuracy will not be the same for each. If the state variables are changed by a factor ω_o (the fundamental a.c. system angular frequency), and reactances and susceptances are used, instead of inductances and capacitances, the integration process may be carried out as a function of the angular displacement of a reference vector rotating at velocity ω_o, with the result that all variables and coefficient matrices, and hence state variable derivatives, are of the same relative orders of magnitude.

Therefore by defining a base angular frequency ω_o, the values to be used for the coefficient matrices are impedances and admittances based on this frequency, for all parts of the network, including the d.c. link. The voltages

and currents may then be scaled to instantaneous phase quantities. Any convenient power-invariant set of bases may be chosen for the network parameters. The integration step will then be an angle rather than a time increment. The resulting equations are as described in Appendix A3.

2.5 MODIFICATION OF REPRESENTATION FOR VARIABLE TOPOLOGY

2.5.1 Mathematical Formulation

Convertor representation involves the interconnection of a series of inductive elements, viz. the smoothing reactor and the convertor transformer windings. The interconnections will vary with changes in valve states and this topology modification is manifested by changes in $K_{\gamma l}$ and L_{γ}. A general power system will have many inductive elements and therefore to avoid involving the whole inductive subnetwork in a topological change due to a convertor valve switching, it may be appropriate to partition the inductive subnetwork. This may be done by segregating convertor (k) branches and (δ) nodes from external system elements (l branches and γ nodes). This segregation will require both $K_{\delta l}$ and $K_{\gamma k}$ to be null matrices (Appendix A4). If k branch flux linkages are specified by

$$\psi_k = L_k I_k \qquad \ldots (2.38)$$

then by analysis as in Section 2.4.3, the equation set (A3.1) - (A3.7) is transformed (Appendix A4) to the set below, where the inductance and capacitance symbols refer to reactance and susceptance matrices as before.

$$\psi_1 = L_1 I_1 \quad \ldots (2.39)$$

$$\psi_k = L_k I_k \quad \ldots (2.40)$$

$$Q_\alpha = C_\alpha V_\alpha \quad \ldots (2.41)$$

$$V_\beta = - R_\beta \left(K_{\beta 1} I_1 + K_{\beta k} I_k + K_{\beta r} R_r^{-1} K_{r\alpha}^t V_\alpha\right) \quad \ldots (2.42)$$

$$V_\gamma = - L_\gamma K_{\gamma 1} L_1^{-1} \left(E_1 - R_1 I_1 - pL_1 I_1 + K_{1\alpha}^t V_\alpha + K_{1\beta}^t V_\beta\right) \quad \ldots (2.43)$$

$$V_\delta = - L_\delta K_{\delta k} L_k^{-1} \left(- R_k I_k + K_{k\alpha}^t V_\alpha + K_{k\beta}^t V_\beta\right) \quad \ldots (2.44)$$

$$I_r = R_r^{-1} \left(K_{r\alpha}^t V_\alpha + K_{r\beta}^t V_\beta\right) \quad \ldots (2.45)$$

$$p\psi_1 = E_1 - R_1 I_1 + K_{1\alpha}^t V_\alpha + K_{1\beta}^t V_\beta + K_{1\gamma}^t V_\gamma \quad \ldots (2.46)$$

$$p\psi_k = - R_k I_k + K_{k\alpha}^t V_\alpha + K_{k\beta}^t V_\beta + K_{k\delta}^t V_\delta \quad \ldots (2.47)$$

$$pQ_\alpha = - K_{\alpha 1} I_1 - K_{\alpha k} I_k - K_{\alpha r} I_r \quad \ldots (2.48)$$

2.5.2 Convertor Nodal Matrix

Referring to the modes of operation as stated in Section 2.2.1.1, an additional restriction must be imposed to satisfy the inductive branch definitions. The case of a completely isolated transformer secondary can not be permitted, i.e. at least one valve in the convertor bridge must be ON when the convertor is in a non-conducting state in order to fix a terminal voltage. This will not affect the remainder of the system since the current path remains open.

The assumption of the incidence matrix $K_{\gamma k}$ being null i.e. the primary windings of the convertor transformer must be connected to either α or β nodes, means that for the

purpose of setting up or modifying L_δ, the transformers may be considered short-circuited at the primary terminals. The transformer phases may then be represented by their leakage reactances referred to the secondaries and connected to the corresponding secondary winding ends.

Considerable improvement in computational efficiency can be obtained if the convertor transformer leakage reactance as viewed from the secondary terminals may be assumed identical for the three phases. This will enable the use of the same nodal solution matrix for any combination of conducting valves within the same mode of operation.

Representation of the modes of operation is made by defining a set of three nodes for each convertor (δ_t, δ_m and δ_b) nominally referring to the top, middle and bottom of the bridge. During normal operation δ_t and δ_b correspond to d_1 and d_2 respectively in Fig. 2.4(a) and the conducting valves will determine the connection of the terminals (a,b,c) to the relevant nodes δ_t, δ_m and δ_b. The designation of these connections is detailed in Appendix A5.

A nodal matrix may then be defined which relates to the non-commutating mode (A). The equivalent (equal) leakage reactance is derived from the convertor transformer matrix L_t by

$$x_{1a} = L_{22} - L_{12} L_{21} / L_{11} \qquad \ldots (2.49)$$

The only other connection to the bridge's node cluster will be either another bridge, earth, or a smoothing reactor. The first two cases can be dealt with by correct node specifications as in Appendix A5.

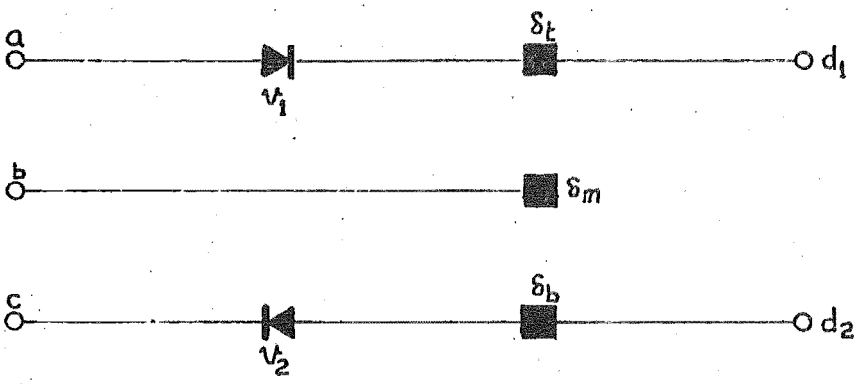

Fig. 2.4(a) Convertor Bridge δ Nodes

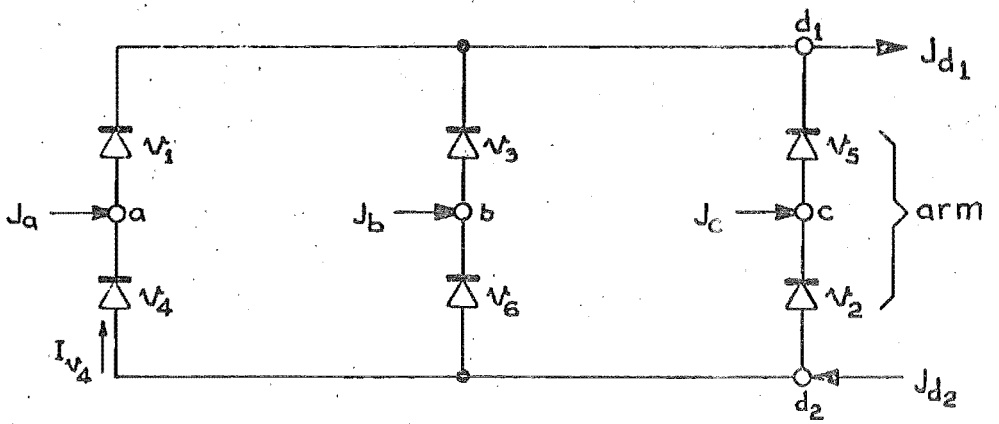

Fig. 2.4(b) Injected Currents

The non-commutating matrix without smoothing reactance included can then be written by inspection (see Appendix A6). The smoothing reactor may be included by connection of the appropriate reactance to the relevant convertor mode. The matrix L_δ is block diagonal with the blocks corresponding to node clusters which are separated in the network by non - δ nodes. This block diagonal form means that a particular convertor switching operation will affect only that part of L_δ corresponding to the relevant convertor's node cluster (as specified in Appendix A5).

The nodal matrix (L_δ) for a particular mode of convertor operation may then be formed. A formula has been derived (Al-Khashali 1976) to perform this nodal modification which will avoid repeated reformation and inversion of L_δ, or parts of its block diagonal structure. This formulation is detailed in Appendix A7 and involves a procedure which adds, removes or changes the connections of a single element in L_δ.

The incidence matrix $K_{\delta k}$ will need to be reformed for each combination of conducting valves however, and this process is outlined in Appendix A8. It will be confined to the bridge nodes (δ), and the permanent external connections of the convertor network will be indicated by zero entries in $K_{\delta k}$ (see Fig. A8.1).

2.5.3 Valve Voltages and Currents

Referring to Fig. 2.4(b), the forward voltage across the top bridge valve of arm p is $(V_p - V_{d1})$ and for the bottom valve it is $(V_{d2} - V_p)$, where V_p corresponds to node a, b or c. Since terminals p, d1, and d2 correspond directly to the δ-nodes defined in Section 2.5.2, the voltages of

which can be evaluated using equation (2.44), the calculation of valve voltages becomes a matter of routine. The relations stated will apply regardless of whether the valve is conducting or not, for, when the valve is conducting, its ends will be set to the same δ-node, and its voltage will then be correctly calculated as zero.

The current relations, on the other hand, are entirely determined by two factors; the currents in the convertor branches, i.e. the smoothing reactor and the transformer windings, and by the prevailing combination of conducting valves.

Considering the set of injected currents shown in Fig. 2.4(b), conducting valves provide the paths for these currents to flow in the system, and the instantaneous values of valve currents can be obtained from these injected currents. The injected currents themselves are obtained directly from the branch currents. I_{d1} and I_{d2} are equal and numerically equivalent to the direct current. The phase injected currents are obtained from the currents in the transformer secondary windings, e.g. for a star-connected secondary, I_a is the negative of the current in the secondary winding connected to node a, and for a delta-connected secondary, the injected currents are given by the difference between the currents in the windings connected to the node.

The relationship between the valve currents in the top and bottom sides of the bridge (I_{vt} and I_{vb}) on arm p, with the injected current at p, J_p, is

$$J_p = I_{vt} - I_{vb} \qquad \ldots (2.50)$$

When the bottom valve vb is OFF:

$$I_{vt} = J_p \qquad \ldots (2.51)$$

and when the top valve vt is OFF:

$$I_{vb} = -J_p \qquad \ldots (2.52)$$

In these two cases an implied supplementary relation, setting the non-conducting valve current to zero, enables the solutions given by equations (2.51) and (2.52) to be obtained. However, when both valves conduct, the supplementary relation must be found elsewhere. The method used considers the three valves on the top half of the bridge, whose currents add up to J_{d1}, i.e.:

$$J_{d1} = \Sigma I_{top} \qquad \ldots (2.53)$$

In this relation, provided p is the only arm with both valves conducting, I_{vt} is implicitly defined.

Equation (2.53) may be re-written, substituting from equation (2.51) for the top conducting valves on phases other than p, to give

$$I_{vt} = J_{d1} - \sum_{q \neq p} J_q \qquad \ldots (2.54)$$

where q are the phases having their top valves conducting.

The current in the bottom valve of phase p may now be calculated using equation (2.50), or by a relation similar to equation (2.54) giving

$$I_{vb} = J_{d2} + \sum_{r \neq p} J_r \qquad \ldots (2.55)$$

where r are the arms having their bottom valves conducting.

It can be seen that no solution is possible when two bridge arms have both valves conducting since there is an

insufficient number of independent equations. A further relation would be provided by considering the current which may circulate in the closed loop formed by the two arms but this entails assumptions which may not be justifiable. In practice the case is likely to arise only in the special circumstance when two valves are fired simultaneously at a time when another pair of valves, which would close the loop, are conducting. Otherwise, there is insufficient voltage across a fourth incoming valve, if the three other valves are already conducting and a firing pulse is applied to the fourth, for it to conduct. For this reason the operating nodes D2, E2 and E3, described in Section 2.2.1.1, have been left out.

CHAPTER 3

COMPUTER IMPLEMENTATION

3.1 INTRODUCTION

The computer programme used to implement the mathematical model described in Chapter 2, is based on the work of Al-Khashali (1976). Various modifications and additional refinements have been carried out with respect to the original functions, to permit the studies carried out in the present investigation. With reference to the general flow diagram illustrated in Fig. 3.1, the various processes have been segregated according to type. Using this modular approach facilitates programme validation and provides flexibility for extensions or modifications, e.g. changes to the convertor control system, change of integration process, change of fault simulation procedure. The programme is written in FORTRAN IV and the main subroutines within each of the different processes are discussed below.

3.2 INPUT AND ESTABLISHING NETWORK EQUATIONS

To avoid the extensive branch list preparation associated with the representation of even simple power systems, an approach in which the programme expands a sample data set for each component into the full network model was adopted. Each data set includes a representative sample of the circuit constants and the single line currents.

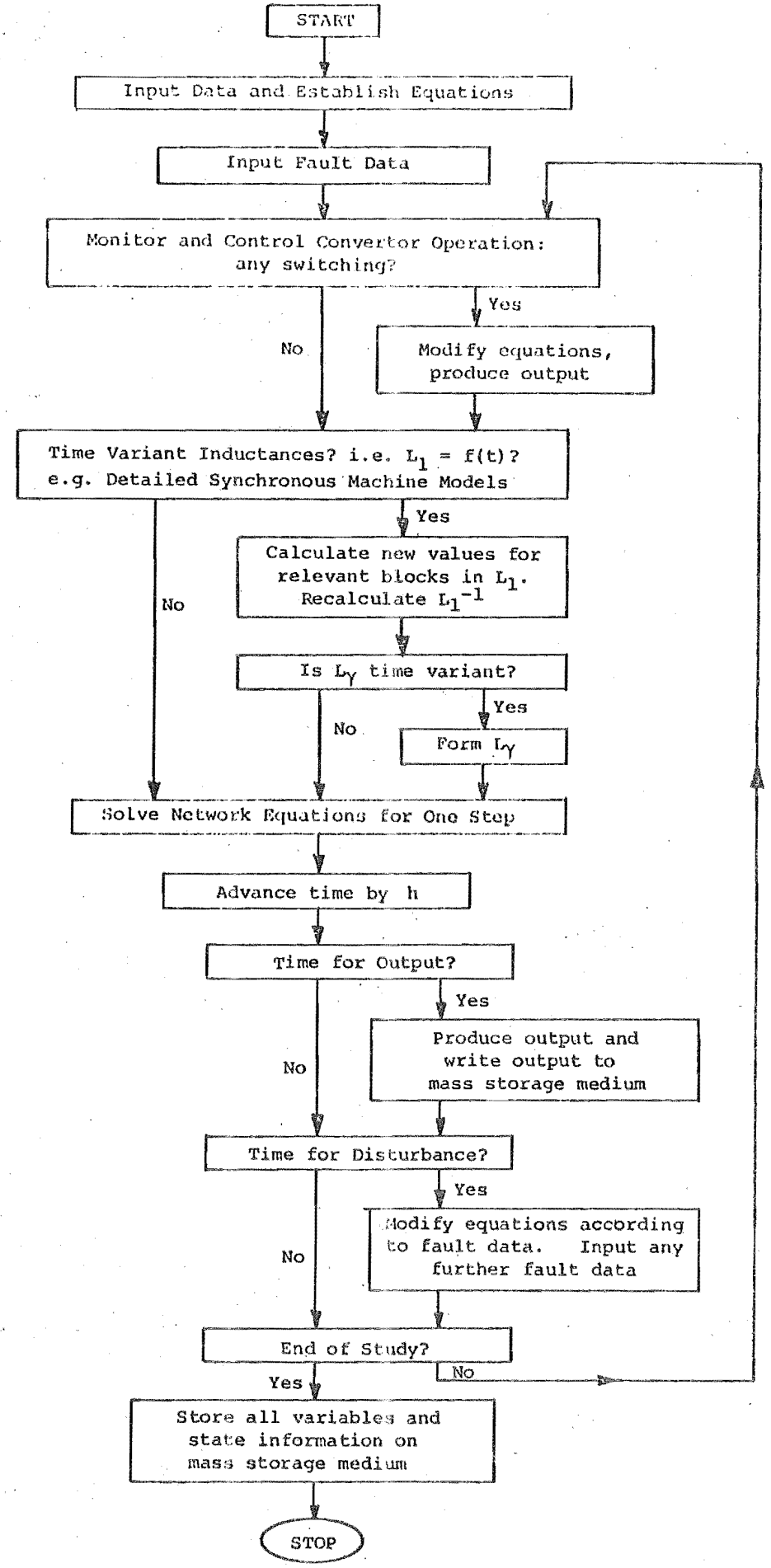

Fig. 3.1 Flow Diagram of Digital Computer Programme Control

In conjunction with a data set containing the systems busbar voltages, the component data may then be expanded into the individual branches and nodes associated with its model, and the instantaneous currents and voltages assigned to them. The network nodes created by data expansion are assigned a node type according to their connected branches, and a set of cross-referencing information is stored relating system busbars to network nodes, first as a group and then partitioned according to the different nodal types.

3.2.1 Initial Conditions

The approximate initial conditions used for currents and voltages in the above input data may be obtained by a steady state load flow analysis of the relevant system. Such an analysis is based on fundamental frequency r.m.s. a.c. quantities and average d.c. quantities. Therefore all variables and component constants must be converted into phase quantities to satisfy the dynamic analysis base system. The single line currents must be calculated from power flows and any source e.m.f.s must be determined. In the case of static convertors or synchronous machines auxiliary calculations must be made to determine initial operating conditions. AC harmonic filters may be assumed to be fully charged to their corresponding phase voltage.

3.2.1.1 Convertor Data. Convertor data comprises three main quantities

- programme control data which identifies the convertor type and its a.c. and d.c. terminals. Convertor bridges, which may be either 6 pulse or part of a 12 pulse group, are referred to as star or delta

depending on the convertor transformer's secondary connections. The latter is designed to provide 30^{o} phase lead in secondary voltage. In addition they may be bottom or top earthed depending on current flow relative to the common reference point, and this is used to distinguish whether the bridge is nominally a rectifier or invertor respectively.

- control system data identifying a.c. system fundamental frequency, initial values of direct current, delay and/or extinction angles, and the control system settings and constants
- circuit constants for the smoothing reactor and convertor transformer(s).

A first approximation to the operational state of the convertor bridges is made by the following process.

Conducting valves in each bridge are determined from knowledge of phase 'a' voltage phase angle θ_a, measured with respect to the steady-state load-flow reference, and taking into consideration the inherent phase shift in the bridge transformer θ_t (0^{o} or $+30^{o}$) and the delay angle α.

Representing the a.c. voltage as a cosine function, the voltage crossover for valve v1 in the bridge, at time $t = 0$, will have occurred "A" degrees earlier. Referring to Fig. 3.2(a), A is given by:

$$A = 60 + \theta_a + \theta_t$$

Valve v1 will, therefore, have started conducting B degrees previous to $t = 0$, where

$$B = A - \alpha$$

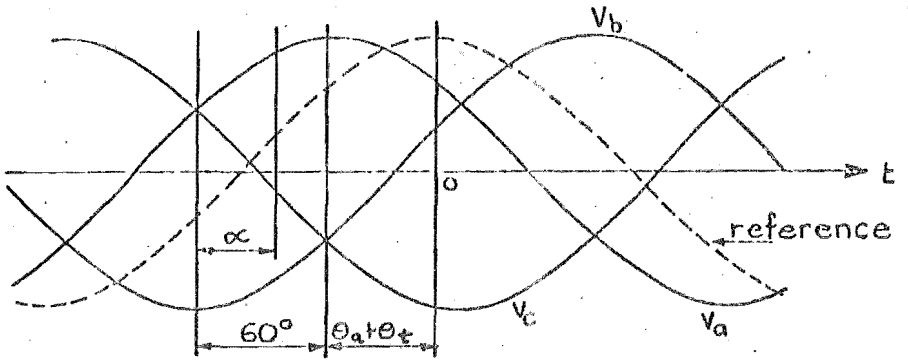

(a) Determination of Conducting Valves

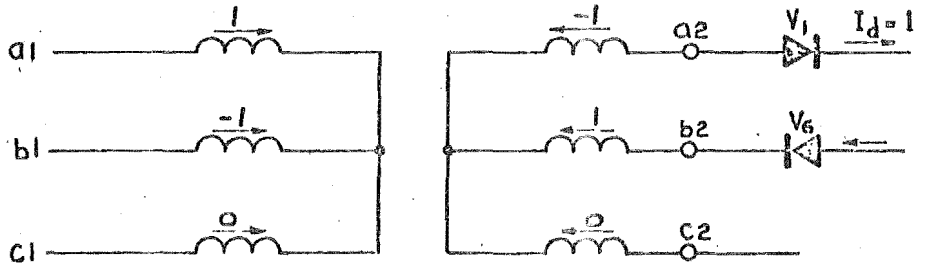

(b) Currents in Star Bridge

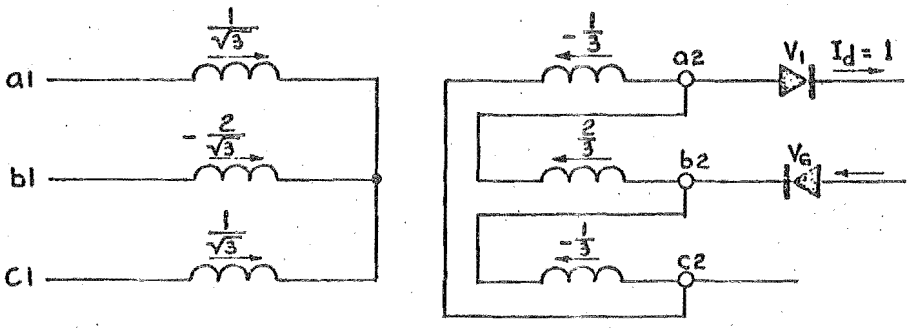

(c) Currents in Delta Bridge

Conducting valves	Winding currents ($I_d = 3$)		
	a	b	c
6 1	-1	2	-1
1 2	-2	1	1
2 3	-1	-1	2
3 4	1	-2	1
4 5	2	-1	-1
5 6	1	1	-2

(d) Delta Winding Currents

Fig. 3.2 Initial Conditions in Convertor Bridges

In this condition valves v1 and v6 are conducting at $t = 0$, and valve v2 is due to be fired at time F_{v2}, which is 60^{o} later than the firing of v1, hence,

$$F_{v2} = 60 - B$$

However, if B is less than zero then v1 is yet to be fired. Conversely, if B is greater than 60^{o} then v1 will have been conducting for more than one firing period indicating that v2 is already conducting. In either case the sequence is changed until the correct pair of conducting valves have been defined. This approach ignores the commutation angle.

A refinement is to adjust the load flow reference angle so that commutation periods are avoided at the convertor. This can be effected by choosing the firing time of the next valve, $k + 1$, to be

$$F_{v_{k+1}} = C$$

where in the above analysis $k = 1$. Then if the steady state commutation (overlap) angle is γ

$$C = 60 - \theta_t - \gamma .$$

This will ensure a maximum time interval exists before any alteration in the convertor topology is effected by a valve commutation. Therefore

$$B = k.60 - C$$

and $$A = k.60 + \alpha - C$$

and the required value for θ_a will be

$$\theta_a^{sp} = (k-1)\cdot 60^o + \theta_t + \alpha - C$$

which can be achieved by altering the original load flow reference angle by $(\theta_a^{sp} - \theta_a)$.

Having established the pair of conducting valves in the bridge, the currents in the transformer windings must be established on both sides. For a star bridge, shown in Fig. 3.2(b), the secondary winding currents of each phase are set equal to the given direct current if its bottom valve is conducting, and to the negative of that if the top valve is conducting; otherwise it is set to zero. Primary (a.c. side) winding currents are set equal to the corresponding secondary currents with the signs reversed.

Current is forced to flow in a secondary winding of a delta bridge even though both valves corresponding to its phase are not conducting. In the case shown in Fig. 3.2(c), the secondary winding of phase 'c' carries a third of the direct current with valves v2 and v5 both not conducting. In general, one winding carries two-thirds of the direct current in one direction while the other two carry one-third each, flowing in the opposite direction. The table shown in Fig. 3.2(d) gives the current distribution in the delta winding for all combinations of normally conducting valve pairs. The primary winding currents are set to $(-\sqrt{3})^{-1}$ times the corresponding secondary currents.

3.2.1.2 Synchronous Machines. Using the terminal conditions provided by the load flow, and assuming balanced conditions, the generators internal e.m.f. is obtained by

$$E_i = V_g / \sqrt{3} + Z_s I_{ga}$$

where Z_s is the synchronous reactance (X_d) and I_{ga} is the generator phase 'a' current as calculated from the power flows.

When filters are present their contribution to fundamental power flow (reactive compensation) must be accounted for, and this is done by

$$I_f \simeq V_g / (\sqrt{3}\, Z_f)$$

where $Z_f \simeq -j / (\omega \sum_i C_i)$ for all the filter branches i.

Field current may be estimated by

$$I_{fd} = \sqrt{2}\, V_g / (\omega\, L_{afd})$$

so that $E_{fd} = R_{fd} \cdot I_{fd}$

The short-circuited damper windings are assumed to have zero current. The rotor angle δ_o may be calculated from the phasor representation in Fig. 3.3, and the relative position angle θ_o is then calculated as

$$\theta_o = 270^o + \delta_o + \phi_{(\text{phase lag})} \pm \beta$$

where β accounts for any transformer phase shift and ϕ is the (lagging) phase angle of the terminal voltage (phase a).

3.2.2 Dynamic Initial Conditions

A steady state analysis such as a load flow, which is based on the assumption of balanced sinusoidal a.c. waveforms, can not provide exact initial conditions for the dynamic analysis of a system which includes convertor and/or detailed synchronous machine models. In the case of a machine, single frequency analyses can not indicate rotor

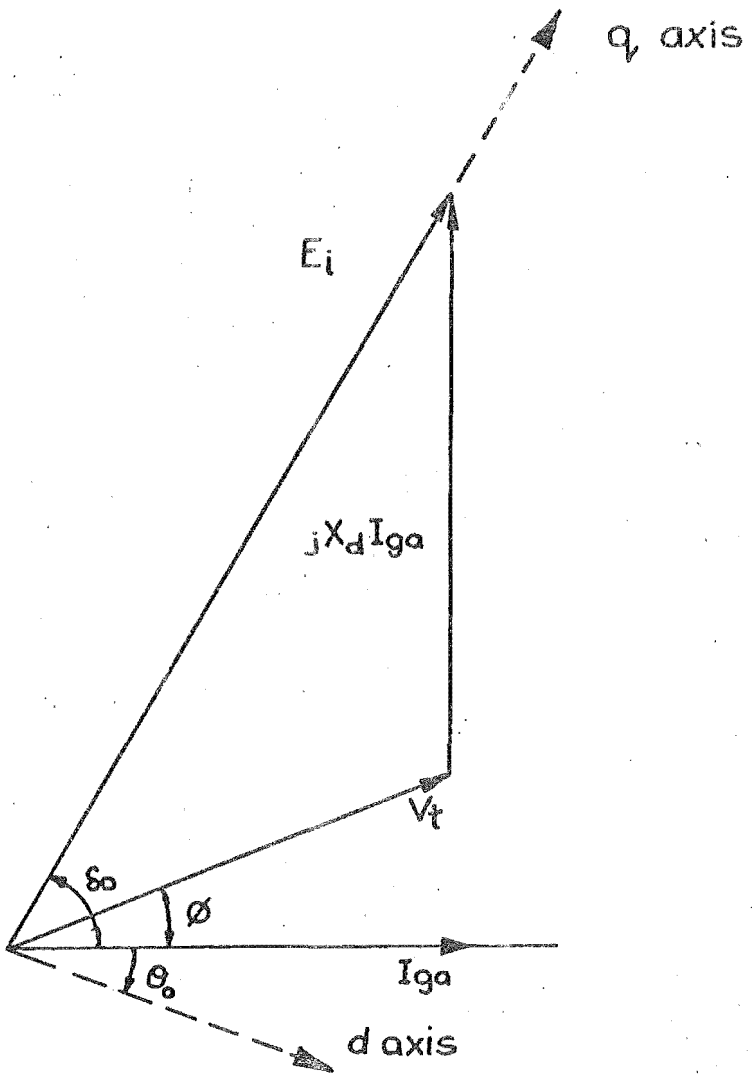

Fig. 3.3 Phasor Diagram of Rotating Machine

currents or position exactly, and in the case of convertors, exact representation of the commutation sequences and filter currents is not possible. As a result initial values for system variables may be in error. It is therefore necessary to perform a preliminary dynamic simulation, using the approximate load flow values as starting points, in order to obtain the desired steady state operating point dynamically. These 'dynamic initial conditions' may be stored and used for several studies on the same system, thus avoiding repetition of data preparation and expansion, and the computation required to achieve 'dynamic initial conditions'.

Both Al-Khashali (1976) and Campos Barros (1976) reported the sensitivity of dynamic analyses of a.c./d.c. systems to initial conditions. The majority of the problems encountered by the former were due to inaccurate specifications of either voltages or currents, or of bridge conduction patterns, especially relating to commutation periods. If these specifications resulted in major changes to the timing of valve firing pulses, e.g. as a result of extinction angle control, the 'dynamic initial conditions' took much longer to attain. Initial values calculated using the formulation in Section 3.2.1.1 have substantially improved this performance so that satisfactory 'dynamic initial conditions' can be attained within 2-3 cycles. Campos Barros's studies of generator-convertor schemes were especially susceptible to problems when a.c. harmonic filters were not present, because the network damping was then low. By temporarily increasing the rotor circuit resistances during the initial condition simulation to reduce the

machine's time constant, faster settling of the system to the desired steady state operating point was achieved.

The overall quality of initial conditions is determined by the use of a fast fourier transform algorithm which analyzes the simulation results, inspecting in particular power flows and voltage profiles, and checking the levels of harmonics.

3.2.3 Network Equations

The procedure above will generate:

(i) the network matrices L_1, L_k, R_1, R_k, C_α and R_r in a compact form as described in Section 3.7

(ii) branch lists for each branch type in terms of the network nodes, together with designations of type and cross referencing information

(iii) initial values for all nodal voltages and branch currents

(iv) the basic non-commutating nodal solution matrix, and initial valve states for all convertor bridges.

The network equations are then established by defining all the incidence matrices including $K_{\delta k}$ and calculating the nodal coefficient matrices L_γ, L_δ and R_β. The latter requires inversion of the matrices L_1, L_k and R_r. An auxiliary connection matrix is also formed for the purpose of calculating valve currents. Initial values for the state variables ψ_1, ψ_k and Q_α are also formed, and using the equation set (2.39) - (2.48), all dependent variables and derivatives of state variables are calculated to form the initial network solution and output.

The dynamic analysis solution may then commence, in most cases initially to obtain the desired operating point dynamically, before beginning investigation of disturbances.

Fig. 3.4 shows a general flow diagram for the process detailed in this section.

3.3 MONITORING AND CONTROL OF CONVERTORS

At each step in the integration process, the convertor valves are tested for current extinction, voltage cross-over and conditions for firing, based on the individual valve currents and voltages. If indicated, changes in valve states are made and/or the control system is activated to adjust the phase of firing. When a valve switching takes place, the network equations are altered by suitable modification of $K_{\delta k}$ and L_{δ} as detailed in Appendices A7-A8. Fig. 3.5 is a generalised flow diagram depicting the above actions which are detailed below.

Since it is not possible to integrate through discontinuities, the integration time must coincide with their occurrence. These discontinuities must be detected accurately since they cause abrupt changes in bridge node voltages, and any errors in the instant of the topological changes will cause inexact solutions.

3.3.1 Valve Firings

When a convertor valve satisfies the conditions in Section 2.2.2.2, it will be switched to the conduction state and the next valve to fire will be set by a ring counter, with its phase of firing set so that in the absence of control action it will be pulsed 60^{o} later. If the valve

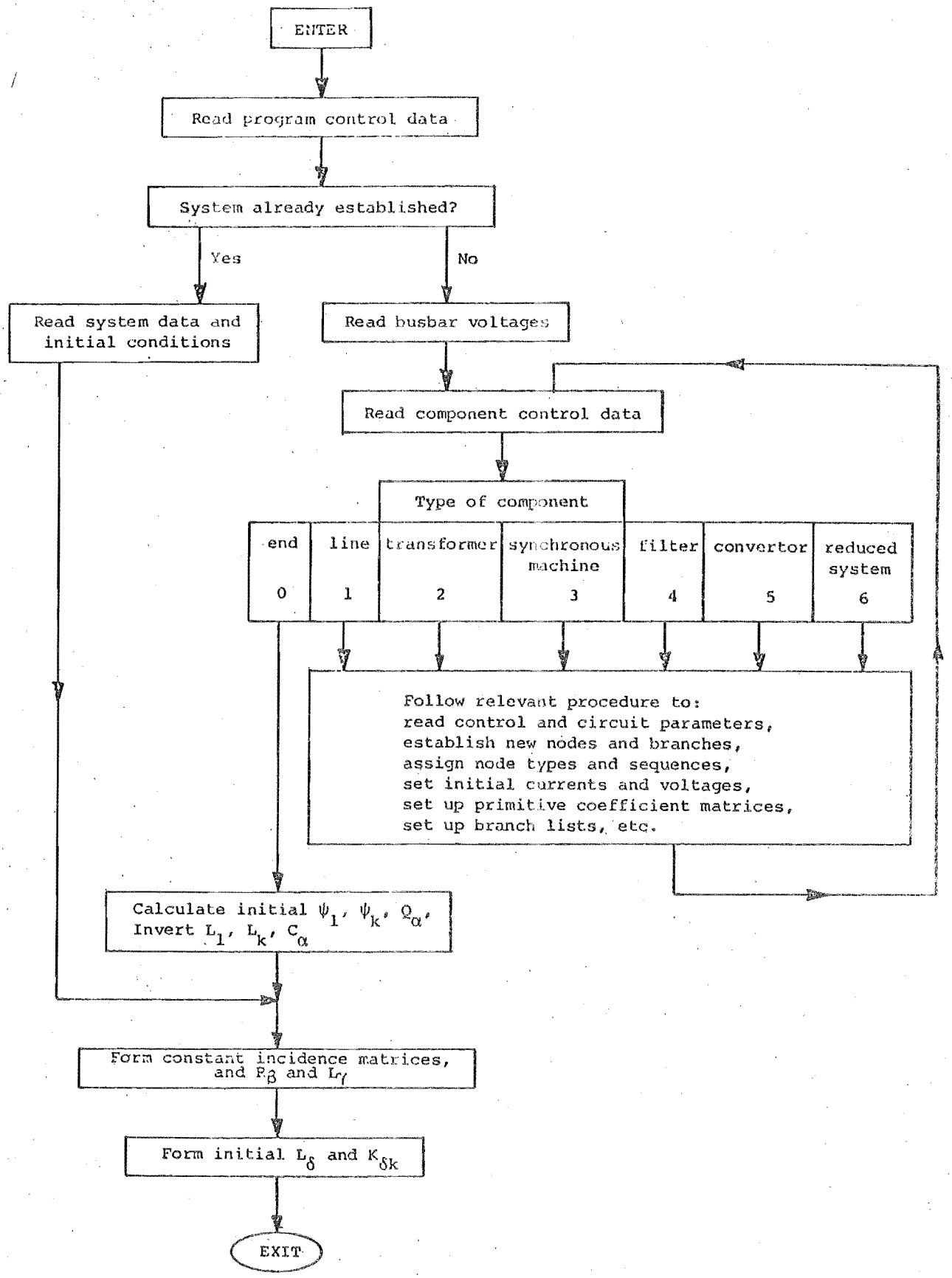

Fig. 3.4 Flow Diagram of Data Input and Initial Value Establishment

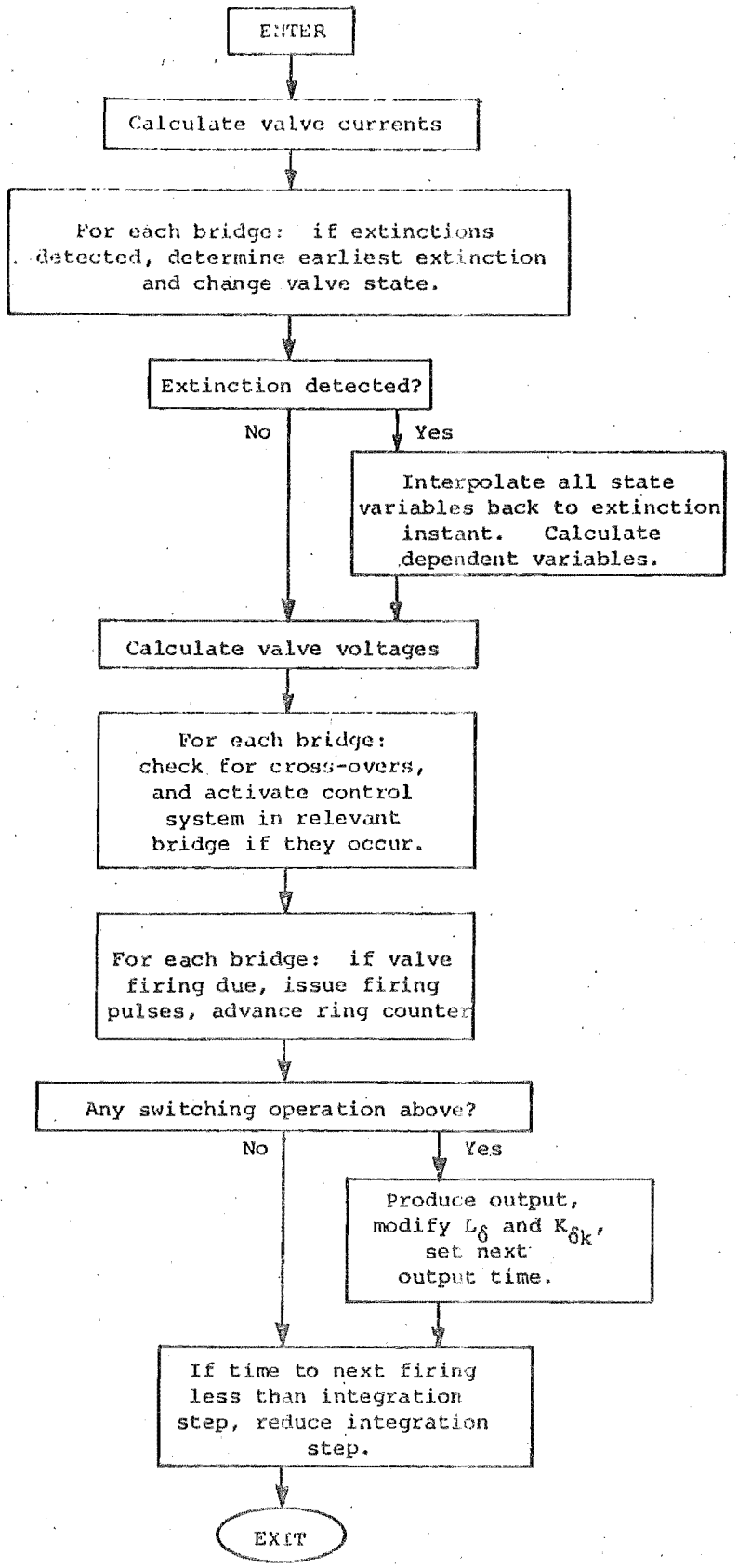

Fig. 3.5 Flow Diagram of Monitoring and Control of HVDC Convertors

forward voltage criterion is not satisfied the pulse is retained for a set period without upsetting the firing instant of the following valve.

Valve firings are therefore predictable, so that if it is detected that a valve is due to fire in the following integration step, the step length may be adjusted so that firing coincides with the end of the step. A tolerance of a fraction of a degree is acceptable in defining firing time, since this corresponds to phase jitter in real systems (Ainsworth 1968).

3.3.2 Valve Extinctions

Valve extinctions can only be predicted at the expense of slowing down the computation process markedly. Sufficient accuracy is achieved by detecting extinctions after they have occurred, as indicated by negative valve currents, and then using linear interpolation to assess the actual turn off instant. Only one valve may be extinguished per bridge at any one time, and the earliest extinction over all the bridges is always chosen for the interpolation process. By defining the current (I) in the outgoing valve at the time of detection (t), when the step length of the previous integration step was h, the instant of extinction (t_x) will be given by

$$t_x = t - h \cdot z$$

where $$z = I_t / (I_t - I_{t-h})$$

All the variables (V) in the equation set (2.39) - (2.48) are then interpolated back to t_x by

$$V_x = V_t - z\ (V_t - V_{t-h})$$

The next integration step will then begin at t_x with step length h. This linear approximation is sufficiently accurate over periods which are generally less than one degree, and is computationally inexpensive.

Caution must be exercised when extinguishing a valve since this may produce a non-conducting condition in the convertor, i.e. the current path is interrupted due to there being no conducting valves in one half of a bridge. Action is taken in such a case to ensure that the valves nearest to the smoothing reactor are OFF so that the convertor side of the smoothing reactor is open circuited, and that the minimum number of valves remain in the conducting state to provide a path within the convertor to the common reference point, thus avoiding the need for defining new network nodes.

3.3.3 Control Action

The convertor control system calculates firing corrections in a bridge, as described in Section 2.2.2.2, when one of its valves experiences a positive going voltage zero crossing for the first time after it was last extinguished. The instant of cross-over is pin-pointed by linear interpolation in the same way as extinction instants were determined, although in this case no discontinuities are created and therefore there is no need to alter the integration process. Actual extinction angles are calculated at this time, and if this angle is less than the safety margin for deionization, the valve is turned ON again to indicate commutation failure. The period used for accumulating current control information is the time between successive voltage crossings, which normally is 60^{o}.

3.3.4 12 Pulse Operation

With direct digital control, it is possible for two bridges in twelve pulse operation to have their controllers drift so that a permanent difference (other than 30^{o}) in their phases of firing occurs. This is particularly so in the constant current control mode, since the absolute value of α_r is not used (whereas the absolute value of δ_i is used for EAC). This imbalanced firing condition may still provide the correct steady state terminal conditions, but will produce uncharacteristic harmonics in both the a.c. and d.c. systems. Therefore this event is prevented by monitoring the relative phases of firing and, in addition to the normal control operation, providing control action to maintain the correct phase shift (30^{o}) between the two bridges' valve firing pulses.

3.4 SOLUTION OF NETWORK EQUATIONS

The differential equations (2.46) - (2.48) are solved for the first integration step, using the initial values provided, and the numerical integration process desired. In Section 2.4.4, it was seen that the implicit trapezoidal method required the evaluation of the changes in state variables, and also the dependent variables, during the iterative process. The number of iterations (i.e. the rate of convergence of the equations) is dependent on the integration step length and the specified tolerance. This iterative process involves the majority of numerical evaluations in the programme, and therefore determines the speed, and accuracy, of the dynamic solution. Therefore,

as detailed in Chapter 2, it must be computationally efficient, which will mean utilising the nature of the problems to be analyzed, such as retaining sparsity in the coefficient matrices.

To ensure fast convergence, the integration step length is automatically adjusted at each integration step by the following method. If the number of iterations taken to achieve convergence at the current time step was i, and h was the step length, then if

$$i > 5, \quad h \text{ is reduced to } 0.95 \cdot h$$

$$\text{and if} \quad i \leq 2, \quad h \text{ is increased to } 1.1 \cdot h$$

If convergence is not attained within 10 iterations, the step length is halved and the integration process is restarted at the previous time step. This latter action, which takes precedence, is a safety measure taken when instability of the process is indicated, e.g. when the step length is much greater than the smallest time constant of the network. The other actions perform fine tuning of the step length to the natural time constants of the network for the following integration period. The optimum step length, with regard to processing time, will vary with the system being studied, but to obey the assumption concerning frequencies of interest, it must be kept below 2.5^{o} for a.c./d.c. systems. In purely a.c. systems the limiting factor is the assumption of constant coefficients over the integration interval.

Actual computer processing time is primarily a function of the step length and the number of system differential equations. However it is also affected by the

system configuration (e.g. number of convertor bridges), and its characteristics (e.g. the presence of time variant parameters such as saturation or unsymmetrical detailed machine models).

3.4.1 Time Variant Nodal Coefficient Matrix

The detailed digital model for synchronous machines contains time variant inductances. Generally the machine's neutral (unearthed) and stator terminals are, by definition, γ nodes. As a result, each time the machine inductance matrix L_1^{-1} is updated, L_γ must be reformed. However in certain instances, for example if the machine is part of a unit type convertor scheme (Calverly *et al.* 1973) and its terminals have harmonic filters connected, then by definition its terminals become β nodes and thus its only coupled γ node is the neutral. In the usually adopted case of phase symmetry, L_γ will then be independent of rotor position and therefore it is time invariant. However if the machine has phase asymmetry, or exhibits saturation, it is still necessary to reform L_γ according to equation (2.26) at each integration step. This requires L_g to be recalculated according to Appendix A1, and inverted to give a new matrix L_1^{-1}. The timing of these calculations, and the logic used to determine if they are necessary, are detailed in Fig. 3.1.

3.5 APPLIED DISTURBANCES

Apart from abnormal convertor behaviour due to terminal conditions, disturbances may be applied by a data set formed at input time, which specifies the type,

and time of application, of the disturbance(s). All types of a.c. system faults are catered for, including their initiation and correct clearance, and these are detailed in Chapter 4. Similarly d.c. fault initiation, detection, clearance and recovery are investigated in Chapter 5. In addition to these fault simulations, disturbances such as network load changes can be modelled by varying the shunt element used to model such loads.

Many types of convertor faults can be initiated, viz. single or multiple valve misfires, single firethrough of a convertor valve, blocking and/or deblocking of a convertor bridge. The latter involves suppression and subsequent reinstatement of the valve firing pulse to the bridge. The accessibility of all convertor bridge control variables allows for easy modification of convertor control settings, and even the actual control schemes, as well as the firing patterns of bridges and individual valves.

Any number and combination of the above faults may be applied at any one time, or during a simulation period.

3.6 OUTPUT AND DATA RETRIEVAL

The dynamic simulation provides, at each integration step, information on all nodal voltages, branch currents and convertor states as well as control information and state variable derivatives. To output all this information would entail a massive output list. Instead a selective procedure is employed in which only certain variables, e.g. valve currents and voltages, are output at regular intervals (say 0.5 to 1.0 msec), as well as at valve switching times,

during the simulation run. In addition, at each of these times, this and other state and dependent variable information is output to a mass storage medium. This enables selection of particular quantities for inspection after the simulation run has finished, without requiring repetition of the simulation. A retrieval programme to utilize this data file to provide graphic plotting or ordinary numeric listing of the selected quantities, or combinations of quantities, has been developed.

The necessity of establishing 'dynamic initial conditions' for a particular system has prompted the development of a facility for storing these conditions on a similar mass storage basis. These conditions can then be used for initiating various studies involving the same system in the same initial state. This will avoid the need to do initial condition runs for each study. Storage of the states at the end of every simulation run also has the advantage that if for some reason a continuation of the simulation is desired at a later stage, it is possible to retrieve this data and extend the simulation period. Alternatively, comparisons over certain periods in a simulation can be made by performing a parallel simulation, e.g. using a different set of controls etc., by retrieving the data stored at the end of the previous period, and re-running the programme for the specified duration of the comparison.

The method of using previously stored established conditions avoids the majority of the input procedure. This is indicated in Fig. 3.4.

3.7 PROGRAMME OPTIMISATION

3.7.1 Scope

The programme was originally designed to handle combined a.c./d.c. systems of reasonable size with flexible configurations. Every practical combination of the plant components discussed in Chapter 2 has been catered for, and the allowable size of the system is only limited by the storage allocated to each type of element.

3.7.2 Sparsity Storage

The coefficient and incidence matrices in equations (2.39) - (2.48) contain a large proportion of zero elements (e.g. Fig. 3.6). Only the non-zero elements need be stored in order to save computer storage and time in performing matrix operations. Further reduction in storage is achieved by storing only a sample of any constant sets which are repeated, i.e. assuming linearity and balance, all three phase matrix elements e.g. multiple-segment transmission line series inductance matrix, and each phase of a bank of single phase transformers. This will not apply to transmission line nodal capacitances (see Appendix A2), nor to resistances since the latter (R_k, R_l, R_r, R_β) are stored as simple diagonal vectors whose indexing information is inherently given by the relative position of the elements.

3.7.2.1 Coefficient Matrices. The representative samples of non-zero matrix elements are stored in a vector of real constants C, and the indexing information is stored in three integer vectors LC, KC, LK, as in the example in Fig. 3.6(c). C contains the non-zero elements of the full

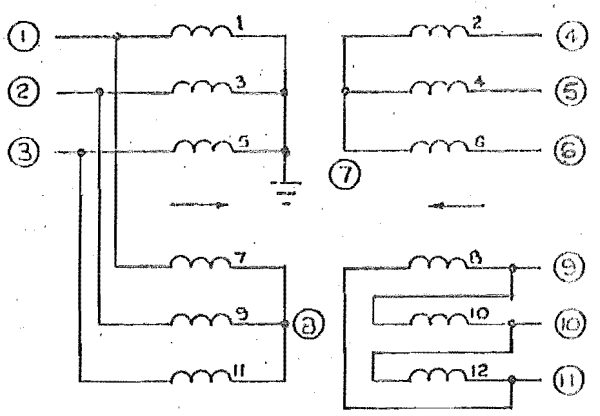

(a) Equivalent Circuit

	1	2	3	4	5	6	7	8	9	10	11	12
1	a	b										
2	c	d										
3			a	b								
4			c	d								
5					a	b						
6					c	d						
7							e	f				
8							g	h				
9									e	f		
10									g	h		
11											e	f
12											g	h

(b) Full Inductance Matrix

C	a	b	c	d	e	f	g	h

LC	1	3	1	3	1	3	5	7	5	7	5	7

KC	1	2	1	2	3	4	3	4	5	6	5	6	7	8	7	8	9	10	9	10	11	12	11	12

LK	1	3	5	7	9	11	13	15	17	19	21	23	25

(c) Compact Inductance Matrix

branch no	1	2	3	4	5	6	7	8	9	10	11	12
from	1	4	2	5	3	6	1	9	2	10	3	11
to	0	7	0	7	0	7	8	11	8	9	8	10

(d) Branch List

K	1	7	3	9	5	11	2	4	6	-2	-4	-6	-7	-9	-11	8	-10	10	-12	-8	12

	1	2	3	4	5	6	7	8	9	10	11	12	13	14	15	16	17	18	19	20	21

L	1	3	5	7	8	9	10	13	16	18	20	22

(e) Node-Branch Incidence Matrix

Fig. 3.6 Storage of Coefficient and Incidence Matrices

matrix, scanned row-wise, ignoring repeated sets. The vector LC gives the relative address in C of the start of information of each row that is defined in the full matrix. KC contains the column numbers of all non-zero elements in the full matrix while LK gives the relative address in KC of the start of information for each row.

The branch and node coefficient matrices (L_l, L_k, L_δ, C_α) are also ordered in such a way that they are composed of block-diagonal sub-matrices of low order. Each block is a square matrix representing a set of mutually coupled branches with few, if any, null elements. The full matrix inverses are therefore identical to the original matrix in structure. This makes it relatively easy to calculate inverse and matrix-by-vector products in a systematic manner.

3.7.2.2 Incidence Matrices. Incidence matrix information is stored in two integer vectors: the coefficient vector (K) and the associated index vector (L).

Taking a node-branch incidence matrix as an example, L gives the relative address of the start of information in K for each node. The coefficient vector K contains the numbers of branches that are connected to each node, preceded by a minus sign if the node happens to be the receiving-end of the branch in question. This is effectively storing the matrix by rows, replacing a +1 by its column number, a -1 by the negative of the column number, and completely ignoring zeros. Fig. 3.6(e) shows the node-branch incidence matrix for the example given.

3.7.2.3 Implementation. Several subroutines are required to perform the tasks of forming, storing and

indexing the coefficient and incidence matrices. A special routine performs coefficient matrix inversion. As well as these tasks, which are basically required at input, the solution of the network equations requires the evaluation of matrix-by-vector products for which general subroutines were also developed.

The product of a compactly-stored incidence matrix D and a vector V is obtained by algebraically adding the elements of V whose relative addresses and signs are given by the elements of K pertaining to each row in D. The product of the transpose of D and a vector can be obtained by a similar modified procedure, and it is therefore only necessary to store one form of incidence matrices. The real coefficient matrix-by-vector product is obtained by summing up the products of the non-zero elements in each row and the elements of the vector V, whose relative addresses are given by the column numbers stored in KC.

Multiple products, such as the expressions given by equations (2.39) - (2.48), are obtained by scanning the expressions from right to left, progressively carrying out single matrix-by-vector multiplications until the final product is reached.

3.8 VALIDATION OF MATHEMATICAL MODEL AND DIGITAL PROGRAMME

The segregation of the processes detailed above, allows for comprehensive testing of the individual parts. Full testing of the mathematical model and programme can only be performed by comparison with results from similar types of studies, or from physically attained results.

The only facilities available for checking purposes on a quantitative basis, were a steady state (load flow) analysis programme, a fault study programme, and a transient stability programme in which the solutions were based on the assumption of balanced, sinusoidal waveforms.

The separation of the convertor monitoring and control logic routines, allows testing of the majority of the programme with an a.c. system, without the need to include the more restrictive d.c. components. Then, using combined a.c./d.c. systems, the remaining routines can be checked.

By comparing results of a dynamic simulation of normal steady state operation over a long period (say 500 msec), with those from a load flow, a reasonably comprehensive check of the model and programme may be obtained. Taking into account the inherent assumptions in load flow analysis (infinite smoothing reactance, fixed commutation reactance, no dynamic control action), one can expect the solutions to be very close. Test cases indicated that discrepancies of less than $1\text{-}2^{o}$ were seen in the control angles (α, γ, δ) for convertors. These are well within the expected tolerance for power system analyses.

These long simulations also provide a means for exposing any possible numerical instability in the integration process(es), or accumulation of truncation and/or round off errors. The use of a different integration process, or step length, for a parallel simulation gives an alternative check.

CHAPTER 4

FAULT STUDIES IN AC SYSTEMS INTERCONNECTED BY HVDC LINKS

4.1 INTRODUCTION

Different analytical models are needed to predict the various effects of a.c. power system faults, depending on the specific information required. Steady state power frequency studies are commonly carried out for the calculation of circuit-breaker ratings and transient stability levels; they normally involve the complete power system, and use linear circuit analysis to obtain information at particular instants of time.

Dynamic simulation studies are also carried out in order to obtain information on transient current and voltage waveforms following the inception of a fault, or its clearance, for the purpose of dynamic testing of switchgear and protective relays. They usually require more detailed representations, but do not normally involve explicit modelling of the complete system.

Conventional a.c. fault algorithms cannot simulate the highly non-linear behaviour of HVDC convertors to fault conditions. The convertors' responses and subsequent effects are often neglected without proper justification. For the sake of analytical simplicity, they are either assumed to maintain a constant P,Q load throughout the fault period, or are disconnected entirely. However, simulations based on simple quasi-steady state representations (Heffernan 1977,

Turner 1980) have shown that the power ratings of HVDC convertors are generally too large to be ignored, and their speed of controllability (much faster than breaker action) may have a profound effect on the entire system behaviour during, and immediately after, the fault. Moreover, a.c. system disturbances will influence the type and characteristics of the d.c. controls required for each particular scheme, and this information can only be obtained through correct simulation of convertor behaviour under such circumstances.

It is the purpose of this chapter to discuss the extent of the applicability of both quasi-steady state and dynamic models, to the analysis of power systems under a.c. fault conditions. The New Zealand a.c./d.c. system is used to test the models with both balanced and unbalanced a.c. faults simulated. The results are used to discuss the extent of the applicability of the models, and particularly, the scope of the dynamic simulation in the design of switchgear, protective systems and convertor controls.

4.2 DYNAMIC MODEL

4.2.1 Introduction

The time variant nature of the current and voltage waveforms in an interconnected a.c./d.c. system, which is subjected to an a.c. fault, can generally only be predicted by dynamic analysis of the interconnected system components. The state variable technique, with its diakoptical handling of the frequent convertor topological changes, is a most convenient method for performing such analyses.

4.2.2 Dynamic Representation of AC System

Modelling of each component in an entire a.c. power system using such techniques is possible, but for a large system this may become economically impractical due to the size and complexity of the system.

The use of an equivalent representation for (part of) an a.c. system, as discussed in Section 2.2.7, has many computational advantages, and by correct network reduction only a negligible reduction in accuracy is sacrificed.

4.2.3 Equivalent Network Representation

To determine an adequate equivalent network for the studies to be carried out, the areas of specific interest must first be identified. For a.c. fault studies in a.c./d.c. networks, the major area of interest will be at the convertor terminals and at the fault location, since these are the most likely areas of overvoltage and distortion effects. Therefore, in general, explicit information will be required at three locations, viz. the rectifier and invertor a.c. terminals, and the fault location.

The New Zealand Power Transmission scheme is used as a test system. It consists of two separate 220 kV a.c. networks of comparable capacity, containing 21 buses in the North Island, and 19 buses in the South Island, which are interconnected by a ±250 kV HVDC transmission link as described in Section 4.2.4. Since this system is not dominated by a particular component (other than the d.c. link), it is appropriate to consider an equivalent network representation, with just the three locations detailed above being modelled explicitly. Effectively then, at each node

of interest a Thevenin Equivalent must be obtained for the a.c. system, as seen looking into the system from the relevant node.

A means of obtaining these equivalents for total system representation is provided by an a.c./d.c. fault study programme, which uses a quasi-steady state representation, based on injected currents at the convertors' a.c. terminals, for the d.c. link (Lake 1978). The programme is based on a nodal system analysis, in which the steady state pre-fault nodal voltages of the a.c./d.c. system are described by the following matrix equation

$$V = Z\,I + Z\,J \qquad \ldots (4.1)$$

where Z is the bus impedance matrix,

I is a vector of nodal injected currents due to a.c. generators, and

J is a vector of nodal currents injected by the d.c. terminals.

This a.c./d.c. fault programme models the links non-linear behaviour during disturbances by assuming the convertors retain controllability, and so maintain the current setting. When a three phase fault occurs in one of the a.c. systems, represented by a current I^f flowing out of the faulted bus p, the quasi-steady state model resolves the d.c. link equations. With the d.c. link on constant current control (at one of the two convertor stations), the magnitude of the current injections, J^f, will remain fixed, but the respective phase angles of the injections will depend on the terminal voltages and the d.c. link operating

conditions (α_r, δ_i).

From the matrix equation (4.1), the following expressions are extracted for the nodal voltages at the convertors and fault buses (Fig. 4.1)

$$V_m^f = V_m + Z_{mm}(I_m^f + J_m^f) + Z_{mn}(I_n^f + J_n^f) + Z_{mp} I^f \quad \ldots (4.2)$$

$$V_n^f = V_n + Z_{nm}(I_m^f + J_m^f) + Z_{nn}(I_n^f + J_n^f) + Z_{np} I^f$$

$$V_p^f = -Z^f I^f = V_p + Z_{pm}(I_m^f + J_m^f) + Z_{pn}(I_n^f + J_n^f) + Z_{pp} I^f \quad \ldots (4.4)$$

where Z^f is the fault impedance,

I^f is the fault current, and

V_m, V_n, V_p are the prefault voltages at the rectifier, invertor and fault buses respectively, in the absence of d.c. transmission.

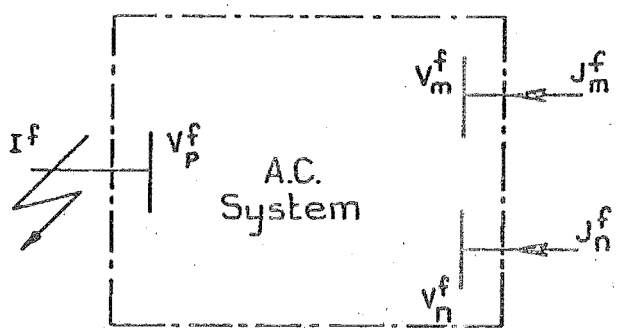

Fig. 4.1 Current Injections from Convertors' and Fault Busbars

Equations (4.2) - (4.4) describe a matrix set containing three interrelated Thevenin equivalents. The unique feature of this interrelation is that each equation contains two terms which couple that equivalent to the other two

equivalents, viz.

$$Z_{kj} \; (I_j^f + J_j^f) \qquad \text{for} \quad \begin{matrix} k \in m,n,p \\ j \in m,n,p \\ j \neq k \end{matrix}$$

where $J_p^f = 0$ and $I_p^f = I^f$.

This equation set can be incorporated into the dynamic simulation with particular ease, provided modification of the equations to allow for the mutual coupling term, which has both real and imaginary components of impedance, is performed. The equations affected are equations (2.39), (2.43) and (2.46) which are modified so that

(i) R_1 now contains off diagonal terms, and

(ii) L_1 contains additional off diagonal terms.

Now that a method of obtaining an equivalent network has been determined, the accuracy of this model at frequencies other than the power system frequency must be examined, since the fault study programme, and thus the Thevenin equivalent, is only applicable at the fundamental frequency. As detailed in Section 2.2.7, the absence of a detailed impedance-frequency locus for each system configuration rules out correct representation at all frequencies. However for frequencies at and above the resonant frequency of the high pass harmonic filter, the a.c. system impedance is swamped. The presence of resonant conditions in the range of the lowest harmonic filter (5th) to the high pass is not expected. Therefore an approximate model which is accurate for frequencies below the fifth harmonic, where resonances are most likely to occur, if at all, is the most feasible. Such is the model proposed by

Giesner (1971), which gives a constant impedance angle up to the fifth harmonic.

The initial test cases presented here used a simple fundamental frequency a.c. network impedance. However this was a data limitation only, since if the impedance-frequency locus is known, it can be modelled in the programme by equivalent networks, such as in Fig. 2.3. In particular, the Thevenin equivalent approach lends itself to the representation in Fig. 2.3(b) where correct system damping can be modelled.

4.2.4 DC System Representation

A schematic of the HVDC interconnection in the New Zealand (N.Z.) power system is shown in Fig. 4.2, where it can be seen that it involves four convertor bridges at each a.c. terminal. The HVDC link involves a bipole line consisting of 530 km of overhead line (South Island), 40 km of submarine cable (Cook Strait) and 37 km of overhead line (North Island).

For a.c. fault investigations, the d.c. line representation may be simplified to a double-bridge monopole equivalent, since this still gives 12 pulse operation, and therefore represents the d.c. system accurately. The transmission line monopole equivalent was represented by 3 pi-sections for the South Island overhead line, a large shunt capacitance for the Cook Strait cable, and a series impedance for the short overhead line in the North Island. The latter was incorporated into the smoothing reactor data at that end due to its relatively small value.

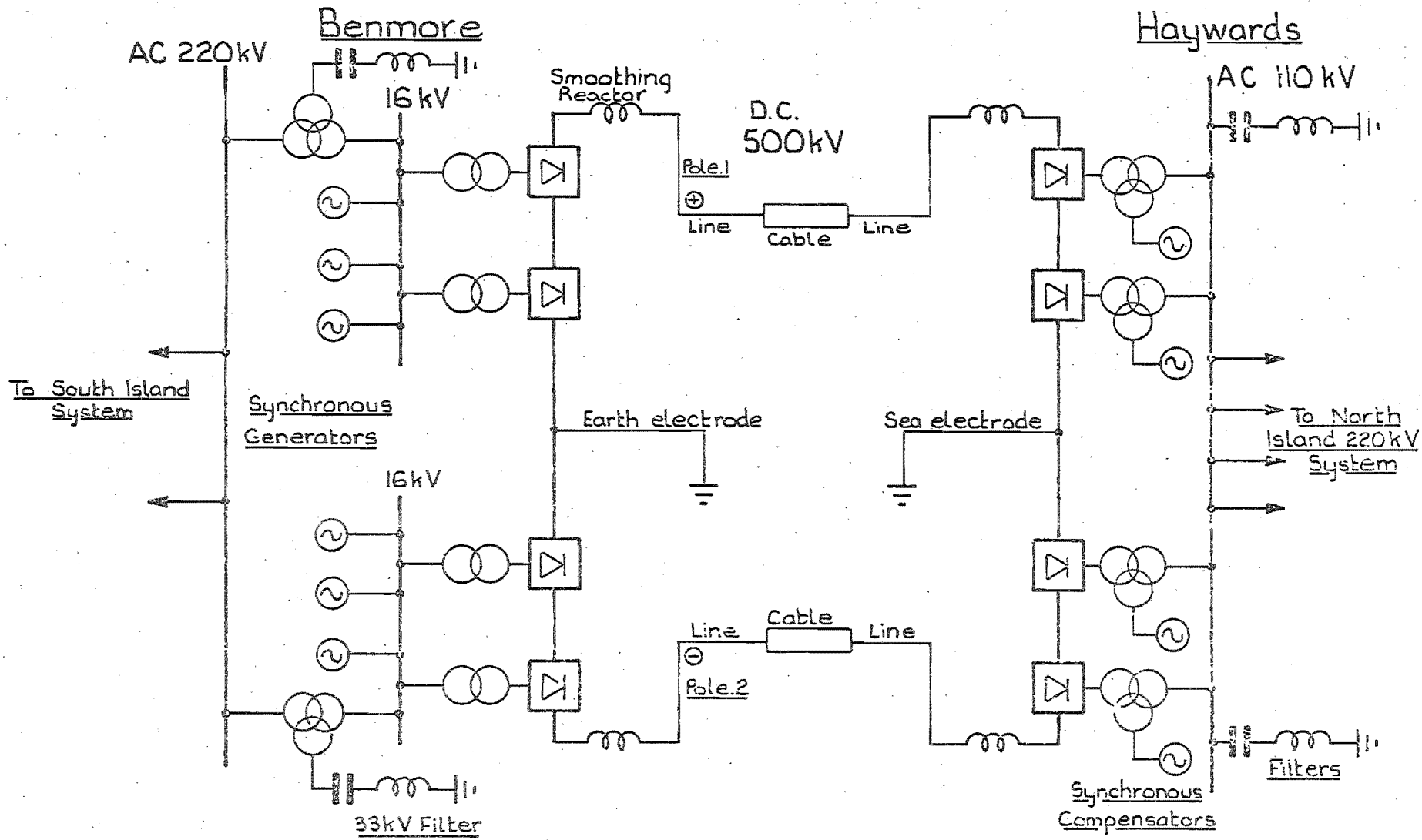

Fig. 4.2 Schematic of N.Z. a.c./d.c. Interconnection

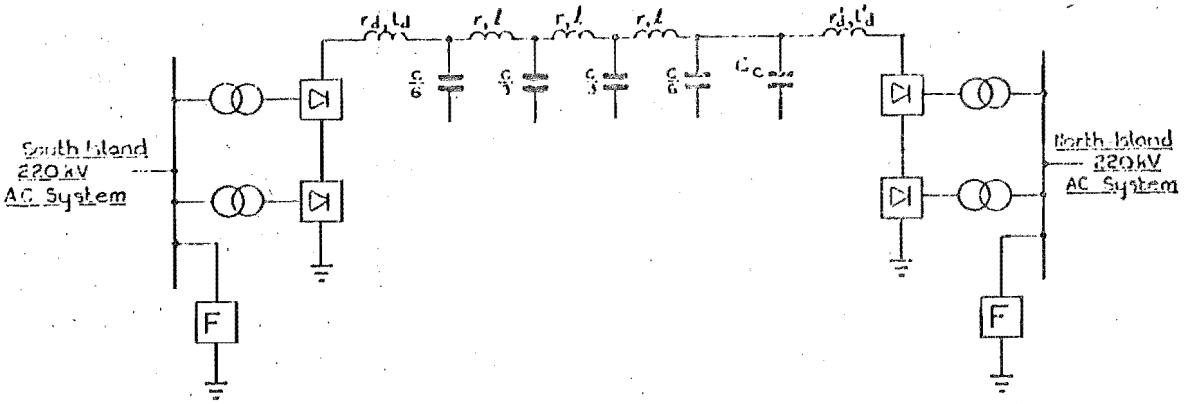

Data Set (in per unit)

S.I. smoothing reactor : $r_d = 0.00042$ $L_d = 0.65807$

N.I. smoothing reactor : $r'_d = 0.00254$ $L'_d = 0.69843$

Overhead line : $r = 0.01087$ $l = 0.07568$ $C = 0.60711$

Submarine cable : $C_c = 1.59974$

Fig. 4.3 Equivalent HVDC Representation for a.c. Faults

This representation is depicted in Fig. 4.3, along with the data set used. Equivalent convertor transformer reactances were calculated using the N.Z. scheme data, and corrected to a two bridge equivalent. Actual a.c. harmonic filter data, corrected to a 220 kV base, was also incorporated from the N.Z. scheme, as was the data for existing smoothing reactors.

The entire data set is detailed in Appendix A9.

4.3 ESTABLISHMENT OF INITIAL CONDITIONS

When a reduced system representation is used to model the a.c. system, the three phase real and imaginary terms of the Thevenin equivalents' branch impedances in equations (4.2) - (4.4) are transferred to the topological matrices R_1 and L_1 respectively, as described in Section 3.2.

The initial conditions are obtained using the process described in Section 3.2.1. The fault study, which provides the Thevenin equivalents, also provides the steady state pre-fault solution required by the dynamic analysis to begin establishment of correct dynamic initial conditions (Section 3.2.2).

If a complete a.c. system representation is used, full component representation is implemented by proper inclusion of component parameters in the R_r, R_l, L_l and C_c matrices. The steady state pre-fault information may also be obtained from an a.c./d.c. Load Flow analysis. In this case, the establishing of realistic initial conditions at the instant of fault occurrence then follows the same pattern as in Sections 3.2.1 and 3.2.2.

4.4 FAULT APPLICATION AND REMOVAL

The simulation of a fault impedance is restricted by the network constraints defined in Chapter 2. Two methods for fault application and/or removal must be considered to allow representation of any type of fault impedance. In general, to satisfy the constraints, fault application will involve either

(i) insertion of a resistive fault branch into a branch list or connection of a fault branch, already established in the branch list, to the fault location; OR

(ii) alteration of the impedance value of a permanently connected fault branch.

The a.c. system representation used, will determine the specification of the nodes at the fault location.

4.4.1 Equivalent AC System Representation

(i) Application by Connection or Insertion of Fault Branch.

There are two types of fault location in equivalent representations.

(a) Convertor Busbar Fault

When the convertor terminals have high pass filters attached, the topology definitions will mean each phase of the terminal busbar is a β node. The existence of a β node at the fault location in the pre-fault branch list, allows the fault application to be simulated by inserting a shunt resistance to ground at the convertor node, at a time corresponding to the fault occurrence. This resistance need not be included in the pre-fault branch list. Matrices R_r^{-1}, R_β and $K_{\beta r}$ must then be reformulated to describe this new shunt resistance. With this topology, practical numerical values for the fault element will not upset convergence of the state variable formulation. Similarly, fault clearance is simulated by removing this shunt resistance, and again reformulating R_r^{-1}, $K_{\beta r}$ and R_β .

An alternative scheme whereby the fault branch, which may be inductive or resistive, is included in the original branch, can also be used for this type of fault location. Fault application or removal is performed by altering $K_{\beta r}$ and R_β for a resistive fault, or $K_{\beta l}$ for an inductive fault. The modifications to the connection matrices require simply setting an element to zero for the prefault and post fault

periods, and setting it to unity on fault application. In both of these cases convergence is again not affected with practical values for the fault element.

However, if the convertor terminal is a γ node, i.e. no high pass filters are present, then the constraints applying to the fault application are the same as for a remote fault location as detailed in (b) below.

Whenever the fault is located at a convertor terminal, only two Thevenin equivalents are required since node p is now identical to either m or n. Therefore equation (4.4) is deleted from the system representation. If the convertors' a.c. systems are asynchronous, then there is no cross coupling and the equation set (4.2) - (4.4) reduces to

$$V_m^f = V_m + Z_{mm} (I_m^f + J_m^f) \quad \ldots (4.5)$$

$$V_n^f = V_n + Z_{nn} (I_n^f + J_n^f) \quad \ldots (4.6)$$

and $$V_p^f = - Z^f I^f = V_j^f \quad \ldots (4.7)$$

where $j = m$ or n.

(b) Remote Fault.

When a network reduction technique such as a Thevenin equivalent is used, a busbar is created at the remote fault location. In the absence of the fault, this bus is effectively open-circuited (infinite shunt impedance to ground). With the Thevenin configuration (source behind impedance model), this busbar will be a γ node in the dynamic analysis. On fault application, insertion of a shunt resistance to ground, as in (a) above, would violate

the original nodal specifications, since the pure resistance shunt element would change the fault node from a γ to a β node. This is not allowed within the topology constraints. If however the shunt contains a reactive component of any size, the original node specification would be maintained. Insertion of this shunt on fault application, i.e. into an already established branch list, would require a large amount of matrix reorganisation (L_1^{-1}, R_1, $K_{\gamma 1}$, L_γ), which would have to be repeated on fault removal. This is to be avoided since the storage scheme for the elemental matrix L_1^{-1} is rather complex. To overcome this, the fault branch is included in the original branch list. Correct simulation of the pre-fault and post-fault periods, as well as the fault period, can then be obtained by setting the relevant element(s) in $K_{\gamma 1}$ to zero and unity respectively. Each alteration of $K_{\gamma 1}$ will require L_γ to be recalculated. However the matrices L_1^{-1} and R_1 remain constant. This sequence is similar to the commutation action in the convertor bridges, where it is seen to not affect the convergence of the numerical integration of the state variables.

(ii) Application by Alteration of Existing Branch Parameters.

The scheme (i) is limited for faults at γ nodes since purely resistive faults cannot be simulated without upsetting the network topology. An alternative to the method (i) for fault initiation and removal, which will be applicable at both fault locations and for any type of fault element, is a method based on the principle of superposition. A fault branch (Z^f), which may be resistive or inductive, is

established in the original branch list. Any value of Z^f which is not infinite in the pre-fault period would create an incorrect system loading. However, very large values for Z^f affect the rate of convergence of the numerical integration of the state variable equations.

This can be avoided by including in the Thevenin equivalent, as seen from the fault point, a generating source exactly equal to the effective loading created by the non-infinite shunt impedance to ground at the fault point. By the principle of superposition, the dynamic model will then see the fault bus as an open-circuited terminal which will have the correct voltage.

This procedure was checked by performing an initial condition study, with a shunt impedance to ground of appreciable magnitude, so that in effect a substantial load was created at the fault point. An equivalent generating source was included in the Thevenin equivalent to compensate for this. The solution then obtained by the dynamic simulation for the pre-fault condition was found to be the same as obtained by a load flow solution. This both justified and proved the application of the method of superposition to avoid the problem of trying to simulate an infinite shunt impedance for the pre-fault conditions.

At fault application time, the shunt impedance is altered to its fault value to form the appropriate faulted network. In the case of a remote fault with a purely resistive fault branch of zero fault resistance, R_r^{-1} will be infinite and R_β will be zero. This would necessitate a very short integration step to achieve a reasonable rate of

convergence for the numerical integration process. Therefore a fault impedance in which the ratio X/R can be selected to avoid convergence problems must be used for remote faults. In the case of a convertor fault (with high pass filters connected), either a resistive (R_r) or inductive (jX_1) fault of any magnitude can be simulated.

Summarising then, in each of the above methods, by establishing the appropriate fault impedance in the branch list the fault can be applied at a pre-selected time, provided a reasonably balanced state has been achieved. The means of establishing this shunt depends on the location and fault branch required, and can be achieved by at least one of the above methods.

Any type of fault can be simulated by each of the above three methods. In a three phase-to-earth fault, each phase will have an equivalent which is grounded through a fault branch. For a single phase fault the two healthy phases will retain their pre-fault configurations. Similarly a phase-phase fault can be simulated by connecting the relevant phases together and if the fault involves earth, they may be connected to ground as well, using one of the methods detailed above.

The usual form of a.c. fault clearance involves the following sequence:

(i) detection of fault with relevant discrimination;

(ii) operation of the relevant circuit breakers to isolate the fault by opening the breakers within 3-10 cycles;

(iii) after a period sufficient for the fault path to deionize, the breaker is reclosed thus completing the original circuit; and

(iv) if the fault re-establishes, the sequence is repeated for up to 2-3 times and then if the fault still persists, the breakers will permanently isolate the fault.

Because of the definition of the fault location in the system model, this sequence of events can be simulated by an action equivalent to circuit breaker action. The actual time of fault clearance is determined by the following sequence of events. At a prescribed time following fault application, say 5 cycles, a flag is set which indicates that fault clearance is to be initiated on the relevant fault branch(es) at the next zero crossing of current in the fault branch(es). Extrapolation is used to predict the time when a zero crossing will occur; i.e. if t_j is the present time step, and h the step length, then

$$t_j = t_{j-1} + h \qquad \ldots (4.8)$$

Therefore if the current in the fault branch at time t_j is I_j, then

$$h' = h\, I_j / (I_j - I_{j-1}) \qquad \ldots (4.9)$$

so that if h' is less than the next integration step (the nominal value as calculated in the integration routine), the next time step will be

$$t_{j+1} = t_j + h' \qquad \ldots (4.10)$$

which will coincide with the zero crossing of fault current. Fault clearance will then be effected as described above by (i) alteration of a connection matrix element or removal of a shunt resistance, or (ii) alteration of an elemental

impedance value to re-establish the pre-fault circuit.

This process is repeated for each of the phases which are faulted. A flow diagram depicting the actions taken for fault application and removal is illustrated in Fig. 4.4.

4.4.2 Full AC System Representation

In a.c. fault simulations with full a.c. system representation, the fault location will generally involve either an α or β node. Therefore either of the methods described in (i) in Section 4.4.1 will be applicable. In the case of γ node fault locations, e.g. faults at the terminals of an isolated generator, the method (i) may be used except in the case of purely resistive faults. In this instance, an adaptation of method (ii) in Section 4.4.1 may be used to correctly simulate the fault.

As an example the full sequence (i) - (iv) in Section 4.4.1 is simulated for a (three phase-to-earth) a.c. line fault, with reference to Fig. 4.5(a) by:

(i) Inserting the relevant fault impedance at the fault point in parallel with the shunt capacitance of the π model corresponding to that location, by alteration of a pre-established connection matrix element.

(ii) Subsequent to the specified circuit breaker operating time, the line is isolated by reforming the connection matrix elements associated with the line ends (breaker locations), on detection of current zeroes there.

(iii) After a specified time, the breakers are reclosed and the fault to ground is removed by reforming the original connection matrices.

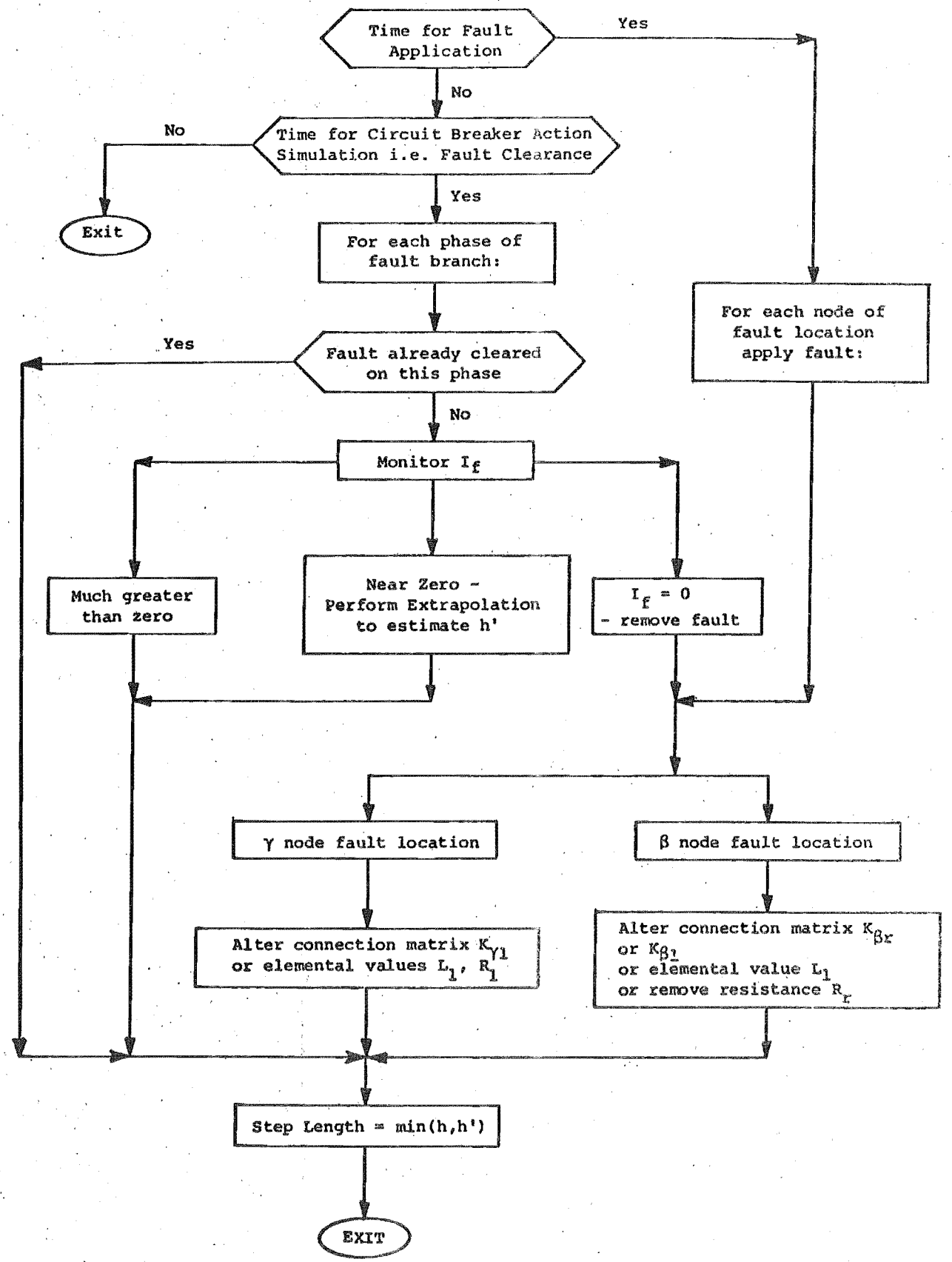

Fig. 4.4 Flow Diagram of Actions Taken for Fault Application/Removal

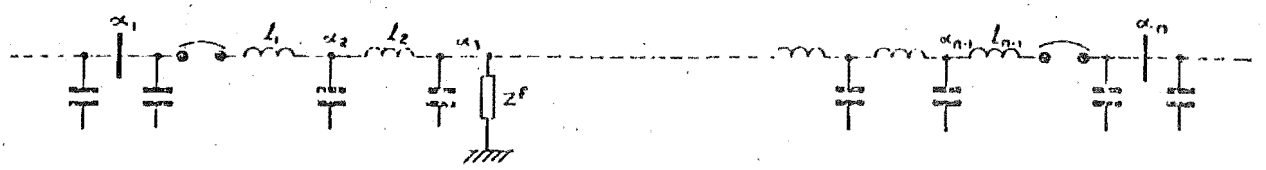

Fig. 4.5(a) Full System Representation of a Line Fault and Circuit Breakers

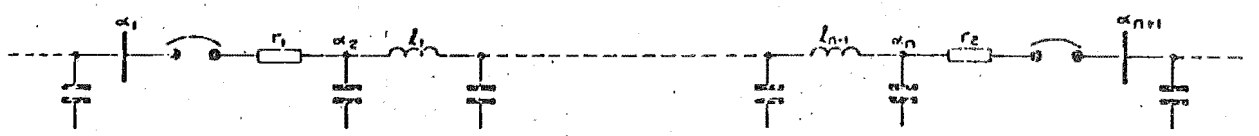

Fig. 4.5(b) Inclusion of Circuit Breaker Resistances

Each of the breaker operations can simulate the inclusion of resistance elements in the make/break sequences. A series resistive element may be included at the relevant line ends (r_1, r_2 in Fig. 4.5(b)), the value of which may be practically zero without affecting convergence patterns, since the line ends are generally connected to other lines, and are therefore in general α nodes. This enables simulation of preinsertion resistors on the reclosing action of the breakers, or of breaker contact resistance increasing with time, on opening of the circuit breakers. The value of this series resistance (see Fig. 4.5(b)) can be altered at any rate.

Opening of the circuit breaker can then be performed by

(i) increasing r_1 and r_2 at a rate defined by the breaker contact resistance vs time behaviour; and

(ii) at a certain resistance, setting elements $\alpha_1 r_{12}$ and $\alpha_{n+1} r_2$ to zero in the connection matrix $K_{\alpha r}$.

Reclosing of the circuit breaker is performed by:

(i) removing Z^f by setting element $\alpha_3 Z^f$ to zero in $K_{\alpha r}$;

(ii) reinstating elements $\alpha_1 r_1$ and $\alpha_{n+1} r_2$ to their original values (1, -1) in $K_{\alpha r}$; and

(iii) decreasing r_1, r_2 to comply with the preinsertion resistor values.

In cases where breaker contact resistance is not modelled, only step (ii) in the opening action is simulated. Similarly in cases where no preinsertion resistance is used, only steps (i) and (ii) are performed, with r_1 and r_2 equal to zero.

4.5 TEST SYSTEM AND RESULTS

The studies carried out were primarily concerned with the fault and immediate post-fault periods. Extensions of the study-periods to investigate system stability are possible, but computationally expensive.

The following a.c. faults, balanced and unbalanced, were simulated with the South Island station rectifying and the North Island convertor inverting.

(i) A three-phase fault in the South Island, resulting in a reduction of the rectifier a.c. voltage to approximately 30% of the pre-fault value (case 22).

(ii) As in (i), except that the fault is applied in the North Island, thus reducing the invertor a.c. voltage to about 30% of the pre-fault value (case 111).

(iii) A three-phase fault in the North Island, close to

the convertor station (case 1).

(iv) As in (iii), but with a single phase fault (case 101).

No attempt was made to optimize the HVDC link controller constants independently for each fault condition under dynamic simulation, but rather a set was used which gave a fast, yet sufficiently damped and stable response, to all a.c. fault conditions tested. A typical fault clearing time of 100 msec (5 cycles) was used in all the test examples.

4.5.1 Fault (i)

The dynamic response of the a.c./d.c. system prior to, during, and after the short-circuit is illustrated by the waveforms shown in Fig. 4.6. Waveform (a) shows the large direct current variation which occurs for about two cycles following the abrupt a.c. voltage changes, i.e. subsequent to fault occurrence (between cycles 2 and 4), and after fault clearance (cycles 7 to 9). Corresponding changes in alternating current take place during those periods, and, due to the relatively slow response of the harmonic filters, very large alternating current waveform distortion occurs. This in turn causes considerable a.c. voltage waveform distortion at the convertor terminals (Fig. 4.6(b)), and at the faulted bus (Fig. 4.6(c)). Fig. 4.6(d) shows the d.c. power variation during the fault. The a.c. disturbance produces no consequential convertor maloperation, and about 80 msec after fault initiation (cycle 6) the d.c. controllers are able to keep the current levels (Fig. 4.6(a)) very close to the specified settings.

Fig. 4.6(a) 22 CONVERTOR DC CURRENTS

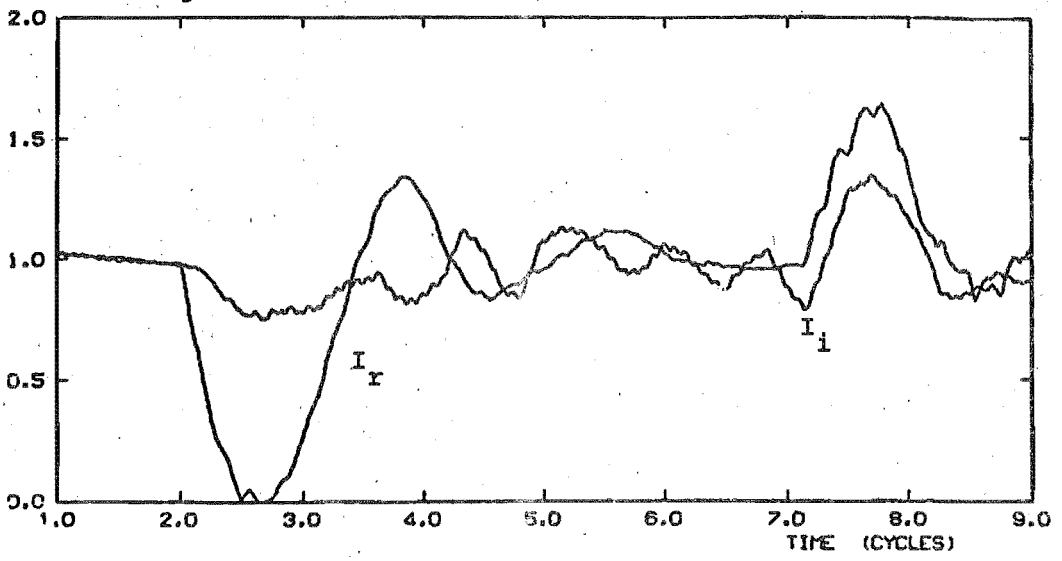

Fig. 4.6(b) 22 RECTIFIER AC VOLTAGES

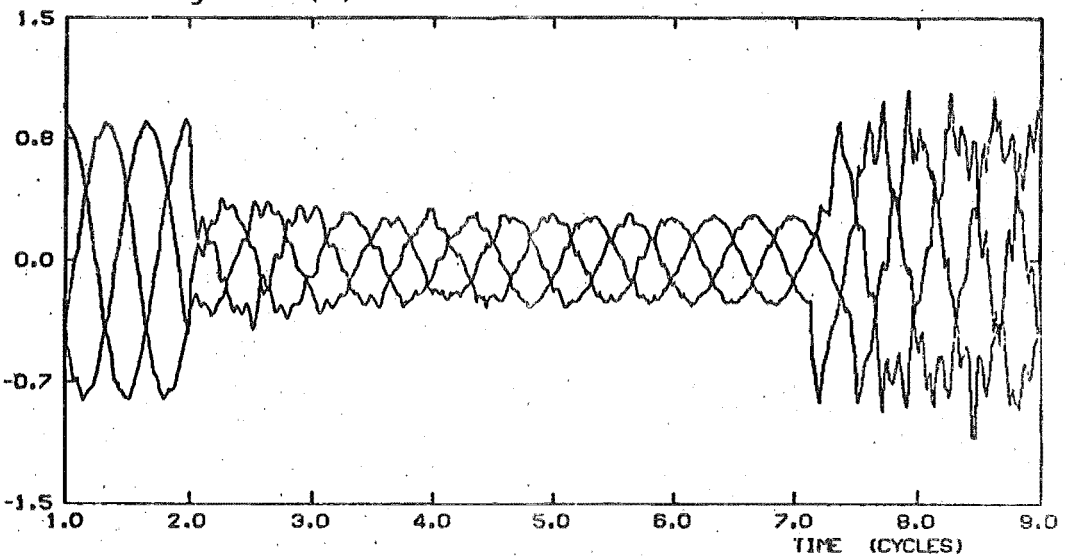

Fig. 4.6(c) 22 FAULT BUS AC VOLTAGES

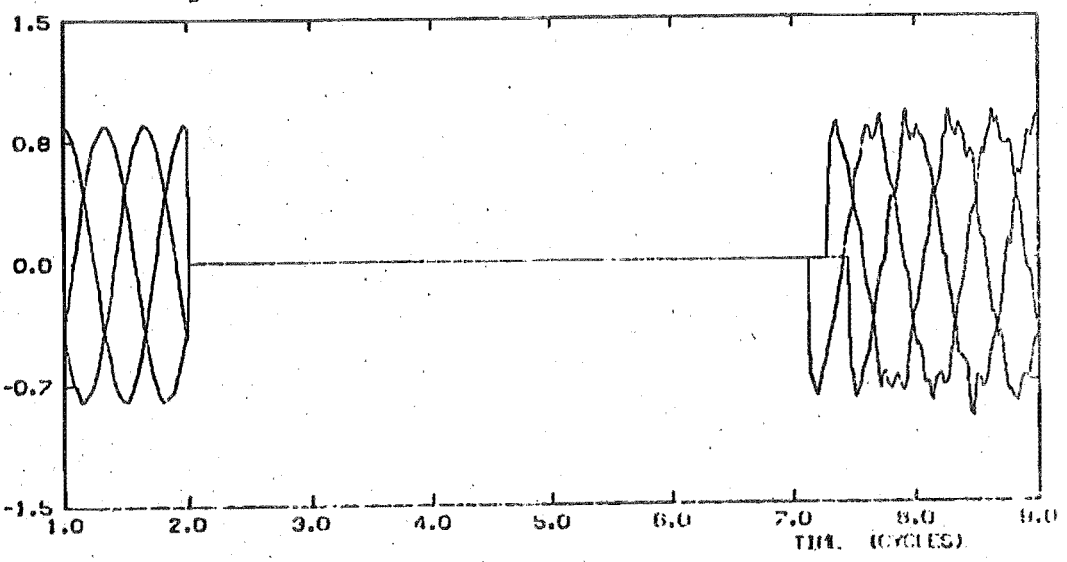

Fig. 4.6(d) 22 CONVERTOR DC POWERS

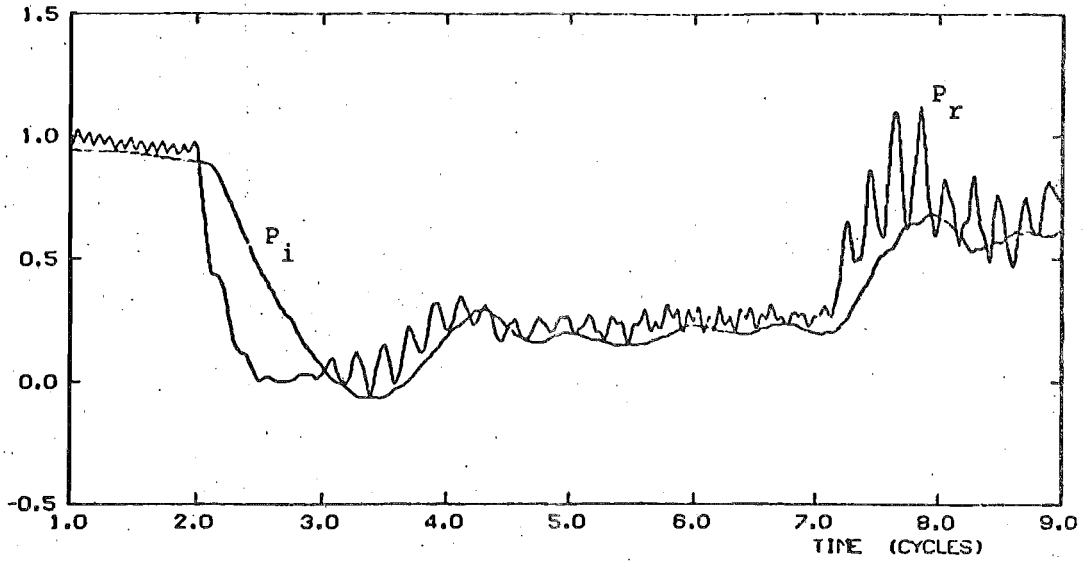

Steady state solutions using a quasi-steady state d.c. model in an a.c./d.c. fault study programme, with the d.c. link operating, or blocked (after the disturbance), were also carried out, and a comparison of results at the instant of fault clearance is made in Table 4.1.

Table 4.1 Comparison of results for case (i) at the fault clearance instant

	DYNAMIC	STEADY-STATE WITH DC LINK	STEADY-STATE WITH DC LINK BLOCKED
α (deg.)	9.5	5.0	Not applicable
δ (deg.)	68.7	73.8	Not applicable
V_r	0.35	0.33/6.8	0.41/16.76
I^f (kA)	13.6	13.8	14.5
Close Generator Current (kA)	-	2.2	2.0
Distant Generator Current (kA)	-	1.4	1.2

It is apparent from the Table that for this particular fault and location, the steady state models provide adequate information for the level of fault current at fault clearance time. The presence of the d.c. link is shown to reduce the current slightly at the point of the fault, and increase it elsewhere.

4.5.2 Fault (ii)

When a similar a.c. fault is placed at the invertor end, the disturbance is sufficient to cause repeated commutation failures in the invertor bridges, producing a large direct current peak of about 300% some 15 msec after fault inception. These convertor disturbances cause extensive current fluctuation (Fig. 4.7(a)), and thus the control angles and current magnitudes at the fault clearing time can not be accurately predicted with the steady state model. For instance, the steady state prediction of fault level for a five cycle clearance is 40% higher than the value obtained from the dynamic simulation.

The current control action during the disturbance causes substantial alternating current and voltage fluctuation, and harmonic distortion, at both ends of the d.c. link. By way of illustration, the rectifier end voltage waveforms of Fig. 4.7(b) show a voltage peak of over 150% during the fault. The voltage waveforms at the fault location following fault clearance are illustrated in Fig. 4.7(c).

Fig. 4.7(a) 111 CONVERTOR DC CURRENTS

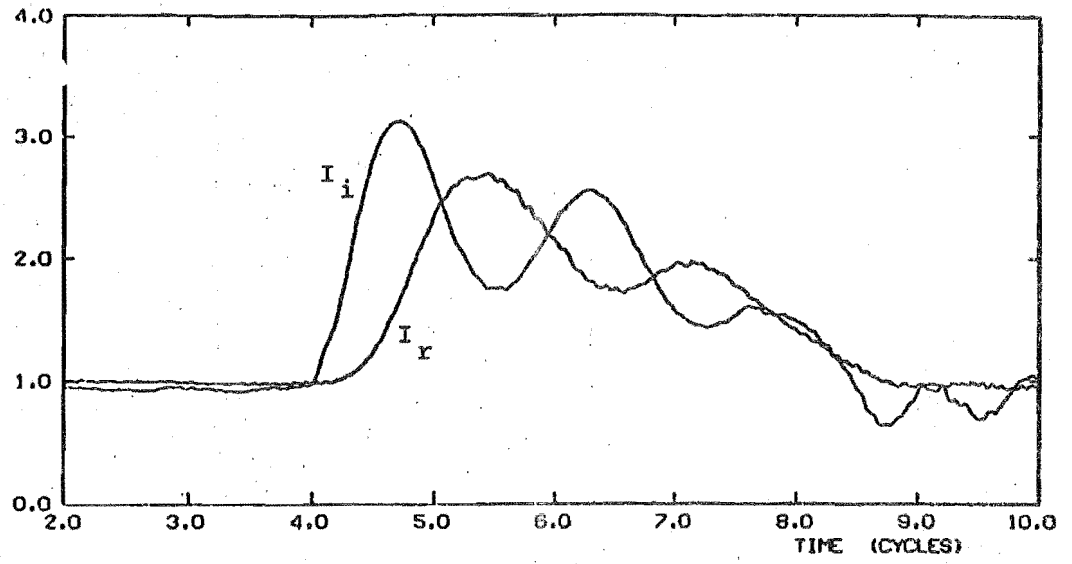

Fig. 4.7(b) 111 RECTIFIER AC VOLTAGES

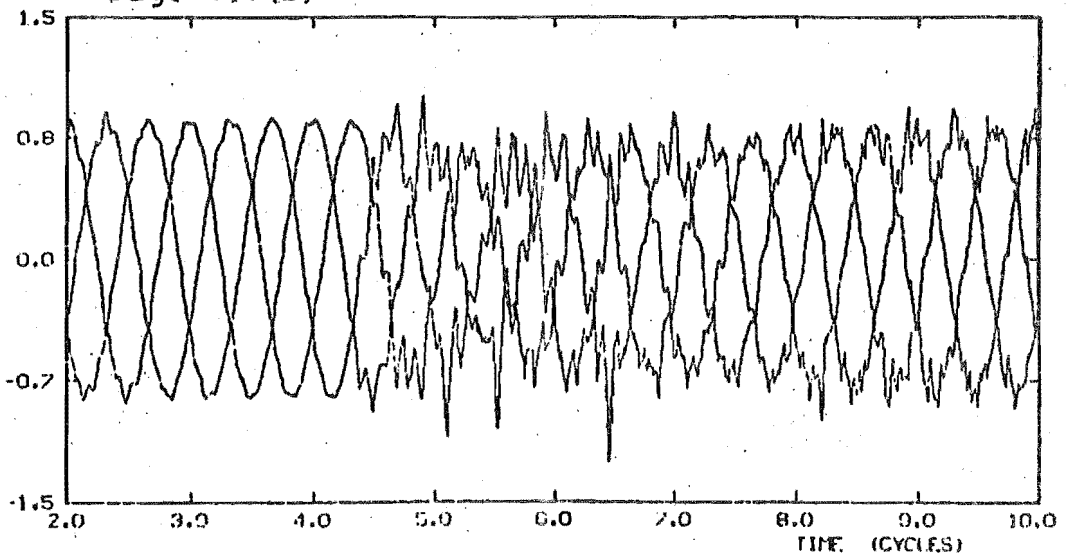

Fig. 4.7(c) 111 FAULT BUS AC VOLTAGES

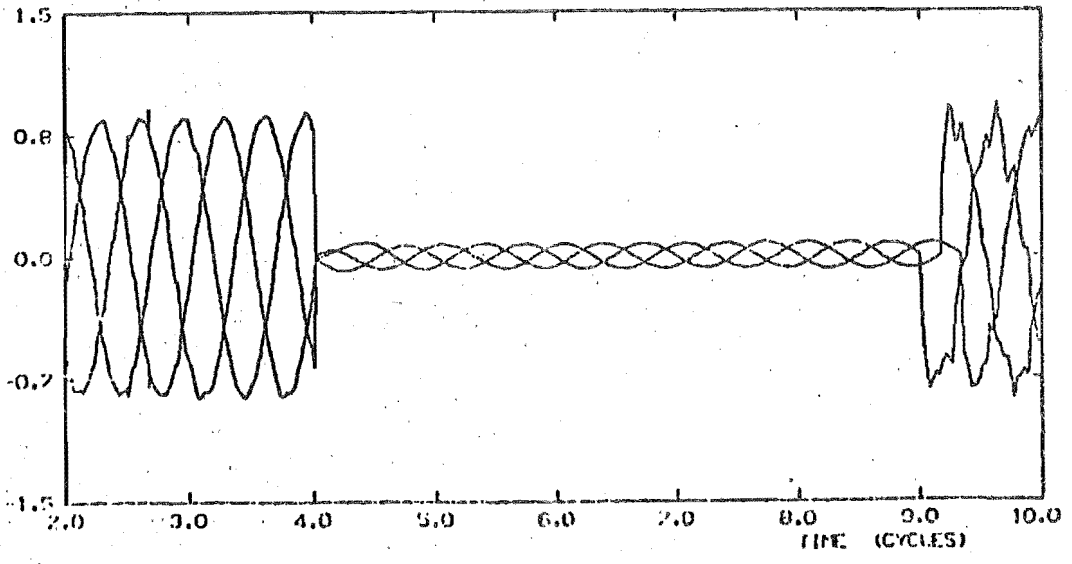

4.5.3 Fault (iii)

A low impedance fault is applied at the invertor a.c. bus, reducing its voltage level to less than 10% of the nominal. The immediate effect is a commutation failure in each of the invertor bridges, with subsequent failures and a continuous d.c. short circuit. The d.c. voltage variation of Fig. 4.8(a) illustrates this effect, and clearly for this fault there is no alternative to the dynamic simulation model.

Fig. 4.8(a) 1 INVERTOR DC VOLTAGES

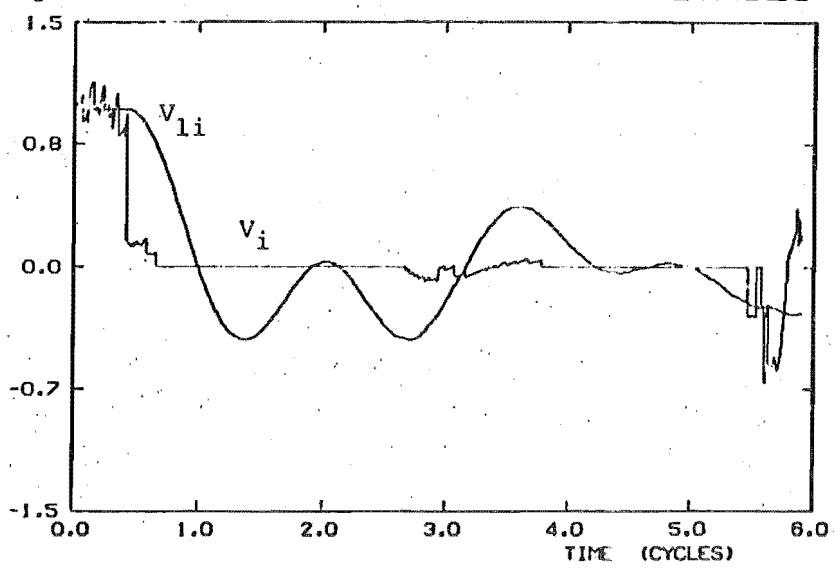

The direct current waveforms, illustrated in Fig. 4.8(b), show a rapid rise due to the invertor d.c. short circuit. This results in correspondingly large variations in the convertor a.c. currents, with peaks of 3 and 4 times normal load values at the rectifier and invertor ends respectively. The rectifier end a.c. current waveforms (Fig. 4.8(c)) are again very distorted and unbalanced.

Fig. 4.8(b) 1 CONVERTOR DC CURRENTS

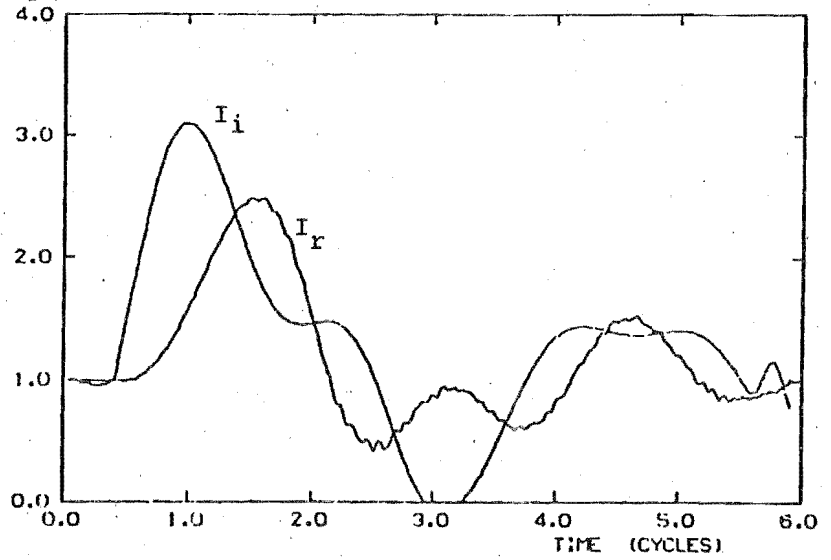

Fig. 4.8(c) 1 RECTIFIER AC CURRENTS

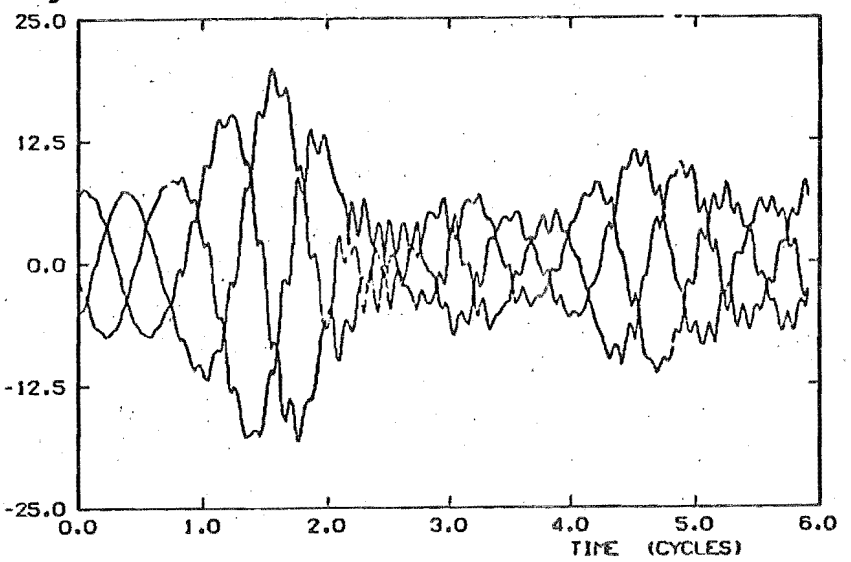

Fig. 4.8(d) 1 INVERTOR AC VOLTAGES

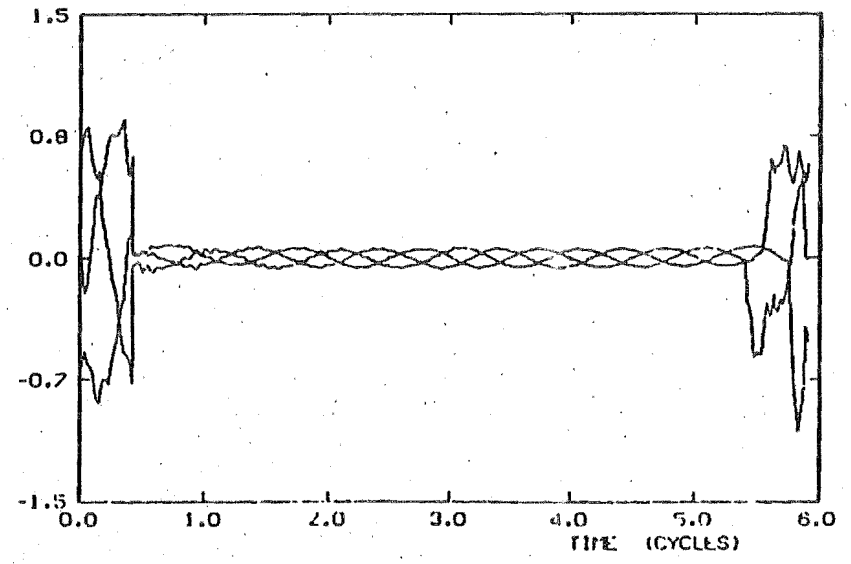

After five cycles, the direct currents are close to the normal settings, but the control angles are close to 90^{o}. Therefore the convertor a.c. currents are almost purely reactive, and cause large voltage regulation at both ends of the link.

The recovery voltages, due to the proximity of the fault, are greatly affected by the convertor behaviour. For instance, Fig. 4.8(d) shows that one of the phases experiences a peak of 135% on fault clearance.

4.5.4 Fault (iv)

A low impedance fault is now applied to one phase only. The collapse of one phase causes an immediate reduction of the invertor d.c. voltage, and a sharp increase of direct current, which results in a series of commutation failures. The initial response of the d.c. link is thus very similar to case (iii), and again, can only be assessed by the dynamic model.

The direct currents and invertor side a.c. voltage waveforms are illustrated in Figs 4.9(a) and (b). The voltage unbalance produces two extended commutation overlaps per cycle. This effect produces a continuous variation of the invertor firing angle (particularly under symmetrical firing control), and causes direct current fluctuation (especially at the invertor). Moreover, the two convertor ends operate with angles close to 90^{o} during the fault, and these two effects result in considerable voltage unbalance, regulation, and distortion of the two healthy phases (Fig. 4.9(b)).

Fig. 4.9(a) 101 CONVERTOR DC CURRENTS

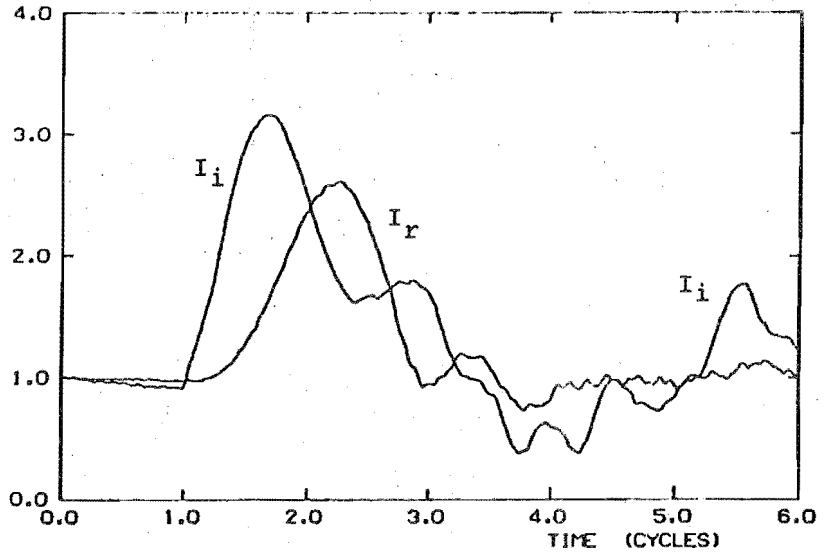

Fig. 4.9(b) 101 INVERTOR AC VOLTAGES

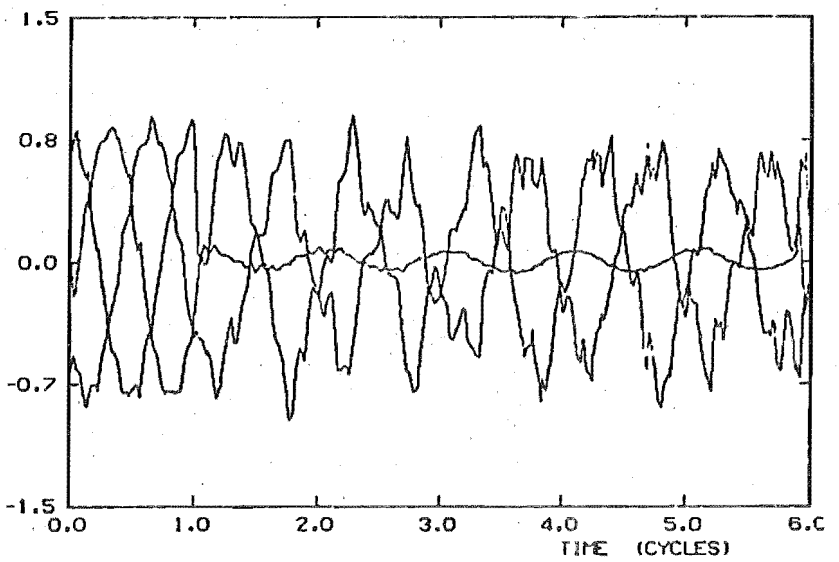

Although some commutation failures still occur 80 msec after fault inception (cycle 5 in Fig. 4.9) their effect on the direct current level is small due to the reduced d.c. voltage present.

4.5.5 Effect of Remote End Representation

An investigation of the behaviour exhibited in the fault studies (i) - (iv) above, indicates that the extent of disturbance to the remote end is governed by the severity of the fault.

Rectifier end faults causing a substantial drop in the rectifier a.c. voltage instigate CCC at the invertor end. This may result in waveform distortion and possible overvoltages at the remote invertor end (see Section 4.5.1 above).

For invertor end faults, the drop in invertor a.c. voltage will demand CCC action at the rectifier which may create waveform distortion and possible overvoltages at the remote rectifier end.

A reduction in the dynamic analysis computation costs may be achieved by using a simplified representation of the a.c. system, remote from the fault location. Inclusion of the a.c. harmonic filters into the a.c. system's Thevenin equivalent, instead of explicitly modelling them in the dynamic analysis, will significantly reduce the number of differential equations to be solved. This simplification may still provide accurate information for the faulted end in the form of actual waveforms at the relevant busbars.

However, because of the simplified remote end representation, waveform information is then limited there. Explicit filter modelling ensures sinusoidal waveforms in the steady state. The effect of including the filters in the Thevenin equivalent is clearly shown in Fig. 4.10(a) for a fault study (case 222) involving the same test system

as in Sections 4.5.1 - 4.5.4 above. The fault is in the South Island, and a simplified North Island representation is used. The invertor voltage waveforms, in the absence of the shunt filters, reflect the effect of square current waves in the convertor transformer windings, and dents due to valve commutations.

Fig. 4.10(a) 222 INVERTOR AC VOLTAGES

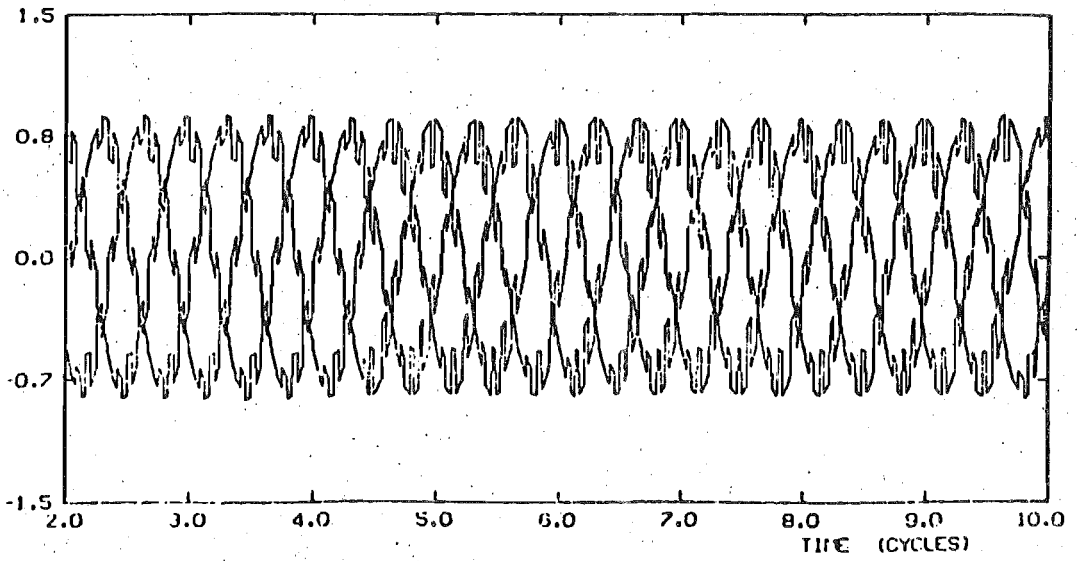

This simplification is valid provided the control action at the remote end is limited, as detailed above, since then the convertor will behave in a near steady state manner, with little or no resultant waveform distortion.

Two parallel studies of the rectifier end fault described above were conducted: one with the invertor filters explicitly modelled (case 321); and one with the filters included in the Thevenin equivalent at the remote end (case 222). The results, presented in Figs 4.10(a) - (e) indicate similar trends. However, the severity of the fault is sufficient to require the invertor to change from EAC to CCC. Under invertor CCC the behaviours are practically identical, but in the transition period where control action alternates between CCC and EAC, differences in invertor

direct current are evident.

The extinction angles measured from the distorted invertor a.c. voltage waveform in case 222 (Fig. 4.10(a)) are different from those obtained from the near sinusoidal waveforms of case 321. The difference is sufficient to cause more control action during the EAC/CCC transition, resulting in the more oscillatory invertor direct current waveform for case 222. Although this error in invertor response (case 222) is directly related to extinction angle measurement, it can not be alleviated in the programme without modification to the basic control principle.

Fig. 4.10(b) 222 CONVERTOR DC CURRENTS

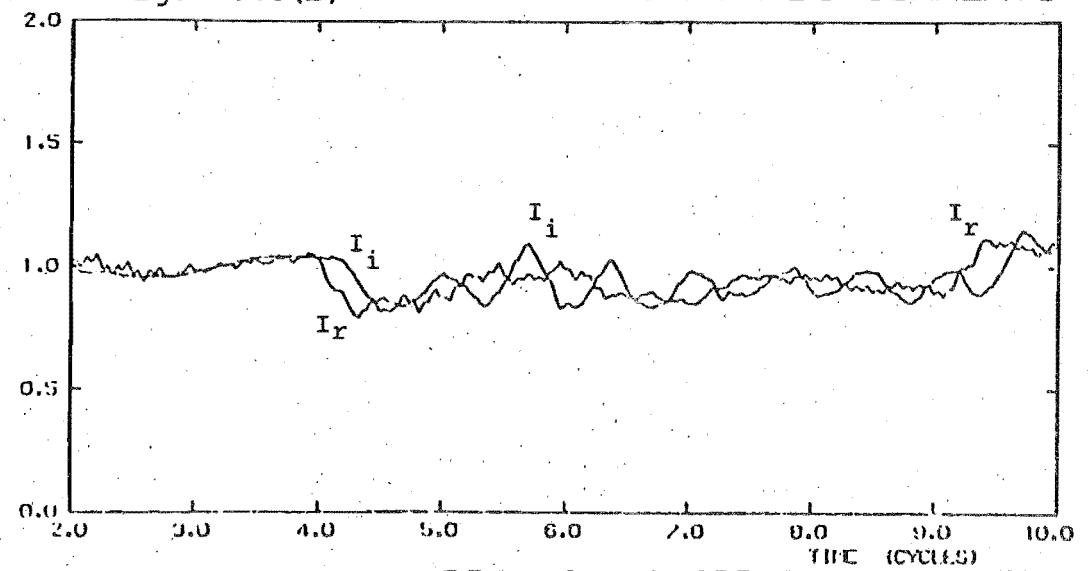

Fig. 4.10(c) 321 CONVERTOR DC CURRENTS

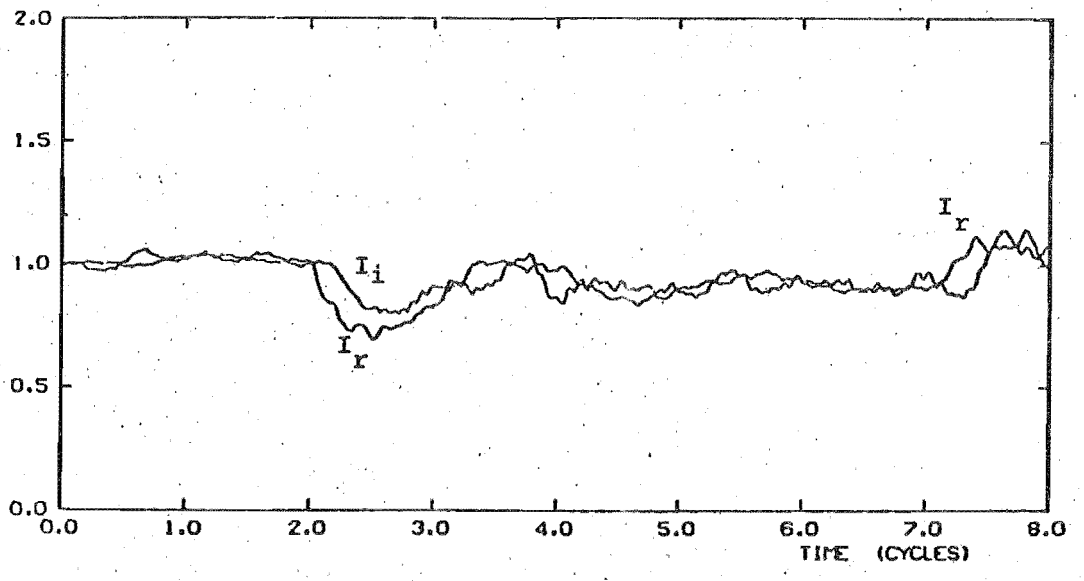

Fig. 4.10(d) 222 RECTIFIER AC VOLTAGES

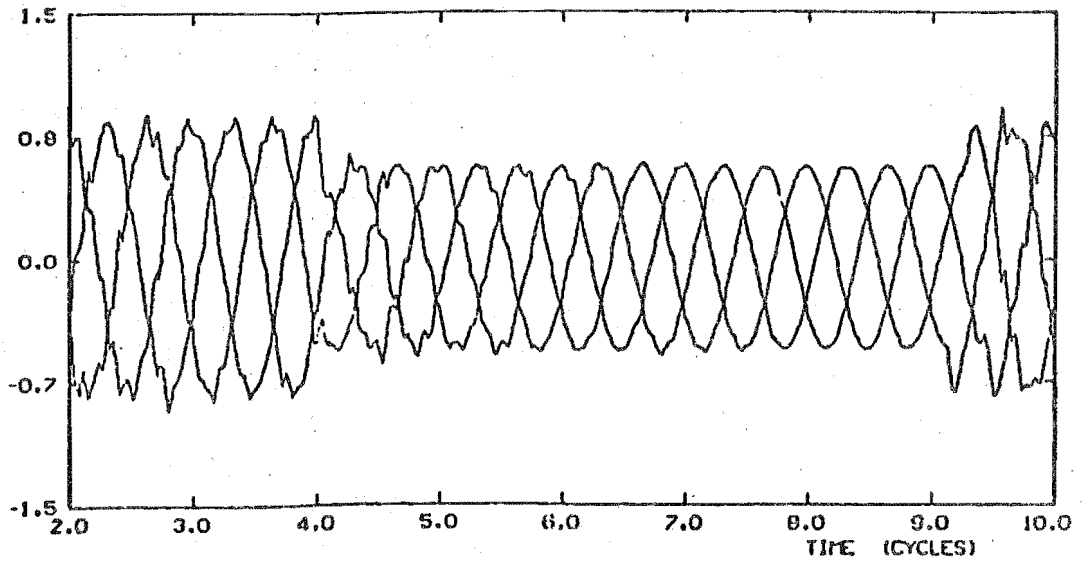

Fig. 4.10(e) 321 RECTIFIER AC VOLTAGES

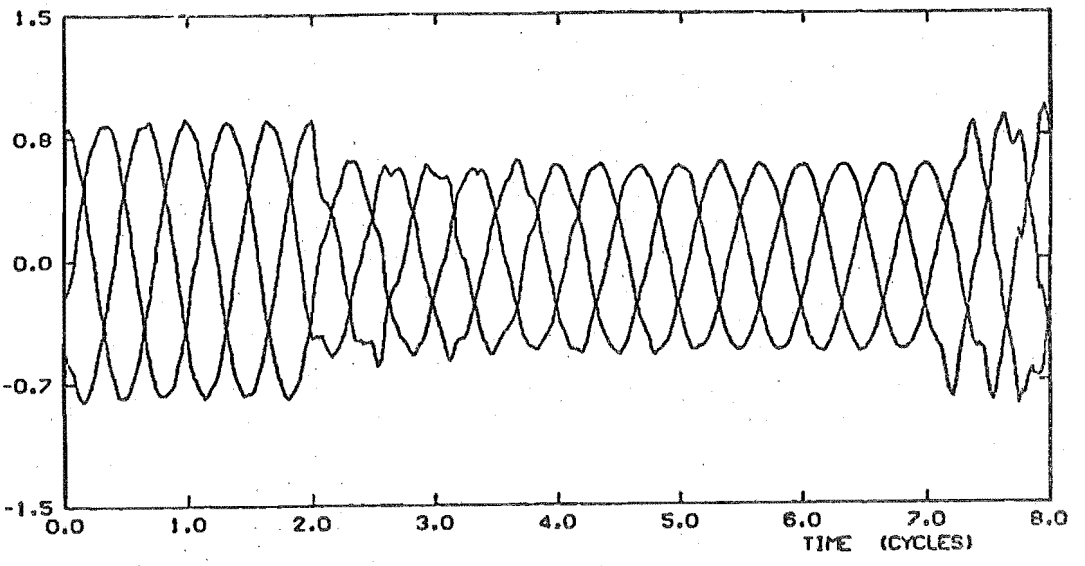

The rectifier direct currents for each case bear a close resemblance, and the rectifier a.c. voltage profiles are practically identical throughout the study period. The behaviour at the fault bus, i.e. fault current levels and recovery voltage behaviour, is also identical for each case. Therefore the waveforms at the fault end are not significantly affected by slight differences in control action at the remote convertor.

Use of a simplified invertor end representation for rectifier end faults is therefore limited by extinction angle measurement errors, which can cause discrepancies in convertor response. The use of the simplified model for a rectifier fault as severe as this is therefore not justified.

However in the case of a mild invertor end fault, this particular limitation will not occur since CCC at the remote rectifier does not require explicit angle measurement relative to a.c. voltage waveforms. The control action at the remote rectifier must, however, be sufficiently minor to not create waveform distortion.

4.6 TIME VARIANT EQUIVALENTS

4.6.1 Effects of Time Variant Thevenin Equivalents

The a.c./d.c. fault study programme, with quasi-steady state d.c. link representation, uses impedance values which are selected to match the time at which calculations are to be made; e.g. for a study in which a circuit breaker will clear the fault after 5 cycles, the simulation uses transient reactances for synchronous machines to obtain information at the breaker operating time. Therefore the Thevenin equivalents derive their numerical values from a fixed reactance system model, the value of the reactance depending on the type of reactance used for the synchronous machines.

However, a dynamic analysis should accurately model the changing state of the system. The use of constant Thevenin equivalents throughout the full study period will not be realistic. They must instead include the time

response of generators throughout the network, since, in the case of a major disturbance, machine effects may be appreciable. This requires a time variant Thevenin equivalent for the network, which can only be obtained from a simulation in time, since a single time solution, such as performed by the fault study programme, can only provide equivalents valid at that single time.

The multimachine transient stability programme used at the University of Canterbury is suitable for the simulation in time of a.c./d.c. systems under a.c. or d.c. faults (Arnold 1976, Turner 1980). The stability programme represents the a.c. system fully, with the d.c. link represented by a quasi-steady state model as a first approximation. At each integration step of the transient stability programme (approximately 10 msec), the full a.c. network is reduced to provide a Thevenin equivalent at each d.c. link terminal. The equivalent at each time step is thus a reduced representation of the a.c. system as seen from the convertor's a.c. busbar, and will include all associated generator effects.

The transient stability study will therefore produce a time variant sequence of network equivalents, the variation of which will be a function of the disturbance investigated. To provide explicit representation of the fault bus, a third Thevenin equivalent is also obtained at each integration step of the transient stability study, by looking back into the a.c. network from that point, in the same manner as the fault study programme did. This is conveniently arranged, since basically each transient

stability solution uses the same set of equations as the fault study programme. Therefore for a two terminal d.c. link, three time variant network equivalent sequences are provided by the stability programme.

The equivalents obtained from the transient stability simulation of the fault condition, are derived using a quasi-steady state approximation to the actual d.c. link behaviour. An improvement of this approximation may be obtained by an extension of the interaction between the dynamic analysis and transient stability programmes. The results from the dynamic analysis can be transformed back into a suitable form for a more accurate transient stability analysis by the following process.

At each integration step of the transient stability study, the dynamic simulation results are processed to provide a.c. power and voltage specifications at the link terminals (Turner 1980). In this way the quasi-steady state approximation to d.c. link performance is replaced by a more accurate representation of the link performance for the purpose of a further transient stability analysis. Consequently, further iterations can be made between the two programme studies to improve convergence between them, as detailed in Fig. 4.11, where each loop indicates in effect an iterative interaction between the two programmes. Obviously, repeated iterations would be very costly.

In order to determine the accuracy of the initial Thevenin equivalents, which were based on a quasi-steady state d.c. link model, two iterations were performed for a severe invertor fault case.

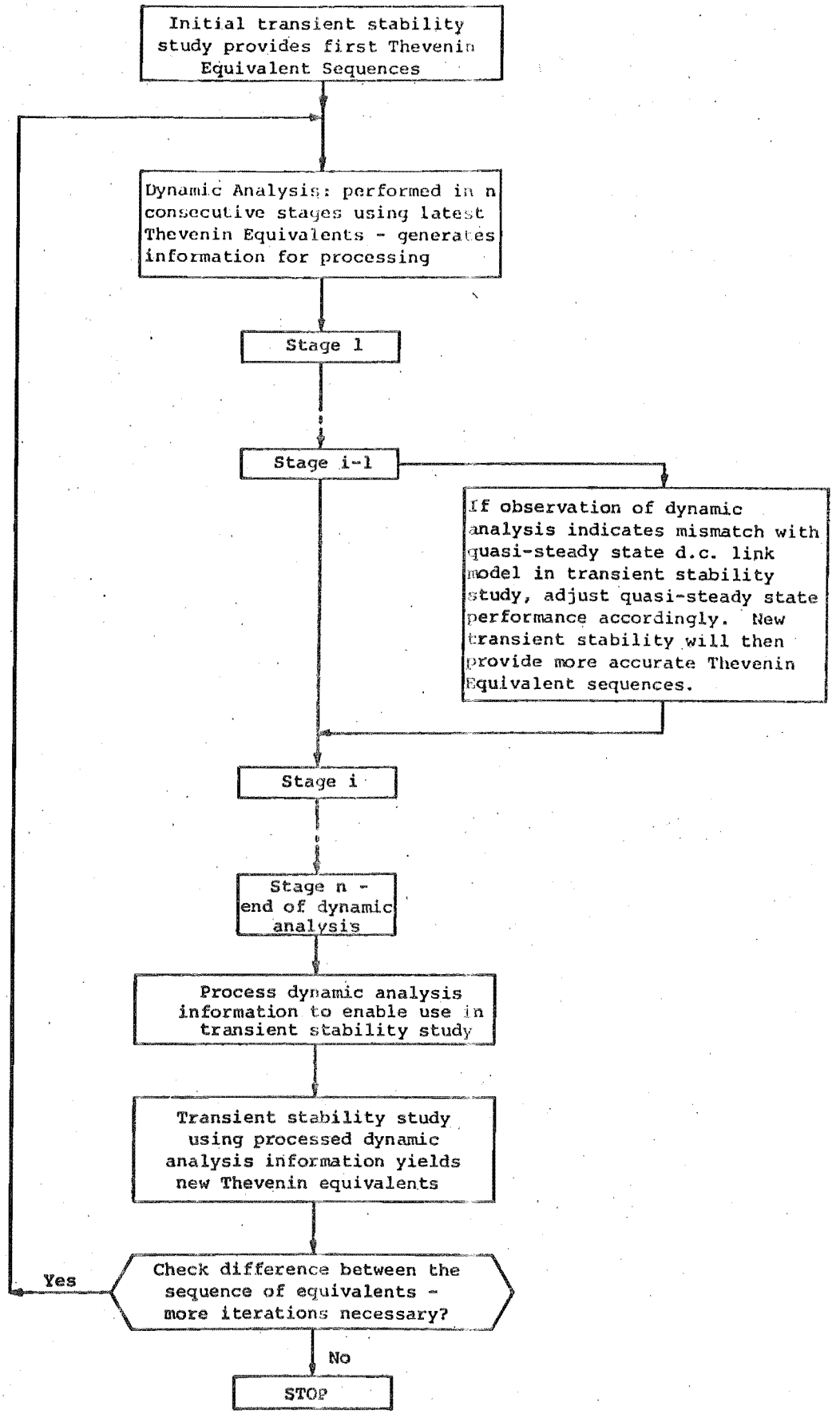

Fig. 4.11 Flow Diagram of Iterative Interaction Between Dynamic Analysis and Transient Stability Computer Programmes.

Inspection of the Thevenin equivalent sequences obtained showed differences of less than 1%. Hence the error in using a Thevenin equivalent determined using the quasi-steady state d.c. link representation, compared with an iterative process, will, in general, be much less than 1%. For the purposes of providing accurate indications of the behaviour of the a.c. systems, in the form of time variant Thevenin equivalents, the quasi-steady state d.c. link approximation has proved to be more than adequate.

In addition, it is possible to observe the trends as a dynamic analysis progresses through consecutive stages, and if necessary, to interactively modify the performance of the quasi-steady state d.c. link model over the period already dynamically simulated, so as to match more closely the dynamic simulation results (see Fig. 4.11). This then provides an updated sequence of time variant network equivalents which can be used in succeeding stages of the dynamic analysis. Although several short duration transient stability runs may be required with this approach, they are less expensive than the alternative, which involves processing the dynamic analysis data as well as performing a transient stability run. In addition the former approach minimises the dynamic analysis computation.

In cases where the full a.c. system is represented, i.e. an equivalent representation is not used, each machine may be represented by a time varying equivalent, or in the case of a system dominating machine, by its full transient equations.

4.6.2 Incorporation of Time Variant Network Equivalents

In the presence of multibridge HVDC convertors, the simulation of waveform dynamics requires a very small integration step (of the order of 0.1 msec). On the other hand the transient stability programme, used to determine the generators' response during disturbances, provides reliable information with integration steps of 10 msec, i.e. one for every 100 dynamic simulation steps.

In the transient stability programme, at each time step, gradual changes of a.c. system parameters from the subtransient to the transient, as obtained from the generators' response, are used to update the injected currents at the terminals of each generator. The updated current injections yield a new Thevenin source voltage, while the Thevenin impedance remains constant.

The r.m.s. magnitude (E) and phase angle (θ) of each Thevenin voltage, as calculated by the transient stability study for each time step t_j, are stored in a data file as a sequence of time variant Thevenin voltages. The rates of changes of these Thevenin voltages over each time step of the transient stability study are small enough to allow a linear interpolation to find an appropriate equivalent at each time step of the dynamic analysis, i.e. at time t_x in the dynamic analysis,

$$E_x = E_j + (E_{j+1} - E_j) \cdot \Delta t \qquad \ldots (4.11)$$

$$\theta_x = \theta_j + (\theta_{j+1} - \theta_j) \cdot \Delta t \qquad \ldots (4.12)$$

where $$\Delta t = (t_x - t_j) / (t_{j+1} - t_j) \qquad \ldots (4.13)$$

and $$t_j \leq t_x \leq t_{j+1} \ .$$

The dynamic analysis then calculates instantaneous phase values for each Thevenin equivalent source voltage at t_x from these quantities, by

$$\begin{aligned} e_a &= E_x \cos (\theta_x + \omega t) \\ e_b &= E_x \cos (\theta_x + \omega t - 120^\circ) \\ e_c &= E_x \cos (\theta_x + \omega t + 120^\circ) \end{aligned} \qquad \ldots (4.14)$$

The necessary modifications to the overall programme control, illustrated in Fig. 3.1, to incorporate a facility for time variant network equivalents, are illustrated in Fig. 4.12.

Careful alignment of the transient stability data file with the dynamic analysis is necessary to correctly identify fault application and removal times. An initial solution at t = 0 by the transient stability programme, which yields information in the form of a load flow, provides the initial Thevenin equivalents. To shorten the establishment of pre-fault initial conditions, the reference angle in the a.c. system(s) is adjusted so that the run begins within a commutation-free period (see Section 3.2.1). Thus all future angles obtained from the transient stability data file must be similarly adjusted.

The dynamic initial conditions are obtained using the constant initial Thevenin equivalents. Fault application initiates the process of obtaining the time variant Thevenin equivalents from the transient stability data file, as described above.

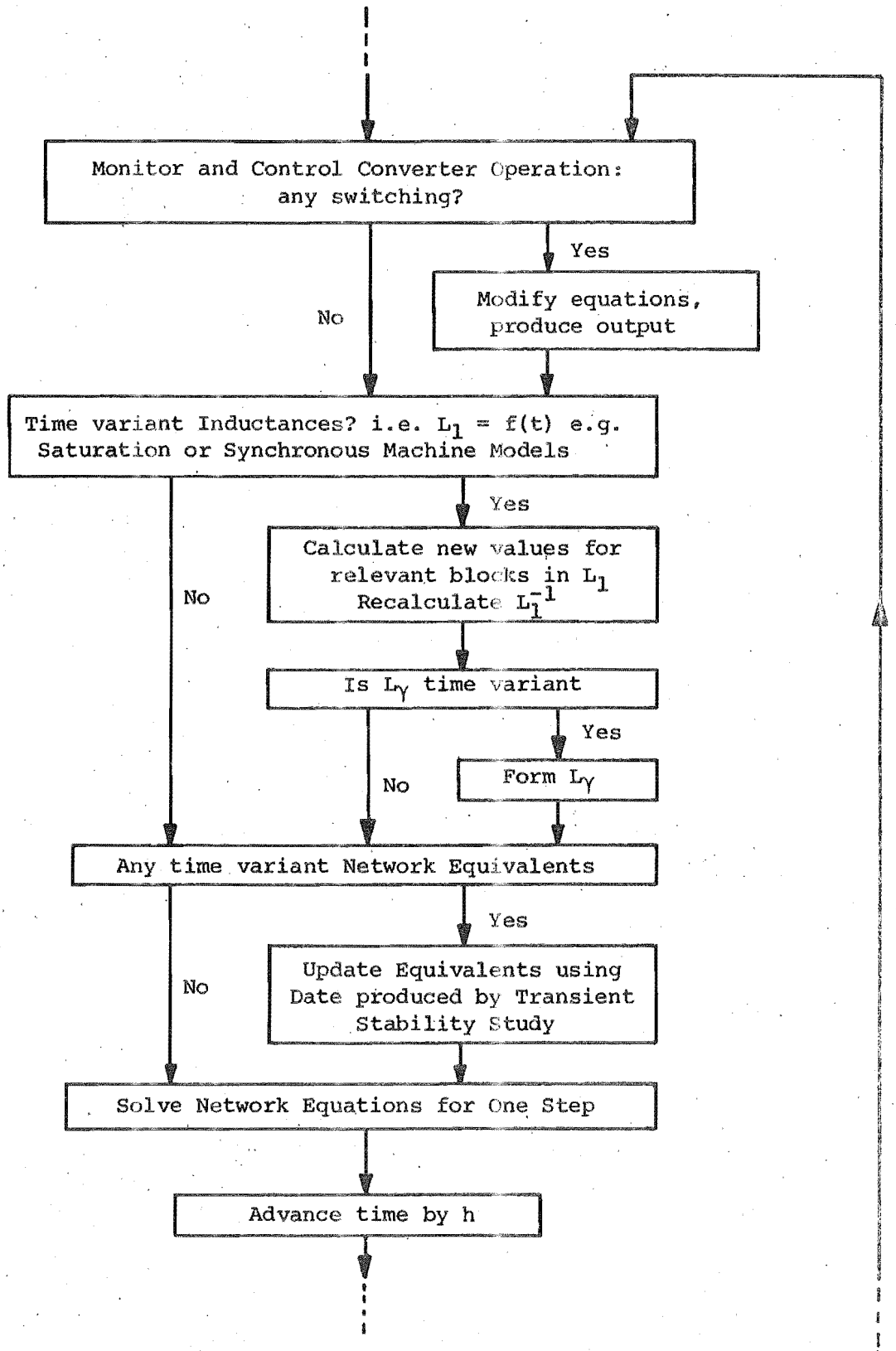

Fig. 4.12 Modification to Programme Control Flow Diagram to Accommodate Time Variant Thevenin Equivalents and Transformer Saturation

If the dynamic analysis is done in stages, as described in Section 3.6, the stage durations must be matched to multiples of the transient stability integration time (10 msec), so that a new equivalent is available to initiate the next dynamic analysis stage.

Since circuit breaker operation will be spread over approximately one half cycle (3 phase fault), a nominal fault clearance time has to be used in the transient stability programme. As a first approximation this gives a reasonably accurate indication of the a.c. system's response to fault clearance. Again, further iterations of the loop indicated in Fig. 4.11 may be used to improve accuracy, although this has not been found necessary.

A consequence of using a time variant equivalent is that frequency deviations occur as the a.c. system(s) swing. Provided control information in the form of I_d, dI_d/dt (both non-zero) and δ_i (from cross-overs) is still available, this will not cause any problems. However α must be measured from the cross-over of voltages (as for δ), if a correct indication of the absolute value of firing angle is required.

Alternatively a reference to the system frequency may be formed so that distortion of the a.c. voltage waveforms does not confuse the firing control pattern when viewed as an absolute firing angle (α). The system swing is then used to modify the interval between firings (ΔF_i), which are 60^o in the steady state. Under disturbed conditions the interval will be ($60^o + \Delta P_i$). To compensate for frequency shift the interval will become

$$\Delta F_i = (60^o + \Delta P_i) \cdot (1 + \Delta\theta/180^o) \quad \ldots (4.15)$$

where $\Delta\theta = \theta_{j+1} - \theta_j$ is the change in Thevenin source angle over the relevant transient stability step. This may also be used to yield a value of α relative to the actual a.c. voltage waveforms.

4.6.3 Results

Two cases were studied to demonstrate the use of time variant equivalents. These were compared directly with a time invariant solution in each case. To offer a wider range of comparison, different time invariant models were used for the two cases. In the first case, the system model was formed using the system generators' subtransient reactances. In the second case, transient reactances were used.

From previous results (Section 4.5), it can be predicted that with a time invariant representation, the fault current level will remain essentially constant throughout the fault period, apart from the effects of d.c. offset related to time of fault occurrence. This will be in contrast to a time variant representation, where a decay pattern relating to subtransient/transient decay effects should be exhibited.

The actual level of fault current depicted in the time invariant cases will be dependent on the generator reactances used. Subtransient values will result in higher levels than a transient reactance model would. For this reason, measures of fault current levels with a time invariant representation can only be done at a time commensurate with the generator reactances used.

4.6.3.1 Invertor End Fault. In order to investigate a particularly severe fault, a three phase fault at the invertor a.c. busbar was simulated. To retain sufficient voltage for valve turn-on, the fault impedance was selected so as to reduce the terminal voltage to approximately 10% of nominal.

As expected, there were significant differences between study 311 (invariant) and study 312 (time variant), since this particular fault is a severe one, which causes the loss of a major power source to the invertor a.c. network. Figs 4.13(a) and (b) indicate the differences in fault current levels. The time variant case shows the natural decay of the envelope of fault current. Closer investigation also shows that the magnitude after five cycles (at time of clearance) is significantly smaller, the r.m.s. magnitude being 24 p.u. compared with 50 p.u.

Fig. 4.13(a) 311 AC FAULT CURRENTS

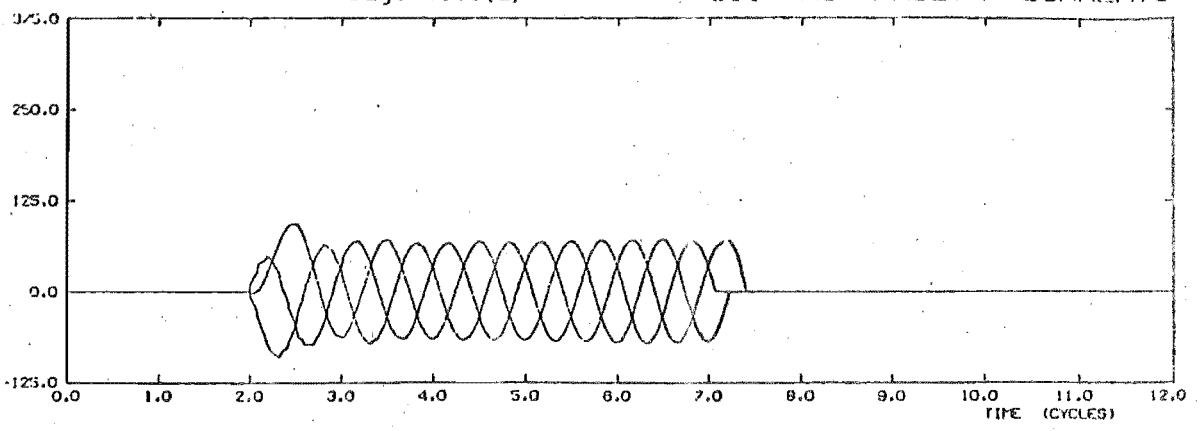

Fig. 4.13(b) 312 AC FAULT CURRENTS

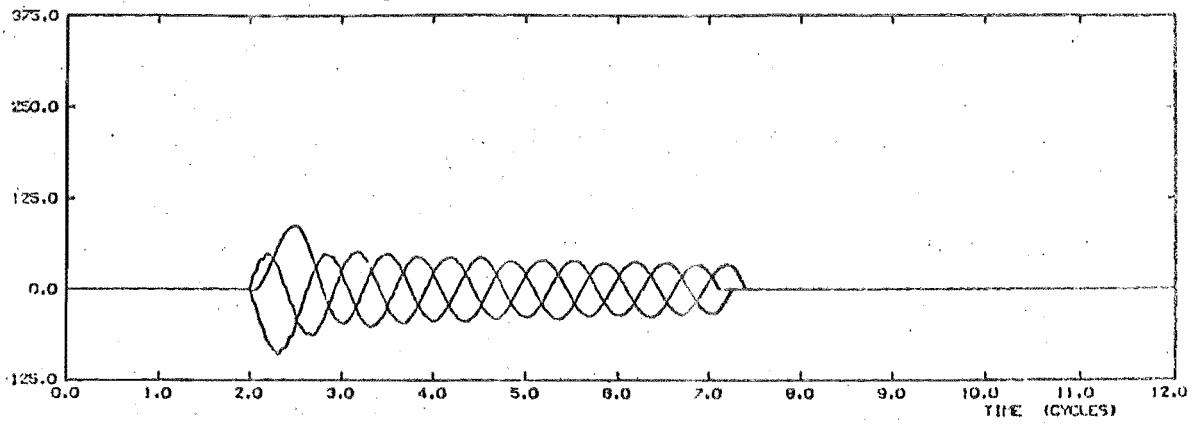

When comparing the case in Section 4.5.3, which used time invariant transient reactances, with the time variant case here, it was seen that the levels of fault current at breaker operating time were nearly identical, since the equivalent used in the former is based on the system equivalent at that time. The use of a time invariant subtransient equivalent is, however, more appropriate in terms of protection ratings, without giving an indication of the fault level at breaker operating times. The use of the time variant equivalent combines both these effects, giving an accurate dynamic analysis.

The decay (apart from d.c. offset decay) is a direct result of the reducing magnitude of the Thevenin source voltage at the invertor, which represents the normal time response of the system's generators. From an initial value of 1 p.u. this reduces to 0.5 p.u. after five cycles. This is depicted in Figs 4.13(c) (magnitude) and (d) (phase angle), which indicate the equivalent sources for each network.

Fig. 4.13(c) 312 THEVENIN VOLTAGES

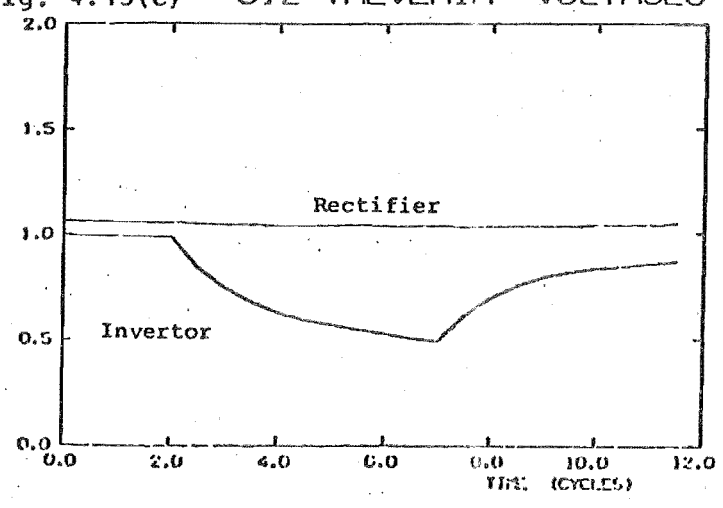

Fig. 4.13(d) 312 THEVENIN ANGLES

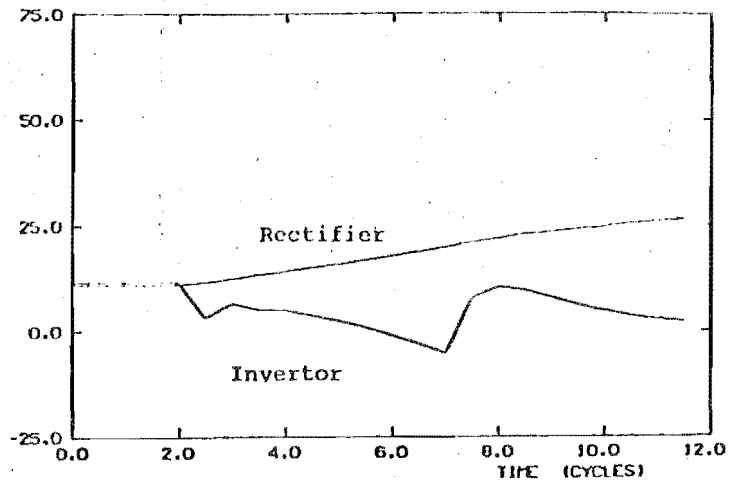

This decay in Thevenin source voltage results in reducing fault current levels and decaying a.c. voltage waveforms at the invertor terminal. The a.c. voltages (Figs. 4.13(e) and (f)) show the differences also, with waveforms (f) indicating a reducing magnitude through the fault period. Of significant interest is the behaviour in the post fault period.

Fig. 4.13(e) 311 INVERTOR AC VOLTAGES

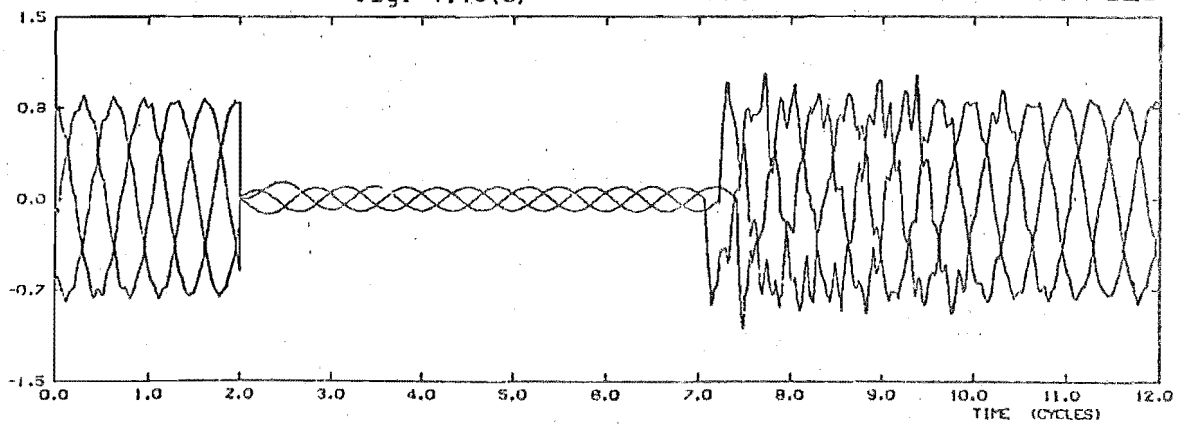

Fig. 4.13(f) 312 INVERTOR AC VOLTAGES

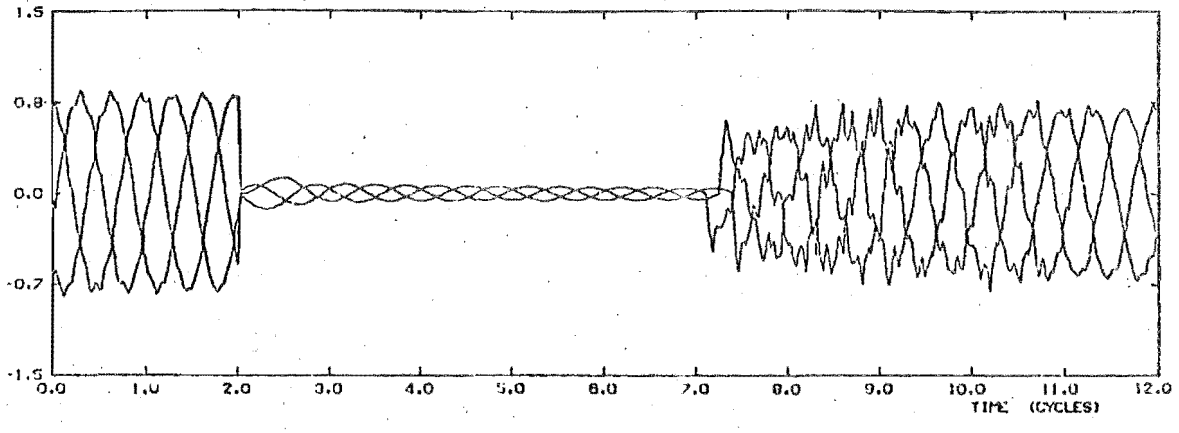

As seen in Fig. 4.13(c), the recovery of the invertor's a.c. source voltage is gradual. Therefore, while voltage levels much in excess of the steady state values are experienced during fault recovery in the time invariant case, this does not occur with the time variant model.

The behaviour of the d.c. link is similar for the initial period. However when the frequency shifts become significant, the timing of calculations of firing corrections, which occur at voltage cross-overs, is altered. As a result different control action is experienced, which leads to a different pattern in the link behaviour. This is indicated in Figs 4.13(g) and (h), which show the d.c. powers in the two cases. The gradual recovery of the invertor source voltage is effected in the gradual recovery of d.c. powers in the time variant case, compared with the relatively abrupt change in d.c. powers in the invariant case.

Fig. 4.13(g) 311 CONVERTOR DC POWERS

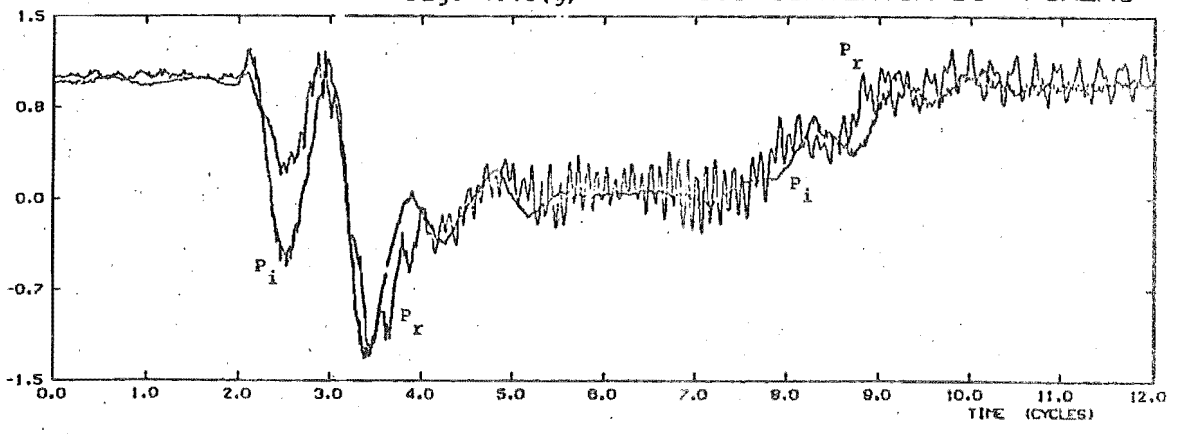

Fig. 4.13(h) 312 CONVERTOR DC POWERS

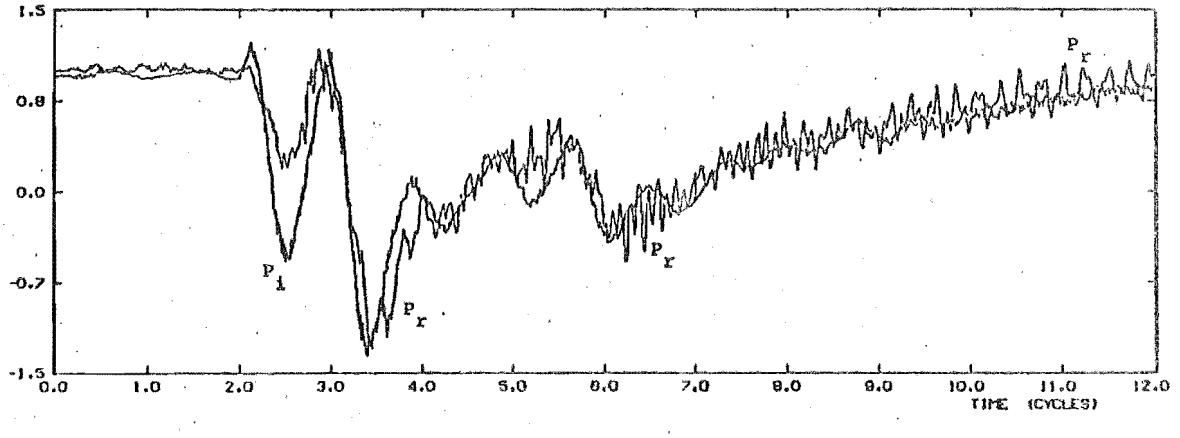

As seen in the results of Section 4.5, considerable distortion is noticeable at the rectifier end. There is little change in source or terminal voltage magnitude there, and the occurrence of overvoltages and distortion is linked closely to the control action of the link. To obtain correct values for these effects, a time variant equivalent must be used.

4.6.3.2 Rectifier End Fault. A three phase fault which was expected to reduce the rectifier a.c. voltage to approximately 65% of nominal was simulated, and the results are illustrated in Figs 4.14(a) - (f). This fault will not have such a severe effect on the d.c. link as did the fault in Section 4.6.3.1.

Fig. 4.14(a) 321 AC FAULT CURRENTS

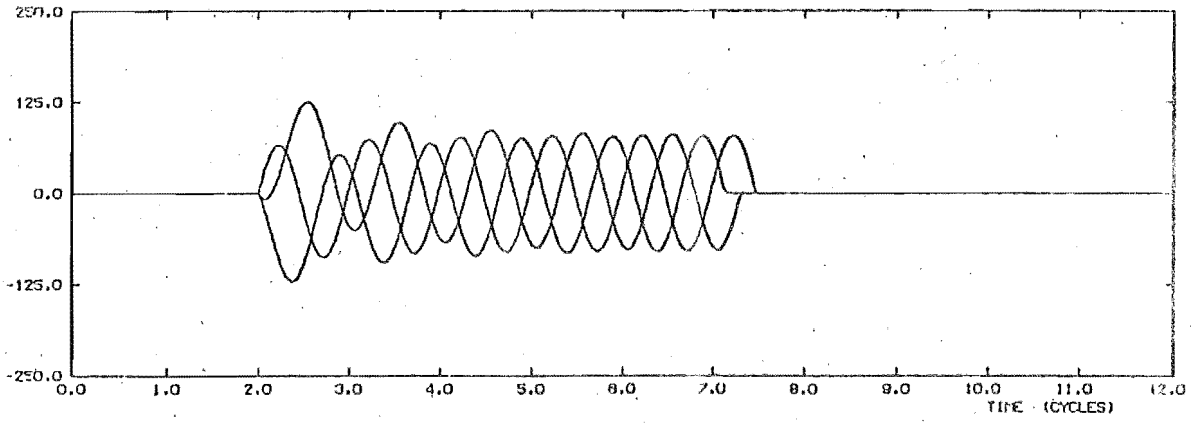

Fig. 4.14(b) 322 AC FAULT CURRENTS

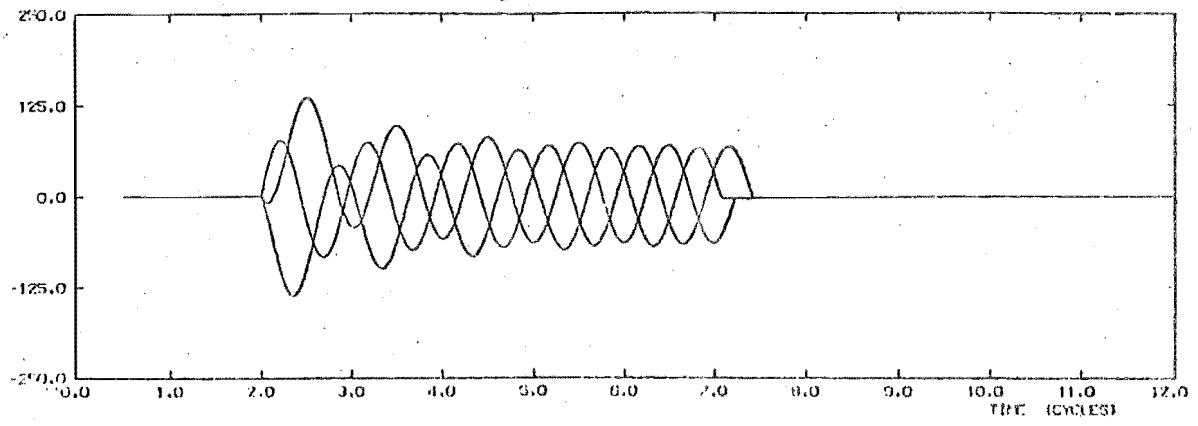

The time invariant case (321) was modelled using a transient reactance model for the a.c. systems. The fault current patterns (Figs 4.14(a) and (b)) are dominated by a d.c. offset, which is due to the instant of switching. Closer investigation showed that fault occurrence coincides with one of the phase voltages being at a maximum, which results in the fault currents of the other two phases having equal and opposite d.c. offsets. By breaker operating time this offset has practically disappeared.

As for the invertor fault (Section 4.6.3.1), post fault recovery showed a gradual rather than instantaneous increase in the phase voltage levels at the fault and rectifier buses for the time variant case (Figs 4.14(c) and (d)).

Fig. 4.14(c) 321 RECTIFIER AC VOLTAGES

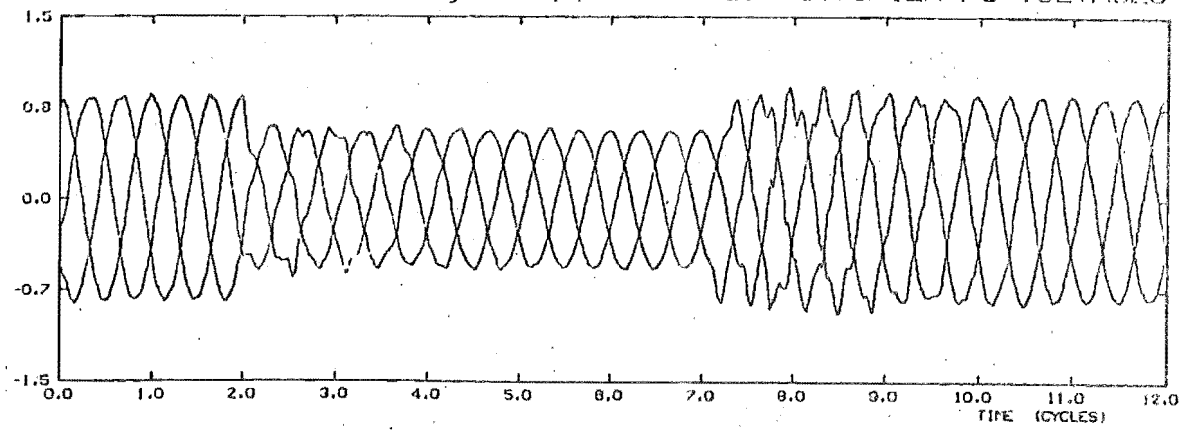

Fig. 4.14(d) 322 RECTIFIER AC VOLTAGES

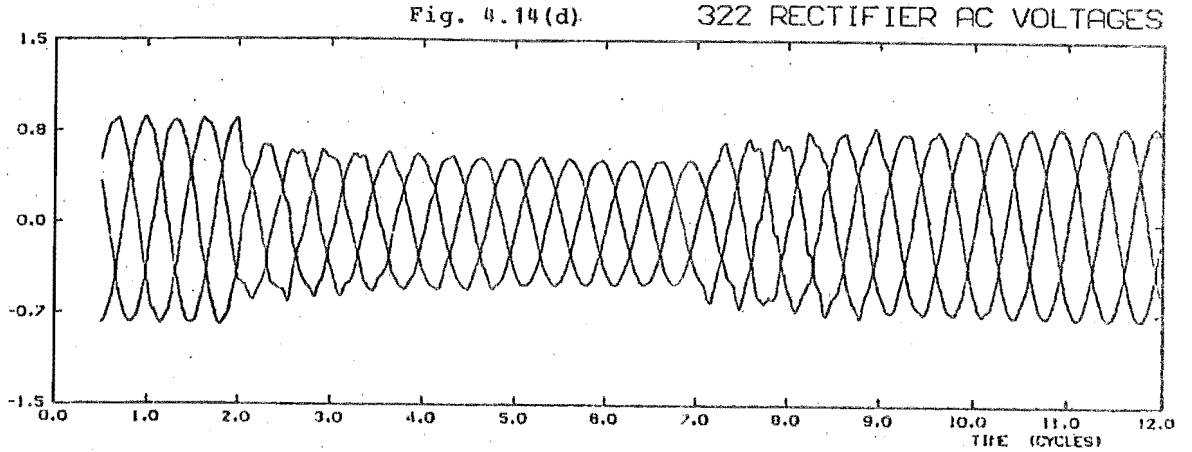

Throughout the fault period, the behaviour of the d.c. link is similar for each case, with rectifier operation at α^{min}, and the invertor controlling current.

This behaviour is sustained post fault, but with the difference that the time variant model has a gradual increase in rectifier a.c. voltage.

Fig. 4.14(e) 321 CONVERTOR DC POWERS

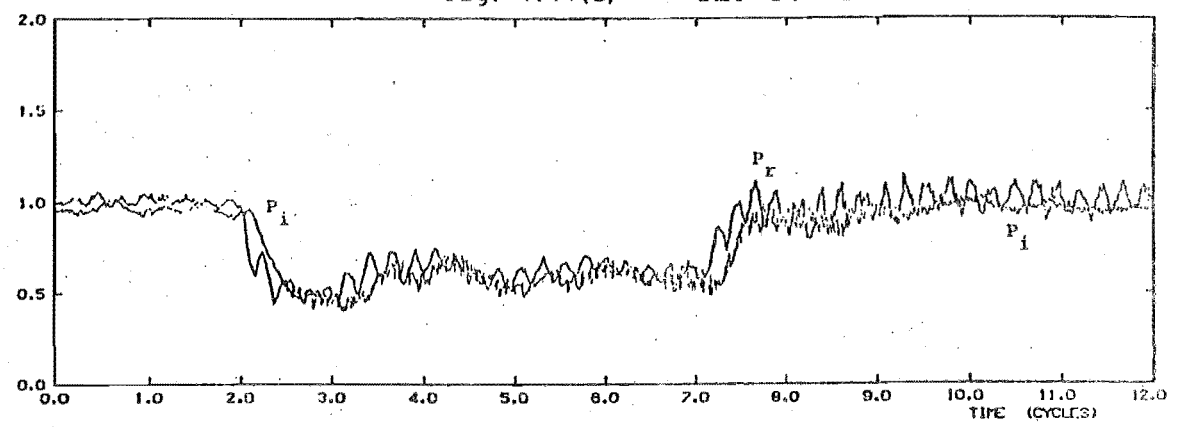

Fig. 4.14(f) 322 CONVERTOR DC POWERS

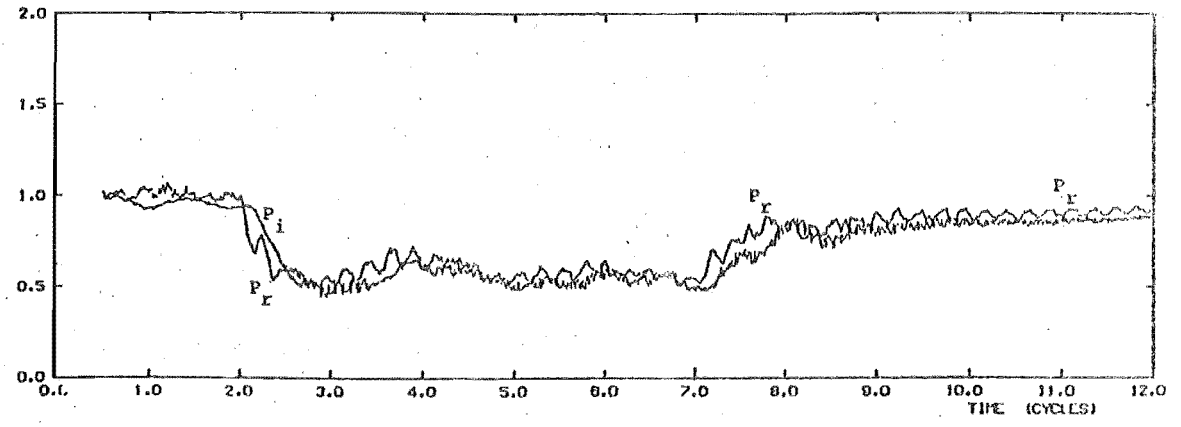

As a result, the invertor continues to control link current, so that the direct current level is equal to the invertor setting. In the time invariant case, however, instantaneous voltage recovery is assumed, and so the rectifier assumes control of current at its setting. As a result of these differences in control action, actual d.c. power transmitted is substantially different in the post fault period (see Figs 4.14(e) and (f)).

As for the invertor fault (Section 4.6.3.1), because the d.c. link is of an asynchronous nature, the a.c. network which is remote from the fault, is not directly affected by the fault. Therefore the only regulation and distortion effects which occur are as a direct result of d.c. link behaviour, i.e. changes in direct current, and the control action implemented. However, as seen in Section 4.5, this can contribute to overvoltages, both during and following the fault.

4.7 TRANSFORMER SATURATION

4.7.1 Introduction

As mentioned in Section 2.2.5, an appropriate modification of the transformer inductance matrix, to take into account the magnetizing characteristics, may be used to model saturation effects. In the coupled circuit model used to represent the transformers, the magnetizing current may be directly formed by summing the instantaneous primary

and secondary currents, with the sign convention as indicated in Fig. 2.1. Multiplication by the magnetizing reactance will result in the instantaneous magnetizing flux linkage, i.e.

$$i = i_1 + i_2 \qquad \ldots (4.16)$$

$$\psi_m = L_m i \qquad \ldots (4.17)$$

where in per unit the magnetizing reactance L_m is equivalent to the self reactance (L_{11}, L_{22}) of the transformer (see Section 2.2.5).

Magnetization curves in general relate the flux linkage of the transformer core to the magnetizing current, i.e. they indicate a relationship for the equivalent instantaneous magnetizing reactance (inductance). When an overvoltage occurs, a large rate of change of flux is created. If the overvoltage is sustained, the resultant flux may be sufficient to push the transformer into the non-linear magnetization region. Typically, high voltage transformers may saturate at 10-20% above nominal flux.

A typical transformer magnetization curve (Dommel 1971 and 1975) is indicated, with hysteresis neglected, in Fig. 4.15(a). As can be seen, the knee point of the curve is tightly defined and the curve may be closely described by a two slope linear approximation as in Fig. 4.15(b), since the slope in the saturated region above the knee is almost linear, and the slope in the unsaturated region is the linear unsaturated value of magnetizing reactance.

In cases where the instantaneous magnetization curve is not defined for a particular transformer, it may be

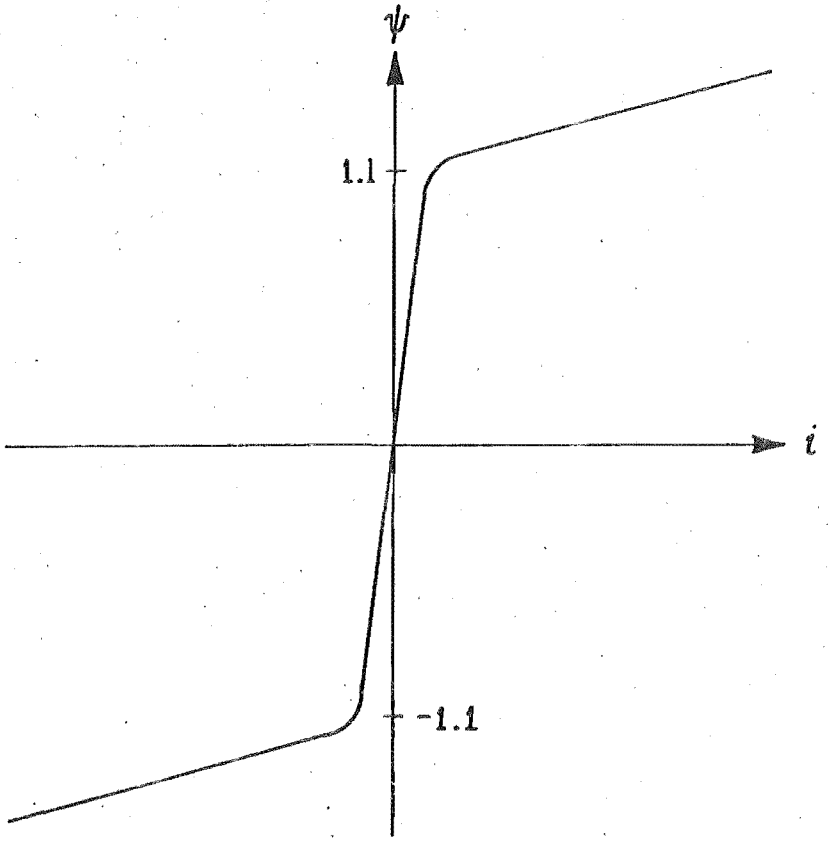

Fig. 4.15(a) Typical Transformer Magnetization Characteristic

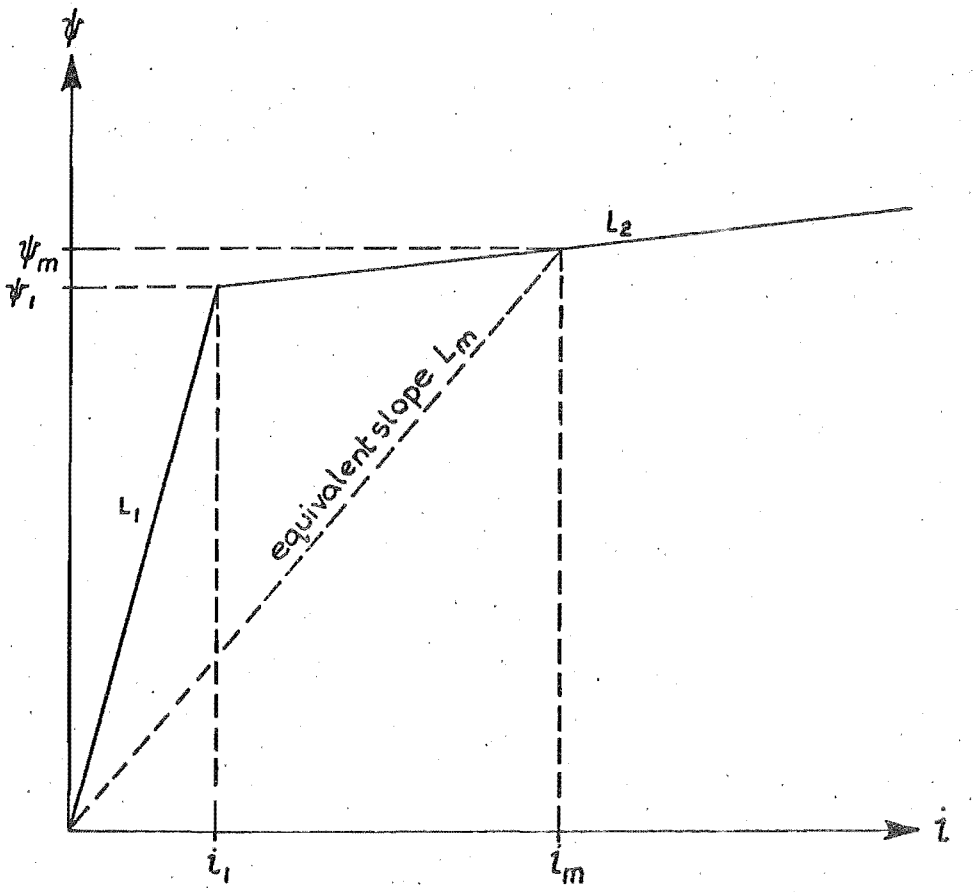

Fig. 4.15(b) Linearised Transformer Magnetization Characteristic

derived from the r.m.s. characteristics usually supplied by the manufacturers, by a conversion technique (Dommel 1975, Prusty and Rao 1980) which ignores hysteresis, eddy current losses and winding resistances.

When a transformer saturates, its operating point on the transformer magnetization curve, which may be expressed as magnetizing flux linkage versus magnetizing current in instantaneous values, is shifted into the non-linear region. In the dynamic analysis formulation instantaneous magnetizing current is directly available, whilst magnetizing flux is expressed by the time integral of the voltage impressed at the transformer terminals. The state space formulation requires constant coefficients over each integration time step, with no discontinuities occurring in flux linkages.

The product of the instantaneous magnetizing current, obtained at time t_j, using equation (4.16), and the constant value for magnetizing reactance over the previous interval (t_{j-1} to t_j), will provide an instantaneous magnetizing flux linkage (ψ_m). This value may then be located on the known magnetizing characteristic to give an updated value for the magnetizing current (i_m). Since flux linkages are continuous through each time step, a new value for the magnetizing reactance (L_m) can then be calculated, i.e. referring to Fig. 4.15(b), if $\psi_m \leq \psi_1$

$$i_m = \psi_m / L_1 \qquad \ldots (4.18)$$

$$L_m = L_1 \qquad \ldots (4.19)$$

if $\psi_m > \psi_1$

$$i_m = \psi_1 / L_1 + (\psi_m - \psi_1) / L_2 \qquad \ldots (4.20)$$

$$\text{and} \quad L_m = \psi_m / i_m \qquad \ldots (4.21)$$

where L_1 and L_2 are the gradients of the dual slope approximation.

To provide a generalised model for cases where the knee point is less well defined, a multislope linearized approximation has been developed, as an extension of the two slope approximation. Alternative numerical techniques for curve fitting have been suggested (Prusty and Rao 1980), but their complexity is not justified for dynamic fault analysis, although the techniques are amenable to the state space formulation.

Since the coupled circuit model's self reactance is based on magnetizing reactance, the transformer matrix L_t may be reformulated as in Section 2.2.5 with L_{11} and L_{22} equal to the updated value of L_m, and since mutual reactance is a function of the self (magnetizing) and leakage reactances, the latter largely independent of core saturation, then

$$L_{12} = L_{21} = \sqrt{L_{11} (L_{22} - x_{1a})}$$

Since saturation will affect each phase independently, data for each phase of the transformer bank must be stored separately. Reconstruction of the system matrix L_1^{-1} can be performed directly, due to its block diagonal structure, by simply inserting L_t^{-1} into the relevant location. If L_γ is dependent on L_t, it must also be reformulated. In the case of convertor transformer saturation, the windings affected are k branches, and L_k^{-1} and L_δ will be the affected matrices. However, the formulation for variable topology

(which segregates convertor branches) is restricted by the assumption in Section 2.5.2 which requires equal reactance matrices for each transformer phase. Therefore in the case of convertor transformer saturation, use of the formulation in Appendix A3 is preferable. The difference in cost is minimal, compared with the complications introduced by non-symmetrical transformer phases. The modifications to the overall programme control (Fig. 3.1) necessary to incorporate a facility for investigating transformer saturation, are shown in Fig. 4.12.

4.7.2 Test Results

To illustrate the effects of transformer saturation, a purely a.c. test system was devised, based on a Thevenin equivalent of New Zealand's South Island 220 kV a.c. system, with an equivalent PQ representation for the convertor load. The system was run at approximately 15-20% above nominal voltage for the following studies.

(i) Obtain steady state conditions dynamically, and then observe the effects of saturation.

(ii) Energize the transformer and connect on to the load, neglecting saturation.

(iii) As for (ii) but with saturation modelled.

The first study was conducted to illustrate the effect of overvoltages occurring in the steady state with balanced conditions, i.e. in the absence of d.c. offsets in magnetizing current. The dynamic analysis will mirror the practical occurrence of d.c. offsets in magnetizing current, as a result of the inrush current phenomena, if the study begins by sudden energization of all transformer phases

connected to the loads. These offsets have a slow decay pattern, governed by the transformer and system parameters, and to remove them entirely would necessitate a very long initial condition study.

By observing that the absolute value of magnetizing current is a maximum when the applied voltage is zero, i.e. the two are in quadrature, the presence of these offsets may be minimized as follows. Using 'point on wave switching', the individual transformer phases are connected to the source at their respective voltage peaks. As a result, the magnetizing current will be zero in theory and so the programme will correctly form this value, along with its correct derivative, so that no (little) d.c. offset results. In the absence of saturation (case 550), the magnetizing current is therefore sinusoidal, and has a very small value (typically 1% of the nominal value) with no d.c. offset. This is indicated in Fig. 4.16(a), where the offset is relatively minimal.

The magnetization characteristic in Fig. 4.15(b) is assumed to have slopes in the ratio 1:4000 (Stigant and Franklin 1973, Say 1976). When repeating the above test with the transformer bank modelled by this characteristic, the magnetizing current (case 551) is seen to be very much larger and distorted (Fig. 4.16(b)). This is due solely to the location of the saturation knee point, as the peak operating voltages are approximately 15-20% above this point. The resultant effect of the peak overvoltage is a distortion of the voltage waveforms, but to a level not easily visible.

The effect of increased magnetizing current is to distort and regulate the secondary voltages. The former is again difficult to compare, but differences of a few per cent in magnitudes are apparent.

Fig. 4.16(a) 550 MAGNETIZING CURRENTS

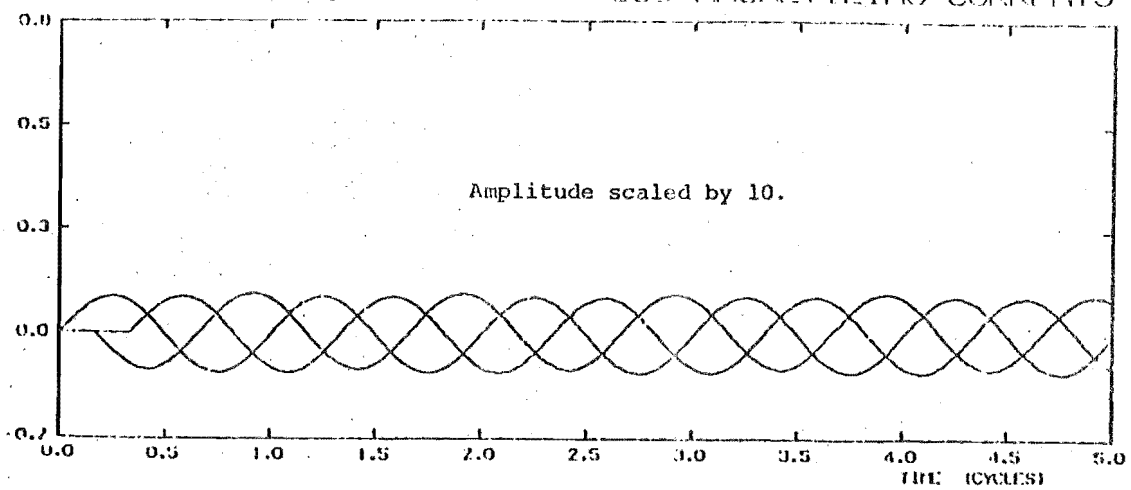

Fig. 4.16(b) 551 MAGNETIZING CURRENTS

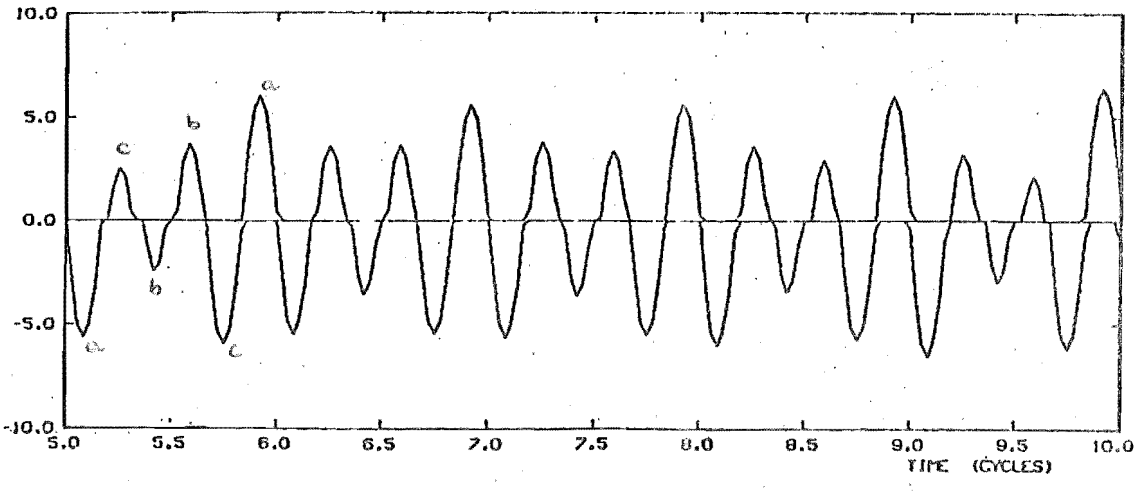

Transformer energization and load connection by instantaneous breaker closure is simulated in cases (ii) and (iii) (552 and 553 respectively), to indicate the effects of saturation (modelled in case 553) in the presence of magnetizing current offset. As discussed above, considerable d.c. offset of the magnetizing currents results from the transformer energization (Fig. 4.17(a)).

In the absence of saturation, i.e. linear magnetizing characteristic, the effect of the d.c. offset on system voltages is minimal.

However, introduction of saturation results in the non-sinusoidal magnetizing current waveshapes indicated in Fig. 4.17(b). The peak values of this current now have the same order of magnitude as the nominal load current, and the consequence is a significant distortion of the system voltages.

Fig. 4.17(a)

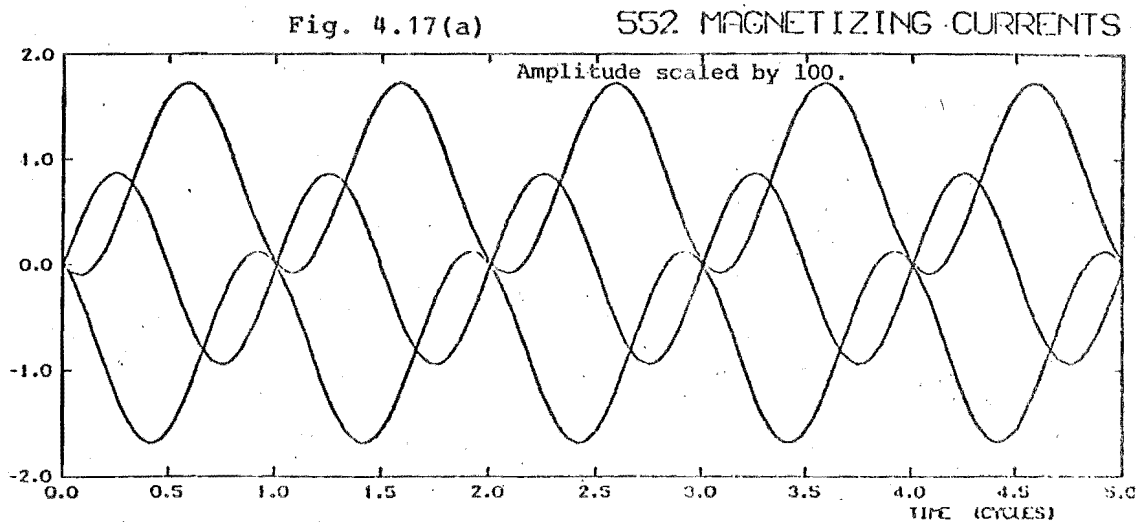

Fig. 4.17(b)

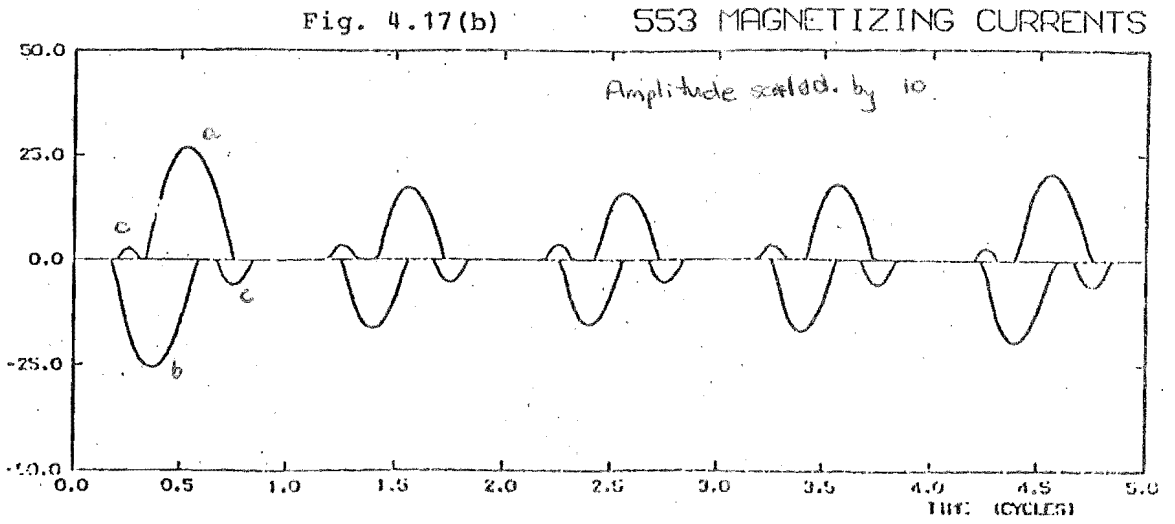

The voltage distortion on the source side of the transformer is largely governed by the strength of the system, which in this case is sufficiently large to produce only a minor effect. The resulting transformer regulation will similarly influence the secondary voltage, and Figs 4.17(c) and (d) indicate these voltages for the two cases. The distortion is least in phase 'a', which has the smallest d.c. offset, but the distortion in phase 'b' (positive half-cycle d.c. offset) and phase 'c' (negative offset) is apparent.

Fig. 4.17(c) 552 SECONDARY VOLTAGES

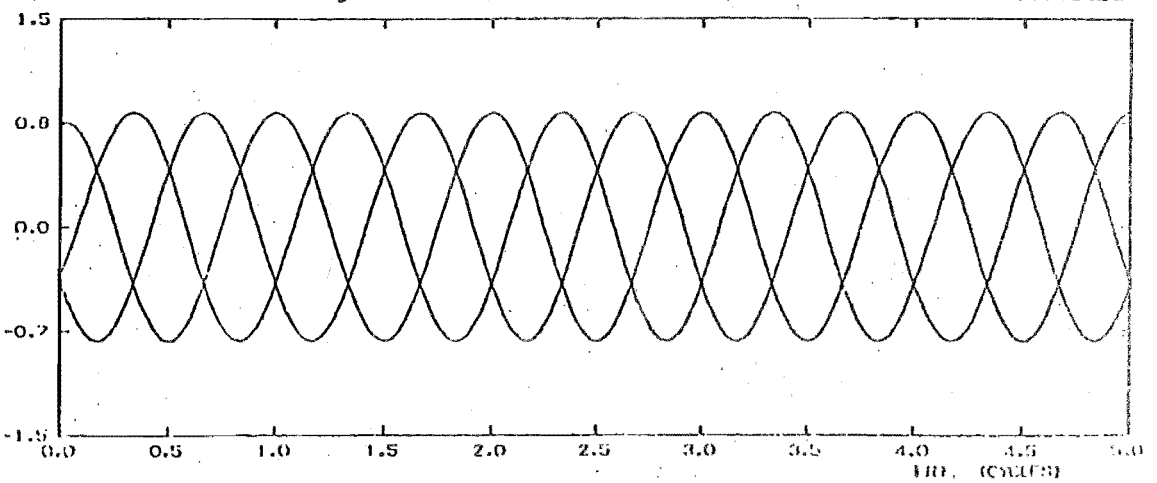

Fig. 4.17(d) 553 SECONDARY VOLTAGES

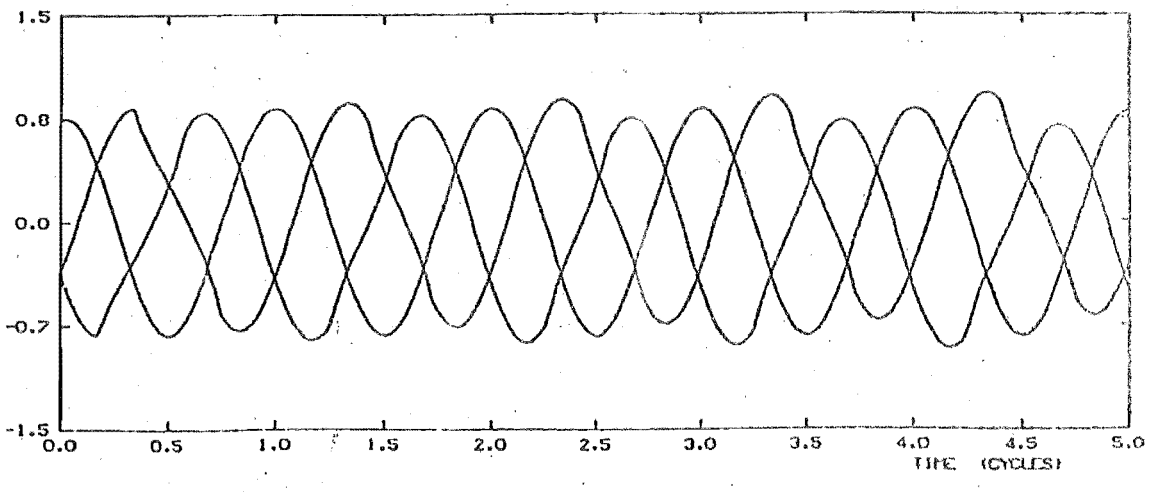

Fig. 4.17(e)

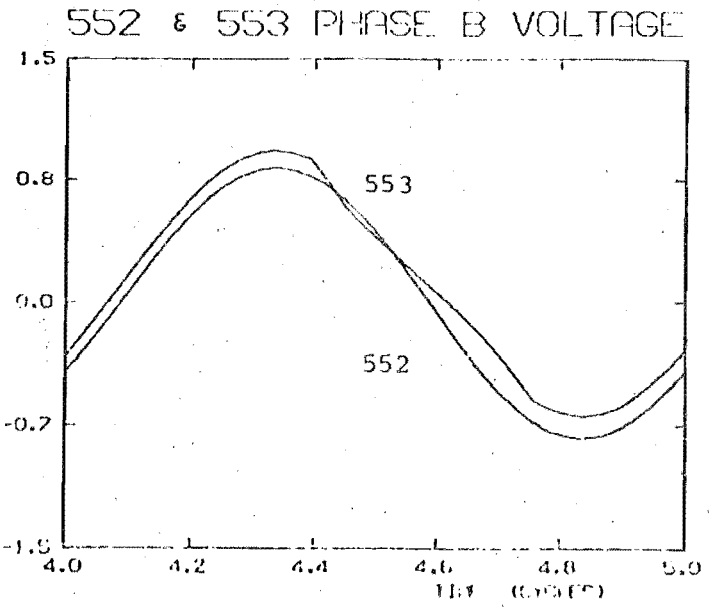

An exploded view for comparison of phase 'b' over one cycle for the two cases 552 and 553 is provided in Fig. 4.17(e). The presence of third harmonic is obvious, creating overvoltages (case 553) greater than those initially assumed in the absence of saturation (552).

4.7.3 Summary

The results obtained for the test system above indicate that the major saturation effect occurs with energization of a transformer, due to the magnetizing inrush current which, dependent on the point on (voltage) wave at which the energizing occurred, may create substantial d.c. offsets. Using a single valued saturation characteristic (i.e. neglecting hysteresis) this has been indicated by the occurrence of significant harmonic distortion of the resultant waveforms. The effects of saturation due to overvoltage as a result of normal operation, i.e. not due to switching aspects, is seen to be relatively minor, even in these cases where significant overvoltages, e.g. 20%, were used with a heavily saturated transformer characteristic above the knee point.

4.7.4 Saturation of Convertor Transformers during AC Faults

In purely a.c. systems, the recovery voltage is often strongly influenced by the transformer magnetizing current, particularly when switching is involved. Various studies and corresponding field tests (Bowles 1974, and Povh and Schultz 1978), have indicated the importance of the consideration of the inrush current phenomena. They found that in systems with pronounced resonance conditions and a low degree of damping, temporary overvoltages may develop when convertor transformers are switched in, or at fault clearance. These overvoltages may last for more than 1 sec, as explained above. Transformer saturation will produce harmonic distortion, and if this coincides with resonant points in a weakly damped system, considerable harmonic voltages may develop. Accurate representation of the a.c. system impedance at all frequencies is therefore necessary, with an appropriate representation of the system damping and transformer resistance to correctly simulate decay of inrush currents.

However the convertor transformers, in the cases studied here, were kept in service throughout the a.c. fault conditions, with the d.c. current regulators trying to maintain constant current throughout the fault. The problem of magnetizing inrush currents does not occur under these operating conditions as seen in Section 4.7.2. However, the presence of overvoltages during recovery may be sufficient, in certain instances, to cause some transformer saturation, with further waveform deterioration.

The case described in Section 4.6.3(i) was investigated for the possibility of saturation occurrence. Since the time invariant case showed a higher level of overvoltage on fault removal, it was selected. If saturation was to occur, one would expect the post fault values of flux linkage (magnetizing current) to exceed their pre-fault values. However, on plotting the magnetizing current for both invertor and rectifier transformers in case 311, it became apparent that the peak-peak values were actually smaller than, or equal to, the pre-fault period values (Figs 4.18(a) and (b). Considerable d.c. offset is present, but this is not due to re-energization problems, and is expected for a study which was based on short initial condition runs, as explained in Section 4.7.2. Taking this offset into account, it is obvious that the subsequent level of magnetizing current due solely to overvoltage levels, as measured by the peak-peak values, is insufficient to cause saturation of either transformer, even though overvoltages were indicated at both terminals.

Fig. 4.18(a) 311 MAGNETIZING FLUX (R)

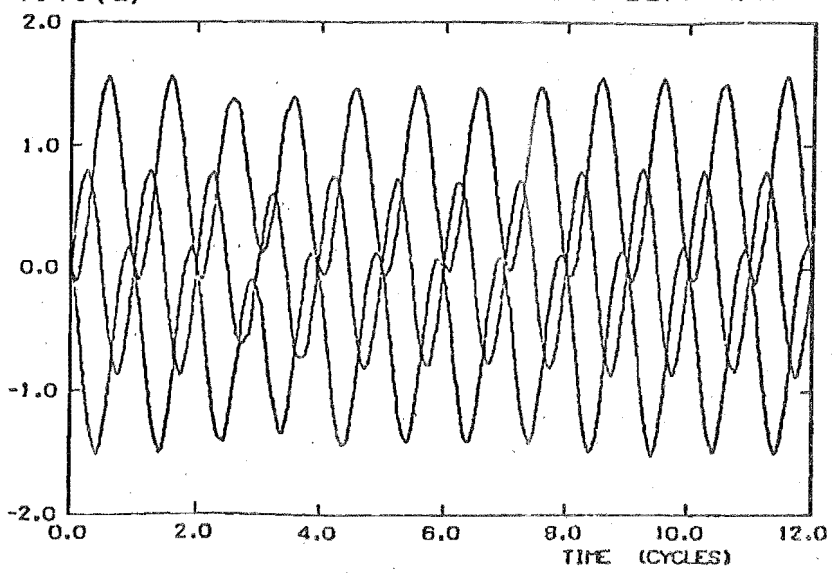

Fig. 4.18(b) 311 MAGNETIZING FLUX (I)

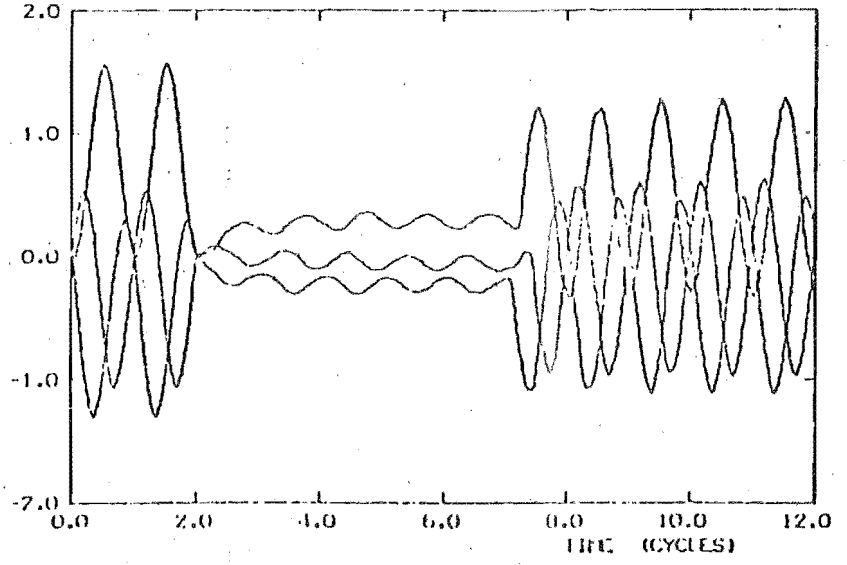

These results indicate then, that the assumption of linear convertor transformer magnetizing characteristics was justified in the studies carried out in this chapter. Indeed this example using time invariant system models was one in which the recovery voltage was significantly higher than is experienced in practice, as shown in Figs 4.13(e) and (f).

The validity of the assumption is constrained, however, to cases where the transformers are not switched. In instances involving energization of convertor transformers, accurate representation of their characteristics is necessary to account for saturation due to inrush currents.

The inrush phenomenon will not occur at the remote end, so that only unlikely overvoltage effects could cause saturation there. At the faulted end, the effect of the inrush phenomenon will be reduced somewhat by the low recovery voltages typically experienced.

4.8 CONCLUSIONS

A computation tool, which utilises a multimachine transient stability programme and a dynamic analysis programme interactively to investigate a.c. faults in a power system containing HVDC plant, has been developed. The former programme provides an accurate time response for the a.c. system, which may be used in a modified Thevenin equivalent form in conjunction with the accurate model of the HVDC plant provided by the dynamic simulation. The resulting accurate and continuous information is essential for studies of combined a.c./d.c. systems, due to the waveform dependent nature of HVDC convertors.

The results presented in this chapter have highlighted:

(i) the differences between fault currents calculated with a quasi-steady state representation of the HVDC link, and those calculated by a dynamic analysis programme;

(ii) the need for an accurate time variant model of the a.c. system, especially with regard to recovery voltage; and

(iii) the effect of saturation on fault recovery.

The advantages of the developed analysis over one which, for example, calculates fault current at a specific instant (Lake 1978) or calculates a time response based on a quasi-steady state HVDC representation (Heffernan 1977), are many. Information on waveform distortion, transient voltage peaks, recovery voltages, and a.c. system response

is provided, which is essential to the reliable performance of switchgear and protective systems.

With the prospective use of faster fault discrimination schemes (Arrillaga and Galanos 1970), which may use control characteristics best suited to the particular fault, the developed model constitutes an essential tool in the design of the proposed control, with regard to switchgear and protection ratings.

CHAPTER 5

DYNAMIC SIMULATION OF DC LINE FAULTS

5.1 INTRODUCTION

To demonstrate fully the applicability of the dynamic model to HVDC disturbances, a type of temporary fault had to be selected which would cause a reasonably long interruption to power transfer. For this reason, convertor faults e.g. valve backfire, bridge short-circuit, commutation failure and valve fire-through were not treated, since, although the valve stresses and/or overcurrents may be critical in some of these cases, the interruption to power transfer is generally small. Therefore it was considered appropriate to investigate in detail the performance of an a.c./d.c. power system which is subjected to a temporary d.c. line fault. It should be noted however, that the developed programme may be used equally to simulate convertor faults.

Most transmission line short circuits are of a temporary nature (e.g. insulator flashovers caused by lightning), and automatic recovery with only temporary interruption is possible. In the case of d.c. transmission however, the absence of circuit breakers precludes the normal a.c. transmission solution of temporary switching and auto-reclosing. With bipolar transmission, faults may involve either one or both poles and/or ground.

Large, sustained fault currents will be prevented by normal constant current control at each convertor, as their

controllers will act to maintain a nett voltage difference across the d.c. link, by driving the firing angles towards 90°. The fault current will then be limited, in the 'steady state', to the difference between the convertors' current settings (i.e. the current margin). However, transiently, discharge of the line will affect the level of fault current. Normally the combined action of the convertor controllers and smoothing reactors will limit the peak rectifier over-current (and also peak fault current) to less than 2-3 times rated current, and after 10-20 msec the fault current will settle to the 'steady state' level of the current margin, with the rectifier and invertor currents at their set values.

However this action will not necessarily be sufficient (depending on fault resistance), even in conjunction with voltage dependent current limiting, to extinguish the fault arc. For sure extinction, both the fault current and the (recovery) restrike voltage across the fault path, must be brought to zero. To achieve this rapidly, the rectifier is usually compelled to act as an invertor, so that both convertors are simultaneously acting as a sink for the energy stored in the link. This energy will thus be fed back into the a.c. networks. Some means of initiating such a protective action for d.c. line faults must be incorporated in conjunction with the normal controller operation. The duration of this emergency control, and of the subsequent time necessary for return to normal power transmission, are important for stability considerations.

The subject of HVDC line faults has been discussed in several papers, each concentrating on a particular aspect of

the disturbance, e.g. the effect of the d.c. line's configuration and characteristics, and the fault location (Hingorani 1970, Kimbark 1970), the maximum expected fault and convertor overcurrents (Peterson *et al.* 1969), and the dynamic behaviour of the convertor plant (Reeve and Kapoor 1972). However, these models are not suitable to analyse the overall fault behaviour from the time of its inception and detection to the final full recovery. A more general approach with varying degrees of system representation, depending on the information required, is described in this chapter. The proposed model is again based on the small step dynamic analysis and multi-machine transient stability computer programmes.

The basic characteristics of temporary d.c. line faults, from detection, through arc extinction and deionization, line re-energisation, and finally full power recovery, are discussed in Sections 5.2 - 5.4. The models used to represent the a.c./d.c. power system are outlined in Section 5.5, and then, using the N.Z. power system, the effects of the various system parameters on the above characteristics are investigated in Sections 5.6 and 5.7.

5.2 OVERCURRENT CHARACTERISTICS OF DC LINE FAULTS

The rectifier and fault overcurrents resulting from a line fault depend on system and fault parameters, fault timing and location, mode of convertor operation, and subsequent control action. Peterson *et al.* (1969) investigated the level of transient rectifier overcurrent by isolating several parameters to determine their effects.

Their analyses were based on a quasi-steady state d.c. representation, and ignored the effects of the a.c. system.

The assumption of a sinusoidal voltage beyond the commutation reactance is not generally valid. The increased rectifier current during the fault period will produce harmonic current imbalances in the a.c. system, which will always result in a.c. waveform distortion for an a.c. system with finite short circuit capacity. Moreover, the extra alternating current required from the a.c. system as I_d increases must be supplied from the a.c. network, which will result in further regulation of the convertor a.c. voltage. Thus a more accurate model of the a.c. network, including a.c. harmonic filters, is necessary for the correct representation of both regulation and commutation effects, as well as for waveform distortion. The use of an infinite a.c. system representation will otherwise yield pessimistic levels of rectifier overcurrent.

The presence of the smoothing reactor will limit the magnitude and rate of rise of overcurrents. Peterson *et al.* (1969) showed that saturation of these reactors under high overcurrent would dramatically increase the peak fault current. For this reason, however, smoothing reactors are normally designed to retain their nominal inductance with up to 2-3 times rated current. The effect of resistances in the convertor transformers and smoothing reactors on peak currents is small.

Since d.c. systems contain only passive elements, the main source of fault current is the a.c. system, with d.c. line discharge contributing additional fault current.

The impedance between a theoretical a.c. infinite bus and the fault location will determine the maximum fault current magnitude. Therefore strong rectifier a.c. systems will result in higher fault and rectifier overcurrents than would a d.c. line fault with a weak (i.e. low S.C.R.) rectifier a.c. system. A d.c. line fault on the line side of the rectifier smoothing reactor is therefore the most severe in terms of location, and a zero fault resistance will be the most severe in any particular location.

The initial overcurrent will be limited by the surge impedance of the d.c. line (which includes the line capacitance, inductance and smoothing inductance). Since control action is only possible at discrete intervals (every 60^{o} for 6 pulse, and 30^{o} for 12 pulse operation), even with instantaneous detection, a transient overcurrent may occur. However control action, initiated by a protection scheme, which retards α_r into inversion, will limit the maximum overcurrent level when compared to normal regulator action (CCC), since the latter will have time delays (circuit time constants) and/or gain limits incorporated in their design to ensure stable operation in the steady state.

Severe oscillations of d.c. voltage and current can occur following normal control action, due to possible resonance effects between the d.c. line and the control system. This highlights the need for an over-riding protection action to not only limit overcurrent stresses, but also to ensure rapid fault clearance and recovery. To provide back up protection, control systems are normally designed so that no more than one commutation occurs in

12 pulse operation after a line fault, before a protective action is taken by the current control system.

Rectifiers operating with minimum firing angles at fault inception will exhibit higher overcurrents than those with firing angles greater than α_{min}, since the effective voltage driving the fault is then greater. Fig. 5.1(a) indicates the effect of the rectifier delay angle, at the time of the fault inception, on the maximum level of rectifier overcurrent. These curves assume instantaneous fault detection, but with the fault applied immediately after a valve firing so that no control action can occur until the next firing instant. The levels are pessimistic in that they assume an infinite a.c. source with zero overlap (commutation) angle (Peterson *et al.* 1969) so that for 6 pulse operation

$$I_{dr}^{max} = (2 + \cos\alpha_r - \sqrt{3}\sin\alpha_r)\pi/6X_c \quad \ldots (5.1)$$

and for 12 pulse operation

$$I_{dr}^{max} = (\sqrt{2} + \sqrt{6} - (2 + \sqrt{3})\sin\alpha_r + \cos\alpha_r)\pi/12X_c \quad \ldots (5.2)$$

To correct for non-zero overlap angle, α is replaced in these equations by $\alpha + \gamma'$, where γ' is the overlap angle during the fault, which is larger than the pre-fault overlap angle. Thus for normal operation, where delay angles are usually less than 30^{o}, 12 pulse operation will have smaller overcurrents than 6 pulse operation.

Fig. 5.1(a) also applies when the abscissa angle depicts the time between fault inception and the previous valve firing. The 12 pulse curve will therefore only be

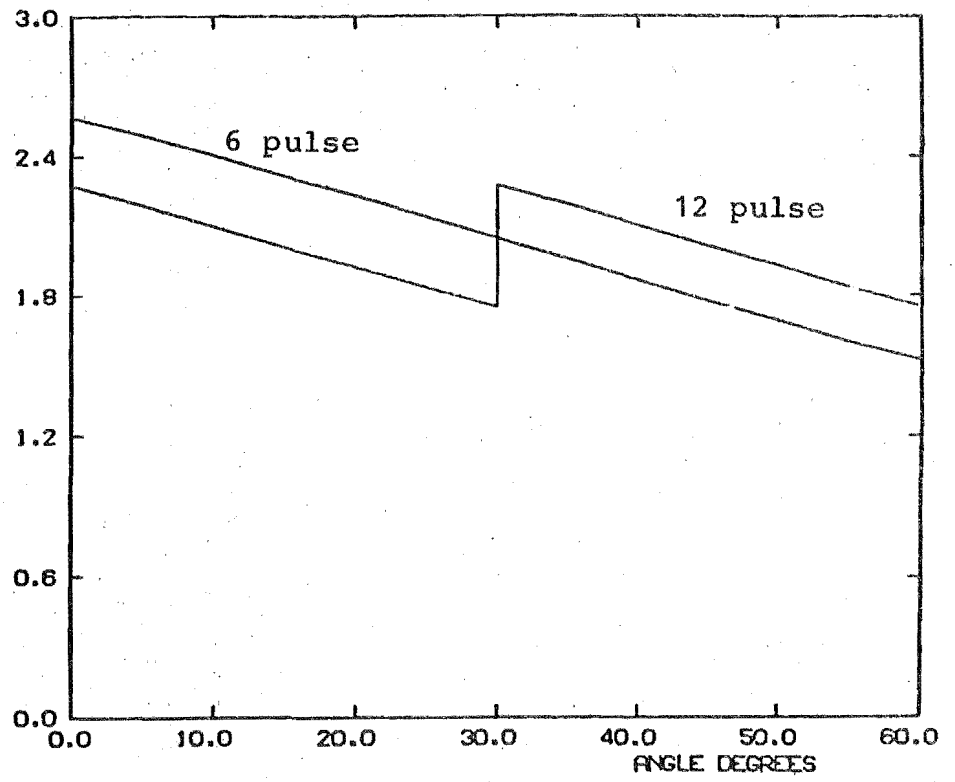

Fig. 5.1(a) Effect of Instant of Fault (and α_o) on I_{dr}^{max}

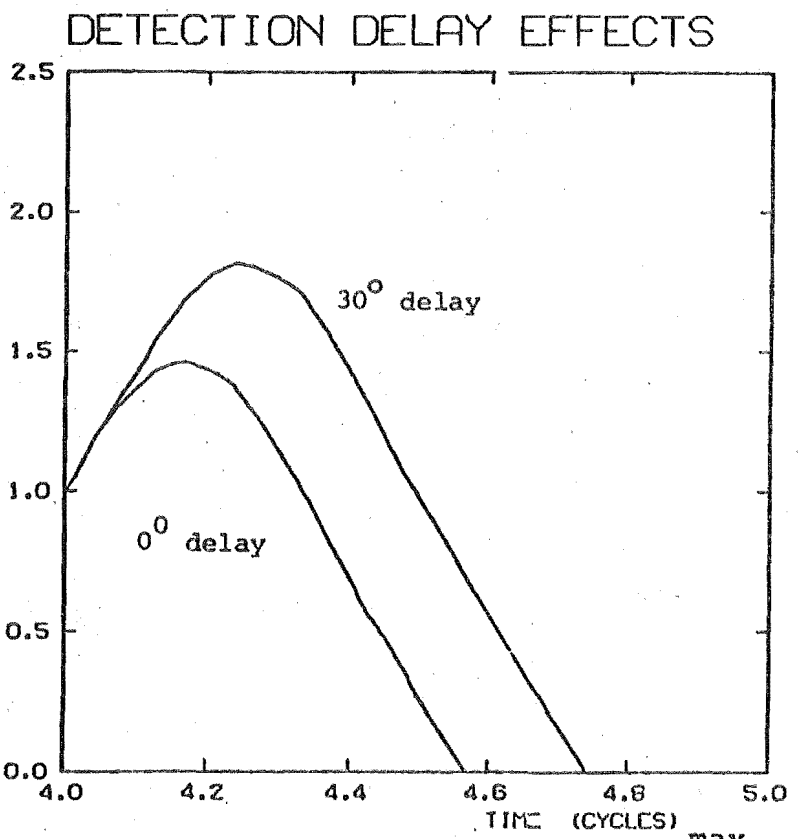

Fig 5.1(b) Effect of Detection Delay on I_{dr}^{max}

applicable from 0^{o} to 30^{o}, and thus 12 pulse operation always has a lower peak overcurrent than does 6 pulse operation. The negative slope of the curves is indicative of the time which must elapse before protective retard action of the rectifier firing angle can be initiated. Again, instantaneous detection is assumed, this time with a constant firing angle of α^{min}. Substantiation of these curves is provided by Foerst in his discussion of Peterson *et al.* (1969). The cumulative effects of initial firing angle and elapsed time before protective action becomes effective can be obtained from these curves.

The effect of non-instantaneous detection on the level of overcurrent is shown in Fig. 5.1(b) for a zero resistance earth fault on the line side of the rectifier end terminal. The nominal firing angle was 25^{o} with the fault applied 10^{o} after the last firing. Calculations based on the above idealised formulae ((5.1)-(5.2)) indicate levels much higher than those obtained by the dynamic simulation, for both instantaneous detection and for detection 30^{o} after fault application.

This indicates the need for the more accurate simulation in which the a.c. system, filters, d.c. system parameters and convertor controls are accurately modelled, in order to assess the effect of voltage regulation, commutation, and waveform distortion. Unless the simulation can accurately represent the actual timing of valve firings in relation to fault occurrence, and the subsequent effects of rapid control action associated with normal or protective action, inaccurate results will be obtained.

The interactive use of the state variable dynamic analysis and a transient stability programme provides accurate simulation of the a.c./d.c. system behaviour over the entire fault and recovery period.

The dynamic analysis requires suitable representation of practical d.c. line fault detection and recovery schemes. Similarly, accurate representation of the expected fault behaviour, including the arc characteristics, must be incorporated into the model.

5.3 DETECTION OF DC LINE FAULTS

Based on the characteristics discussed in Section 5.2, a d.c. line fault detection and protection scheme must:

(i) respond rapidly to d.c. line faults independent of convertor or plant parameters, and of fault location;

(ii) not respond to convertor faults, a.c. system(s) faults, or reduced d.c. voltage due to operational changes (e.g. step changes in d.c. voltage);

(iii) preferably involve only local detection to avoid dependence on telecommunications; and

(iv) be able to determine if convertor restart has been successful.

Various early methods of detection suffered from a variety of drawbacks (Erinmez 1971), such as confusion with other types of faults (e.g. convertor or a.c. system faults, Uhlmann 1960), or detection speeds which were not satisfactory (e.g. in the use of voltage level detection).

On the occurrence of a line fault, a travelling wave (Fortescue 1918) runs along the conductor, away from the

fault point, in both directions at equal speeds. These waves, and their subsequent reflections, create high voltage and current gradients at the convertor stations.

Since, as described in Section 5.2, the protection must be fast acting, the detection scheme must be able to identify the travelling waves set up on the transmission lines by each type of fault, and to discriminate between them.

The polarity of these travelling wave gradients, with respect to line voltage, holds enough information to determine whether the fault is bipolar or monopolar, and to indicate the pole(s) involved. In the case of a monopolar fault, travelling waves are also induced on the healthy pole by virtue of mutual coupling action. Investigations into possible overvoltage thereon, by Hingorani (1970) and Kimbark (1970), have shown that in certain circumstances the coupling action as a result of a monopolar fault may be sufficient to cause a flashover on the healthy pole. The magnitudes of overvoltages induced on the line by coupling action are dramatically influenced by the d.c. line terminations. Fault location and type, as well as line characteristics, will also affect the over-voltage magnitude at the terminals. As indicated in Section 5.2, convertor control will have no effect on the first wave reflections at the terminals, which in general involve the peak overvoltages.

Because of the d.c. link smoothing reactors, invertor faults and a.c. system changes will cause considerably lower gradients of line voltage and current at the rectifier than

will d.c. line faults, since there is much more inductance between the detection unit and the fault location. Similar discrimination is possible with current gradients, since the two types of travelling waves initiated by the fault are interrelated.

The fault resistance will also affect the travelling wave gradients. In the case of a high resistance ground fault close to the invertor end of a long line, information obtained at the rectifier end, based exclusively on voltage magnitude and gradients, may not be sufficiently reliable, since it may be indistinguishable from voltage information resulting from operational changes or a.c. faults. Resorting to comparison of current at either end is also unreliable, and would require signal transmission. The use of current gradient however, is a reliable signal which can be formed by the use of an instrument transformer (Erinmez 1971).

It was established by Erinmez (1971) that for rapid, accurate d.c. line fault detection with complete discrimination of fault locations, it is best to use the weighted sum of the direct voltage and direct current gradients at the convertors, for each pole of the d.c. line. This meant measuring

$$\eta = K_5 \, dV_{dc} / dt + K_6 \, dI_{dc} / dt \qquad \ldots (5.3)$$

which will be directly related to the travelling waves initiated by the fault, and contains information relating to the fault type, size and location. Since the terminations of the d.c. line will affect the gradients of the travelling

waves, this must be considered in setting suitable detection levels.

Also, by suitable choice of K_5 and K_6, restraints may be put on η to ensure that a monopolar fault is not seen as a fault on the healthy pole of a bipole system, due to the voltage which may be induced thereon by mutual coupling action. Of course if this induced voltage is sufficient to initiate a flashover on the initially unfaulted pole, an extremely undesirable condition, then η must be such as to initiate the detection/protection scheme associated with that pole as well. On detection of a line fault, the convertor bridges associated with the faulted pole(s) will then undergo the relevant protective action as described below.

5.4 FAULT CHARACTERISTICS

5.4.1 Arc Extinction and Deionization

Normal grid/gate pulse control techniques in an HVDC transmission system have been shown to provide the best means of clearing line faults and re-establishing normal operation. Fast convertor blocking is normally used only for internal station faults, and is not necessary for d.c. line faults, where a method of fast retardation of firing angles is most effective.

On detection of a line fault, by driving the rectifier into inversion (say $\alpha_r = 120^o$ to 135^o), the bridge side voltage will rapidly drop appreciably below the line side value, forcing the rectifier current to extinguish more quickly than it would under normal CCC

action. Similarly the drop in line voltage at the invertor due to the line fault will extinguish the invertor current quickly.

However, this condition of zero energy transfer into the link will not immediately extinguish the fault. In the case of a d.c. link such as in the N.Z. scheme, the combination of a long overhead line (with smoothing reactors) and a relatively long submarine cable represents a lightly damped oscillatory RLC circuit with a natural frequency of approximately 50 Hz. This circuit represents a significant energy storage capacity. With no external sources, i.e. once both convertors have shut down, the time for the energy in this circuit to dissipate is determined by the relative magnitude of the circuit resistances, which will be made up from three components:

(i) d.c. line resistance;

(ii) earth fault resistance; and

(iii) arc resistance.

The value of the line resistance will be known for a particular line. This value will vary a little with loading of the link, but it is sufficiently accurate to use the nominal value for its representation. Therefore to decide upon the interval necessary for complete arc extinction, the properties of the arc, as well as the specific earth resistance, must be established. In tests where a line side rectifier fault of zero earth resistance was simulated, with the d.c. line disconnected, Kohler (1967) determined the most important properties of a free burning arc, i.e. the arc voltage and the arc path deionization time. His

investigations, using current levels equal to the normal current margin (which is valid in the absence of line discharge currents), indicated that:

(i) The arc voltage drop for arc lengths of 0.4 to 2.0 metres seemed to be independent of fault (rectifier) current and of arc length, and had an average value of 2 kV per metre of arc.

(ii) The deionization time, measured from the instant when the arc current goes below 1A (0.5% rated current), must be from 20-50 msec to prevent reignition of the arc on convertor restart. Higher line recharge voltages were found to require slightly longer deionization periods.

(iii) A minimum interruption time of 100-150 msec may be sufficient to restore full d.c. transmission if the fault is of a temporary nature.

In these tests by Kohler, the d.c. line was not simulated, so that the only storage element involved was the d.c. smoothing reactor. For this reason, relatively quick extinction was achieved - of the order 20-30 msec. However when the line storage elements are represented, the extinction time will be longer, depending on the decay of the energy stored in it.

The values used for earth resistance will then greatly affect the time necessary to achieve this current extinction, since as discussed above, the magnitude of resistance in the fault circuit will determine how quickly the naturally oscillating fault voltage (and fault current) envelope decays. In general, earth resistances of at least

the magnitude of the tower footing resistance must be expected. Typically this may range from 5 ohms up to approximately 20 ohms.

Since, as detailed above, the arc voltage drop is relatively constant, the arc resistance is dependent on the instantaneous arc current. Therefore the arc resistance must be calculated as a function of the instantaneous arc current, and will range from a few ohms to a large value.

Since the fault impedance will be predominantly resistive, the fault voltage and current will be in phase. With a naturally oscillating current waveform, the period of which is dependent on the line parameters (normally in the range 10-60 Hz), there will be several instances at which the arc may extinguish. However if the voltage impressed across the still ionized arc path has sufficient peak amplitude to sustain further arc current, i.e. the voltage at the fault location is greater than 2 kV per metre of arc, then the arc path will continue to conduct current. Once the maximum value of voltage (line - earth value) is insufficient to reignite the still ionized arc path after current has passed through zero, then the current will remain at zero. The deionization time, representing the period taken for the arc path to deionize, will then be measured from this time on.

The majority of HVDC schemes, including the N.Z. scheme investigated here, have higher direct voltage and direct current ratings than the test system used by Kohler. Therefore the more conservative specification (Uhlmann 1975) of 100 msec was used as a safe deionization interval for the

purposes of this work.

After this time, the arc path will generally be sufficiently deionized to withstand normal voltage. During the arc extinction and deionization periods, the rectifier maintains a firing angle in the range $120^{o} - 135^{o}$ (nominally 125^{o} say). Normal invertor controller action (CCC) would have driven the invertor delay angle towards its minimum in an attempt to maintain link current at I_{di}^{sp}.

In the New Zealand scheme, the presence of a large capacitance (submarine cable) at the end of a long overhead line can create oscillations in link voltage. If invertor operation is only limited to a minimum firing angle of 90^{o}, these oscillations can force the line voltage to change polarity following line fault occurrence. Normal d.c. link operating principles do not permit this polarity change, since a resonance effect between the d.c. line and the control system may sustain the oscillations in line voltage. These oscillations will extend arc extinction times unless a protection scheme is implemented which overrides the invertor CCC, and maintains EAC. Such a scheme, using the same detection principle as for the rectifier end, was modelled, with the result that current extinction at the invertor was enhanced.

5.4.2 Convertor Restart

On completion of the deionization period, it is appropriate to initiate the restart procedure for the link. In most cases the line is restored to normal voltage and pre-fault power. If re-energization at full voltage is not acceptable (e.g. due to wet or dirty insulators), then a

lower voltage may be used by bypassing one or more of the convertor bridges, or by the use of constrained control action i.e. larger minimum limits on α_r and δ_i .

Various methods have been suggested for attempting resumption of normal power transfer. Basically the transmission cannot restart itself, since operation at the completion of deionization is with both convertors in inversion, i.e. $\alpha_r = 125^o$ and $\delta_i = \delta_0$. A starting order is therefore needed to remove the protective control action and to release the normal control systems of the convertors. The actual time required for the d.c. link to regain nominal voltage and current will depend on the properties of the d.c. line and the convertor controls. Generally, fast restart with a speed of power recovery conducive to stable operation, but with avoidance of overswings in both d.c. voltage and current, is required. Oscillations of these parameters may otherwise occur at the natural frequency of the line, and may be sufficient to cause arc restrike or to put additional stress on other plant. For this reason, restart by an instantaneous release of the normal controllers is not practical.

Alternative restart methods based on alteration of the convertors' reference settings can be achieved by increasing the settings linearly with time. However one must ensure sufficient current margin is maintained, which may be done either by delaying invertor controller release with respect to the rectifier, or by using a slower rate of increase in the setting at the invertor end. This will allow the line to recharge to the specified nominal voltage,

and the convertor currents to increase towards the setting.

However, with fast acting control systems this may be simplified. After completion of the deionization period, the protective control enforced at each convertor may be removed. As in the above instance, once the rectifier recharges the line, the invertor will be able to receive power, and the link current will begin to increase. Since the control system is fast acting, with corrections at every commutation, there need not be any violent overshoots in d.c. voltage or current, even though pre-fault settings are retained, provided this line recharge is done smoothly under the control of a starting control unit.

To avoid overswings in d.c. voltage (and current), the start control unit of the d.c. link may be designed to increase the direct voltage exponentially to the nominal value, with minimum overshoot, rather than as a sudden step. This unit usually operates only for start-up or re-energization following a line fault. The time constant of the exponential increase must be long compared to the natural frequency of the line (e.g. 100 msec cf. 20 msec), to ensure stable, controlled recovery of the d.c. system from the fault condition is obtained. A similar method is used in practice on the New Zealand scheme with an equivalent time constant near 100 msec.

If the line fault persists, or the arc restrikes due to inadequate deionization, the above process may be repeated a few times with increased deionization periods and/or reduced restart voltages, and then, if it still persists, the faulted pole will be removed from service.

However, if the restart is successful, normal operation will resume.

5.5 POWER SYSTEM REPRESENTATION

5.5.1 DC Network

The New Zealand Power Transmission scheme was again used as the test system. To investigate d.c. line faults a sufficient number of pi-sections must be used to accurately simulate the behaviour of the d.c. line. Since we are only interested in effects at the two convertor terminals and at the fault point which are not of a high frequency nature (e.g. switching transients, overvoltage phenomena), it was considered sufficient to use a pi-model for every 50 miles of overhead line.

Since the termination of transmission lines affects the reflection of travelling waves, it is pertinent to accurately represent the line's terminal parameters, particularly in the N.Z. case for the cable and overhead line section at the N.I. terminal.

With 4 bridges in 12 pulse operation at each convertor, on a 2-pole system, and for the purpose of analyzing a bipole fault to ground, it was considered appropriate to use a monopole equivalent of the bipole transmission line. This means modelling a monopolar line, the parameters of which are identical to an equivalent of the existing bipole line. Analysis of a single pole fault on a bipole system would require explicit representation of each pole and any mutual effects.

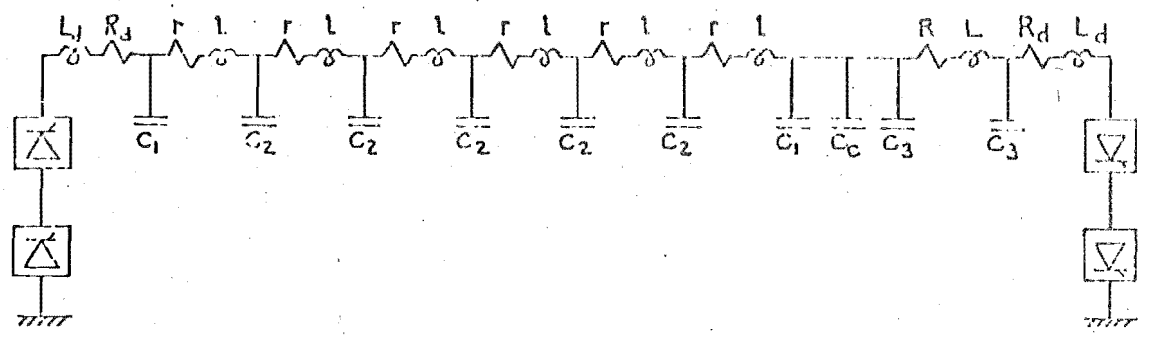

Data in per unit

Smoothing Reactors : $L_d = 0.65807$ $R_d = 0.00042$

S.I. overhead line : $l = 0.09686$ $r = 0.00509$ $C_1 = C_2/2 = 0.064752$

N.I. overhead line : $L = 0.040362$ $R = 0.00212$ $C_3 = 0.026983$

Submarine cable : $C_c = 1.599743$

Fig. 5.2 Monopole Equivalent for N.Z. HVDC Link in DC Line Fault Studies

Thus an equivalent representation of the four bridge convertors and the bipole line system of Fig. 4.2, is a model involving double bridge convertors, i.e. in 12 pulse operation, with a monopole line between convertors, as in Fig. 5.2, using the data indicated, as derived from Appendix A9.

As has been indicated in previous sections, the parameters used to model the d.c. fault are particularly crucial to the fault behaviour. The dynamic simulation permits modelling the fault by either a zero (dead short circuit) or non-zero fault impedance, by connecting a shunt element at the faulted node. The zero impedance fault is simulated by modifying the nodal capacitance C_α^{-1} accordingly. For non-zero fault resistance (or impedance), the shunt element is a non-zero resistance R_r (or impedance $R_1 + jX_1$),

which may be connected as indicated in Section 4.4.

5.5.2 AC Network

The dynamic simulation of d.c. faults is mainly concerned with the behaviour of the d.c. system. Therefore by using an equivalent representation of each a.c. network as seen from the convertor's a.c. busbars, it is not necessary to explicitly model a.c. busbars beyond those at the convertor terminals.

As detailed in Section 2.2.7, provided the a.c. harmonic filters and convertor transformers are modelled explicitly, a suitable representation, especially in the absence of a suitable impedance frequency locus for the a.c. system, is a modified Thevenin equivalent (see Fig. 2.3(b)).

For this equivalent to be a realistic representation of the a.c. network it must include all associated generator effects.

In a real power system subjected to a d.c. line fault, with subsequent temporary loss of power transfer, the behaviour of the a.c. system will be determined by the relative size of this loss to the a.c. system capacity. Where it is significant, an appreciable effect will be exerted on the a.c. system generators.

Transient stability studies may be used to represent the behaviour of generators during such disturbances, and from them, the time varying Thevenin equivalents of the a.c. networks can be obtained. These equivalents will be influenced by the subtransient and transient effects experienced by the system generators.

Typical variations of the equivalent Thevenin source for each a.c. network are depicted in Figs 5.3(a) (r.m.s. magnitude) and (b) (phase angle) where curves (i) and (ii) represent the rectifier and invertor a.c. network equivalents respectively.

Fig. 5.3(a)

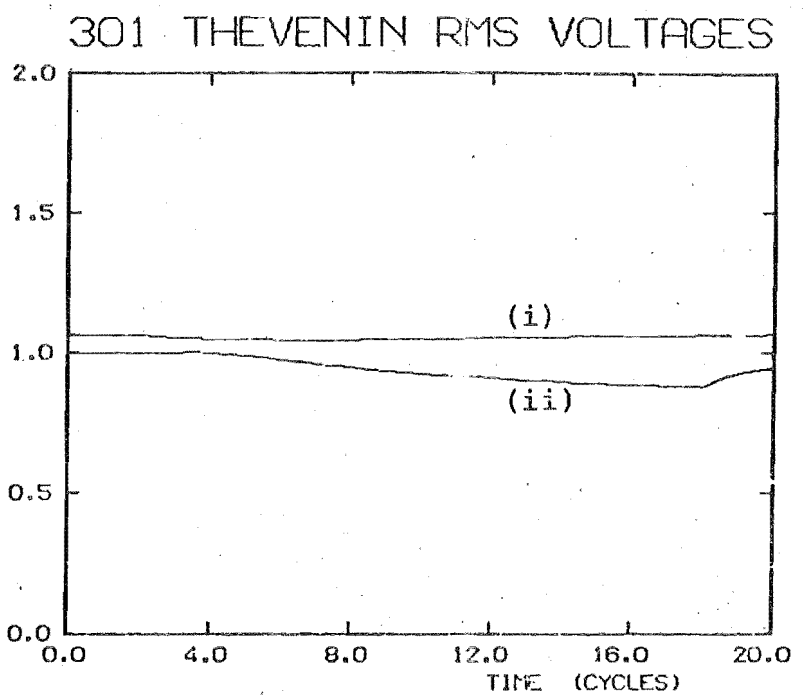

Fig. 5.3(b)

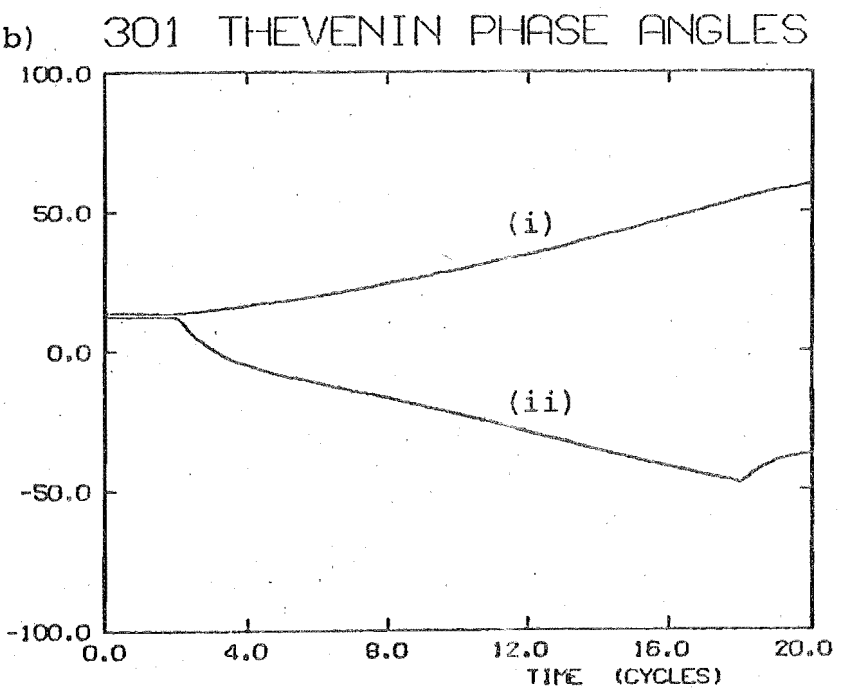

The disturbance investigated was a loss of full d.c. transmission at 2 cycles, and subsequent resumption of full transmission at 18 cycles, using the New Zealand a.c./d.c. system, as depicted in Appendix A9, as the test system.

As expected, during the fault the two a.c. networks swing in opposite directions, since effectively the rectifier suffers from a surplus of generation and the invertor from a loss of generation. The curves indicate the relative strengths of the two a.c. networks, with the invertor suffering a 10% reduction in its a.c. voltage. Although the presence of the harmonic filters would tend to elevate the invertor a.c. voltage, the large local loads, which are connected to the rest of the North Island a.c. system by long a.c. tie lines, cause a nett a.c. voltage reduction. The reference angle there swings appreciably, especially in the subtransient period, as its machines slow down due to the loss of power injection. At the rectifier end the loss of a $P + jQ$ load results in slightly elevated voltage levels with the filters still connected, and increased system frequency as the generator speeds up, as shown by the curves (i).

These preliminary investigations indicated the need to incorporate in the dynamic analysis, the time variant behaviour of the a.c. system, by regularly updating the Thevenin equivalents. The formulation set out in Section 4.6.2 was used with the following modifications. As a result of the loss of control information over a long period when the link is shut down, and in order to maintain the firing angles at $\alpha_r = 125^o$ and $\alpha_i = 180^o - \delta_o$, compensation for a.c. system frequency shift by a time shift of the firing pulse instant was necessary. This was done on the basis indicated

in Section 4.6.2. If, however, firing control was based on detection of actual voltage cross-overs and direct measurement of delay angle (i.e. individual phase control), this would not have been necessary.

The use of the interactive process indicated in Fig. 4.11 allows the d.c. fault clearance times, indicated by the dynamic analysis, to be correctly simulated in the transient stability analysis. The transient stability analysis may ramp the d.c. power to closely match the actual response as indicated by the dynamic analysis, thus avoiding the need for further interaction. In all other aspects, e.g. the alignment and initiation of the use of the time variant equivalents, the interaction will be exactly as detailed for a.c. faults in Section 4.6.

The representation for each convertor and its associated a.c. system is depicted in Fig. 5.4, where Z_{THEV} may be adapted to comply with the configuration in Fig. 2.3(b).

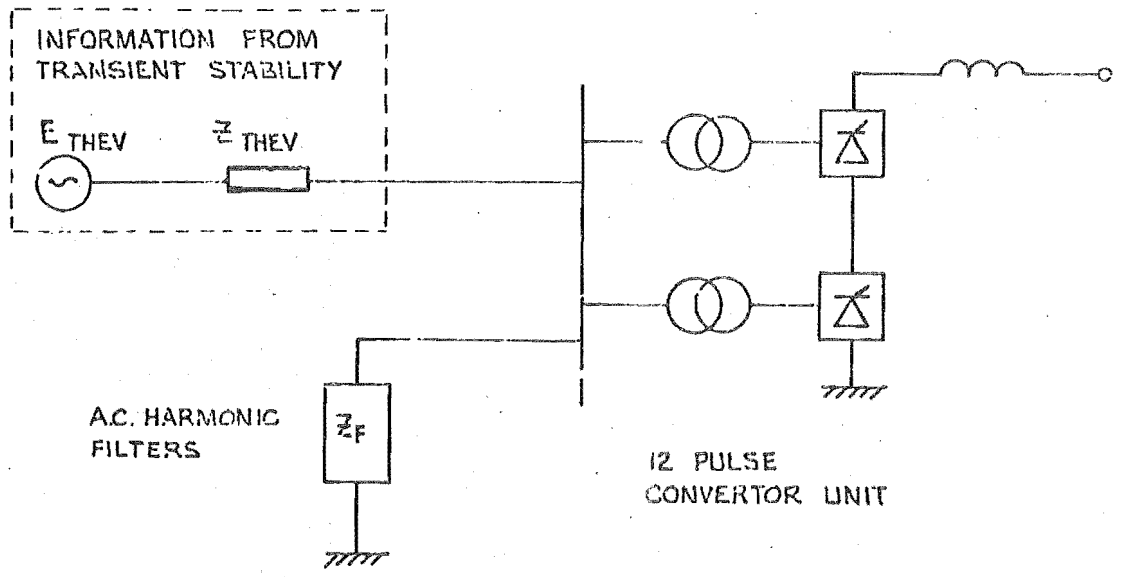

Fig. 5.4 Representation of each Convertor and Associated a.c. Network

5.6 RESULTS

5.6.1 Fault Application

Once satisfactory dynamic initial conditions for the test system were achieved (2 cycles of simulation were necessary), a decision as to when to apply the fault was made. For a d.c. system operating at nominal convertor angles, and provided with a protection principle based on the detection of travelling waves, the worst type of line fault in terms of overcurrent has been shown to be one in which a zero resistance fault occurs immediately adjacent to the line side of the rectifier smoothing reactor, immediately after a valve firing in one of the rectifier bridges. Thus for 12 pulse operation it will be a full 30^{o} before any retard action becomes effective. Initiation of the fault may be performed by alteration of the relevant connection matrix element ($K_{\alpha r}$ or $K_{\alpha l}$) for an already established branch element, or by insertion of a new branch element (R_r) and reformation of $K_{\alpha r}$.

5.6.2 Fault Detection

In Section 5.3, detection principles were formed based on travelling wave information. This related to the rectifier terminal only, but in Section 5.4 it was found that arc extinction was enhanced by inclusion of a similar principle at the invertor. However a different set of levels for K_5, K_6 and η were necessary to provide fault discrimination.

In the state variable formulation, the detection principle is implemented by monitoring the rates of change

of the state variables ψ_1 and Q_α on each pole of the d.c. line at each convertor terminal, where 1 is the smoothing reactor branch and α is the node relating to the convertor's line side termination. Equation (5.3) may then be rewritten as

$$\eta = K_5\, p\psi_1 + K_6\, pQ_\alpha \qquad \ldots (5.4)$$

An indication of the relative detection times for the two convertor units is shown in Figs 5.5(a) (convertor direct currents) and (b) (line side convertor voltages), by dynamic simulation of a 20 ohm earth fault applied as indicated in Section 5.6.1. An indication of the travelling wave initiated by the fault can be obtained from this graph, as can the natural frequency of the d.c. line. The rectifier detection unit is seen to respond almost instantaneously to the fault, as the voltage gradient is very high. The protective action initiated, with the next firing pulse retarded, is seen to be effective after 30^o, as predicted. This is indicated by a change in the rate of rise of rectifier current. The time delay associated with the travelling waves on the line is indicated by the invertor detection delay of around 5 msec between fault initiation and identification. Alteration of the constants K_5, K_6 and η can alter this value, but inspection of Fig. 5.5 shows detection occurs near the peak voltage and current gradients; and since the fault is at the far end of the line, these levels indicate good discrimination. Invertor current is seen to extinguish after approximately 8 msec, and the rectifier current 6 msec later. The oscillation of invertor line voltage is seen to be of about 50Hz frequency.

Fig. 5.5(a) 301 DETECTION RESPONSES

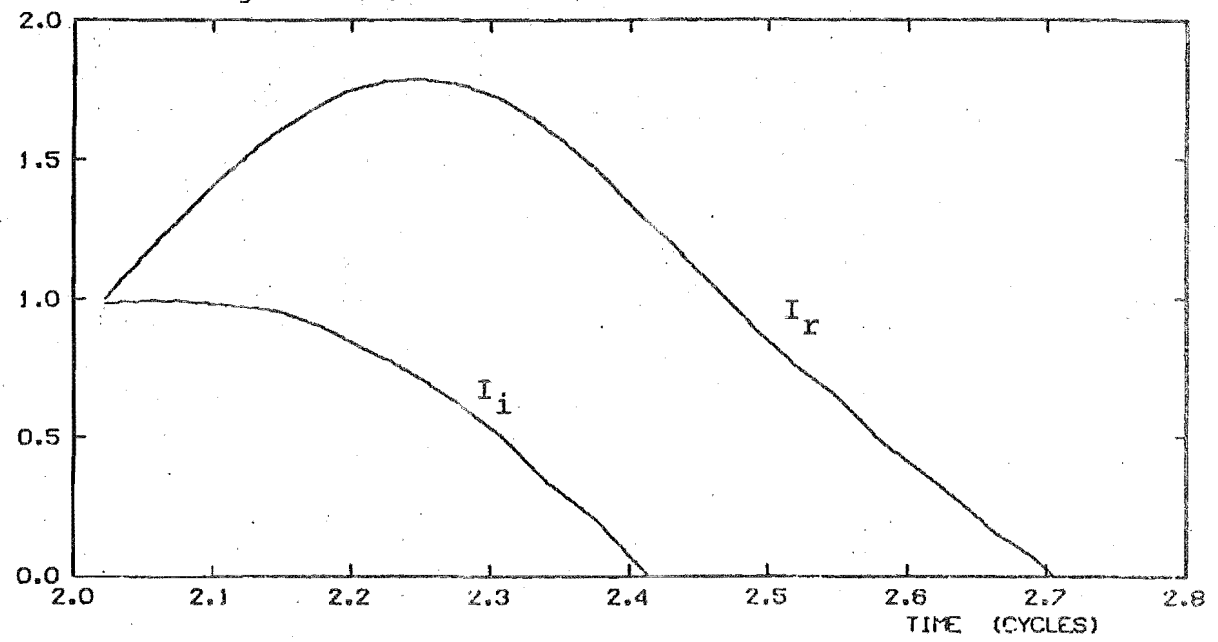

Fig. 5.5(b) 301 DETECTION RESPONSES

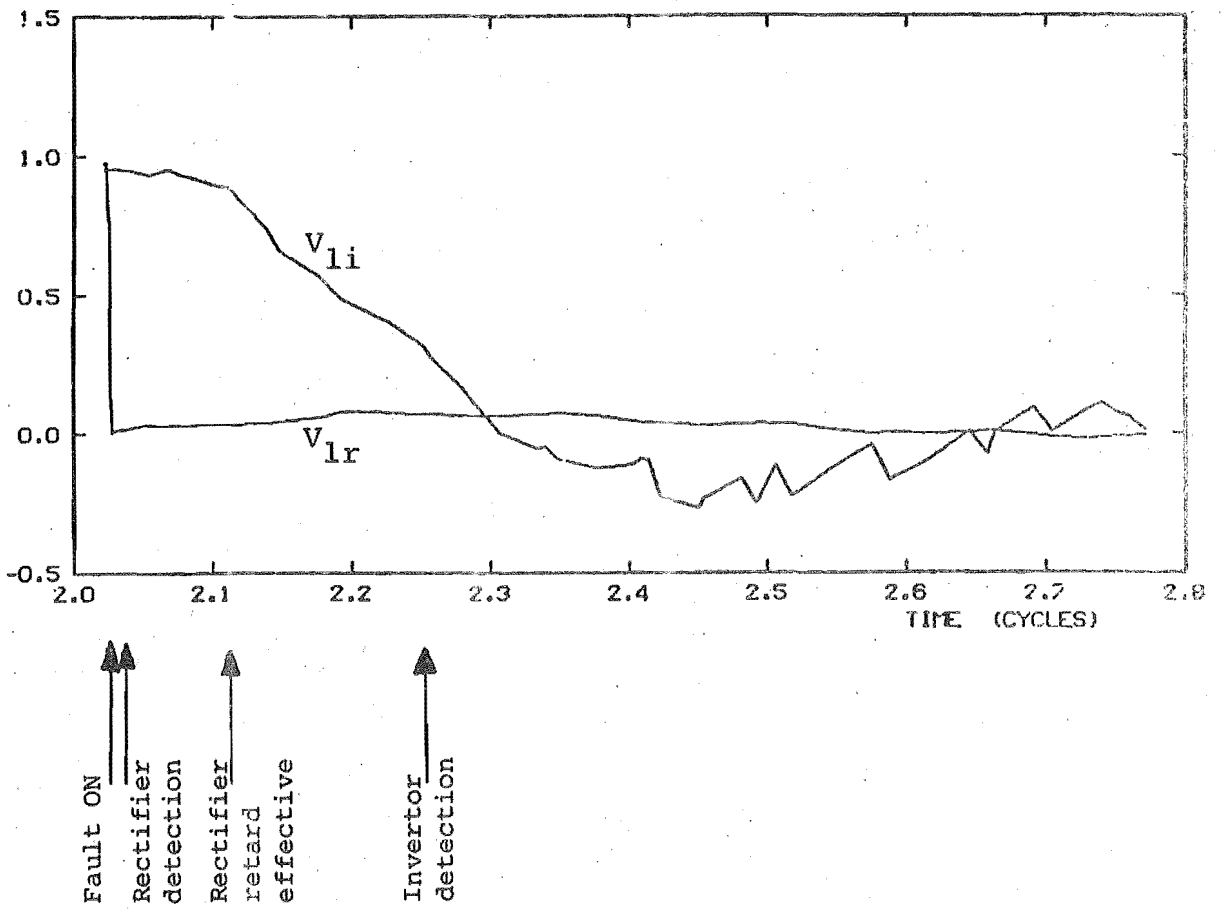

Fig. 5.5 Coordination of d.c. Line Fault Detection Action

The envelope of the fault voltage is seen to have a peak of around 0.15 p.u. or about 30 kV, which will promote a healthy arc.

5.6.3 Arc Extinction and Deionization

As indicated in Section 5.2, the levels of rectifier overcurrent and peak fault current are dependent on the timing of the line fault relative to the convertor control, the location of the fault, and the magnitude of the fault's resistance to earth. However it was noted in Section 5.4 that a crucial factor in investigating d.c. line faults is the time taken for the fault arc to extinguish. In the absence of a current source this will be entirely dependent on the characteristics of the d.c. line, and of the fault path. The assumption of a dead short circuit, whilst the most onerous with respect to overcurrents and extinction times, is contrary to the real situation.

To examine the effects of various earth resistances on the decay of fault current, it is appropriate to consider the situation once the rectifier has shut down, since prior to this time it will act as a source which is sustaining the fault current. Subsequent to rectifier turn off, the only fault current source is the energy stored in the d.c. line, and as discussed in Section 5.4.1, the fault current will thus decay exponentially with a time constant dependent on the total circuit resistance.

The combined a.c./d.c. system described in Section 5.5 was subjected to a d.c. line fault (nominally 20Ω earth resistance) at the time described in Section 5.6.1, using the detection principles in Section 5.6.2, and studied until

the rectifier current became zero (with $\alpha_r = 125^o$). Over this period (approximately 14 msec), it was found that the fault voltage and energy states of the d.c. line were relatively independent of the earth resistance. Slight variations in peak rectifier overcurrent, fault current level, and fault voltage are evident, but these have negligible effect on the decay of fault voltage. This can be indicated by considering the nett energy absorbed and dissipated by the d.c. line and the fault, when the source (rectifier) is present. Therefore, the effects of earth resistance on the time taken for the arc to extinguish can be investigated by using the d.c. line energy states at the time the rectifier turns off.

By modelling the d.c. line as a simple, separate system, with these states as initial conditions, a simple and computationally inexpensive comparison can be made between various earth resistances with respect to fault current. This is advisable since, for practical values of earth resistance, step lengths below 0.1^o are necessary to achieve a reasonable rate of convergence in the numerical integration process.

Since arc voltage is largely independent of fault current, the effective arc resistance will vary inversely with fault current. The total fault resistance, simulated at the appropriate point, is thus a combination of the time variant arc resistance (calculated at each time step as the ratio of the specified constant arc voltage drop to the actual fault current), and the specified earth resistance. For the N.Z. scheme the direct voltage rating is ±250 kV

and an insulator flashover may thus be expected to sustain an arc of nearly 2 metres, with a voltage drop of around 4 kV.

Studies for earth resistances of 2, 5, 10 and 20 ohms were conducted, and the corresponding fault currents are illustrated in Figs 5.6(a) - (d) respectively. The extinction times achieved are summarised in Table 5.1.

Table 5.1 Arc Extinction Times as a Function of Earth Resistance

	EARTH RESISTANCE (OHMS)			
	2	5	10	20
TIME (msec)	110	100	90	80

It is apparent that each halving of the earth resistance increases arc extinction by approximately a half cycle, which at the natural line frequency of around 50 Hz is about 10 msec. The arc extinctions occur at the zero crossings of arc current, provided the peak arc voltage is below the arc sustain level (approximately 2 kV/metre). The arc path resistance then increases effectively to infinity, since no current flows, and provided restriking does not occur, the fault branch may be removed or disconnected. This action is invoked at the completion of the specified deionization time, when it is assumed the arc path is completely deionized. If arc restriking is to be simulated, the fault branch may be reinserted or reconnected depending on the method being used (see Section 5.6.1).

Fig. 5.6(a)

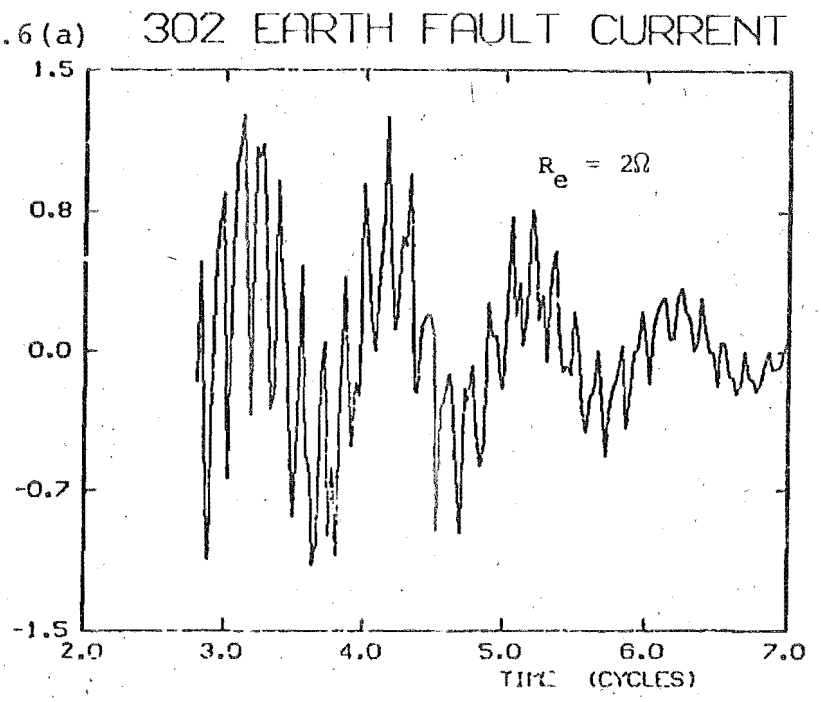

Fig. 5.6(b)

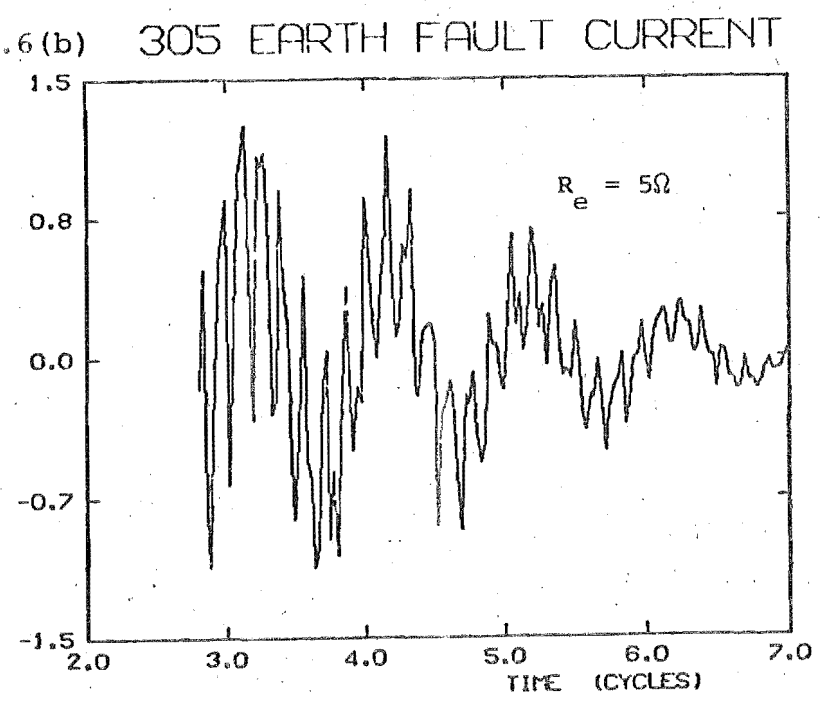

Fig. 5.6(c) 310 EARTH FAULT CURRENT

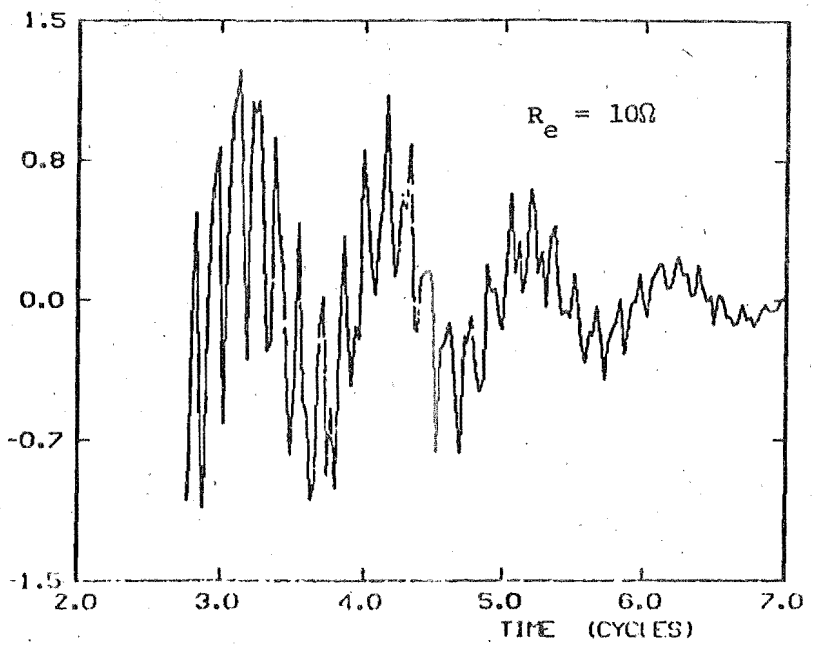

Fig. 5.6(d) 320 EARTH FAULT CURRENT

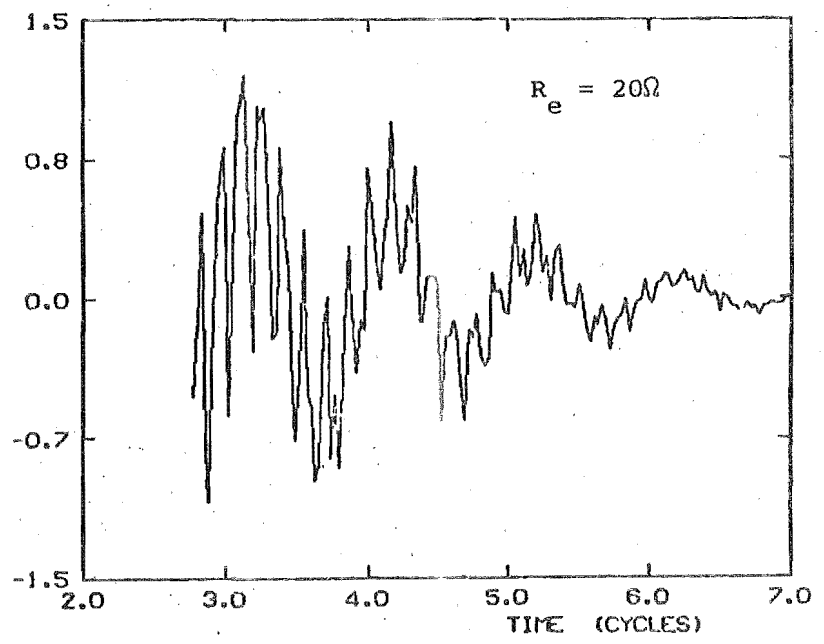

5.6.4 DC Line Recharge and Power Transmission Restart

As outlined in Section 5.4.3, close co-ordination of convertor controls is necessary following deionization to ensure that the restart period does not suffer from severe oscillations in voltage and/or current. A line recharge process which results in large overshoots of line voltage may cause the arc to restrike or may cause additional stress to other line components, resulting in consequential failures. With a scheme which uses linear ramping of firing angles, such as when normal control action is used with a limit on maximum angle advance, this is a distinct possibility. By ramping of the convertor settings, with suitable delay at the invertor, this may be avoided. However, Figs 5.7(a) and (b) depict the results of applying such a linear ramping of current settings, with a limit on the maximum firing angle change per firing, to the New Zealand test system's controllers. The angle advance limit was set at 15^{o} to allow nominal voltage to be attained nearly a cycle after controller release. The responses indicated, although exhibiting rapid line recharge, are oscillatory in nature. This is a consequence of the particular d.c. line characteristics. The voltage oscillations and line travel time also result in large oscillations in the direct current. Obviously then, a recharge process based on the ramping procedure is unacceptable for the N.Z. scheme, since the overvoltages indicated (30% above nominal) could be detrimental to the system's recovery from the fault condition.

A d.c. line recharge start control unit, to be used instead of linear ramping methods for the (re-)energization of a d.c. line, must be capable of attaining nominal line voltages quickly, but with a well damped, minimum overshoot. The time constant of the d.c. line (approximately 20 msec for the N.Z. scheme) will give an indication of the rate of response which may be acceptable.

To recharge a d.c. line from $\alpha_r = 125^\circ$ and $\delta_i = \delta_o$, it is best to control α_r by a start control function, whilst maintaining $\delta_i = \delta_o$. This ensures the rectifier recharges the line fully before the invertor begins to draw power. This will mean that both the rectifier and invertor constant current controllers will be inoperative, since the invertor is controlled by EAC and the rectifier by the start control function. A function which will exhibit the above characteristics is one in which α_r is controlled exponentially.

Following the completion of the deionization period, α_r is stepped from 125° to 90° over one firing instant. Subsequent firing action is then controlled by the recharge function

$$\alpha_r = \alpha_o + (90^\circ - \alpha_o) \exp(-k\Delta t) \qquad \ldots (5.5)$$

where α_o is the control angle which will give nominal line voltage, and

Δt is the elapsed time since transfer of the convertor control to the restart unit (i.e. from when $\alpha_r = 90^\circ$).

The constant k will determine the response rate.

Fig. 5.7(a) 301 LINEAR RECHARGE (I)

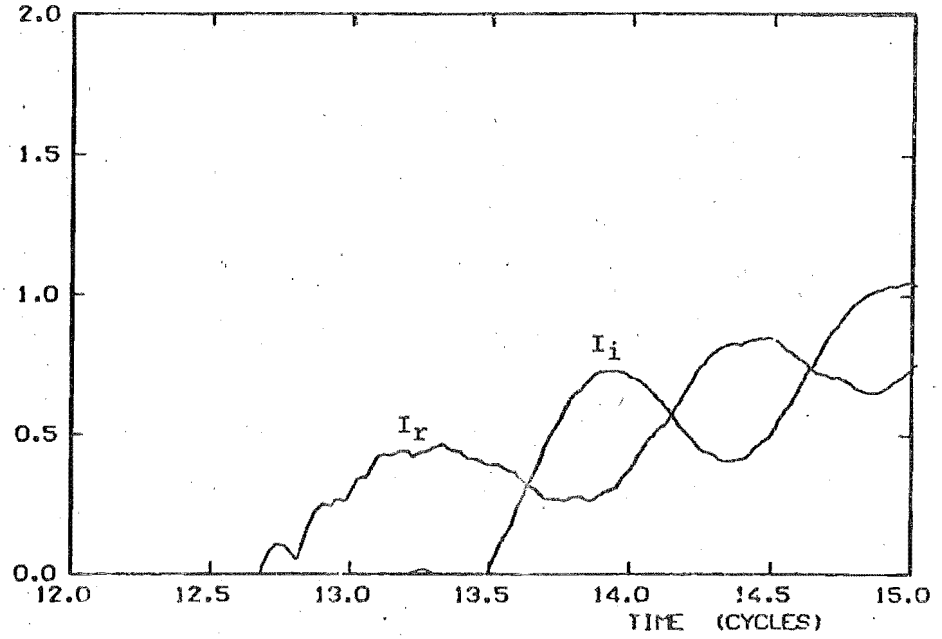

Fig. 5.7(b) 301 LINEAR RECHARGE (V)

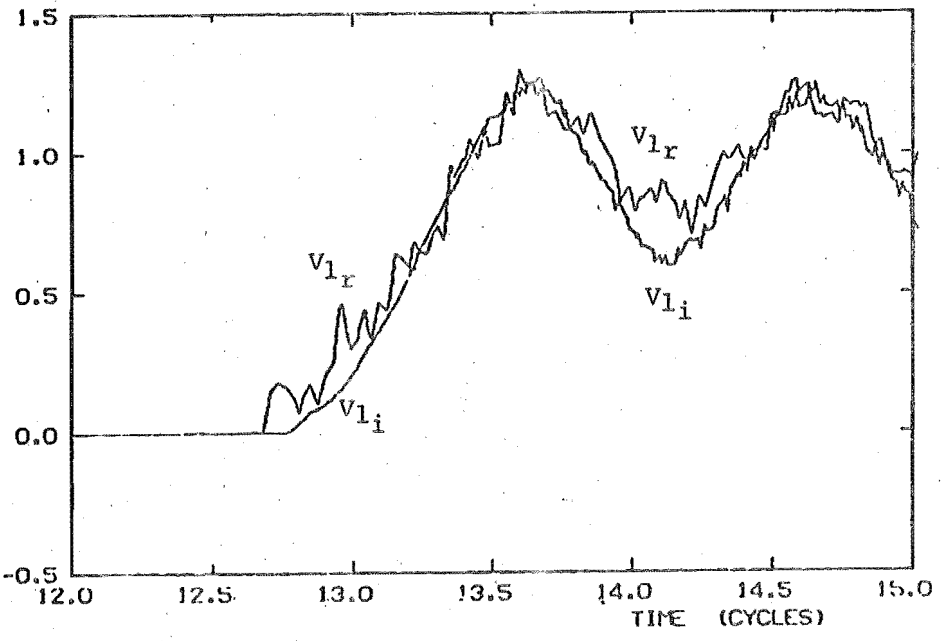

Fig. 5.7 Effect of Linear Recharge on DC Link Restart

Figs 5.8(a) and (b) indicate respectively α_r and $\cos\alpha_r$ (which is proportional to the ideal no load voltage), for various values of k, as a function of elapsed time (Δt). In this case $\alpha_o = 10^o$. For a d.c. line which has a time constant of approximately 20-25 msec, it is desirable to have no more than 63% of nominal voltage when Δt = 25 msec, in order to obtain critical damping of the no load voltage rise. Curve (ii) exhibits this characteristic, and actually achieves nominal voltage when Δt is approximately 100 msec. Fig. 5.8(b) shows that, ideally, little overshoot of line voltage should occur. Other factors beside α_r affect the line side voltage (e.g. reflection of travelling waves). However, by designing the start control unit on an idealised basis to exhibit critical damping, a realistic approximation to the expected response may be achieved. In the N.Z. scheme an equivalent recharge time of approximately 100 msec is used. Therefore the selection of k = 2.4 is realistic and justified. Selection of a slower rate (e.g. k = 2) would have been detrimental to the total response time without markedly enhancing restart performance with respect to protection problems and possible arc restrike.

The recharge process is implemented by adjusting the firing instant F_{j+1} by

$$\Delta P_{j+1} = \alpha'_{j+1} - \alpha_j \qquad \ldots (5.6)$$

where $$\alpha'_{j+1} = 10 + 80 \exp(-2.4\,\Delta t) \qquad \ldots (5.7)$$

and where Δt is measured to F_{j+1}.

Fig. 5.8(a) RECHARGE FUNCTION (ALPHA)

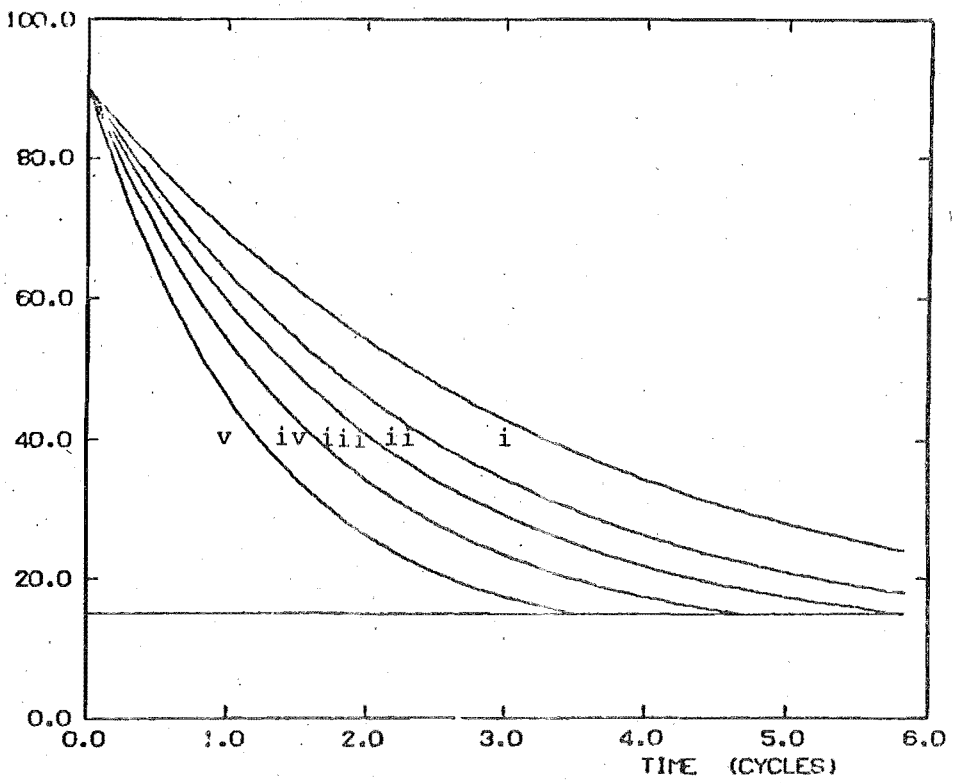

Fig. 5.8(b) COSINE RECHARGE FUNCTION

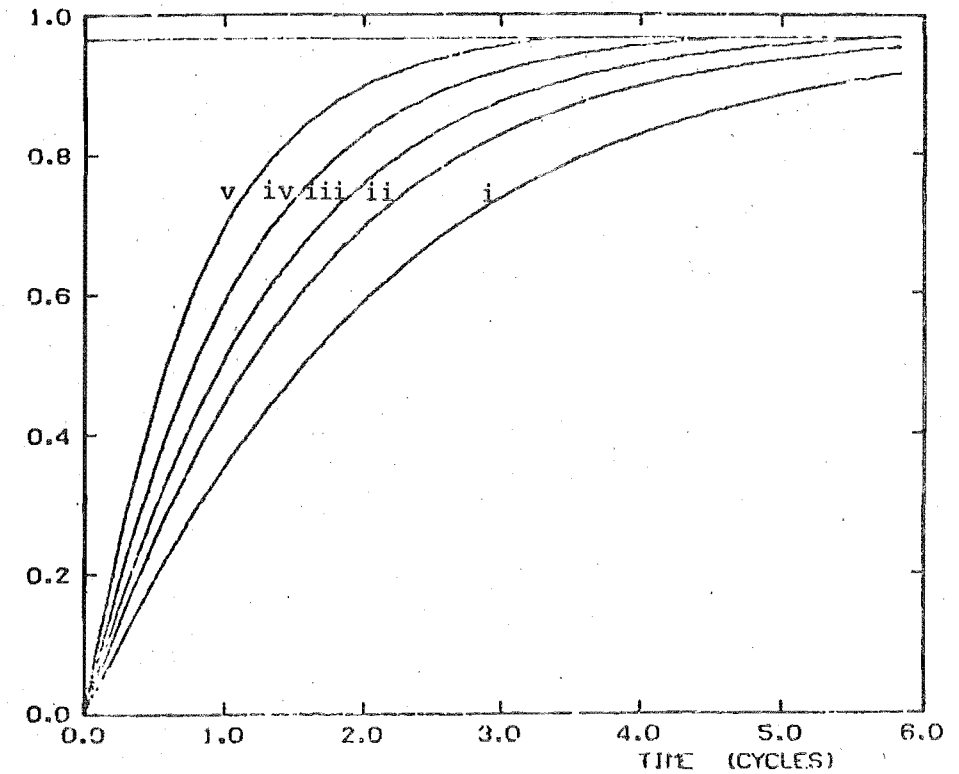

Fig. 5.8 Characteristics of Exponential Recharge

k values : i 2.
ii 2.4
iii 3.
iv 4.
v 5.

When the d.c. line is fully recharged to nominal voltage at the correct polarity, conditions are conducive to resumption of normal power transfer. At this time α_r will be close to nominal and δ_i will be on its specified optimum value. The rectifier then switches from the line recharge controller to constant current control, whilst the invertor maintains EAC.

5.7 FULL SIMULATION OF A DC LINE FAULT

A temporary 20 ohm earth resistance bipole fault at the d.c. line's terminal connection with the rectifier smoothing reactor was investigated from the time of fault initiation through to full fault recovery and normal power transmission, using the developed dynamic analysis programme and the interactive facility of a transient stability programme as indicated in Section 4.6. A flow diagram indicating the co-ordination of the special control functions designed for protection and recovery of d.c. line faults is shown in Fig. 5.9. The results are indicated in Figs 5.10(a) - (g).

The fault was applied as indicated in Section 5.6.1, using the detection process described in Section 5.6.2. Two phases at the rectifier continue to conduct current for an extended period (Fig. 5.10(f)), as α_r is retarded to 125^o. The initial rectifier overcurrent occurs 4 msec after the fault is applied. The peak is only 80% above the setting and decays to zero, 15 msec after fault initiation. The invertor has already shut down by this time.

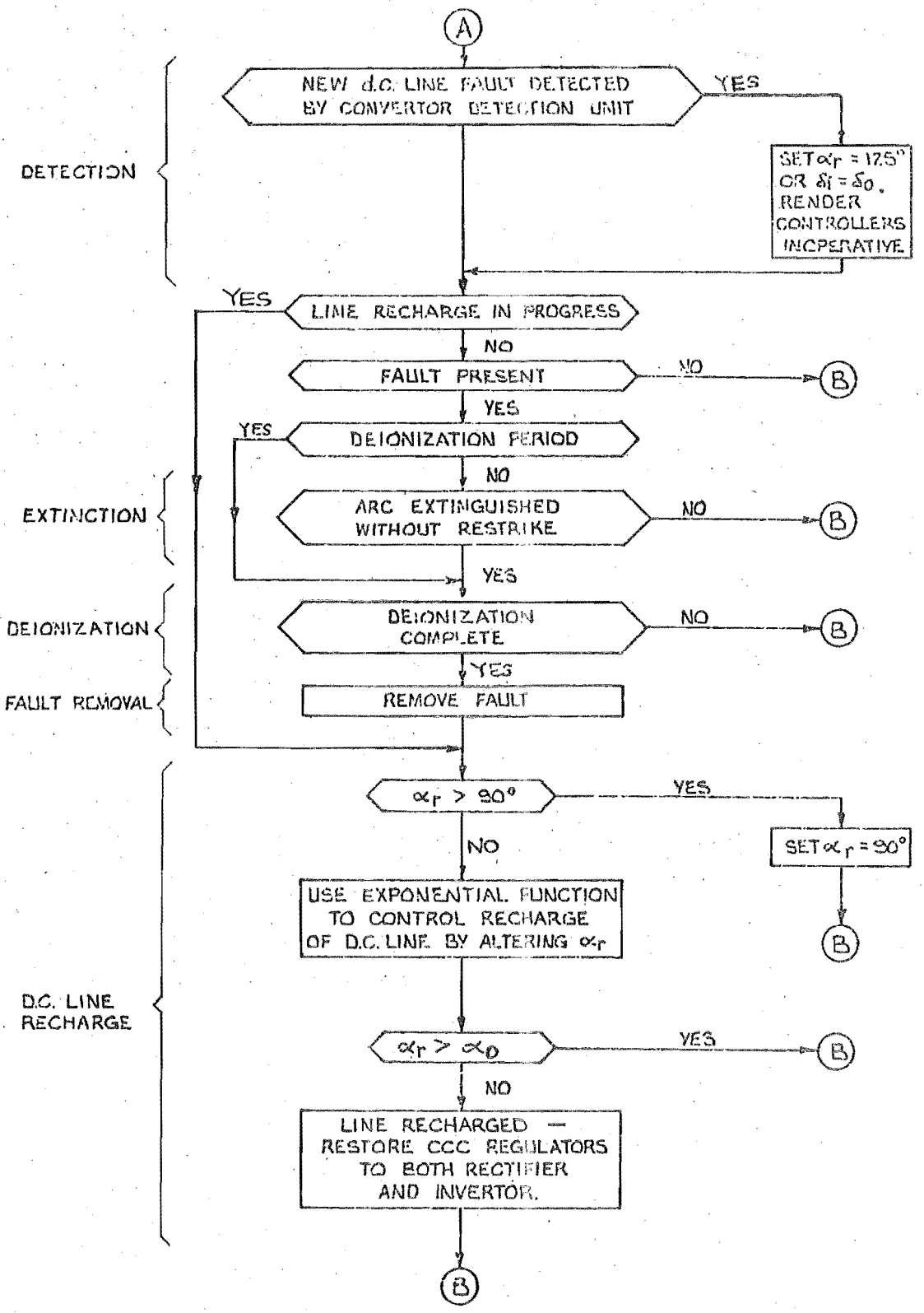

Fig. 5.9 Flow Chart of Coordination of Special Control Characteristics for d.c. Line Fault Protection

The Figs 5.10 illustrate the existence of voltage oscillations with the invertor voltage reaching 50% of the rated voltage with reverse polarity. The invertor line voltage oscillation is then seen to die out within approximately 80 msec as a result of the protective action taken, whereby the invertor is kept on EAC control (as indicated in Section 5.4.1). Even with this protective action, a slight negative power level, indicating fault contribution, exists for a short time prior to invertor shut down. The rapid decay in invertor direct current is illustrated by the a.c. current waveforms. Due to the continued presence of the harmonic filters, a residual current level remains throughout the fault, with considerable initial harmonic content as indicated by the a.c. voltage waveforms. This is even more evident at the rectifier end due to the large initial increase in direct current and also due to the large change in control angle, which does not occur at the invertor end under EAC. The rectifier voltages exhibit a large regulation effect, as well as distortion, during the over-current period as a result of the harmonic content and phase imbalance evident in the a.c. current waveforms. The distortion of voltages at each end is seen to reduce quickly as the residual (filter) currents become settled. In each case this takes about five cycles, giving an indication of the relatively slow time response of the harmonic filters.

During the same period the line voltages are seen to decay, and as indicated in Fig. 5.6(d), extinction of the arc occurs some 80 msec after fault initiation.

Fig. 5.10(a) 301 CONVERTOR DC CURRENTS

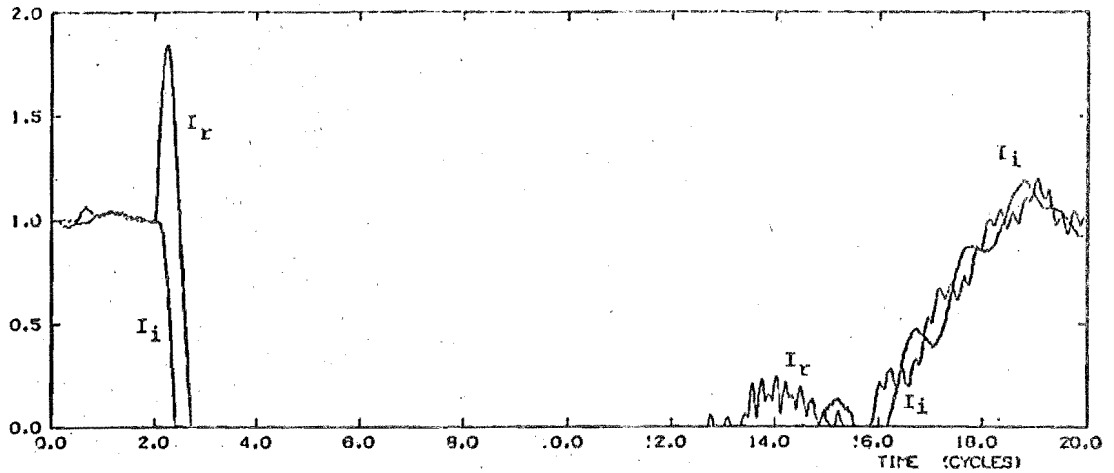

Fig. 5.10(b) 301 CONVERTOR DC VOLTAGES

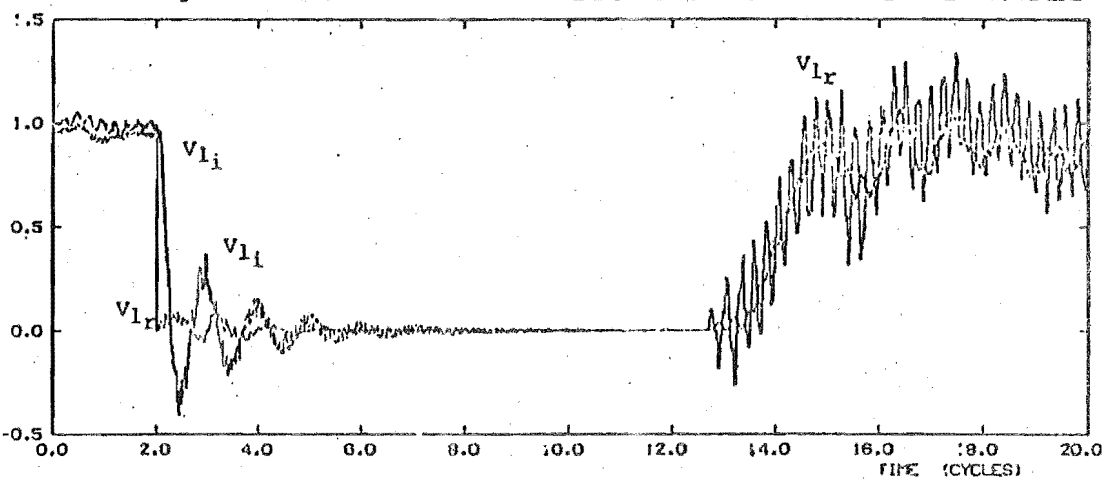

Fig. 5.10(c) 301 CONVERTOR DC POWERS

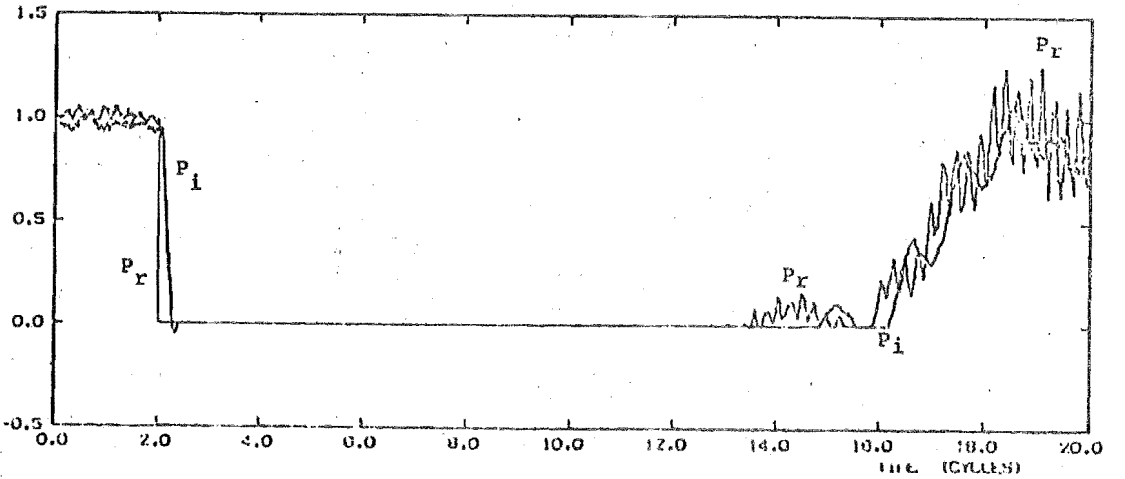

Fig. 5.10(d) 301 RECTIFIER AC VOLTAGES

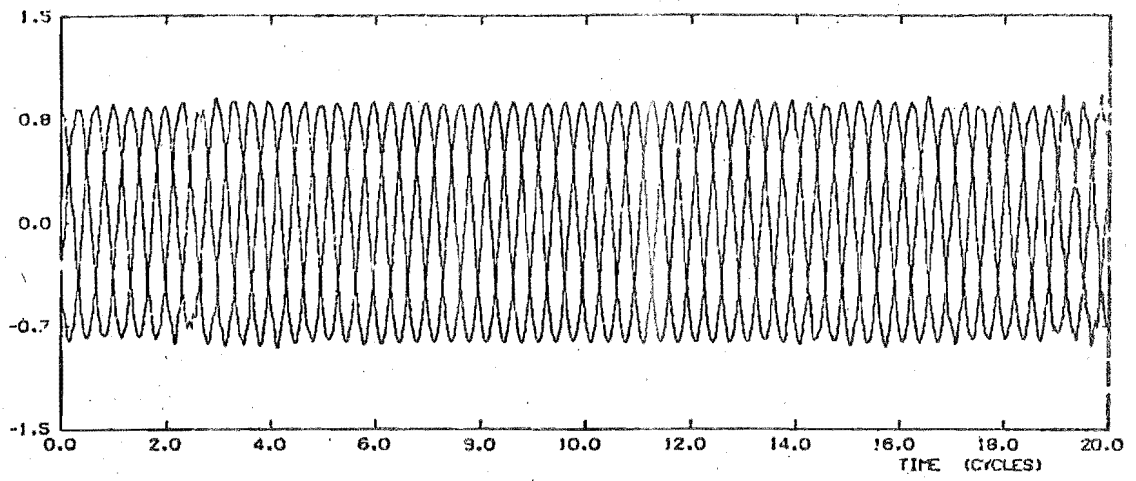

Fig. 5.10(e) 301 INVERTOR AC VOLTAGES

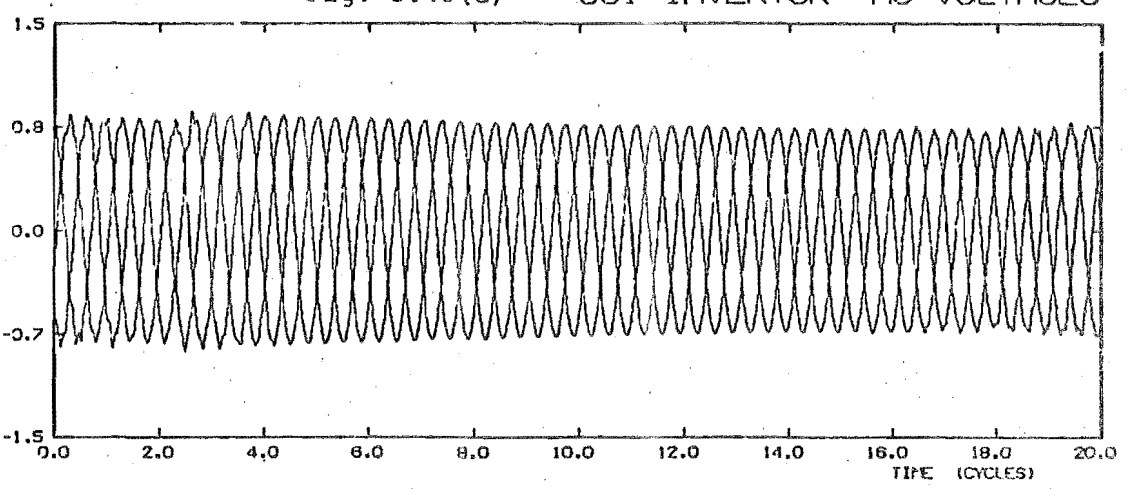

Fig. 5.10(f) 301 RECTIFIER AC CURRENTS

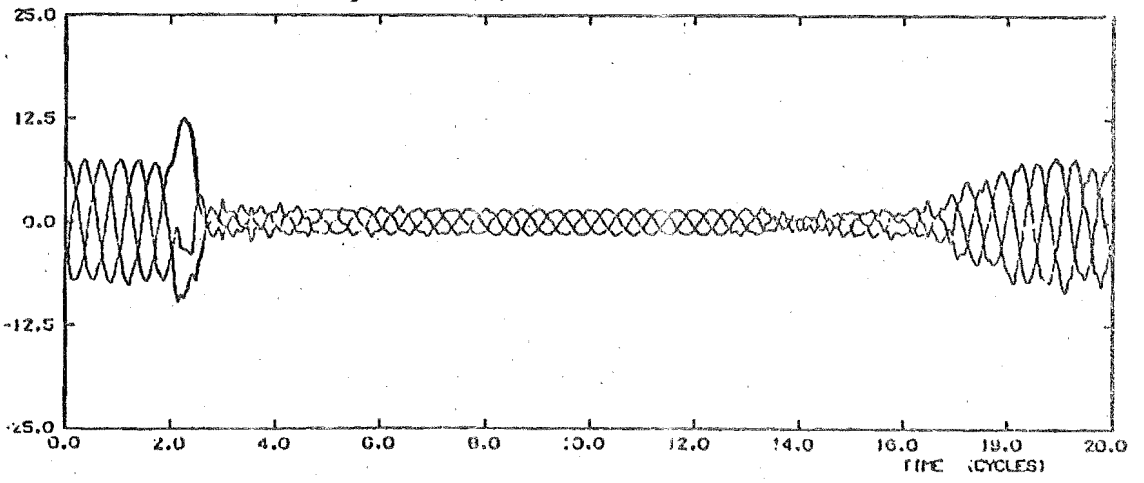

Fig. 5.10(g) 301 INVERTOR AC CURRENTS

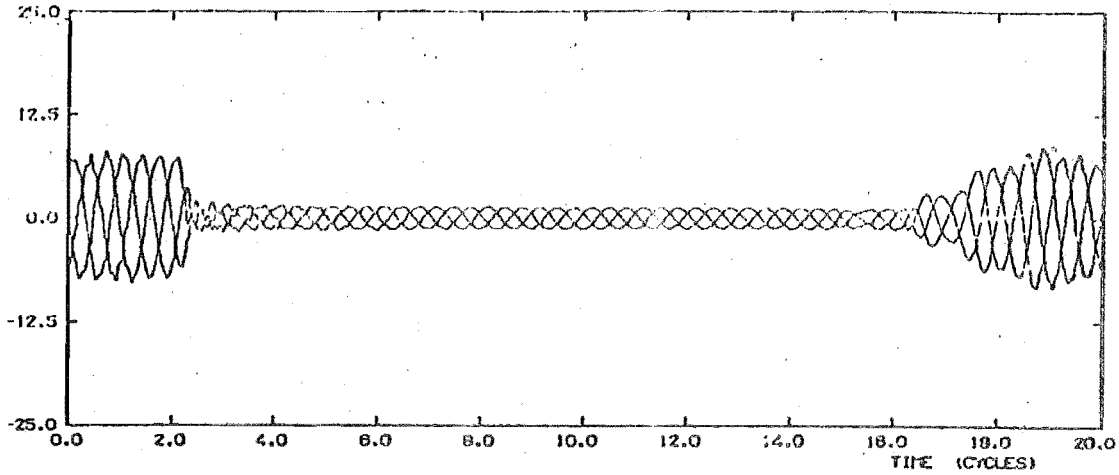

The deionization period then extends for approximately 100 msec. With no control action throughout this period, and with only filter currents being supplied by the source, the voltage waveforms become sinusoidal since the filter currents are balanced. However the effect of the a.c. system's response to the d.c. link shut down, as obtained from the transient stability study and indicated in Figs 5.3(a) and (b), is manifested as a form of modulation in both convertor a.c. voltage waveforms. The amplitude variation is especially noticeable in Figs 5.10(d) and (e).

Some 200 msec after fault initiation, the arc is assumed to be completely deionized, and the fault branch is removed. The convertors' protective control is replaced by the line recharge control to commence fault recovery. As indicated in Section 5.6.4, the invertor maintains EAC and the rectifier angle is progressively advanced, initially from 125^{o} to 90^{o}, and then under control of the exponential recharge function. The rectifier direct current and both line voltages indicate this process. The current involved in line recharge is seen to be relatively small, and the

d.c. voltages are seen to climb relatively quickly (in 60 msec) to about 80% of nominal voltage; the invertor voltage increase being delayed by the travel time of the line. Because the invertor is on EAC, the invertor does not conduct current until the line is charged to about 90% of nominal. The recharge time, measured from deionization until the line is recharged and convertor current has begun to increase, is seen to be about 80 msec. This is marginally faster than was anticipated, and is indicated by small oscillations in line voltage. These oscillations are only about 10% above nominal at the invertor, with slightly larger oscillations at the rectifier. The reasons for these oscillations being larger than predicted can be found by inspecting the r.m.s. values of the Thevenin voltages (Fig. 5.3(a)), where the invertor value is seen to be some 10% down from nominal, whereas the rectifier value is 5% above nominal. By designing the recharge function for pre-fault values of the Thevenin voltages (E_r, E_i), and control angles α_r and δ_i in Section 5.6.4, the nett voltage difference across the link with different source voltages, such as in Fig. 5.3, is significantly larger than it would be at the pre-fault levels. The direct voltage at the rectifier end is therefore greater than the response characteristic was designed for. As a result, the oscillations in line voltage are slightly greater than predicted. To reduce this oscillation, a value for α_o of 30^o appears to be more suitable than 10^o, since this results in the same no load voltage difference for the d.c. link as when the pre-fault voltage is used.

A new family of curves similar to those of Figs 5.8(a) and (b) may be constructed using the recharge equation (5.5) with an appropriate k value selected. In order to indicate the effects of the r.m.s. voltages at each convertor, instead of plotting $\cos\alpha_r$ as in Fig. 5.8(b), the following function could be plotted:

$$E_i^o \, E_r \cos \alpha_r \; / \; (E_i \, E_r^o)$$

where E_i^o and E_r^o are, respectively, the pre-fault invertor and rectifier Thevenin voltages, and E_i and E_r are the corresponding values at fault recovery time, as obtained from a preliminary transient stability study.

The use of a recharge function designed using these principles will result in the line being charged more slowly and to a voltage lower than nominal (in this case 10% lower due to the reduced invertor a.c. voltage).

Following the recharge period, which is completed 280 msec after fault initiation, the convertor currents are seen to increase quickly and steadily to the set values. This increase takes place with the rectifier on CCC, and the invertor on EAC. The current is seen to reach its setting after 60 msec with only a minor initial overshoot, indicating that the CCC constants used are adequate. At this time (cycle 19) the d.c. power levels are not at their pre-fault values since the invertor a.c. voltage is still depressed, although it is increasing steadily with the reinjection of link power. As indicated in Fig. 5.3, it will take some time for the pre-fault a.c. voltages to be regained.

The effect of control action and direct current increases during the convertor restart period is again indicated by distortion of the a.c. voltages. At the rectifier, significant changes in α_r occur, as well as current modulation due to direct current changes. This behaviour is similar to that immediately following the fault initiation when the time response of the filters was also found to be significant. The distortion is less at the invertor since it is under EAC with steady current increase.

Convertor behaviour, i.e. the firing pattern, is settled ($\pm 5^{o}$ change in firing angle at the rectifier) and thus extension of the dynamic analysis beyond the time indicated is not justified. Therefore a total dynamic analysis time of 400 msec is suitable for this investigation. Beyond this period a quasi-steady state approach, as given by a transient stability programme, will be suitable for investigation of stability aspects.

5.8 CONCLUSIONS

The techniques outlined in this chapter have shown that transient ground faults on one or both poles of a d.c. line may be cleared quickly by convertor control, without the need for a mechanical breaker as is the case in a.c. systems. The main factors influencing the duration of the interruption due to the fault have been investigated, and these have been shown to be dependent on:

(i) the fault resistance (including arc characteristics) which will control the rate of arc current extinction;

(ii) the time necessary for deionization of an arc; and

(iii) the restart procedure which involves recharging the d.c. line to nominal voltage and resumption of power transfer.

To investigate these effects, it was essential to use a dynamic analysis programme with a small integration step (0.05 - 0.1 msec), in order to identify the variation in energy states in an a.c./d.c. system due to the frequently changing convertor topology. Since a.c. current and voltage waveforms are greatly influenced by the dynamic behaviour of the harmonic filters and convertor controllers, this information on actual a.c. waveforms is essential to determine if any distortion or overvoltage effects occur. This programme also allows accurate co-ordination of the detection and protection schemes necessary for the recovery of the d.c. link from a fault condition. The prospective use of microprocessor identification and control of particular fault conditions makes it essential to provide accurate assessment of such applications by a simulation tool.

The behaviour of the generating sources in the a.c. systems following a disturbance has been shown to be sufficiently important to necessitate a time variant representation for the a.c. system. Utilisation of an interactive facility developed with a multi-machine a.c./d.c. transient stability programme has made this feasible.

The test results indicate that the interruption and recovery times may be optimised by means of faster detection

schemes, fault development control for extinction and deionization, and also by control of line re-energization. At no time are any convertor faults initiated as a result of the fast control action taken, nor are excessive stresses put on the convertor plant.

The effect of earth resistance on overcurrents and arc extinction has been shown to be important in considering tower footing resistances for d.c. transmission lines. Similarly, careful insulation design is possible by observing likely overvoltages on the healthy pole of a bipole system subjected to a monopole fault. As has also been shown, overvoltages can occur on line re-energization, and these factors must be taken into account for design purposes.

The effect on the a.c. system during such a fault has been seen to be relatively mild, with acceptable over-voltages and only limited waveform distortion occurring, when compared with the a.c. fault cases studied in Chapter 4. For faults with high earth resistance, the complete interruption interval has been shown to be 200-300 msec. The interruption time will increase as fault resistance decreases (i.e. extinction time increases), deionization time increases (due to system ratings), or protection and co-ordination speeds reduce, making the upper limit of 350 msec realistic.

In a.c. systems, interruption times of 500 msec, even with rapid reclosure, are experienced. Moreover, a.c. fault current levels of many times the full load ratings occur, whereas d.c. fault currents are of the same order of magnitude as the rated link current.

Thus the behaviour of a d.c. system under line fault conditions has been found to be more favourable than that of an a.c. system with rapid reclosure facilities, by virtue of simple modifications to the normal convertor controller actions.

An interesting feature of d.c. transmission is that minimum outage time does not necessarily provide an optimum response in terms of system stability. It has been suggested in the literature (Dougherty and Hillesland 1970) that outage time should be matched to the frequency of machine angle oscillations in the a.c. system(s). This may mean that re-energization control should include information of generator swings to improve stability following d.c. line faults. Further development of the interactive facility with the transient stability programme could be performed to investigate such a possibility.

CHAPTER 6

MODELLING OF FAST EXCITATION CONTROL WITH GENERATOR-CONVERTOR APPLICATIONS

6.1 INTRODUCTION

In the last decade, several contributions to the literature (see References in Anderson and Fouad 1977) have indicated the need for fast acting methods of excitation, capable of providing fast field forcing for improvement of system stability under abnormal operating conditions. As a result of this enquiry, excitation systems have been proposed which have a time response very much faster than those of the traditional AVRs, such as indicated in the IEEE Committee report of 1968. To obtain these fast response times, the designs may involve feedback of the generator output voltage to a three phase full wave bridge rectifier (Goto, Isono and Okuda 1971). The output of this bridge is then applied to the field windings. The power source of such excitation systems is therefore an integral part of the generator (Cotzas, Hesse and Lane 1979).

Self excited synchronous generators using thyristor controlled bridge exciters have many advantages over those using conventional rotating d.c. exciters, including easier maintenance and operation, and, because high initial response is possible, transient stability of the generator and connected network may be improved. The form of the proposed bridge design ranges from simple diode schemes with auxiliary

control, to bridges which may be operated as true rectifier bridges, thus providing the required excitation under all expected load conditions as well as under no load and fault conditions.

To provide full control, however, it is necessary to consider the possibility of allowing the exciter bridge to operate transiently as an invertor. This will then give the excitation system a negative voltage ceiling as well as a positive voltage ceiling. Some modifications have also been proposed whereby negative field current can be obtained. To ensure safe invertor operation, the negative ceiling normally has an absolute amplitude less than that of the positive ceiling voltage. An excitation system with the above characteristics may then be capable of providing high initial field voltage forcing for good system stability under abnormal operating conditions.

Whereas the effect of normal AVR responses could be modelled adequately by the use of constrained algebraic relationships applied to the fixed field voltage (E_{fd}) in the model of Section 2.2.3 (Campos Barros 1976, Brandwajn and Dommel 1979), the proposed thyristor bridge excitation circuits must be explicitly modelled, to accurately represent the dynamic behaviour of the excitation circuit.

The application of such excitation schemes to generators operating in various system arrangements is considered. Firstly, to demonstrate thyristor bridge excitation, its steady state performance in a simple a.c. system is investigated. The normal application of such excitation systems in this context is to control the

terminal voltage of the generator by modification of the exciter's thyristor firing angles. The ability of the thyristor exciter to perform this function under normal operational demands, or due to a.c. system faults, is indicated in the following sections.

The mismatch between traditional excitation controllers and those of an HVDC transmission scheme have been highlighted in earlier work (Arrillaga, Arnold *et al.* 1977). These studies of interconnected a.c./d.c. systems indicated that normal convertor control had a time response much faster than that of traditional AVR systems. This meant the two control systems were not always matched to give optimum performance.

It has recently been suggested that interconnection of a synchronous generator and an HVDC convertor in a unit type concept could reduce HVDC scheme costs (Calverley *et al.* 1973, Krishnayya 1973). The application of fast acting thyristor exciters to such systems could also eliminate the need for rectifier control if the speed of response of the exciter could be designed to approach that of normal convertor control. This would not only eliminate the need for controlled rectifiers, but also eliminate the mismatch between rectifier and generator control systems.

Bowles (1977) in preliminary studies using analogue simulators for such isolated generator-diode rectifier unit schemes, has indicated their feasibility and also possible protection limitations. A digital computer model of a unit type connection of diode rectifier and synchronous generator with fast thyristor excitation is described in this chapter,

and is used to investigate the steady state and fault behaviour. This unit scheme model, which may have 6 or 12 pulse conversion, can be connected to a normal d.c. line, invertor and invertor end a.c. system.

6.2 MODELLING OF THYRISTOR BRIDGE EXCITATION SYSTEMS

The present model for the field circuit (aligned in the rotor's d-axis) is a fixed e.m.f. in series with the field circuit's inductance and resistance as in Fig. 6.1.

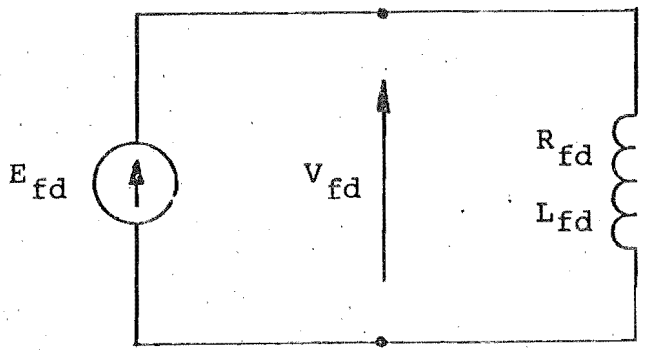

Fig. 6.1 Representation of Field Circuit by Fixed e.m.f.

Typically, models for excitation systems in dynamic analyses have used constrained algebraic relationships applied to the field voltage, E_{fd}, or when a more accurate model is needed, additional differential equations to describe the voltage regulator and exciter performance are used. These models are based on assumptions which, in the case of thyristor controlled exciters, are not always valid. For instance the field inductance is not infinite, so some ripple will always be present on the field current; the commutation reactance as seen by the thyristor bridge is

reasonably large (a combination of machine subtransient reactance and excitation transformer leakage reactance) so considerable harmonic current may flow in the stator windings unless filter equipment is provided; and normal excitation is usually at a high delay angle to provide adequate excitation ceilings. Therefore analyses based on assumptions of perfect smoothing, no waveform distortion, and firing angles and commutation angles less than 60^{o} will be in error. As was found in the case of HVDC convertor performance, an accurate assessment of the dynamic behaviour of a thyristor bridge (excitation) system can only be obtained with the use of a detailed bridge model.

The proposed model of a thyristor excitation circuit will in effect replace the fixed field voltage, E_{fd}, by a variable d.c. voltage which will be supplied, via excitation bridge and transformers, from the generator terminals. The field circuit in Fig. 6.1 is thus replaced by a circuit as in Fig. 6.2, where a single star-star transformer for 6 pulse exciter bridge operation is depicted.

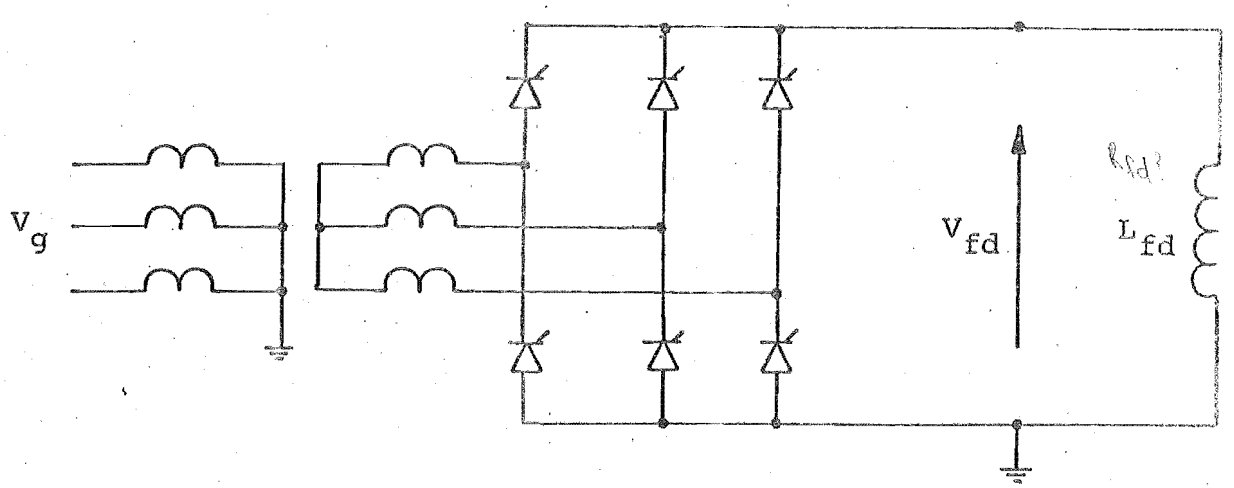

Fig. 6.2 Dynamic Representation of Thyristor Bridge Exciter

The incorporation of the above model for an excitation system into the programme described in Chapter 3 is relatively straightforward with regard to component representation. This can be seen by comparing the model with that used to represent HVDC convertor bridges. The same formulation will apply for an excitation bridge. However a limit is encountered in the machine representation.

Because the machine's field circuit is now also a part of the excitation bridge circuit, its branch would be identified as a k (convertor) branch (compare with smoothing reactor identification in HVDC convertors). All other generator branches must then be k branches (i.e. part of the same subnetwork) due to the presence of stator-rotor and d-axis mutual inductances. To allow this, no generator connections could involve γ nodes without violating the topology constraint on $K_{\gamma k}$ and $K_{\delta l}$ (both null). Since this likelihood is high, e.g. ungrounded stator star point (neutral), or generator terminals usually being directly connected to a transformer, the alternative formulation must be used where convertor subnetworks are not segregated, and all inductive elements are modelled as l branches. The inclusion of the field circuit, its excitation transformers and its thyristor bridge into the synchronous machine representation is necessary to satisfy the formulation. This requires some modification of the input routine for synchronous machines.

Initial condition specifications will apply as in Section 3.2.1 with the realisation that the rotor field current and the exciter bridge current are identical for the calculations in Sections 3.2.1.1 and 3.2.1.2.

6.3 EXCITATION CIRCUIT P.U. SYSTEM

6.3.1 Excitation Transformer Ratio

In the absence of saturation, and with perfect d.c. side smoothing, the field voltage (equal to $R_{fd}\ I_{fd}$) will be directly proportional to the field excitation (E_i) as indicated in Section 3.2.1.2. The ratio of this voltage to a.c. input voltage, when the bridge operates with a fixed delay angle, will be constant provided the a.c. source impedance and the field circuit are fixed. Therefore to obtain the desired bridge output voltage (equal to the voltage required by the generator field winding), it is only necessary to select the proper turns ratio for the excitation transformer. Variation of the field voltage to suit particular operating conditions can then be made via delay angle control.

To provide adequate excitation ceilings, the nominal delay angle is usually selected (Cotzas, Hesse and Lane 1979) to allow for an 'excitation margin' of near 50% under normal operating conditions; i.e. by fully advancing the firing angle, the field voltage may be raised by 50%. This would indicate a delay angle of around $45^{\circ} - 50^{\circ}$ for normal generator operation. By an increase in the nominal delay angle to near 60°, a ceiling of 2 p.u. can be achieved since the field voltage is roughly proportional to the cosine of delay angle. Thus by designing the excitation system so that a nominal delay angle of 60° will provide 1 p.u. terminal voltage at rated power, the necessary transformer turns ratio will be defined by the required field voltage for these operating conditions.

The definition of a particular turns ratio for the excitation transformer will also provide a means of fixing a non-arbitrary base for rotor quantities.

6.3.2 Base System

With the field circuit configuration as in Fig. 6.2, it is obvious that the rotor circuit per unit quantities must be calculated relative to a d.c. system set of bases. The base quantities used for the rotor circuit may be fixed by any arbitrary means, such as fixing rated field current as a base value (Anderson and Fouad 1977).

In addition, the direct phase model of the synchronous machine requires that invariant base sets are selected, since for per unit systems in electromagnetically coupled circuits, it is essential to select the same voltampere and time base in each part of the circuit. Normally the base time value is the same in every circuit in an analysis. It can be shown (Lewis 1958) that the choice of a common time (frequency) base forces the voltampere base to be equal in all circuit parts, and also forces the base mutual inductance to be the geometric mean of the base self inductances, i.e.

$$L_{srB} = L_{rsB} = \sqrt{L_{sB} \cdot L_{rB}} \qquad \ldots (6.1)$$

which will ensure the per unit mutual inductances retain reciprocity.

An inspection of the equations for a synchronous generator (equations (2.5) - (2.6)) shows that by choosing three base quantities involving voltage, current and time, all other base quantities will be fixed. This will apply

to both the stator and rotor circuits, and, using the method described in Appendix 9, the stator base quantities fixed are apparent power (MVA), equal to rated stator power, rated line-line voltage (kV) and rated generator speed (radians/sec).

As stated above, the voltampere base and the time base must be the same for both rotor and stator. Therefore there is only one "free" base quantity in the rotor circuit.

The choice of the remaining rotor base quantity depends on the nature of the stator-rotor coupling. As indicated in Section 6.3.1 the excitation system transformer ratio fixed the level of field voltage. In accordance with the per-unit system used for HVDC convertors then, the d.c. (rotor) side transformer voltage is used for the remaining rotor base quantity.

This is different to the base system normally adopted for representation of synchronous machines where the remaining rotor base quantity is a field current obtained from the rated voltage on the no-load saturation curve's air gap line. However this system is normally used in conjunction with an equation set which has undergone Park's transformation, and with fixed or constrained values for the field voltage. For the purposes of an investigation involving dynamic representation of the thyristor excitation, the base system using field voltage is more appropriate.

Obviously, because the stator voltampere base is much larger than the MVA rating of the rotor (field) circuits, some rotor quantities will be large, thus making the corresponding per unit quantities numerically small.

However, this problem will arise irrespective of the base parameter used.

Data for a detailed synchronous machine was compiled from a set relating to machines at Kingsnorth, England, which was used by Campos Barros (1976). The per-unit system contained therein used the rated field current to define a suitable base system for the rotor circuit. For this reason a change in the per-unit data set to the base system described above, which is more conducive to simulation of the proposed excitation circuit, was necessary.

6.3.3 Validation of P.U. System

The original data base is indicated in Appendix A10, and the modified base for use in thyristor excitation applications is included for comparison. To check the conversion of data from that detailed by Campos Barros (1976) (using a different per-unit system) to the required per-unit system and voltage bases, a simple test case was devised which used the system to be investigated ultimately. The data conversion is indicated in Appendix A10.

The preliminary system involved a fixed excitation generator working into a PQ load via a transformer. In order to ascertain whether the specification of rotor voltage base, which results in some rotor per unit quantities having much smaller numerical per unit values (by orders of magnitude), affects convergence, round off errors and accuracy, some tests were performed. The two data sets were shown to produce identical working conditions for a full operating range provided the per unit values of rotor quantities were calculated to the same degree of

accuracy in the data input and initial condition establishment routines.

6.4 INITIAL CONDITION PROBLEMS

The susceptibility of simulations involving detailed machine models to inaccurate initial conditions was indicated by Campos Barros (1976) to be a major problem in his work, which involved generator-rectifier systems. Various explanations, mainly relating to the presence of the HVDC convertor unit, were forwarded to explain the appearance of d.c. components in the stator currents, and fundamental frequency components in the rotor currents.

6.4.1 Transformer Magnetization Effects

Investigations into transformer behaviour (Section 4.7) have shown that a considerable amount of offset in line currents can occur due to a component relating to the magnetizing current. In the transformer model used, initial values for the primary and secondary line currents are assumed to be equal (in per unit). Since magnetizing current will be the difference between the two, or in the convention used (see Fig. 2.1) the sum of I_1 and I_2, the initial value of magnetizing current is therefore forced to be zero in each phase of the transformer bank.

The correct value of magnetizing current however, is directly proportional to the magnetizing flux in the linear magnetizing region of a transformer. Since flux is related to impressed voltage (in per unit) by

$$v = d\psi/dt \qquad \ldots (6.2)$$

and the instantaneous voltages are based on cosine relations, the flux relationships will be sinusoidal, i.e. the flux waveform will lead the voltage waveform by 90^{o}, and will have the same per unit maximum value.

The magnetizing current calculated by the programme will therefore have a fundamental frequency component, and a d.c. component initially equal to the difference between the assumed initial zero value and the actual value which may be calculated from a knowledge of the impressed voltage waveform. The rate of decay of this magnetizing current offset (d.c. component) is largely dependent on the circuit (transformer) resistance involved. Since this is usually low for power transformers, the time taken for the offset to disappear is considerable.

In Section 4.7 a method to eliminate the d.c. component of magnetizing current was devised and illustrated for a simple system involving a source e.m.f., transformer and load. The method involved the use of point-on-wave switching, in which each phase of the transformer and load was connected when the respective phase voltage was a maximum. Since peak (absolute) voltage corresponds to a zero of magnetizing current, if each phase is connected at a voltage maximum, the correct zero value for magnetizing current at the switching instant will be obtained so that no resultant offset occurs.

Preliminary investigations into fixed excitation, detailed synchronous machine models, using a system involving the generator with transformer and load, showed a d.c. component in the stator currents and a corresponding

fundamental frequency component in the rotor circuit. This was related to the connected transformer windings, and therefore the viability of using the point-on-wave switching technique to eliminate transformer magnetizing current offset, and thus the effects on the generator's stator and rotor, were examined.

In the first instance, initial conditions were calculated for the system assuming full load current, and the dynamic analysis was initiated assuming instantaneous values calculated from the initial full load current conditions with all load phases connected. Using the approximate initial conditions calculated in the absence of magnetizing current, as in Section 3.2.1.2, resulted in a d.c. component in the stator currents, the magnitude of which depended on the initial value error for the magnetizing current of each phase. In the case where one phase voltage was a maximum at the initial time step, no resultant offset occurs in that phase, although both other phases had offsets of equal and opposite magnitudes. This offset was approximately equal to the r.m.s. value of the fundamental frequency component. As a result, d.c. offset of the stator currents occurred, with a corresponding fundamental frequency component in the rotor circuit. Since the magnetizing current was rated at only 1% of load current, the effect is rather small overall, and only slight errors occur in the results (again around 1%).

In the second case, the procedure of instantaneously connecting full load at the initial time step was replaced by one involving point-on-wave switching of the load circuit.

It began by using zero stator currents, which required the initial conditions to be calculated for a no-load condition. This required new initial values for I_{fd}, θ_o etc. to be used in the dynamic analysis. By this method, the offset was shown to be significantly reduced or even entirely eliminated.

However the effect of progressively connecting each single phase load was detrimental to the generator behaviour, since it required large changes in field current from the initial no load value to the full load value. In a simple e.m.f. source representation this was not a problem with point-on-wave switching, but in this case significant differences in generator states, with substantial changes in rotor currents, occur for quite some time. These effects are more significant than the original problem, thus ruling out the possibility of using this method to eliminate transformer magnetizing d.c. components.

To counter this problem, instantaneous energization of all three phases from no load initial conditions was investigated. Although an improvement in the speed of attaining steady state conditions over the previous case was experienced, the level of magnetizing current offset was similar to that observed in the first case.

In summary then, no programme techniques could be shown to eliminate transformer magnetizing current d.c. offset, which occurs due to the use of approximate initial conditions, without severely impairing the overall performance of the test system.

6.4.2 Generator Energization

As indicated in the last section, the problem of inaccurate initial values for the currents in the magnetically coupled coils of a transformer can affect the duration of the dynamic analysis needed to obtain accurate initial conditions. By analogy it would seem that the same problems could occur with initial values in a generator modelled by coupled coils, i.e. involving (implicit) magnetizing inductances.

Campos Barros (1976) indicated that problems had arisen in cases involving a fixed excitation synchronous machine, especially where the load was an HVDC convertor as in Fig. 6.3. He showed that when a.c. harmonic filters were present, any unexpected generator components due to inaccurate initial values quickly disappeared. However, without the filters, as might be the case in an isolated generator-rectifier scheme, this decay was not so apparent since the circuit damping resistance, previously provided mainly by the filters, was now small. Therefore the initial condition period had to be significantly extended to eliminate the stator current d.c. components, and the fundamental frequency components of rotor current present.

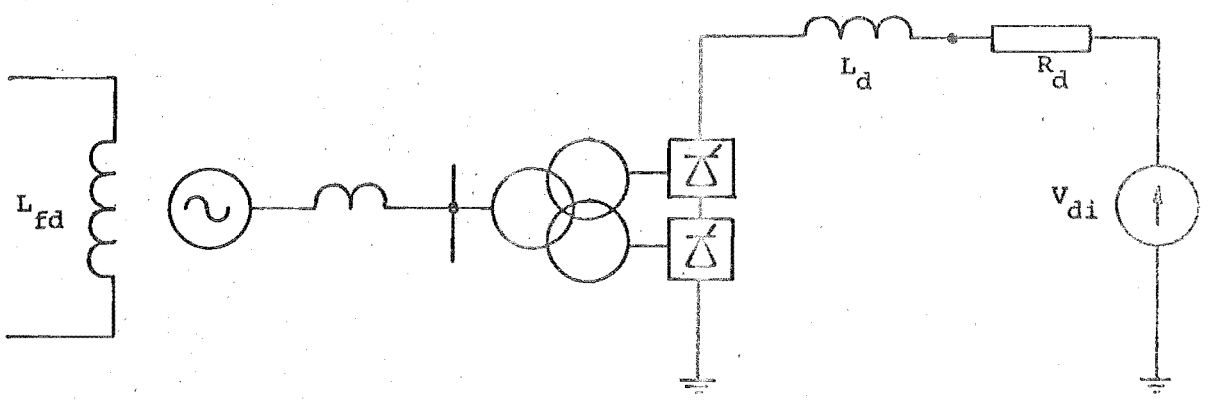

Fig. 6.3 Schematic of Fixed Field Synchronous Generator-HVDC Convertor System

As detailed in Section 3.2.1.2, initial values are calculated using a classical analysis based on positive sequence values only. This approach is satisfactory provided only small unbalances in terminal voltages and currents exist. More accurate calculations accounting for unbalances (e.g. convertor load) by estimating negative and zero sequence currents have been suggested (Brandwajn and Dommel 1979, Gross and Hall 1978), but the initial values thereby calculated, ignore 3rd and higher harmonic effects. Therefore again, some simulation time is required for the steady state operating point to be obtained dynamically, albeit shorter than without these more accurate calculations.

Modification of the rotor damper's resistances to inflated values allows the time constants of the machine to be artificially reduced, so that the initial value errors disappear more rapidly and the machine moves quickly to its steady state. By analogy with the transformer magnetizing offset case, this provides increased rates of decay to initial value errors which were caused by assuming balanced and sinusoidal steady state conditions in the generator. This artificial method is sufficiently adequate, with decay rates fast enough to not require the more laborious solution entailing more accurate initial value specifications.

Although the majority of these unexpected generator components is thereby removed, the components due to transformer magnetizing current offset will remain. Campos Barros also suggested starting from no load conditions, but as indicated in Section 6.4.1 this can have dramatic effects

on the generator circuit as it goes from no load to full load, without removing transformer magnetizing current offset.

Fig. 6.4 indicates the rotor currents from an initial condition study (case 0093) involving a fixed excitation, detailed generator model which is connected via parallel transformers to a rectifier in 12 pulse operation (all modelled explicitly). The short d.c. link is a simple inductive model and the invertor is modelled as a constant d.c. voltage source (see Fig. 6.3). The reason for using these simplistic models for the d.c. line and invertor system, is to enable generator problems to be isolated by eliminating possible contributory effects from a controlled invertor and naturally resonating link. Increased damper resistances are also used in the initial condition period to accelerate the decay of unexpected generator current components.

Fig. 6.4 0093 ROTOR CURRENTS

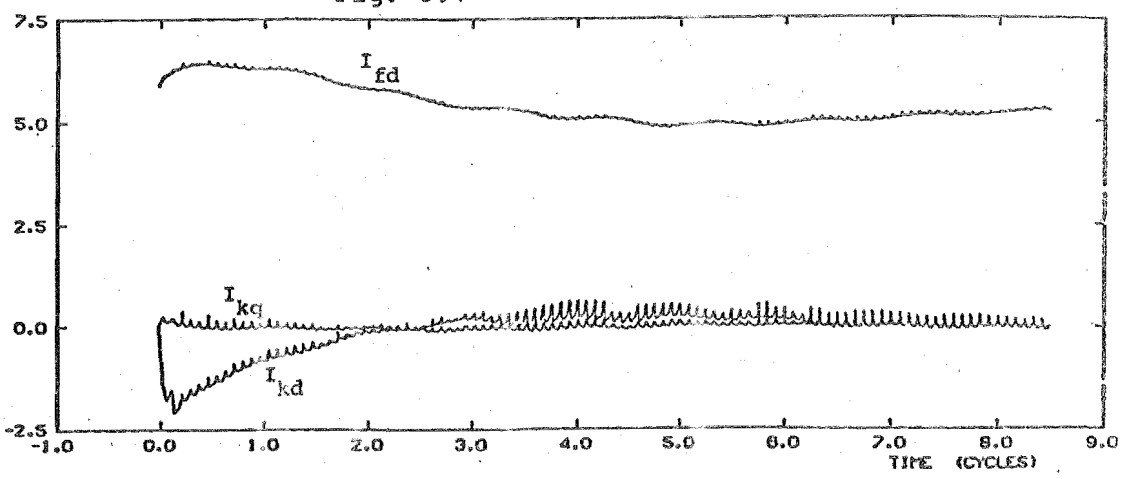

The field current waveform in Fig. 6.4 contains significant 12 pulse ripple which can be directly related to the short circuit existing during the 12 commutation processes occuring every cycle. Also evident is a fundamental frequency component which is related to stator current d.c. offset. This occurs because of inaccurate initial values for transformer currents, viz. ignoring the magnetizing current effect, as explained in Section 6.4.1. Inspection of the actual magnetizing current verified the presence of a considerable offset in two phases of approximately 3% of load value. This correlates with the magnitude of the fundamental component of field current.

The other, more obvious, effect is a continuous change in the d.c. level of field current. This is not cyclic, but occurs very slowly with some decay of its envelope pattern, although even after ten cycles it is still not settled. This behaviour is not related to the effects already mentioned, nor is it related to inaccurate initial values due to calculations based on positive sequence currents, since increased damper resistances have been used to ensure that such effects decay quickly. This initial decay is demonstrated in Fig. 6.4 over the first two cycles.

Closer inspection of the test system and the method of calculating initial conditions (see Section 3.2.1) reveals that the analysis of the system to obtain initial values uses a quasi-steady state model for the d.c. link based on fundamental components in the a.c. system.

The generator parameters are then calculated for a positive sequence network using these fundamental a.c. quantities. However the actual system will, in the absence of harmonic filters, display considerable distortion, which will effectively result in a reduced r.m.s. level of terminal voltage. As a consequence the initial values of rotor angle and excitation parameters, as well as the d.c. link variables, will be different to those estimated in the absence of distortion. Therefore the effect indicated in Fig. 6.4 is an illustration of the shift to a new set of operating conditions (I_{fd}, I_d, α_r etc.) under the fixed excitation which was calculated erroneously.

Since excitation is fixed, the rectifier firing control will control the operating point shift. In this case the reduced effective terminal voltage caused a decrease in direct current. Control action responded by advancing α_r which resulted in a restoration of I_d back towards the setting. The amount of control via α_r was insufficient however, and only a change in the excitation voltage will restore I_d fully. Additional increases in E_{fd} would allow both α_r and I_d to return to their nominal values.

In summary then, to dynamically obtain a given steady state condition, several aids must be implemented:

(i) the correct initial values must be calculated to eliminate transformer magnetizing current effects on the generator;

(ii) effects due to slight inaccuracies in initial values based on balanced conditions must be

eliminated by increasing damper resistances; and

(iii) the correct operating point must be found by taking into account the effect of waveform distortion etc.

Point (iii) will be discussed later with reference to a relevant system. Point (ii) has already been discussed and successfully solved above. The solution to (i) is outlined below.

6.4.3 Solution of Magnetizing Current Initial Value Problem

Experience has shown that if energization, i.e. connection to source, of each transformer phase is performed at peak voltage, only the fundamental frequency component of current will be present in the ensuing dynamic analysis. This indicates that the initial zero value specified for magnetizing current is correct, as explained in Section 6.4.1. However, this method of selective energization of a transformer phase was found unacceptable in Section 6.4.2 for systems involving detailed generator models and/or convertor bridges. Therefore a means of exactly calculating the initial instantaneous magnetizing current must be established, and this value used implicitly in specifying different initial primary and secondary winding currents. Equation (6.2) shows that since

$$\int \cos u \, du = \sin u \qquad \ldots (6.3)$$

the magnetizing flux (current) waveform is a sine waveform, with a maximum magnitude equal (in per unit) to the maximum voltage magnitude scaled by the magnetizing admittance (Y_m), i.e., if

$$v = V_m \cos \omega t \quad \ldots (6.4)$$

then

$$i_m = Y_m V_m \sin \omega t \quad \ldots (6.5)$$

Therefore knowledge of the voltage impressed on the transformer will allow accurate estimates of magnetizing current to be calculated, which in turn will be used to calculate different per unit values of primary and secondary current. This then correctly specifies the initial value of magnetizing current, and so its only component is of fundamental frequency and no d.c. offsets occur in the line currents.

6.5 VALIDATION OF EXCITATION SYSTEM MODEL

To test the model proposed in Section 6.2 to represent a thyristor bridge direct excitation system, the simple test system in Fig. 6.5 was used. The rating of the exciter transformer was made excessively large to amplify the effects of excitation control. The data for the scheme is indicated in Appendix 10, where it is noted that the load circuit is designed to represent reasonably closely a PQ equivalent of the proposed HVDC link to be used in later tests. With the high rating of the exciter circuit, nominal voltage was provided by a thyristor delay angle of 80°. This gave excellent opportunity for large ceiling voltages of either polarity with small changes in control angle.

The proposed tests were designed to investigate the validity of the excitation model, and for this reason the first test was to examine the feasibility of the model under steady state conditions.

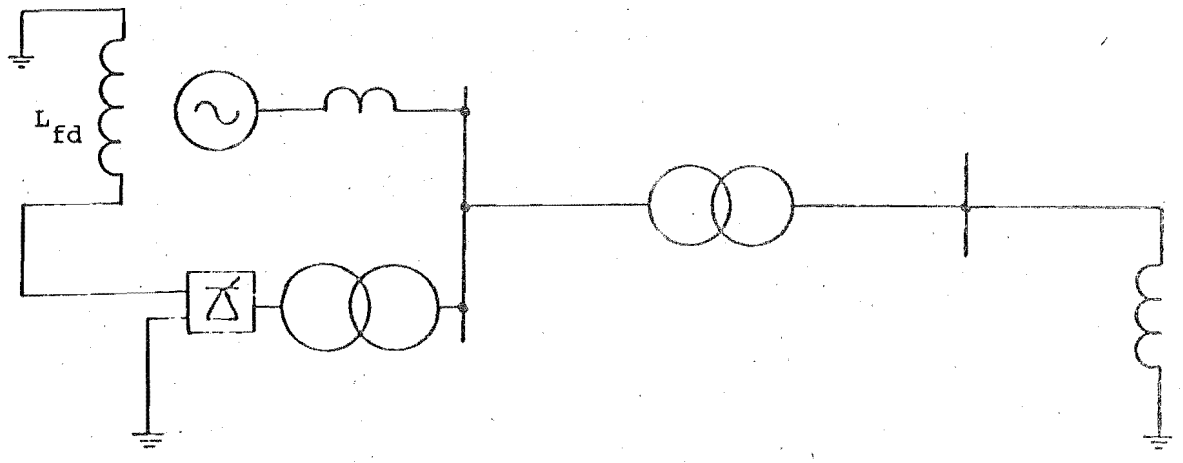

Fig. 6.5 Schematic of System used to Validate Thyristor Bridge Exciter Model

6.5.1 Steady State Conditions

Using a normal single phase (positive sequence network) steady state analysis, the r.m.s. values of the a.c. system quantities were determined for a fixed loading condition. Using the method in Section 3.2.1.2, the initial values for the generator (θ_o, I_{fd}) were determined. These values then gave an indication of the necessary firing angle of the exciter bridge. At this stage, the effect of any transformer magnetizing current was neglected, although increased rotor damper winding resistances were used.

The waveforms for this case (0195), illustrated in Figs 6.6(a) and (b), give an indication of the generator's terminal voltage and its rotor currents for an initial condition study using the initial values described above. The slowly decreasing 'average' field current, and consequent reduction in terminal voltage magnitudes, can be directly related to the initial specifications of θ_o and α_e. Since the thyristor bridge is simulated in the same way as a convertor bridge, its firing pulses, in the absence of any control signals, occurred at regular intervals and were not measured relative to actual voltage cross-overs (α).

Fig. 6.6(a) 0195 GENERATOR VOLTAGE

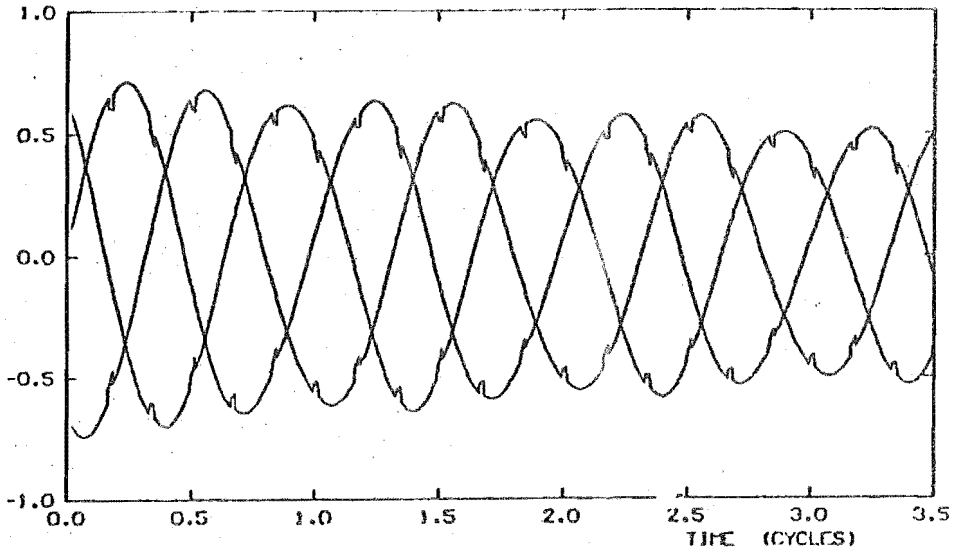

Fig. 6.6(b) 0195 ROTOR CURRENTS

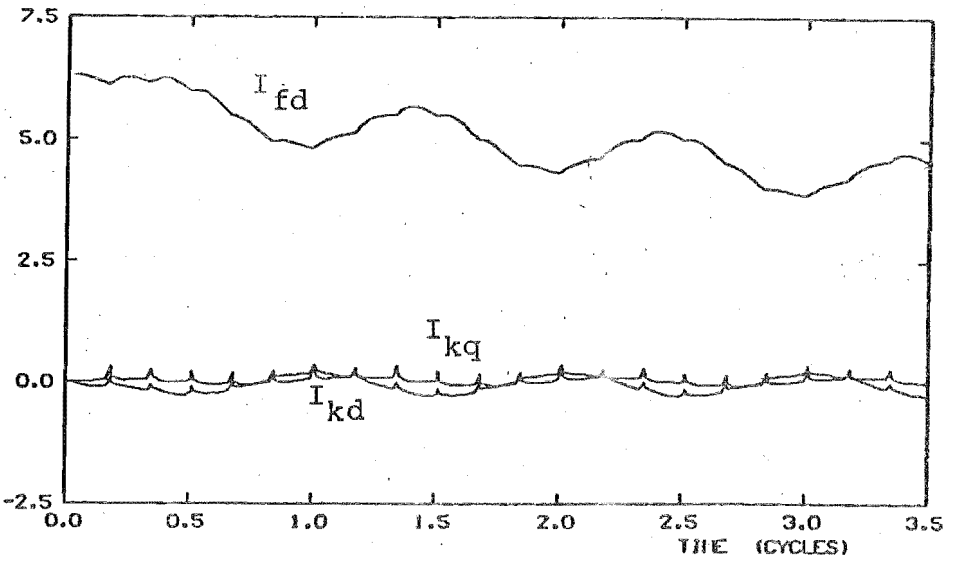

Investigations of the actual waveform cross-overs and the firing instants showed that the exciter valves were actually firing at an angle greater than 80^{o}. This was found to be due to small inaccuracies in the initial value calculations, especially in θ_{o}, which resulted in different voltage phase relationships to those predicted. Obviously then, the effect of any errors in the initial rotor angle will affect the voltage phase angles, and thus the timing of exciter

valve firings, and consequently the level of field voltage and current.

Also significant in the figures is a 50 Hz component in the rotor current, and a d.c. component in the terminal voltages. This is entirely due to transformer magnetizing currents, as explained in Section 6.4. Because of the feedback effect - i.e. any d.c. component in the exciter transformer windings will be impressed on to the bridge, and thus the field current - the offset magnitude is much greater than with the fixed excitation system investigated in Section 6.3.

To clarify the above problems, a new set of initial values were calculated, to a greater degree of accuracy than above, in an attempt to obtain a constant 'average' field current. The results for this case (1195) are indicated in Figs 6.7(a) and (b) where it can be seen that the drift in field current has been eliminated almost entirely, resulting in constant maximum phase voltage magnitudes. However, the component due to transformer magnetizing current is still significant.

To eliminate this effect the method proposed in Section 6.4 was utilised, as detailed in Appendix 10, for this particular case. The resultant waveforms for this case (2195) are shown in Figs 6.8(a) and (b). The magnetizing currents' d.c. components in both the load and exciter transformers are significantly reduced (compare Figs 6.9(a) and (b)) by this method. The component still present is due to the inability to correctly specify the initial values of r.m.s. magnitude and phase angle for the terminal voltage.

Fig. 6.7(a) 1195 GENERATOR VOLTAGE

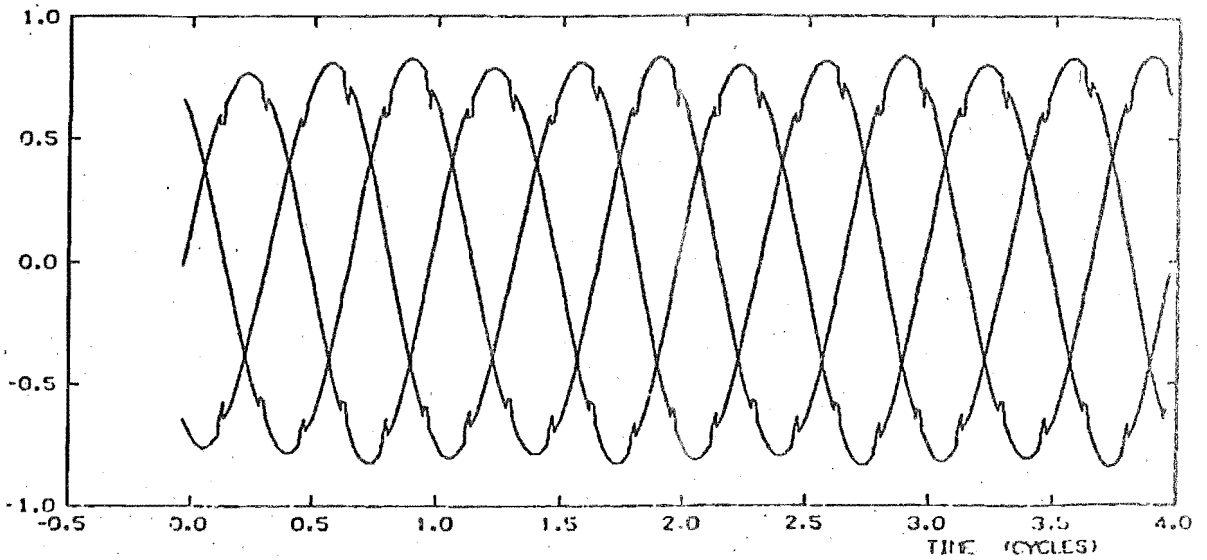

Fig. 6.7(b) 1195 ROTOR CURRENTS

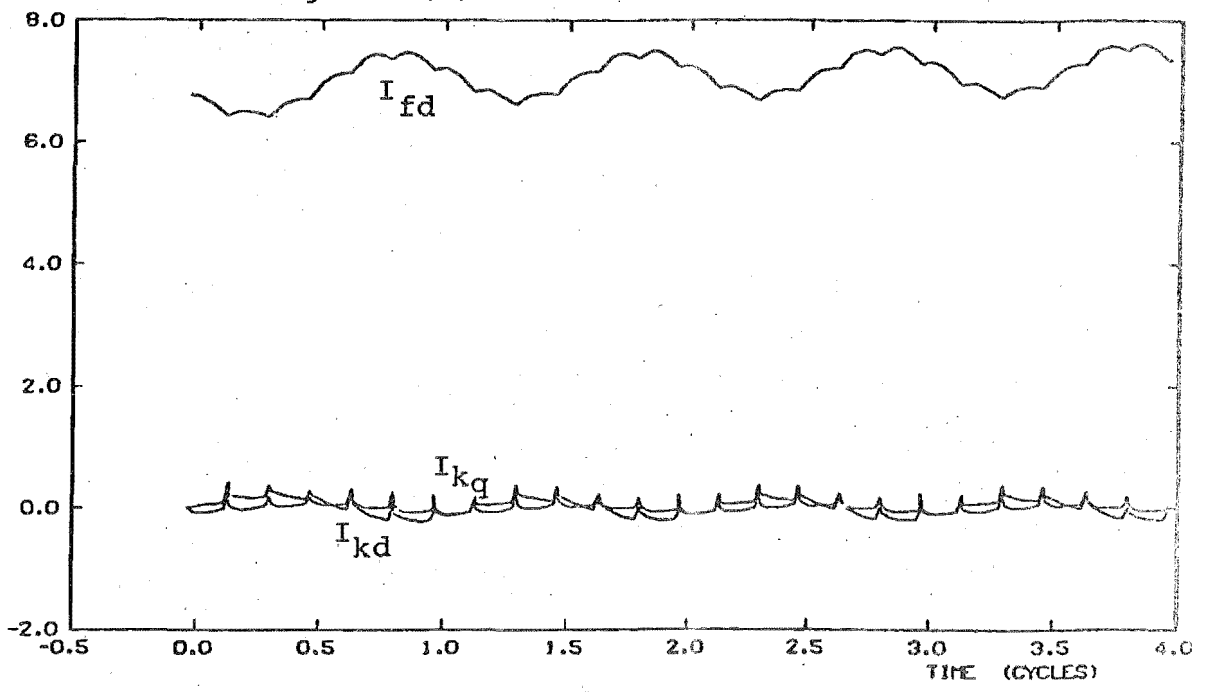

Fig. 6.8(a) 2195 GENERATOR VOLTAGE

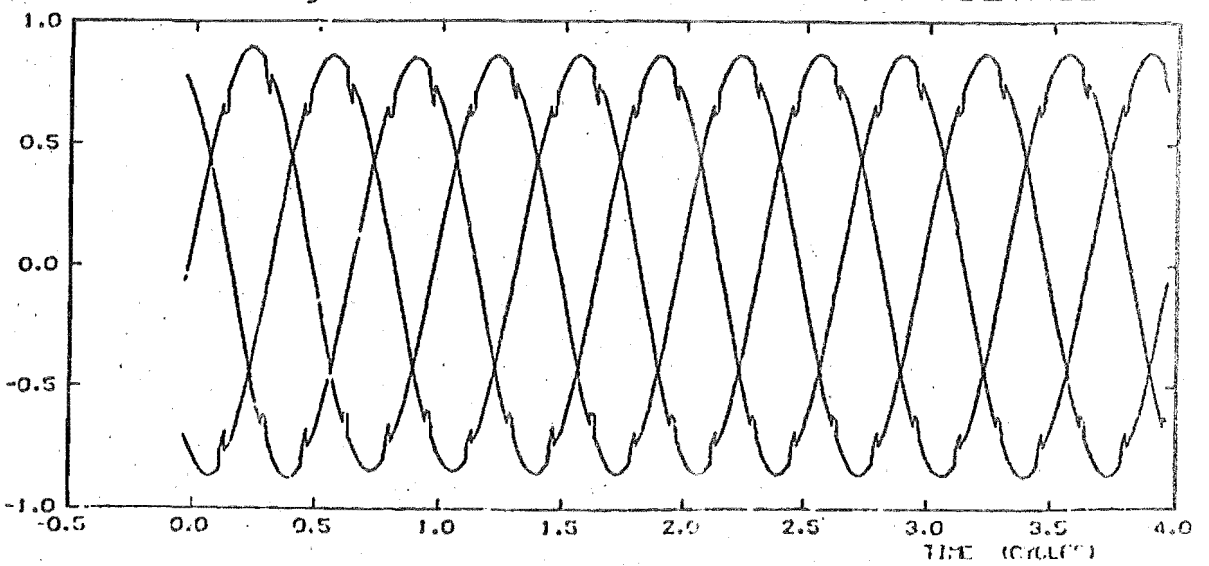

Fig. 6.8(b) 2195 ROTOR CURRENTS

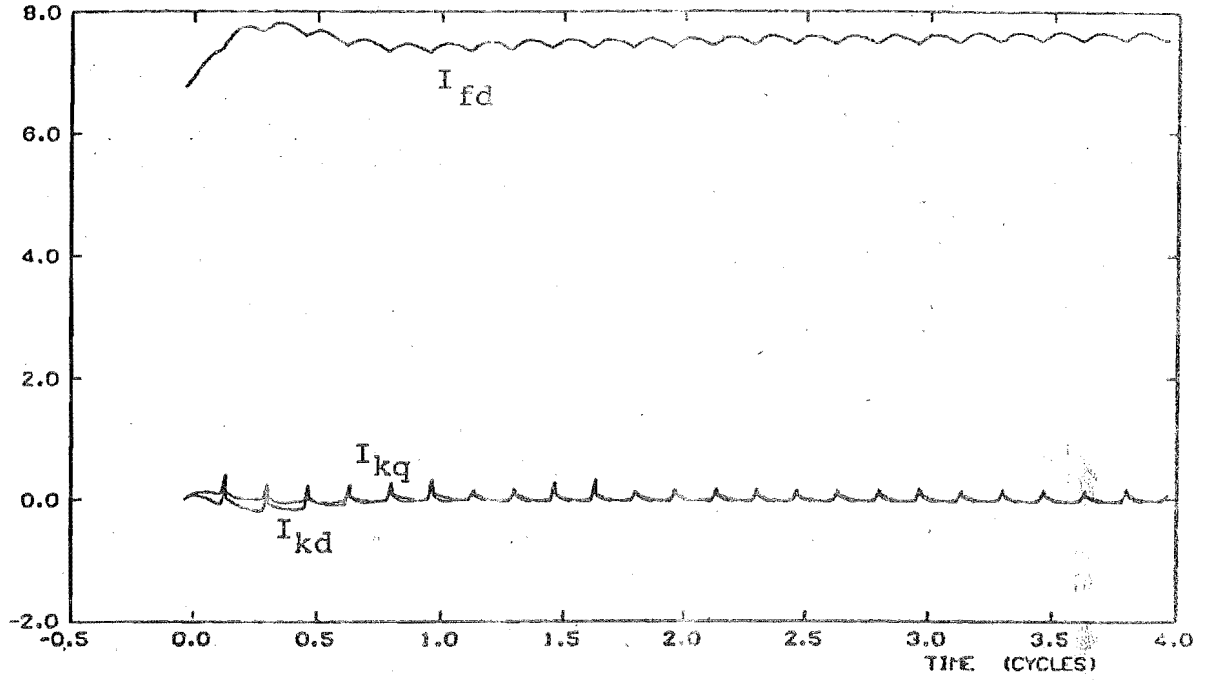

Fig. 6.9(a) 1195 MAGNETIZING CURRENTS

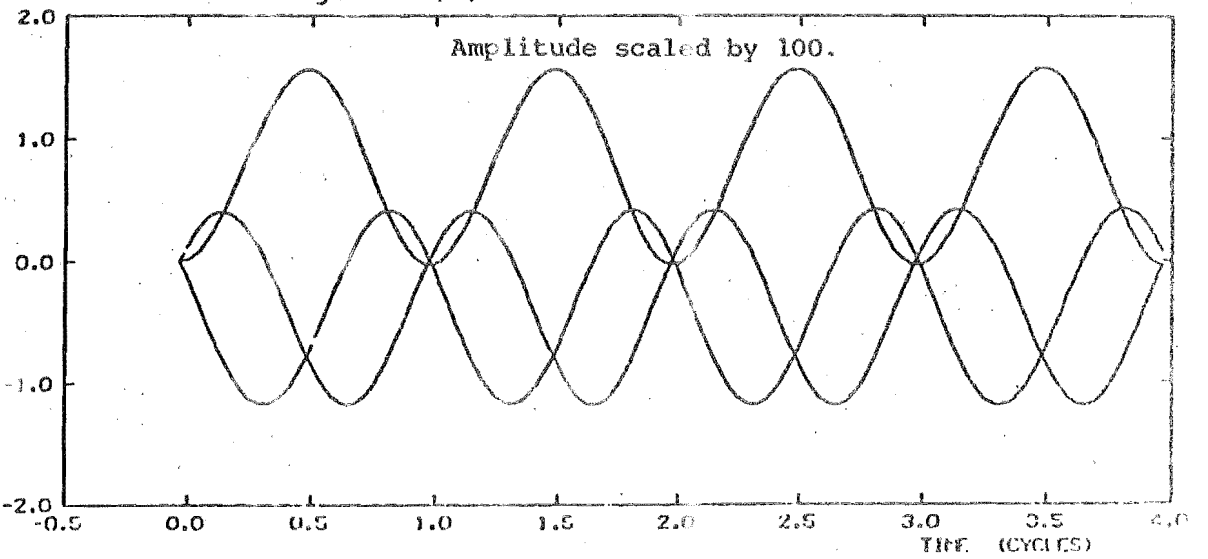

Fig. 6.9(b) 2195 MAGNETIZING CURRENTS

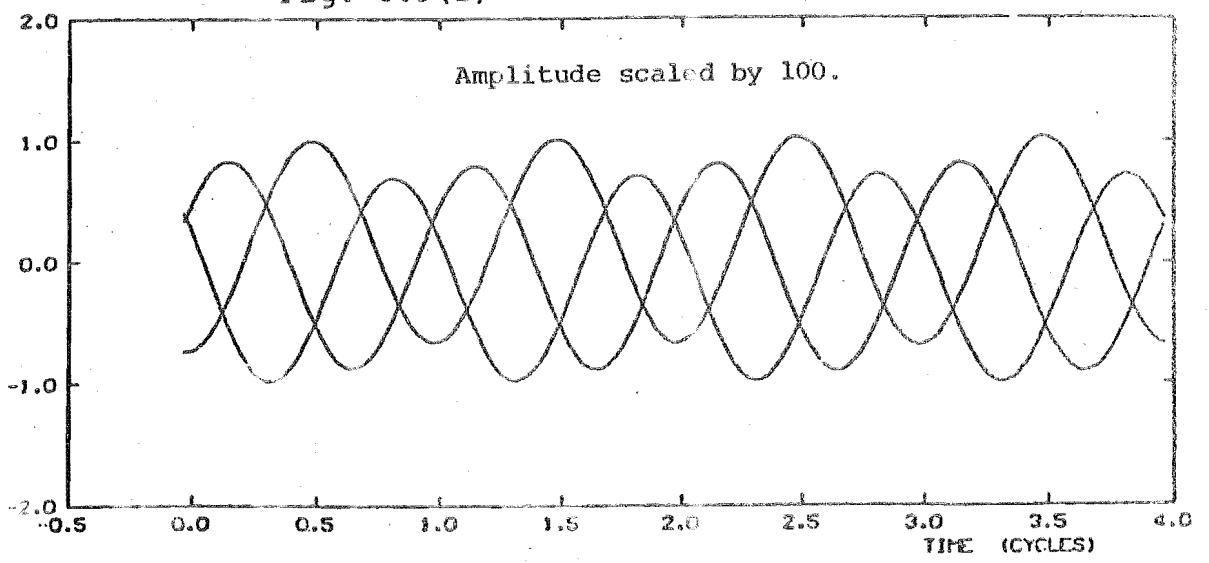

The use of increased damper resistances has ensured that the generator settles to its initial state rapidly (within one cycle). The field current is then very settled with a dominant 6 pulse ripple, as expected for the output of a 6 pulse bridge. The magnitude of this ripple could be reduced by changes in the system parameters. The terminal voltages are also balanced, with a small amount of distortion due to the presence of the (over-rated) excitation circuit. Again, this distortion (during commutation periods) could be reduced by better design.

From these results then, it is seen that with careful calculation of initial rotor angle, exciter firing angle and field current, combined with a good approximation for initial values of transformer magnetizing current, the system quickly settles to the specified operating condition. This validates the use of the excitation model and solves all the initial condition problems normally associated with simulation of such a circuit.

The ability of the system to perform under disturbed conditions must also be investigated to show the feasibility of modelling the excitation system by the above means.

6.5.2 Disturbed Conditions

A preliminary test to show the desired response to a temporary demand for increased generator terminal voltage was performed primarily to illustrate the practicality of the exciter's thyristor firing angle control in regulating terminal voltage. Similarly, a simulated three phase fault in the a.c. system was studied to investigate the required exciter response. These tests were not designed to

investigate the actual voltage regulation control parameters, but merely to illustrate the feasibility of the proposed model in responding to certain demands.

In the first instance (case 3195), the initial conditions provided by the settled case in Section 6.5.1 were used to start the study. The exciter firing pulse train was advanced 10^{o} for 2½ cycles so that the new firing angles were 70^{o}. The effect on field current is readily observed in Fig. 6.10(a) where it is seen to steadily increase to approximately 115% of its original level. The terminal voltages (Fig. 6.10(b)) have similarly increased to nearly 110% of their original level. This illustrates the quick action possible using thyristor control of the excitation circuit.

Fig. 6.10(a) 3195 ROTOR CURRENTS

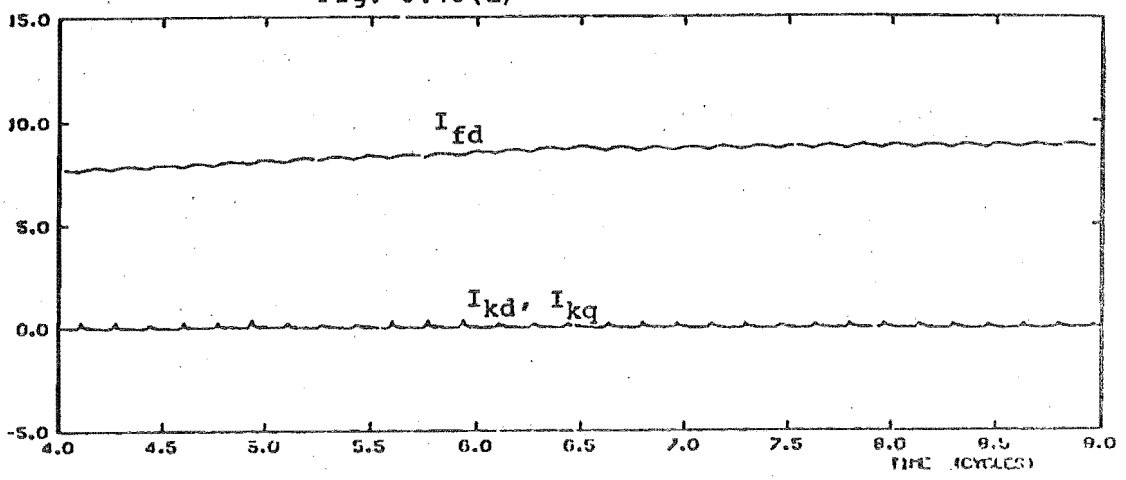

Fig. 6.10(b) 3195 GENERATOR VOLTAGE

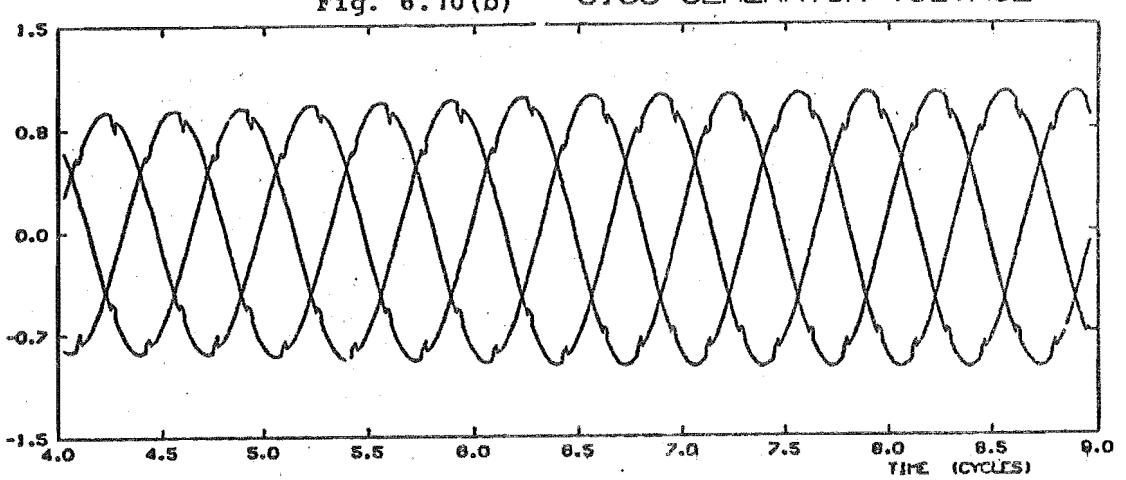

As explained, the actual control response is not simulated here, the major interest being to illustrate the ability of the model to indicate excitation circuit response, and the resultant generator effects. After 2½ cycles the pulse train was retarded so that the original firing angle was restored. With the increase in terminal voltage due to the period of increased excitation, returning the exciter firing angle to near 80^{o} stabilises the generator terminal voltage at its new level.

It is obvious from this simple example that the effect of fast excitation control can be simulated using the proposed model. As a further example, the performance under disturbed conditions was investigated. The disturbance simulated was a remote three phase fault which, in the absence of excitation control, would result in a 15% reduction in generator terminal voltage. Campos Barros (1976) simulated several similar faults (mainly at the generator terminals) with a fixed excitation model for the machine.

The instant of fault occurrence affects the level of d.c. offset which will be present in the stator currents. For severe faults the offset can be significant, and in studies of a three phase fault at the generator terminals the field current was shown to have a corresponding fundamental component, in certain cases with a magnitude greater than the pre-fault d.c. level. As indicated in Section 6.5.1, stator d.c. or rotor fundamental frequency components are magnified by feedback in the test system used here.

Preliminary investigations of a three phase fault close to the generator terminals verified this effect with the peak value of the fundamental components due to the instant of fault approximately equal to 80% of the pre-fault field current level. Therefore to avoid confusion, these effects were reduced by simulating a remote fault for which classical analysis predicted a generator terminal voltage drop of 15%.

In conjunction with the fault application, a signal was delivered to the exciter's firing control to advance its grid pulses. This forced earlier firing in the exciter, thus creating more field voltage. As a result, field current and generator terminal voltage increased, the latter to its pre-fault level after just three cycles of pulse train advance. These effects (for case 4195) are indicated in Figs. 6.11(a) and (b).

Fig. 6.11(a) 4195 ROTOR CURRENTS

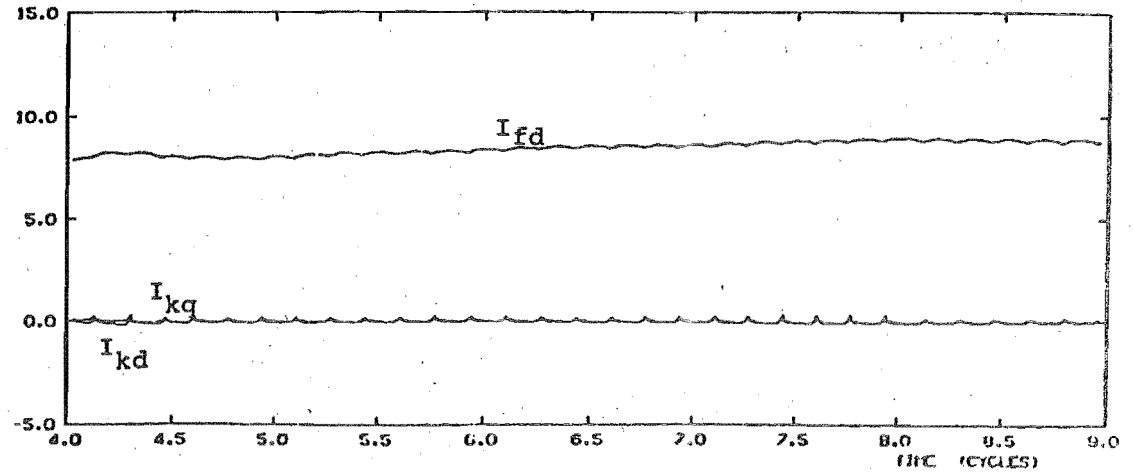

Fig. 6.11(b) 4195 GENERATOR VOLTAGE

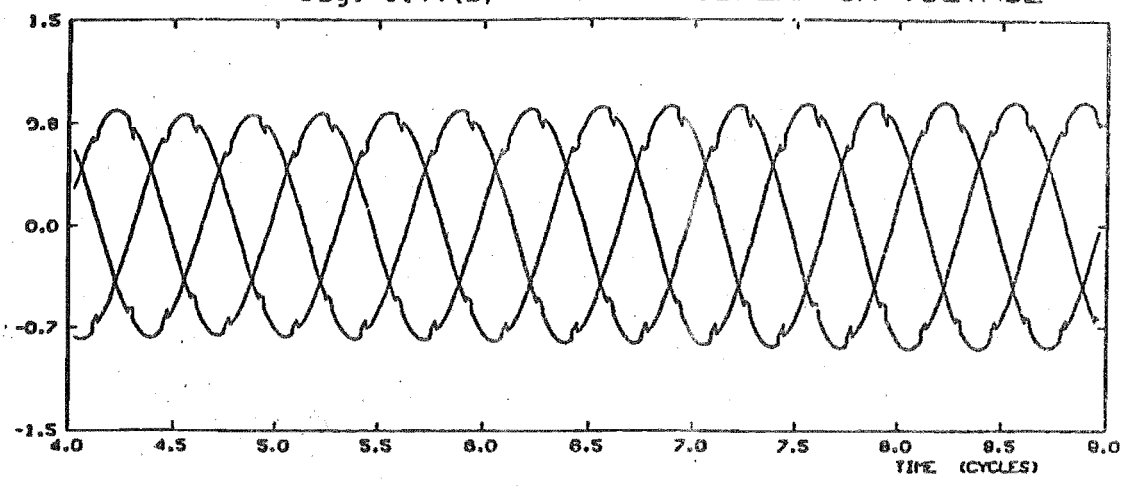

6.6 ISOLATED GENERATOR-RECTIFIER APPLICATIONS

The concept of the generator-HVDC convertor unit was advocated during the last decade (Calverley *et al.* 1973, Krishnayya 1973) in an effort to reduce HVDC system costs. Since the terminal costs of HVDC schemes dominate, any such reduction improves the economic feasibility of HVDC as an alternative to a.c. transmission. This concept proposed operation without a.c. harmonic filters, as indicated in Fig. 6.12. The elimination of a.c. filters, a.c. switchyard, etc., by the use of unit type connections would not only remove associated operational problems (Kimbark 1971), but would render HVDC an even more attractive alternative for power transmission from remote sites.

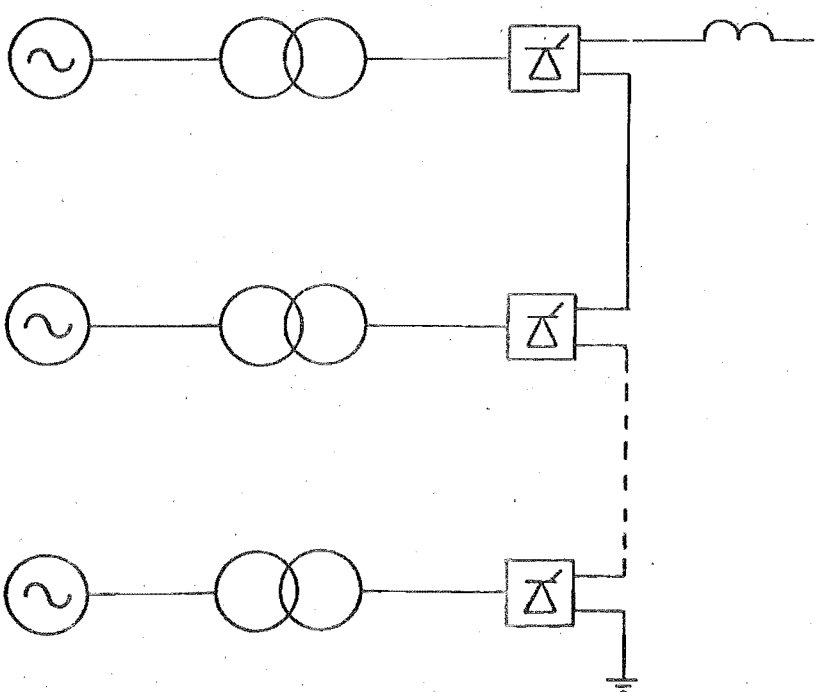

Fig. 6.12 Schematic of Unit Type Scheme

The effect of operation without harmonic filters was analysed by Bonwick and Jones (1972), and subsequently, dynamic analysis of the performance of a synchronous machine supplying a rectifier load was performed by El-Serafi and Shehata (1980) with particular attention to the harmonic analysis of resultant waveforms. From these studies, the capability of generators to withstand the harmonic currents in the machine windings was assessed, and suggestions for design refinements were made to ensure the unit type application was feasible. Normal hydro generators should be capable of operating in a unit type connection with twelve pulse convertor loads.

Investigations by Arrillaga, Arnold *et al.* (1977) highlighted the mismatch that exists between the traditional controllers of synchronous generators (AVRs) and HVDC convertors. These investigations of unit type connections of generator and convertor (as in Fig. 6.12) showed that there was no real need for both types of control (i.e. excitation and convertor), since each generator operates independently and is connected directly to the convertor transformers, in isolation.

The replacement of the controlled convertor at the sending end of an HVDC link by a diode rectifier was proposed (Bowles 1977, Jotten *et al.* 1978) for applications involving isolated (e.g. hydro, mine-mouth) generation infeed by HVDC, where voltage (power) reversal was not required. The economic gains to be achieved by an isolated generator-diode rectifier scheme can be substantial, since much of the equipment normally associated with HVDC convertors, e.g.

a.c. filters, bus work, circuit breakers, buildings, control and communication systems can be eliminated or reduced. The reliability of the simpler diode rectifier would also be much greater than the corresponding thyristor bridge in the absence of the grading, control, communication and damping requirements of a controlled bridge.

A further advantage of diode rectifier operation is that harmonic generation is minimised, and in general, would be below the tolerable levels of hydraulic generators thus ensuring the feasibility of a.c. filter removal and unit type operation.

These advantages, which are detailed by Bowles (1977), show that for isolated generation, the generator-diode rectifier technique offers substantial reductions in associated HVDC equipment and a more flexible, more reliable and more easily maintained and operated convertor unit.

The feasibility of such schemes however, is very much dependent on their ability to perform control and protective functions. Such functions, including the synchronous generator's excitation must therefore be examined to determine the feasibility of the system. To provide adequate control and protection, the excitation must be fast acting (Evans and Brown 1977), such as provided by the thyristor bridge excitation circuits detailed above. As indicated, these excitation systems can only be accurately simulated by dynamic analysis.

The following sections will investigate firstly the performance of a fixed excitation generator model with a controlled rectifier load, and secondly a fast thyristor

excitation-generator model with an uncontrolled rectifier. Preliminary investigations into the latter's performance under d.c. fault conditions will also be conducted.

6.7 FIXED EXCITATION GENERATOR-CONTROLLED RECTIFIER SYSTEM STUDIES

During certain a.c. conditions, the Kingsnorth HVDC scheme may operate with one of its large generators feeding the d.c. link in isolation. Studies of this configuration were reported by Arrillaga *et al.* (1977(2)). These studies were not concerned with excitation effects, although Campos Barros (1976) did perform a preliminary study of the effect of excitation on the performance of a system such as in Fig. 6.12. He concluded that with a 25% change in excitation voltage, although the field current altered significantly over a few cycles, a similar, opposite current was induced in the rotor's d-axis dampers, with the result that the nett rotor flux remained practically constant with no resultant effect on the generator's performance.

However, investigations into thyristor excitation of a.c. generators (Section 6.5) have shown that using the same generator data, significant changes in terminal voltage magnitudes can be obtained by rapid alteration of the effective field voltage. Therefore the system illustrated in Fig. 6.3 (using the data set in Appendix A10) was investigated to determine not only its response to excitation changes, but also its steady state performance and the possible interaction between convertor controls and excitation.

As indicated in Fig. 6.4, this system (0093) took some time to attain reasonable steady state conditions. Some of the reasons for this have been discussed in Section 6.5. However in addition to these reasons, the absence of a.c. harmonic filters contributes markedly to initial condition problems. Their absence removes a source of the reactive power requirements of the convertor, and as a result the initial conditions predicted by classical analysis (assuming balanced sinusoidal waveforms) are inaccurate. A higher level of excitation (and field current) will be necessary to provide this extra reactive power in the absence of sinusoidal waveforms, and thus give the operating condition predicted.

However, initial condition problems associated with non-sinusoidal waveforms, due to the absence of harmonic filters, occur not only in relation to discrepancies in reactive power and excitation level assumptions, but also in the initial specifications of line currents. These line currents, ignoring magnetizing components, are obtained directly from knowledge of the convertor valve states, so that in the absence of harmonic filters the stator currents have square wave shapes (as for 12 pulse operation). Whereas sinusoidal stator currents will correctly identify the correct voltage magnitude and phase relationship as predicted by θ_o, this will not be true for non-sinusoidal currents, since the derivatives of current are now zero in the commutation free periods.

The result is seen in Fig. 6.13(a) where initial values for terminal voltages are clearly excessive.

Fig. 6.13(a) 0093 GENERATOR VOLTAGE

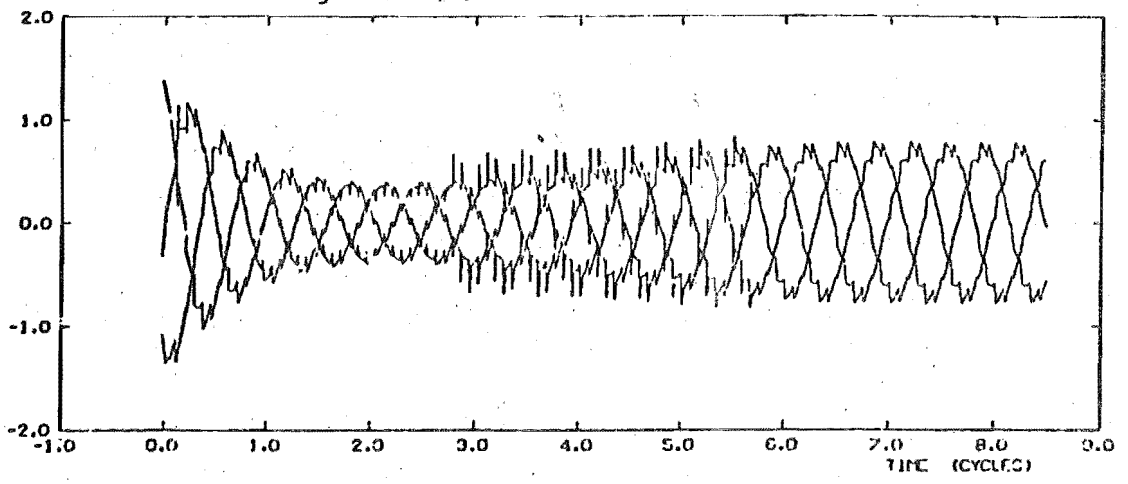

Fig. 6.13(b) 0093 RECTIFIER CURRENT

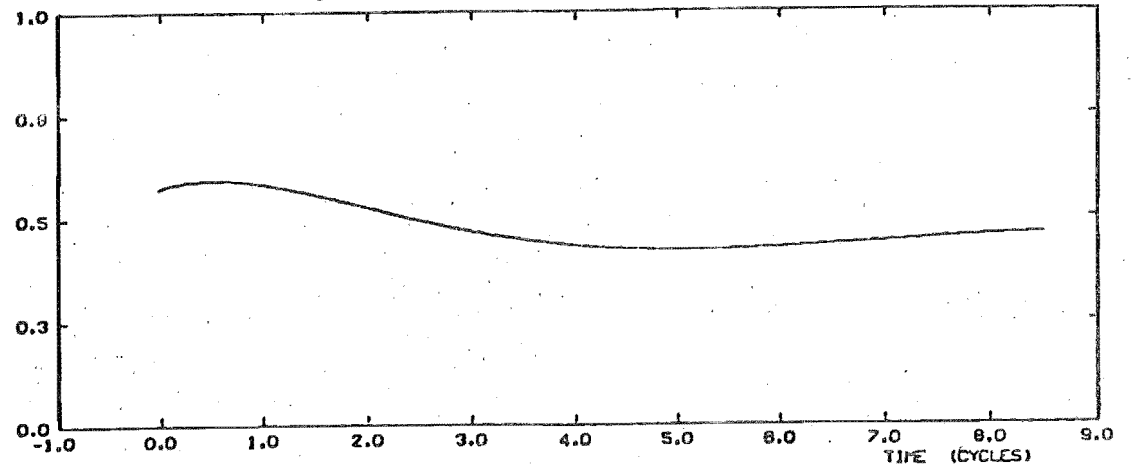

During the initial condition period, because of the excessive generator terminal voltage, I_d increases above its initial specification (Fig. 6.13(b)). Therefore the initial convertor response is to retard α_r.

The error in voltage waveform is, however, quickly eliminated with high rotor resistance, as seen by inspecting the field current response in Fig. 6.4, and the terminal voltages in Fig. 6.13(a). Consequently, as a result of this

fast (increased rotor damping) generator response, and the increased regulation due to increased direct current, the voltage waveform becomes depressed, which results in a decreasing direct current. Therefore the convertor controller then acts to advance α_r towards α^{min}.

Inspection of Fig. 6.13(a) indicates these changes in rectifier firing angle, with a large amount of distortion occurring as a result of firing retard action, and then, with firing angle at a minimum for a sustained period, a minimal amount of distortion is apparent (cycles 5.5 to 8.5).

With the fixed level of excitation predicted by classical analysis, it is seen that after some 5 cycles of simulation, the system has settled at a reasonably constant operating point. This operating point has a reduced direct current level (90% of nominal) and a reduced field current (83% of nominal). As a result of the deficiency in direct current, the rectifier firing angles have been advanced to α^{min}.

Moreover, the extra demand for reactive power in the absence of harmonic filters has resulted in depressed generator terminal voltages. Figs 6.4 and 6.13(a) and (b) indicate that continued operation with α^{min}, but with a step change in excitation voltage to 115% of nominal, results in an increase of around 10% in both the field current and convertor current after just two cycles. By further increasing the excitation voltage, the desired convertor current (I_d^{sp}) could be attained. The time taken for this to occur would be controlled by the magnitude and rate of the change in excitation voltage.

The difference in exciter and convertor controller time responses, however, makes an objective investigation of this behaviour difficult. Elimination of one of the controllers, which are both performing the same basic operating task, would be of more interest. The ability of fast excitation control, with high ceiling voltage limits, to perform this function will determine whether excitation control is sufficiently rapid to eliminate the need for fast convertor control. If this can be shown to be true, then considerable savings in HVDC convertor terminal costs could be achieved in remote applications.

To investigate the effect of excitation control, the controlled rectifier in the above case can be replaced by a diode rectifier, and the fixed excitation, E_{fd}, by a thyristor bridge excitation circuit.

6.8 FAST THYRISTOR BRIDGE EXCITED GENERATOR-UNCONTROLLED RECTIFIER SYSTEM STUDIES

The system illustrated in Fig. 6.14, with test data as detailed in Appendix A10.4, is used to analyze the steady state performance and the initial response to d.c. line or remote end a.c. faults.

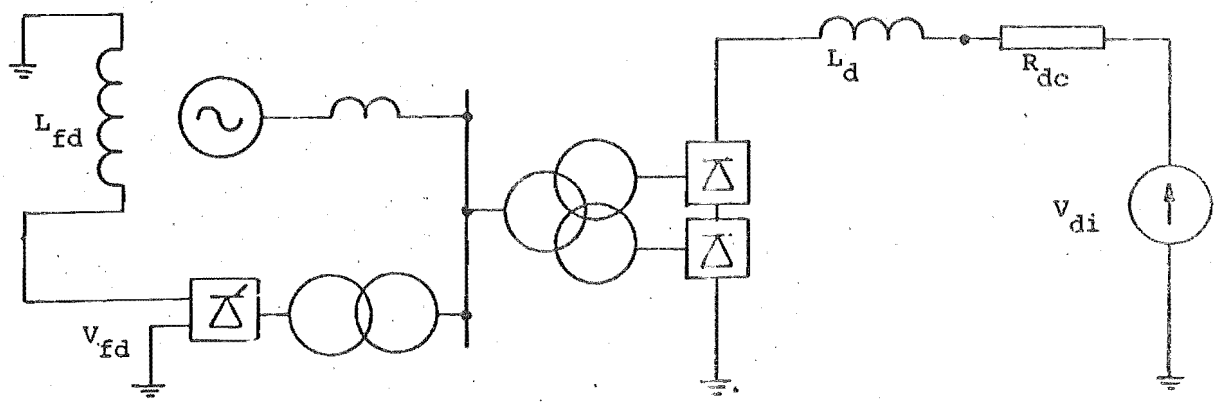

Fig. 6.14 Schematic of Thyristor Bridge Excited Synchronous Generator-HVDC Diode Rectifier System

6.8.1 Preliminary Studies

As indicated in Section 6.7, zero values for line current derivatives, as a result of non-sinusoidal waveforms, create errors in matching terminal voltage conditions to those predicted by the analysis in Section 3.2.1.2. However, adjustment of the rotor angle θ_o, whilst retaining the same initial values of line currents, provides a closer approximation to the required steady state operating point.

In the test case, an adjustment of some 15^o was necessary to get reasonable magnitudes for the generator and convertor terminal voltages. Table 6.1 indicates the approximate instantaneous magnitudes of rectifier voltage obtained for several values of θ_o at time zero, with all other parameters constant.

Table 6.1 Effect of Initial Rotor Angle on Initial Conditions

θ_o	-18.5	-9.25	0.0	4.25	5.0	9.25
V_{dr}(p.u.)	7.2	5.3	3.3	2.4	2.2	1.4

The initial condition calculations of Section 3.2.1.2 predicted an initial rotor angle of -9.25^o, yet specified a rectifier d.c. terminal voltage of 2.2 p.u. As can be seen in Table 6.1, these two conditions are incompatible, and only by adjusting θ_o from -9.25^o to $+5.0^o$ are the correct waveforms, as specified by the load flow analysis, attained.

At this stage no other changes were made to enhance the initial condition period. The initial condition period for case 0193 extends from cycles 0 to 1.5 in Figs 6.15(a) (generator voltage), (b) (rotor currents) and (c) (rectifier current).

Fig. 6.15(a) 0193 GENERATOR VOLTAGE

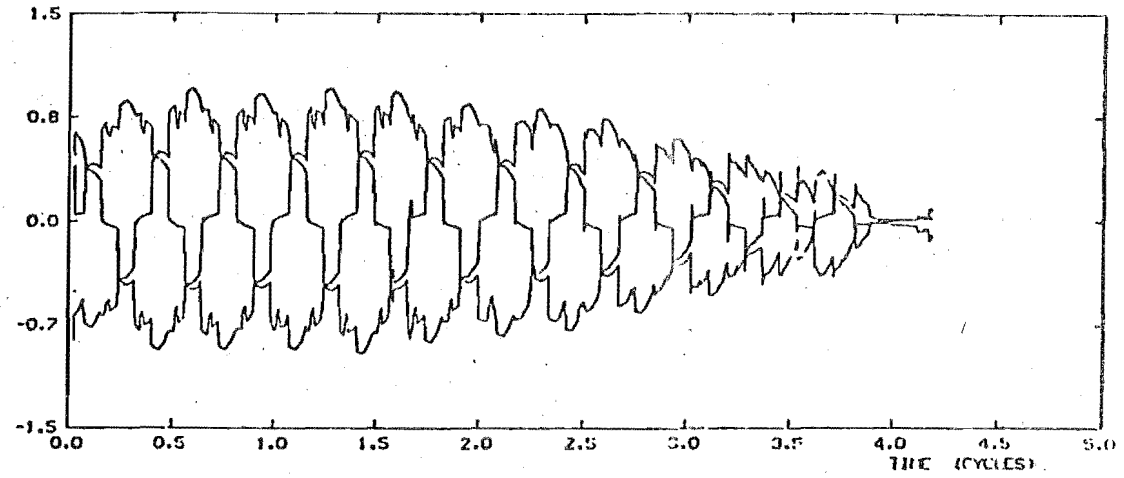

Fig. 6.15(b) 0193 ROTOR CURRENTS

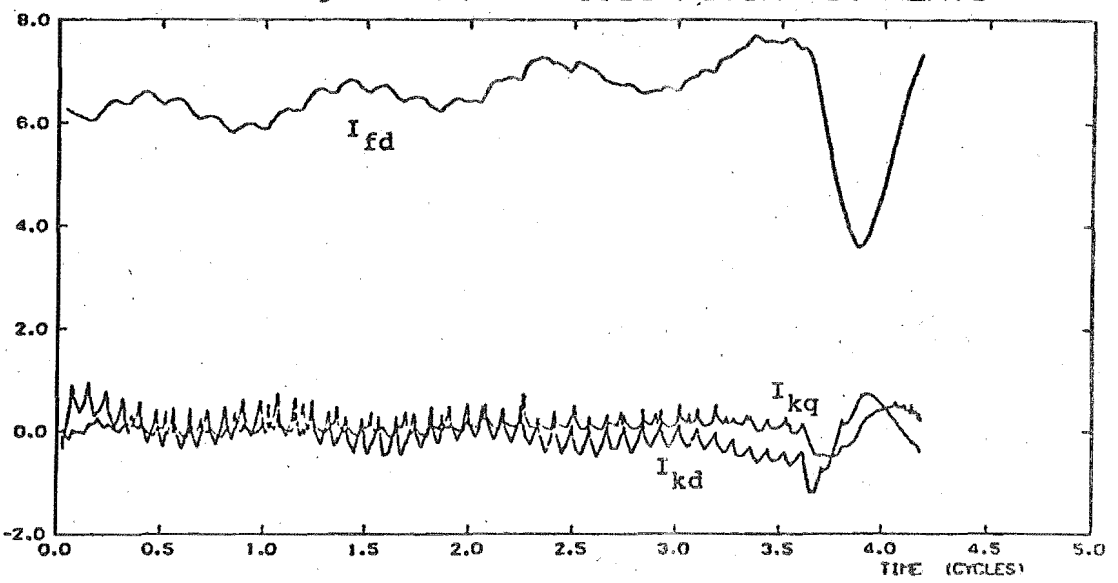

Fig. 6.15(c) 0193 RECTIFIER CURRENT

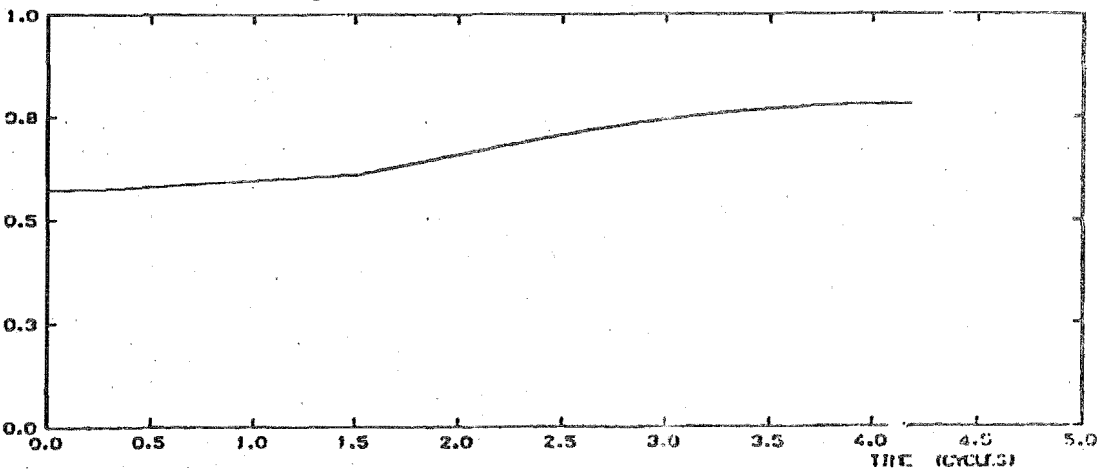

During this period, it can be seen that the transformer magnetizing current problem is present (50 Hz component of field current), and that the average value of field current excitation is resulting in a generator voltage that is some 15% above that predicted by the initial value calculations.

As a result, the rectifier voltage is high, and with a constant invertor d.c. voltage, the d.c. line current is increasing slowly. Because of the high generator voltage and the feedback effect of the excitation circuit, in the absence of any control action, the excitation voltage will continue to increase. Obviously then, some better means of obtaining initial conditions is required.

6.8.2 Initial Condition Improvement

Using the techniques described in Section 6.4 for reducing magnetizing current errors and initial value errors in generator specifications, attempts were made to obtain initial conditions more quickly. However as explained before, a change in θ_o was necessary to compensate for d.c. current flow in all windings. This alters the initial values of terminal voltage, and thus the initial values of magnetizing current. Better estimates for initial values of magnetizing current can be obtained by observing the voltage waveform at time $\theta_o + 90^o$. By scaling these values by the magnetizing admittance, and adjusting for the correct phase relationship, this will give correct values for the initial magnetizing current, assuming constancy over the 90^o period. Increased damper resistances were also used to speed up the initial response as explained in Section 6.4.

Fig. 6.16(a) 2193 GENERATOR VOLTAGE

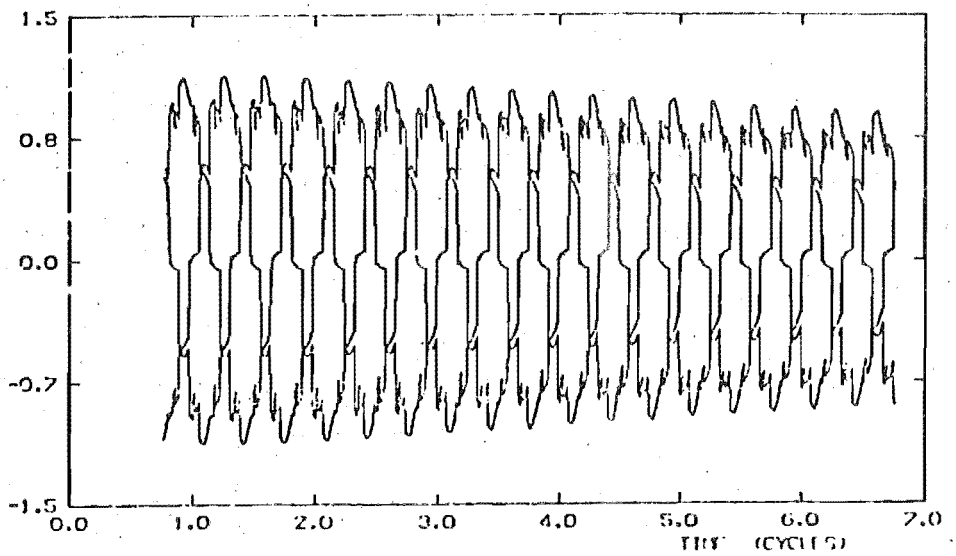

Fig. 6.16(b) 2193 ROTOR CURRENTS

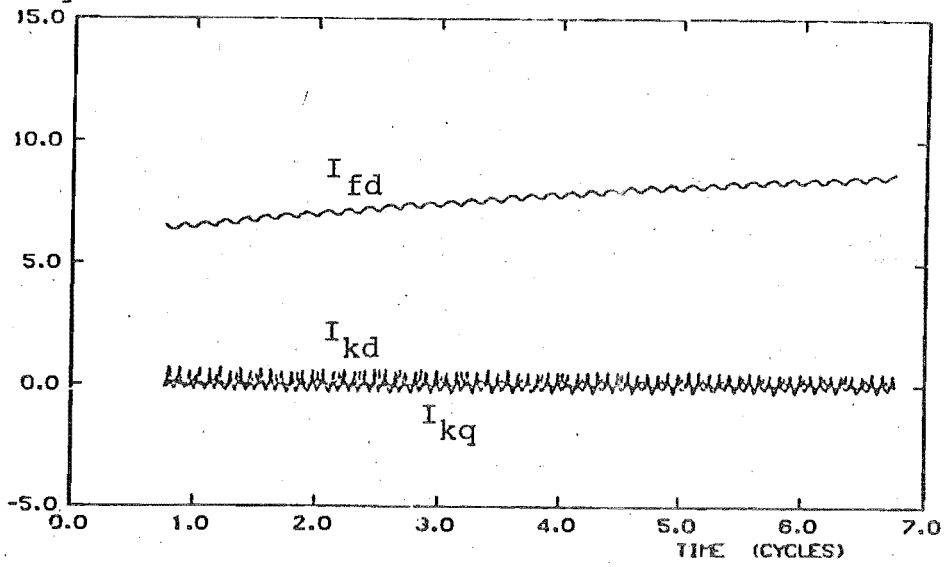

The results for this case (2193) are illustrated in Figs 6.16(b) (rotor currents) and (a) (generator voltage). The former indicates a steadily increasing average level, with a dominant 6 pulse ripple. The fundamental frequency component is no longer evident due to the more accurate specification of magnetizing currents. However the high level of terminal voltage is still a problem, since this

results in higher than predicted rectifier currents. These could be reduced by excitation control (retarding α_e) but this process would take some time to settle to the required operating point.

The above methods have attempted to begin from full load steady state conditions, and without control, settle dynamically to the operating point. With excitation based on terminal conditions, it is not possible without some excitation control to reach a stable operating point. As seen in Section 6.4, this operating point can not be accurately predicted by the use of equations based on balanced, sinusoidal waveforms. However, alteration of the field parameters will allow the specified rectifier current (or power) to be obtained.

An alternative method of attaining initial conditions was investigated, based on the start-up procedure of an isolated generator-diode rectifier. Starting from no load conditions (θ_o, I_{fd}, α_e), which can be estimated accurately by equations based on balanced and sinusoidal waveforms (see Appendix A10), the rectifier current is allowed to increase from zero to full load. The rate of current increase is controlled by the nett direct voltage difference, which will be a function of both the generator excitation and the effective control at the invertor end. The latter is simulated by increasing the fixed source (V_{di}) from zero to full load at a rate corresponding to normal start-up control action.

Fast start-up can be achieved by α_e control. The amount of control will determine whether the start-up

(especially the rate of rise of I_d) is under-damped (or even unstable) or over-damped (too slow). Figs 6.17(a) - (e) indicate a start-up (case 5193) which exhibits close to critical damping of the direct current response. Full load current is achieved within four cycles with nominal generator voltage and field current. The excitation action is indicated by the field voltage.

Fig. 6.17(a) 5193 EXCITER VOLTAGE

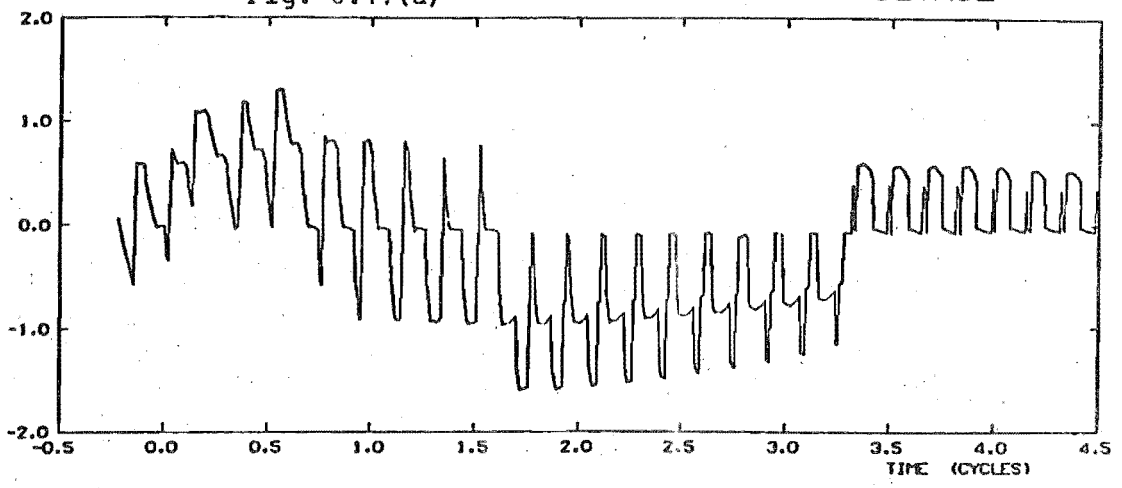

Fig. 6.17(b) 5193 ROTOR CURRENTS

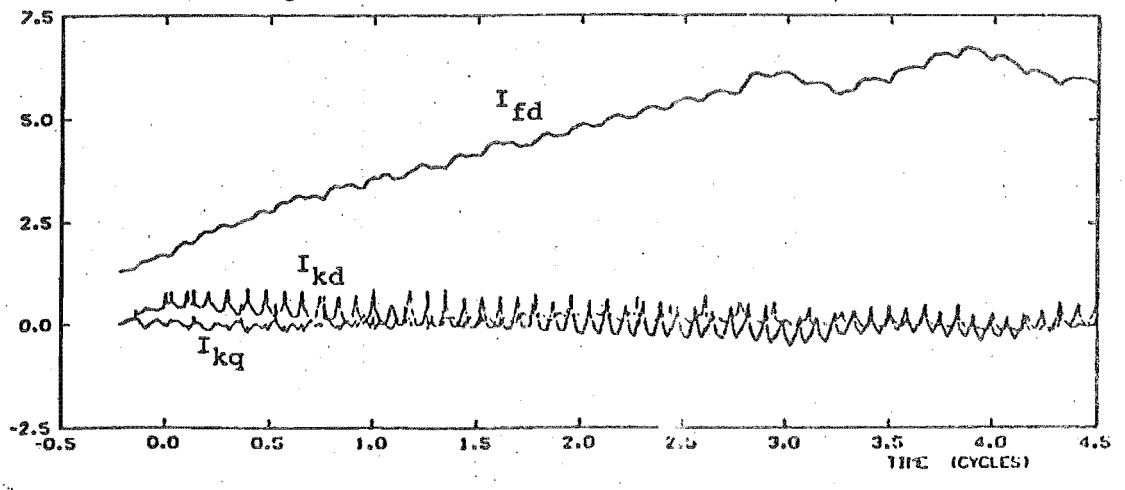

Fig. 6.17(c) 5193 GENERATOR VOLTAGE

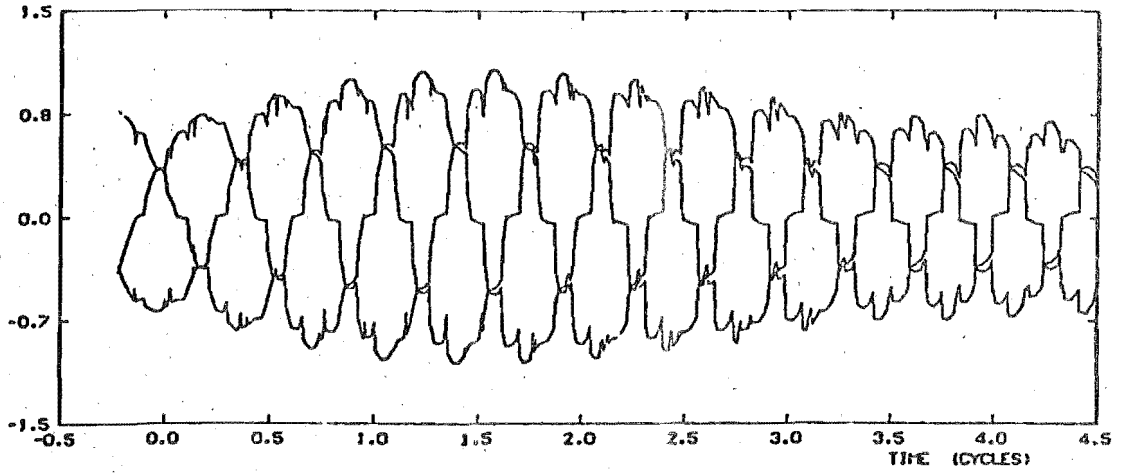

Fig. 6.17(d) 5193 RECTIFIER CURRENT

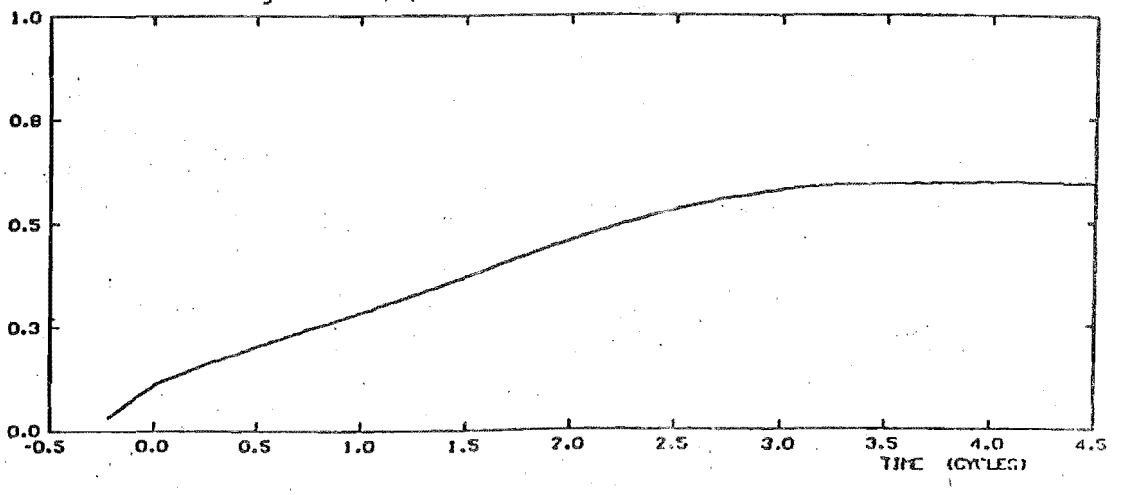

Fig. 6.17(e) 5193 MAGNETIZING CURRENTS

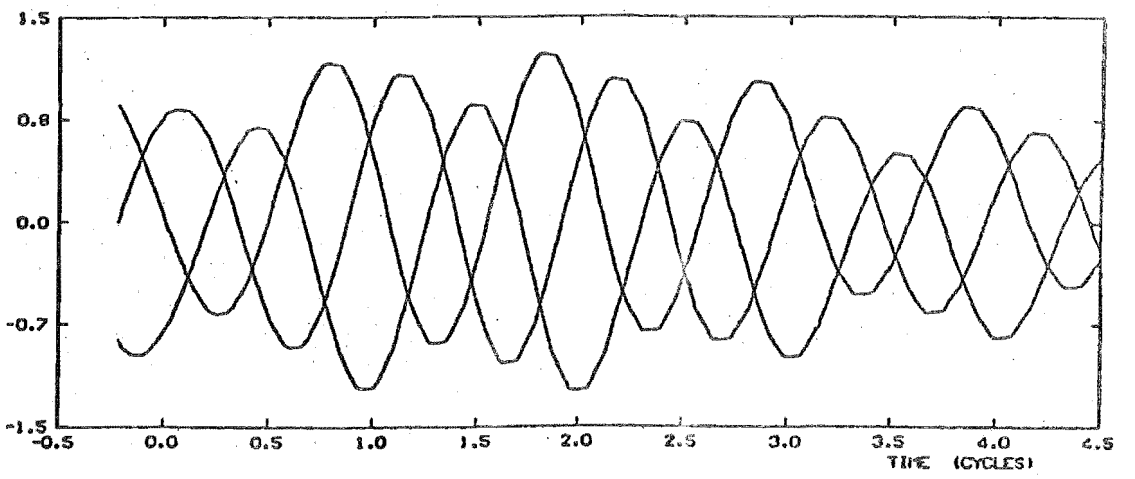

Initially, positive field forcing ($\alpha_e = 60^o$) gives a rapid increase of field and rectifier current. A stabilising period ($\alpha_e = 85^o$) followed by de-excitation (with $\alpha_e = 110^o$) controls the rate of rise of current, and returns the terminal voltage to near nominal, where α_e is reset to 85^o.

The field current waveform indicates a steady climb from its no load value (0.013 p.u.) to a value approximately equal to the full load value predicted by classical analysis (0.0675 p.u.). As expected, a 6 pulse ripple is evident, and in the last cycle of simulation small deviations around a slowly increasing level occur due to the control action occurring in the thyristor bridge. These deviations are not related to magnetizing current offset, since Fig. 6.17(e) shows only a small amount of offset in these currents.

This study has therefore indicated the performance during simulated start-up, using both positive and negative excitation, with the system attaining the desired operating point (I_{dr}, I_{fd}, α_e) within 5 cycles, compared to the earlier study (Figs 6.16(a) and (b)), which attempted to begin with full load initial conditions.

An attempt to increase the speed of start-up resulted in under-damped responses, as indicated in Figs 6.18(a) and (b), where curves A and B represent 2 and 1 cycles of field forcing respectively, and curve C the case of Figs 6.17(a) - (e).

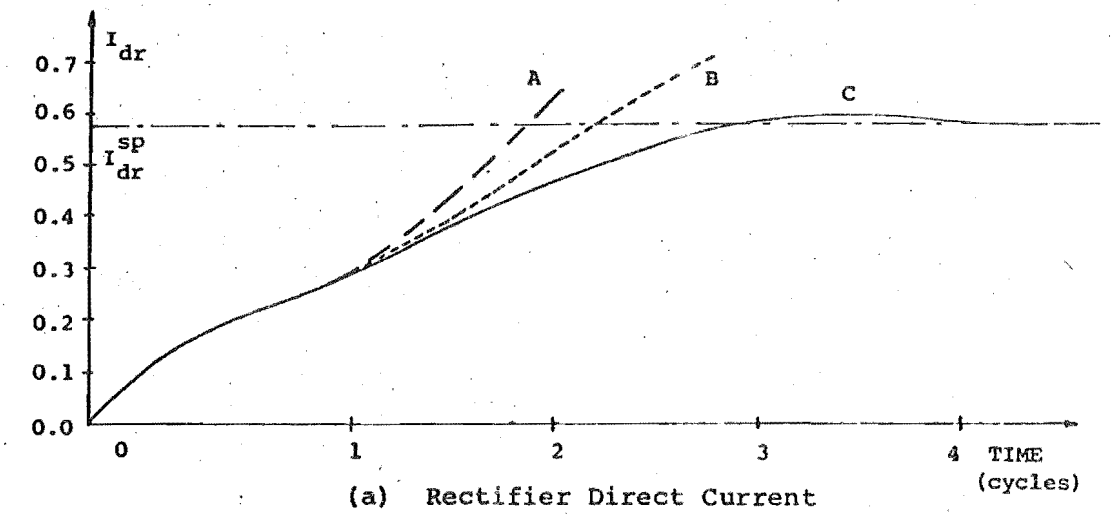

(a) Rectifier Direct Current

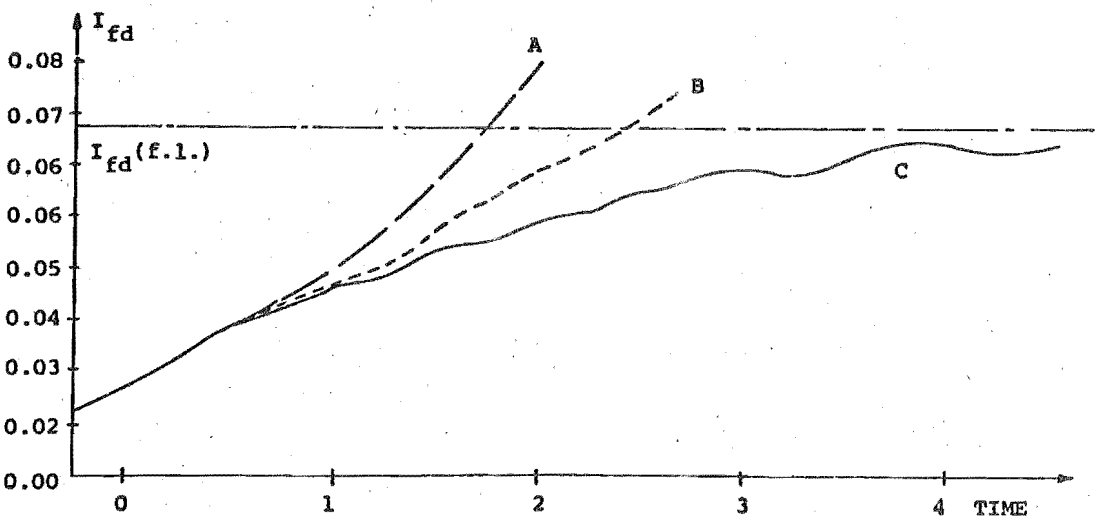

(b) Generator Field Current

6.8.3 Fault Studies

In addition to achieving suitable initial conditions, the previous simulations have displayed the applicability of fast excitation control in depressing or boosting the generator voltage in a short period of time. This can be extended to the simulation of faults where, as explained earlier, the ability of the exciter to provide sufficient protection and control of the scheme will determine the suitability of isolated generator-diode rectifier applications. Bowles (1977) has performed preliminary investigations of fault conditions using simulator techniques.

The digital computer model developed here, provides a further tool which may be used to more accurately investigate the feasibility of these schemes under both normal and abnormal operating conditions. From these studies the need for protective action additional to that provided by excitation control may be ascertained, whether it be in the form of an a.c. circuit breaker, requiring additional a.c. buswork, or a d.c. circuit breaker.

In Figs 6.15(a) - (c) and 6.19(a) - (b), the initial response of the generator to a d.c. line fault is illustrated for a period of 3 cycles.

Fig. 6.19(a) 0193 EXCITER VOLTAGE

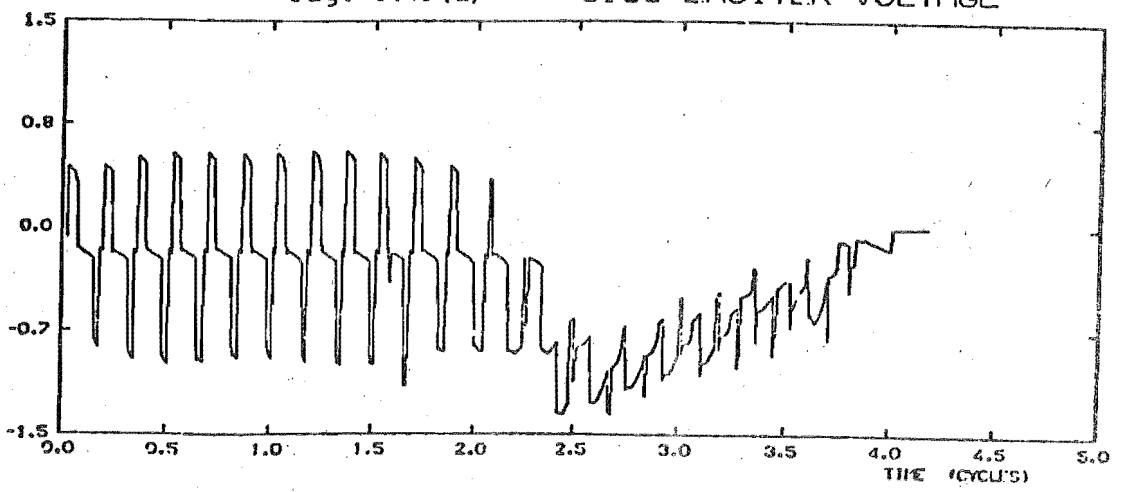

Fig. 6.19(b) 0193 STATOR CURRENTS

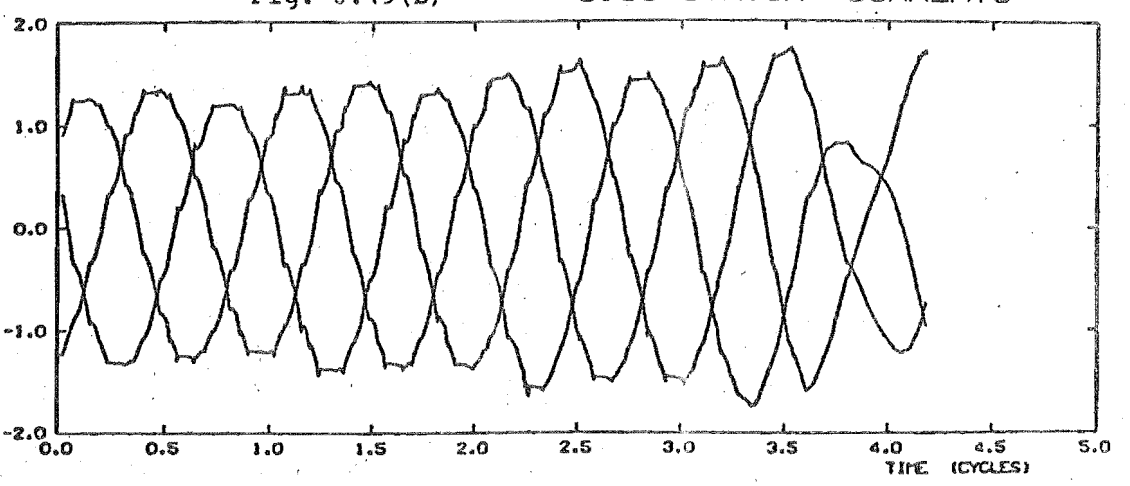

The excitation system is presumed to detect the fault within ½ cycle, and to retard the thyristor firing angles by 40^{o} so that the exciter bridge is on full retard (i.e. α^{max}). This is illustrated in Fig. 6.19(a). The fault also causes an increase in voltage regulation. In conjunction with de-excitation, this causes the generator terminal voltage to decrease rapidly, which in turn extends commutation periods and further depresses the voltage. The voltage depression in this case limits the peak over-currents to some 50% above the setting within two cycles of fault occurrence. Continued simulation shows the generator terminal voltage collapses 2½ cycles after fault occurence, with the result that unacceptable commutation failures occur in the exciter and convertor bridges.

Whereas the de-excitation effected by thyristor control will limit the d.c. over-current, it is necessary to remove the source (generator) completely to clear the fault. This is normally performed by convertor control action (see Chapter 5), but in the diode rectifier application this is not possible. The alternative is to use circuit breaker action.

Normally, low a.c. voltage will be detected and a protective action initiated whereby a.c. circuit breakers will interrupt the a.c. line (fault current) at current zeroes. However, although such breakers need only have limited duty due to the restricted fault current (Fig. 6.19(b)), isolation of each phase at current zero cannot be guaranteed in the presence of an HVDC convertor. If one phase is cleared at a current zero (i.e. on extinction

of a valve), the next valve commutation will be hindered by a reduced commutation voltage. As a result of the extended commutation period, d.c. short circuits may occur and alternating current zeroes cannot be guaranteed. Therefore the operation of an a.c. circuit breaker alone, may not be a viable protection auxiliary to fast excitation control.

Recently (Bowles *et al.* 1976), proposals have been forwarded for the use of a direct current circuit breaker. Simulator studies carried out by the proposers showed that the use of a high speed breaker to guard against d.c. line faults, and faults within the receiving system, allowed the performance of an isolated generator-diode rectifier scheme to approach that of a conventional controlled rectifier scheme. This required the d.c. circuit breaker to have a trip-reclose sequence of around 5 cycles. It was indicated that invertor commutation failures would not require breaker action provided the excitation system was fast enough.

The simulation of a.c. circuit breaker operation in dynamic analysis, indicated in Chapter 4, can also be applied to d.c. circuit breaker operation, i.e. the sequence of operations and non-linear resistance characteristics of the proposed breaker could be easily incorporated in the state space formulation. Studies of an isolated generator-diode rectifier scheme, subjected to a variety of fault conditions, could then be undertaken to determine the feasibility of fast excitation control and a.c. and/or d.c. circuit breaker action providing effective and co-ordinated protective control.

6.9 CONCLUSIONS

Various studies conducted on typical and proposed generator-convertor systems have illustrated the versatility of the developed model for investigating the dynamic behaviour of synchronous generators provided with thyristor bridge excitation control, and the effect of fast thyristor bridge excitation in isolated generator-rectifier applications for both controlled and uncontrolled rectifier schemes.

Future work could utilize the developed model to investigate the feasibility of various configurations of generator-rectifier schemes and, in particular, their controllability and protective sequences, with a view to obtaining the most economic, practical solution to HVDC infeed from a remote source.

CHAPTER 7

CONCLUSION

Recent technological developments, coupled with real cost reductions and a steady improvement in reliability, have resulted in HVDC transmission emerging commercially as an attractive complement to a.c. power systems. This is particularly so with regard to the increasing requirement for bulk power transfer into urban centres. The location of new generating sources (hydro, nuclear, mine mouth, etc.) is invariably remote from the load centres, and the advantages of HVDC when long overhead transmission and/or underground/submarine cables are necessary, coupled with the higher transmission power density possible over a given right of way, make HVDC at least comparable to EHVAC with regard to reliability and economic and environmental aspects.

However one of the problems generated by increased utilisation of high capacity d.c. links is that a larger portion of the a.c. system load is fed from 'remote' generation, with the result that a link may be feeding into a relatively weak system, i.e. where the ratio of convertor a.c. bus short circuit level to transmitted d.c. power is less than say 2.5. The resultant effects possible include increased overvoltages on load rejection, susceptibility to commutation failures during voltage disturbances, and difficulty of rapid re-start of d.c. transmission following faults. The system must in general be able to withstand

these overvoltages, or their effects must be limited by protective devices (overvoltage control) or by convertor control.

The accurate simulation of transient phenomena associated with such disturbances is vitally important in the design of HVDC schemes, particularly if they are to feed into a relatively weak a.c. system.

Over the last two decades, digital computer programmes for a.c. network solutions were developed which were more attractive than the traditional analogue network analyser on the basis of cost, convenience and size/accuracy of representation. Traditionally, the simulation of transients associated with HVDC transmission has also been performed by analogue models, such as special purpose HVDC simulators, since they provide the required detailed modelling of the convertor equipment. Such modelling was not possible with the level of programming developed for a.c. network solutions.

However the simulators, although indispensable in the practical introduction of HVDC, have the inherent limitations associated with any analogue or physical model. More recently, digital methods have been developed to complement these analogue simulators. However to date their application to the simulation of transients in inter-connected a.c./d.c. systems has also been limited by the trade-off necessary between the size and accuracy of system representation, and the cost of running the programme. This trade-off has resulted in programmes which use either a simplified (quasi-steady state or normal mode) representation

for the HVDC link(s), or a reduced representation of the a.c. network. Transient stability programmes have, with tenuous justification, tended to use the former simplification, whilst retaining full a.c. network representations. Programmes designed to analyse the transient performance of convertors have tended to use a simplified a.c. network representation.

It has been shown in this thesis that by combining the full a.c. network representation of a transient stability analysis with a detailed d.c. link model, it is possible to obtain a digital computer simulation which not only models the entire a.c./d.c. system accurately throughout the dynamic analysis period, but also has a computation cost comparable with those simulations which used inaccurate simplifications for the a.c. network representation.

Explicit modelling of essential a.c. components (e.g. convertor transformers, harmonic filters) has been retained. Special provision for the detailed modelling of important synchronous machines has been included, along with an exact equivalent for the rest of the a.c. network, obtained via the transient stability programme. The waveform dependent topology of the bridges can be simulated for all modes of operation, with a multisegment pi-equivalent representation of the d.c. line. The accessibility of all system variables allows various types of convertor control systems to be simulated.

The developed dynamic analysis programme was used for the investigation of a.c. faults (Chapter 4), convertor maloperation and d.c. line faults (Chapter 5), and these

topics have been the subject of two publications (Appendices A11 and A12 respectively). Included in the programme for these investigations are facilities for representing non-linearities (such as transformer saturation), phase unbalance and circuit breaker operation, and d.c. line fault protection schemes.

The use of the programme in the preliminary investigation of prospective applications, such as the isolated generator-diode rectifier schemes, has been indicated in Chapter 6, and the development of an accurate model for fast excitation systems provides a tool which will be essential in the determination of the practicality of such schemes. A novel technique for harmonic elimination has been developed by Baird *et al.* (1979), and a configuration involving an isolated generator with fast excitation control feeding a d.c. link which utilises this new technique could make diode rectifier schemes more attractive. The development of the dynamic analysis programme to study diode rectifier schemes, and in particular those that incorporate the elimination technique, offers an area of research which could be exploited.

Many of the initial condition problems previously associated with dynamic analyses, which contributed appreciably to their running costs, have been isolated and eliminated during the course of this research. A supportive package provides a means of post processing results (e.g. to obtain a harmonic analysis of phase quantities), and a post-simulation graphics package provides flexibility in the presentation of results.

A parallel development of the interaction between the dynamic analysis and transient stability programmes has enabled exact transient stability studies to be carried out during severe disturbances (Turner 1980). This work has been extended to study the utilisation of the d.c. link to provide transient stability improvement following a.c. disturbances. These investigations demanded the interactive facility of the two programmes, at least until a time when the convertor's behaviour could be accurately represented by a quasi-steady state representation and the a.c. waveforms were reasonably balanced and sinusoidal. This time could only be determined from a study using the developed dynamic analysis computer programme.

BIBLIOGRAPHY

B1 BROMBERG, E. "An Annotated Bibliography of High Voltage Direct Current Transmission 1932-1962", IEEE, New York, 1963, 520 items.

B2 BROMBERG, E. "An Annotated Bibliography of High Voltage Direct Current Transmission 1963-1965", IEEE, New York, 1967, 378 items.

B3 LAVA, V.S. "An Annotated Bibliography of High Voltage Direct Current Transmission 1966-1968", Library Bonneville Power Administration, Portland, U.S.A., 1968, 498 items.

B4 HWANG, H.H., IMAI, R.R. and SIMMONS, T.C. "Bibliography on High Voltage Direct Current 1969-1976: Part A", Paper A77-541-6 presented at IEEE PES Summer Meeting, Mexico City, July 1977, 201 items.

B5 HWANG, H.H., IMAI, R.R. and SIMMONS, T.C. "Bibliography on High Voltage Direct Current 1969-1976: Part B", Paper A77-542-4 presented at IEEE PES Summer Meeting, Mexico City, July 1977, 146 items.

B6 KIMBARK, E.W. "Direct Current Transmission, Vol. I", Wiley Interscience, 1971, 476 items.

REFERENCES

ADAMSON, C. and HINGORANI, N.G. "High Voltage Direct Current Power Transmission", 1st Ed., Garraway Ltd, London, 1960 (Book), 284 pp.

AINSWORTH, J.D. "Harmonic Instability Between Controlled Static Convertors and AC Networks", Proc. IEE, Vol. 114, No. 7, July 1967, pp. 949-957.

AINSWORTH, J.D. "The Phase Locked Oscillator - A New Control System for Controlled Static Convertors", Trans. IEEE, Power Apparatus and Systems, Vol. PAS-87, No. 3, March 1968, pp. 859-865.

AINSWORTH, J.D. and MARTIN, C.J.B. "Principles of Control for HVDC Transmission", Proceedings IEE International Conference (No. 22) on HVDC, 1966, Paper 30, pp. 158-160.

AL-KHASHALI, H.J. "Generalised Dynamic Modelling of High Voltage AC-DC Transmission Systems", University of Manchester Institute of Science and Technology, 1976, 103 pp. (Thesis: Ph.D.: Engineering).

ANDERSON, P.M. and FOUAD, A.A. "Power System Control and Stability", Iowa State University Press, Ames, Iowa, U.S.A., 1st Ed., 1977, 464 pp.

ARNOLD, C.P. "Solutions of the Multimachine Power System Stability Problem", University of Manchester Institute of Science and Technology, 1976. (Thesis: Ph.D.: Engineering).

ARRILLAGA, J., AL-KHASHALI, H.J. and CAMPOS BARROS, J.G. "General Formulation for Dynamic Studies in Power Systems Including Static Convertors", Proc. IEE, Vol. 124, No. 11, November 1977, pp. 1047-1052.

ARRILLAGA, J., ARNOLD, C.P., HEFFERNAN, M.D. and CAMPOS BARROS, J.G. "Stability of Isolated Generator-HVDC Convertor Units", IEEE Summer Power Meeting, Mexico City, July 1977, A77-508-5.

ARRILLAGA, J. and BALDWIN, D.G. "Direct Digital Closed Loop Control of HVDC Convertors", Proc. IEE, Vol. 121, No. 12, December 1974, pp. 1567-1571.

ARRILLAGA, J., CAMPOS BARROS, J.G. and AL-KHASHALI, H.J. "Dynamic Modelling of Single Generators Connected to HVDC Convertors", Trans. IEEE, Power Apparatus and Systems, Vol. PAS-97, No. 4, July-August 1978, pp. 1018-1029.

ARRILLAGA, J. and GALANOS, G. "Fault Development Control in AC/DC Convertors", Proc. IEE, Vol. 116, No. 7, July 1969, pp. 1201-1208.

ARRILLAGA, J. and GALANOS, G. "Fault Detection Scheme for a Direct Digital Control of AC/DC Interconnections", Proc. IEE, Vol. 117, No. 4, April 1970, pp. 785-793.

ARRILLAGA, J. and GALANOS, G. "Theoretical Basis of a Digital Method of Grid Control for HVDC Convertors", Trans. IEEE, Power Apparatus and Systems, Vol. PAS-89, No. 8, November/December 1970, pp. 2049-2059.

ARRILLAGA, J., GALANOS, G. and POWNER, E.T. "Direct Digital Control of HVDC Conductors", Trans. IEEE, Power Apparatus and Systems, Vol. PAS-89, No. 8, November/December 1970, pp. 2056-2065.

ARRILLAGA, J. and GIESNER, D.B. "Limitations of Short Circuit Levels by Means of HVDC Links", IEEE Summer Power Meeting, July 1970, 70CP637-PWR.

ARRILLAGA, J. and GIESNER, D.B. "Recovery of Mercury-Arc HVDC Interconnections from Backfire Faults", Proc. IEE, Vol. 119, No. 11, November 1972, pp. 1611-1615.

BAIRD, J.F. and ARRILLAGA, J. "Improvements in and Relating to Static Convertors", New Zealand Patent Application 190713, 1979.

BARTON, T.H. and DUNFIELD, J.C. "Inductances of a Practical Slip Ring Primitive: I - An Analytical Study and II - Experimental Study", Trans.IEEE, Power Apparatus and Systems, Vol. PAS-85, No. 2, 1966, pp. 140-151.

BONWICK, W.H. and JONES, V.H. "Performance of a Synchronous Generator with a Bridge Rectifier", Proc. IEE, Vol. 119, No. 9, September 1972, pp. 1338-1342.

BOWLES, J.P. "AC System and Transformer Representation for HVDC Transmission Studies", Trans. IEEE, Power Apparatus and Systems, Vol. PAS-89, No. 7, 1970, pp. 1603-1609.

BOWLES, J.P. "Overvoltages in HVDC Transmission Systems Caused by Transformer Magnetizing Inrush Currents", Trans. IEEE, Power Apparatus and Systems, Vol. PAS-93, No. 1, January/February 1974, pp. 487-493.

BOWLES, J.P., VAUGHAN, L. and HINGORANI, N.G. "Specification of HVDC Circuit Breakers for Different System Applications", Proc. CIGRE Conf. Paris, July 1976, Paper 13-09, 13 pp.

BOWLES, J.P. "HVDC System Developments and Concepts - the Diode Rectifier", Paper presented to CIGRE SC14 Meeting and Colloquium, Winnipeg, Canada, June 1977.

BRAMELLER, A., SCOTT, M.R. and JOHN, M.N. "Practical Diakoptics for Electrical Networks", Chapman and Hall, London, 1969, 242 pp.

BRANDWAJN, V. and DOMMEL, H.W. "Simulation of Turbine Generators in Electromagnetic Transients Programs", Electrical Power and Energy Systems, Vol. 1, No. 2, July 1979, pp. 118-124.

CALVERLEY, T.E., OTTAWAY, C.H. and TUFNELL, D.H.A. "Concept of a Unit Generator Convertor Transmission System", Proc. IEE International Conf. on HVDC (No. 107), London, 1973, Part I, pp. 53-59 with discussion Part II, pp. 58-67.

CAMPOS BARROS, J.G. "Dynamic Modelling of Synchronous Machines Connected to HVDC Transmission Systems", University of Manchester Institute of Science and Technology, 1976, 82 pp. (Thesis: Ph.D.: Engineering).

CARTER, G.W., LEACH, W.I. and SUDWORTH, J. "The Inductance Coefficients of a Salient Pole Alternator in Relation to the Two-Axis Theory", Proc. IEE, Vol. 118, Part A, June 1961, Paper 3587S, pp. 263-270.

CONCORDIA, C. "Synchronous Machines, Theory and Performance", John Wiley, New York, 1951, 224 pp,

CORY, B.J. (Ed.) "High Voltage Direct Current Convertors and Systems", Macdonald, London, 1965, 269 pp.

COTZAS, G.M., HESSE, M.H. and LANE, L.J. "Electrical Design and Steady State Performance of Generrex Excitation System", Trans. IEE, Power Apparatus and Systems, Vol. PAS-98, No. 6, November/December 1979, pp. 2251-61.

CRESAP, R.L., SCOTT, D.N., MIDDLESTADT, W.A. and TAYLOR, C.W. "Damping of Pacific AC Intertie Oscillations via Modulation of the Parallel Pacific HVDC Intertie", CIGRE Conference, August-September 1978, Paris, Paper 14-05, 9 pp.

DOHERTY, R.E. and NICKLE, C.A. "Synchronous Machines: I and II; An Extension of Blondel's Two-Reaction Theory", Trans. AIEE, Vol. XLV, 1926, pp. 912-947.

DOMMEL, H.W. "Nonlinear and Time Varying Elements in Digital Simulation of Electromagnetic Transients", Trans. IEEE, Power Apparatus and Systems, Vol. PAS-90, November/December 1971, pp. 2561-2567.

DOMMEL, H.W. "Transformer Models in the Simulation of Electromagnetic Transients", Paper 3-1/4 presented at 5th Power Systems Computation Conference, Cambridge, England, September 1975, 16 pp.

DOUGHERTY, J.J. and HILLESLAND, T. Jr. "Power System Stability Considerations with Dynamically Responsive DC Transmission Lines", Trans. IEEE, Power Apparatus and Systems, Vol. PAS-89, No. 1, January 1970, pp. 34-45.

DUKE, R.M. "A Thyristor-Controlled Regulating Transformer", University of Canterbury, Christchurch, N.Z., 1979 (Thesis: Ph.D.: Engineering) 245 pp.

DUNFIELD, J.C. and BARTON, T.H. "Effect of MMF Permeance Harmonics in Electrical Machines (With Special Reference to a Synchronous Machine)", Proc. IEE, Vol. 114, No. 10, October 1967, pp. 1443-1450.

ELLERT, F.J. and HINGORANI, N.G. "HVDC for the Long Run", IEEE Spectrum, August 1976, pp. 36-42.

EL-SERAFI, A.M. and SHEHATA, S.A. "Digital Simulation of an AC/DC System in Direct Phase Quantities", Trans. IEEE, Power Apparatus and Systems, Vol. PAS-95, No. 2, 1976, pp. 731-742.

EL-SERAFI, A.M. and SHEHATA, S.A. "Effect of Synchronous Machine Parameters on its Harmonic Analysis Under Thyristor Bridge Operation", Trans. IEEE, Power Apparatus and Systems, Vol. PAS-99, No. 1, January/February 1980, pp. 59-68.

ERINMEZ, A. "Direct Digital Control of HVDC Links", University of Manchester Institute of Science and Technology, 1971 (Thesis: Ph.D.: Engineering).

EVANS, W.A. and BROWN, W.A. "Alternator Field Control of an HVDC Link", Proc. IFAC Symposium, Melbourne, February 1977, pp. 345-348.

FITZGERALD, A.E. and KINGSLEY, C. Jr. "Electric Machinery", 2nd Ed., McGraw Hill, New York, 1961, 568 pp.

FORTESCUE, C.L. "Method of Symmetrical Coordinates applied to the Solution of Polyphase Networks", Trans. AIEE, Vol. 37, Part II, July-December 1918, pp. 1027-1140.

FOTIN, F.P. *et al.* "Tests of Powerful High Voltage Thyristor Valves on a Test Plant in the Town of Togliatt", CIGRE Conference, Paris, 1976, Paper 14-1, 6 pp.

GIESNER, D.B. "The Dynamic Behaviour of AC/DC Power Systems Under AC Fault Conditions", University of Manchester Institute of Science and Technology, 1971, 163 pp. (Thesis: Ph.D.: Engineering).

GIESNER, D.B. and ARRILLAGA, J. "Behaviour of HVDC Links Under Balanced AC Fault Conditions", Proc. IEE, Vol. 118, No. 3/4, March/April 1971, pp. 591-599.

GIESNER, D.B. and ARRILLAGA, J. "Behaviour of HVDC Links Under Unbalanced AC Fault Conditions", Proc. IEE, Vol. 119, No. 2, February 1972, pp. 209-215.

GIESNER, D.B. and ARRILLAGA, J. "Recovery of HVDC Interconnectors from Disturbances in the Thyristor Bridges", Trans. IEEE, Power Apparatus and Systems, Vol. PAS-91, November 1972, pp. 2333-2340.

GOTO, M., ISONO, A. and OKUDA, K. "Transient Behaviour of Synchronous Machine with Shunt Connected Thyristor Exciter under System Faults", Trans. IEEE, Power Apparatus and Systems, Vol. PAS-90, No. 5, 1971, pp. 2218-2227.

GROSCHUPF, E., JOTTEN, R., MULLER, R. and MUTSCHALER, P. "Methods and Results of Computer Simulations of AC, HVDC and HVDC-AC Systems", Proceedings IEE International Conference (No. 107) on HVDC, London, 1973, pp. 109-113.

GROSS, G. and HALL, M.C. "Synchronous Machine and Torsional Dynamics Simulation in the Computation of Electromagnetic Transients", Trans. IEEE, Power Apparatus and Systems, Vol. PAS-97, No. 4, July/August 1978, pp. 1074-1086.

HAY, J.L. and HINGORANI, N.G. "Dynamic Simulation of Multiconvertor HVDC Systems by Digital Computer: Part I Mathematical Model", Proceedings 6th Power Industry and Computer Applications Conference, Colorado, 1969, pp. 512-520.

HAY, J.L. and HINGORANI, N.G. "Dynamic Simulation of Multiconvertor HVDC Systems by Digital Computer: Part II Computer Programme", Proceedings 6th Power Industry and Computer Applications Conference, Colorado, 1969, pp. 521-535.

HAY, J.L. BHATTI, J.S. and HINGORANI, N.G. "Simplified Dynamic Simulation of HVDC System by Digital Computer: Part I Computer Programme", Trans. IEEE, Power Apparatus and Systems, Vol. PAS-90, No. 2, 1971, pp. 859-864.

HAY, J.L. BHATTI, J.S. and HINGORANI, N.G. "Simplified Dynamic Simulation of HVDC System by Digital Computer: Part II Design of Controller and Test Results", Trans. IEEE, Power Apparatus and Systems, Vol. PAS-90, No. 2, 1971, pp. 805-875.

HAYWOOD, R.W. and PATTERSON, W.A. "Applications of Control on the Eel River and Nelson River HVDC Schemes to Enhance Operation of Interconnected Systems", CIGRE Conference, Paris, 1976, Paper 14-04, 12 pp.

HEFFERNAN, M.D. "Stability of Hydrogenerators Connected to HVDC Convertors", University of Canterbury, Christchurch, N.Z., 1977, 90 pp. (Report: M.E. in Engineering).

HINGORANI, N.G. "Transient Overvoltages on a Bipolar HVDC Overhead Line Caused by DC Line Faults", Trans. IEEE, Power Apparatus and Systems, Vol. PAS-89, No. 4, April 1970, pp. 592-610.

HINGORANI, N.G. and BURBERRY, M.F. "Simulation of AC System Impedance in HVDC System Studies", Trans. IEEE, Power Apparatus and Systems, Vol. PAS-89, No. 5/6, 1970, pp. 820-828.

HINGORANI, N.G. and HAY, J.L. "Dynamic Simulation of an HVDC System on a Digital Computer", Proc. IEE International Conference (No. 22) on HVDC, 1966, pp. 119-124.

HINGORANI, N.G. and HAY, J.L. "Representation of Faults in the Dynamic Simulation of HVDC Systems by Digital Computer", Proc. IEE, Vol. 114, No. 5, May 1967, pp. 629-638.

HINGORANI, N.G., HAY, J.L. and CROSBIE, R.E. "Dynamic Simulation of HVDC Transmission Systems on Digital Computers", Proc. IEE, Vol. 113, No. 5, May 1966, pp. 793-802.

HINGORANI, N.G., HAY, J.L. and KITCHIN, R.H. "Dynamic Simulation of HVDC Power Transmission Systems on Digital Computers - Generalised Mesh Analysis Approach", Trans. IEEE, Power Apparatus and Systems, Vol. PAS-87, 1968, pp. 990-996.

IEEE COMMITTEE REPORT. "Computer Representation of Excitation Systems", Trans. IEEE, Power Apparatus and Systems, Vol. PAS-87, June 1968, pp. 1460-1465.

JARRET, G.S.H. and MIDDLETON, R.M. "Operational Experience of HVDC Systems throughout the World during 1971-1972", CIGRE Conference, Paris, 1974, Paper 14-09, 15 pp.

JONES, C.V. "The Unified Theory of Electrical Machines", Butterworths, London, 1967, 542 pp.

JOTTEN, R. *et al.* "Control in HVDC Systems - the State of the Art. Part I: Two Terminal Systems", Paper 14-10 presented by Study Committee No. 14 (DC Links) at CIGRE Conference, Paris, August/Setpember 1978, 18 pp.

KAPOOR, S.C. and REEVE, J. "Analysis of a Pole-to-Pole Short Circuit on Bipolar HVDC Convertors", Trans. IEEE, Power Apparatus and Systems, Vol. PAS-92, May/June 1973, pp. 886-892.

KIMBARK, E.W. "Power System Stability - Vol. III: Synchronous Machines", Dover Publications Inc., New York, 1968, 322 pp.

KIMBARK, E.W. "Transient Overvoltages Caused by Monopolar Ground Fault on Bipolar DC Line: Theory and Simulation", Trans. IEEE, Power Apparatus and Systems, Vol. PAS-89, No. 4, April 1970, pp. 584-592.

KIMBARK, E.W. "Direct Current Transmission, Vol. I", Wiley Interscience, 1971, 508 pp.

KOHLER, A. "Earth Fault Clearing on an HVDC Transmission Line, with Special Consideration of the Properties of the DC Arc in Free Air", Trans. IEEE, Power Apparatus and Systems, Vol. PAS-86, No. 3, March 1967, pp. 298-304.

KRISHNAYYA, P.C.S. "Stresses on Generators and Transformers of Block and Double Block Connections proposed for HVDC Power Stations Infeed", Proc. IEE International Conference on HVDC (No. 107), London, 1973, Part I, pp. 279-280.

KRON, G. "The Application of Tensors to the Analysis of Rotating Electrical Machinery", General Electric Review, Schenectady, 1938, 187 pp.

KRON, G. "Tensors for Circuits", 2nd Ed., Dover Publications, 1959.

KRON, G. "Diakoptics - the Piecewise Solution of Large Scale Systems", Macdonald, London, 1963.

KRON, G. "Tensor Analysis of Networks", Macdonald, London, 1965 (1st published 1939, Wiley).

LAKE, C.B. "A Computer Programme for AC Fault Studies in a.c./d.c. Systems", University of Canterbury, Christchurch, N.Z., 1977 (Report: M.E.: Engineering).

LAST, F.H. and MIDDLETON, R.M. "A Survey of the Performance of HVDC Schemes throughout the World for 1968/1969", CIGRE Conference, Paris, 1970, Paper 14-05, 11 pp.

LAST, F.H. and MIDDLETON, R.M. "A Survey of the Performance of HVDC Schemes throughout the World for 1970", CIGRE Conference, Paris, 1970, Paper 14-07, 15 pp.

LEWIS, W.A. "A Basic Analysis of Synchronous Machines, Part I", Trans. AIEE, Power Apparatus and Systems, Vol. PAS-77, Part III, August 1958, pp. 436-455.

MILIAS-ARGITIS, J. and GALANOS, G. "Dynamic Simulation of HVDC Transmission Systems", Paper presented at IEEE PES Winter Meeting, New York, January 1976, A76-118-0, 4 pp.

MILIAS-ARGITIS, J., GALANOS, G. and GIANNAKOPOULOS, G. "A Digital Method for the Control of Power Flow in HVDC Interconnections", Paper presented at IEEE PES Winter Meeting, New York, January/February 1977, A77-024-3, 7 pp.

MILIAS-ARGITIS, J., GIANNAKOPOULOS, G. and GALANOS, G. "Power Flow Control in Multiterminal HVDC Systems", Paper presented at Proc. IEE 2nd International Conference on Power Electronics, "Power Semiconductors and Their Applications", London, September 1977, pp. 150-153.

MILIAS-ARGITIS, J., GIANNAKOPOULOS, G. and GALANOS, G. "Dynamic Simulation for Multiterminal HVDC Systems", Trans. IEEE, Power Apparatus and Systems, Vol. PAS-97, No. 2, 1978, F77-533-3, pp. 587-593.

MASSACHUSETTS INSTITUTE OF TECHNOLOGY (MIT) ELECTRICAL ENGINEERING DEPARTMENT STAFF. "Magnetic Circuits and Transformers", M.I.T. Press, Massachusetts, 1943.

O'REGAN, P.G. and DILLON, C.T.G. "Digital Computer Simulation of Transients in HVDC Convertors with Harmonic Filters", Proc. IEE, Vol. 117, No. 2, February 1970, pp. 421-430.

PARK, R.H. "Two Reaction Theory of Synchronous Machines: Generalized Method of Analysis: Pt I", Trans. AIEE (IEEE), July 1929, Paper presented at AIEE Winter Meeting, New York, January-February 1929, pp. 716-730.

PETERSON, H.A., PHADKE, A.G. and REITAN, D.K. "Transients in EHVDC Power Systems: Part I - Rectifier Fault Currents", Trans. IEEE Power Apparatus and Systems, Vol. PAS-88, No. 7, July 1969, pp. 981-9.

POVH, D. and SCHULTZ, W. "Analysis of Overvoltages caused by Transformer Magnetizing Inrush Current", Trans. IEEE, Power Apparatus and Systems, Vol. PAS-97, No. 4, July/August 1978, pp. 1355-1365.

PRUSTY, S. and RAO, M.V.S. "New Method for Predetermination of True Saturation Characteristics of Transformers and Non-linear Reactors", Proc. IEE, Vol. 127, Part C, No. 2, March 1980, pp. 106-110.

REEVE, J. and CARR, J. "Dynamic Digital Simulation of HVDC Convertor Control and its Application to System Studies", Trans. IEEE, Power Apparatus and Systems, Vol. PAS-93, No. 1, 1974, pp. 296-302.

REEVE, J. and KAPOOR, S.C. "Analysis of Transient Short Circuit Currents in HVDC Power Systems", Trans. IEEE, Power Apparatus and Systems, Vol. PAS-90, No. 3, May/June 1971, pp. 1174-1182.

REEVE, J. and KAPOOR, S.C. "Dynamic Fault Analysis for HVDC Systems with AC System Representation", Trans. IEEE, Power Apparatus and Systems, Vol. PAS-91, No. 2, 1972, pp. 688-696.

REEVE, J. and KAPOOR, S.C. "Digital Simulation of Travelling Waves in HVDC Transmission Lines", Trans. IEEE, Power Apparatus and Systems, Vol. PAS-91, November/December 1972, pp. 2342-2355.

ROBINSON, G.H. "Harmonic Phenomena Associated with the Benmore-Haywards HVDC Transmission Scheme", N.Z. Engineering, January 1966, pp. 16-29.

RUMPF, E. and JARRETT, G.S.H. "A Survey of the Performance of HVDC Systems throughout the World during 1973-1974", Paper presented in the name of Study Committee No. 14 (DC Links), CIGRE Conference, Paris, 1976, Paper 14-07, 20 pp.

SAY, M.G. "The Performance and Design of Alternating Current Machines: Transformers, Three Phase Induction Motors and Synchronous Machines", 3rd Ed., Pitman, London, 1958, 664 pp.

SAY, M.G. "Alternating Current Machines", 4th Ed., Pitman, London, 1976, 543 pp.

SMITH, I.R. and SNIDER, L.A. "Prediction of Transient Performance of Isolated Saturated Synchronous Generator", Proc. IEE, Vol. 119, No. 9, September 1972, pp. 1309-1318.

STIGANT, S.A. and FRANKLIN, A.C. "J and P Transformer Book", Newnes-Butterworth, London, 10th Ed., 1973, 770 pp.

TURNER, K.S. "Transient Stability Analysis of Integrated AC and DC Power Systems", University of Canterbury, Christchurch, N.Z., 1980, to be Submitted (Thesis: Ph.D.: Engineering).

UHLMANN, E. "Clearing of Earth Faults on HVDC Overhead Lines", Direct Current, Vol. 5, No. 2, September 1960, pp. 45-47, 65-66.

UHLMANN, E. "AC Network Stabilisation by DC Links", CIGRE Conference, Paris, 1970, Paper 32-01, 12 pp.

UHLMANN, E. "Power Transmission by Direct Current", Springer-Verlag, Berlin/Heidelberg, 1975, 389 pp.

WILLIAMS, S. and SMITH, I.R. "Fast Digital Computation of 3-Phase Thyristor Bridge Circuits", Proc. IEE, Vol. 120, No. 7, July 1973, pp. 791-795.

APPENDIX A1

DETAILED SYNCHRONOUS MACHINE COEFFICIENT MATRIX

This matrix, L_g in equations (2.5) - (2.6), is a 6 x 6 matrix which can be partitioned into stator, stator-rotor, and rotor terms, i.e.

$$L_g = \begin{bmatrix} L_{ss} & L_{sr} \\ L_{rs} & L_{rr} \end{bmatrix}$$

where

$$L_{ss} = \begin{bmatrix} Laa + La_2 \cos 2\theta + L_{a4} \cos 4\theta & -L_{ab} - L_{ab2}\cos 2(\theta+30^o) - L_{ab4} \cos 4(\theta+30^o) & -L_{ac} - L_{ac2}\cos 2(\theta+150^o) - L_{ac4} \cos 4(\theta+150) \\ -L_{ab} - L_{ab2}\cos 2(\theta+30) - L_{ab4}\cos 4(\theta+30) & L_{bb} + L_{b2}\cos 2(\theta-120^o) + L_{b4} \cos 4(\theta-120^o) & -L_{bc} - L_{bc2}\cos 2(\theta-90^o) - L_{bc4}\cos 4(\theta-90^o) \\ -L_{ac} - L_{ac2}\cos 2(\theta+150) - L_{ac4} \cos 4(\theta+150) & -L_{bc} - L_{bc2}\cos 2(\theta-90) - L_{bc4} \cos 4(\theta-90) & L_{cc} + L_{c2}\cos 2(\theta+120^o) + L_{c4} \cos 4(\theta+120^o) \end{bmatrix}$$

$$L_{sr} = \begin{bmatrix} L_{afd} \cos \theta & L_{akd} \cos \theta & - L_{akq} \sin \theta \\ L_{bfd} \cos (\theta-120) & L_{bkd} \cos (\theta-120) & - L_{bkq} \sin (\theta-120) \\ L_{cfd} \cos (\theta+120) & L_{ckd} \cos (\theta+120) & - L_{ckq} \sin (\theta+120) \end{bmatrix}$$

$$L_{rs} = L_{sr}^{t}$$

and

$$L_{rr} = \begin{bmatrix} L_{fd} & L_{fkd} & 0 \\ L_{fkd} & L_{kd} & 0 \\ 0 & 0 & L_{kq} \end{bmatrix}$$

Similarly, the torque matrix is a 6 x 6 matrix derived from L_g by

$$\frac{d}{d\theta} L_g = \begin{bmatrix} \frac{\partial L_{ss}}{\partial \theta} & \frac{\partial L_{sr}}{\partial \theta} \\ \frac{\partial L_{rs}}{\partial \theta} & \frac{\partial L_{rr}}{\partial \theta} \end{bmatrix}$$

where $\frac{\partial L_{rr}}{\partial \theta} = 0$ and $\frac{\partial L_{rs}}{\partial \theta} = \left(\frac{\partial L_{sr}}{\partial \theta} \right)^{t}$

APPENDIX A2

TRANSMISSION LINE REPRESENTATION

HVDC and EHVAC multiconductor lines or cables are defined by their series impedance ($R + jX$) and shunt admittance (B_c) matrices per unit length. Their equivalent circuit is represented by an appropriate number of pi-segments, the elements of which are derived from the physical geometry of the conductors, earthing and conductor-earth resistivities.

A method for calculating these matrices is described by Al-Khashali (1976), and results in the following:

Defining the B matrix, whose order is the number of conductors, including earth wires, and whose general element is given by:

$$B_{ij} = \log_e (D_{ij}/d_{ij})$$

where D_{ij} = distance between the ith conductor and the image of the jth conductor;

d_{ij} = distance between the ith and jth conductors ($i \neq j$); or

d_{ij} = radius of ith conductor ($i = j$).

The capacitance matrix per unit length is $C = 2\pi\varepsilon \cdot B^{-1}$.

The useful part of C corresponds to the "live" conductors since the earth wires are at earth potential and may, therefore, be eliminated. This is achieved by discarding the rows and columns in C corresponding to the earth wires.

The resistance and inductance matrices (series impedance) are given by:

$$Z = R_c + R_e + jw\ (L_g + L_c + L_e)$$

where suffixes g, c and e signify, respectively, the effects of geometry, conductor and earth path.

The contribution of the geometry to the total inductance is obtained directly from the B matrix as $L_g = \mu B/2\pi$.

The effect of the conductor on the resistance at low frequencies is limited to the d.c. resistance per unit length and, where skin effect is significant, a corrected power frequency value may be used. The internal inductance L_c is constant and is calculated using the concept of geometric mean radius. The earth return contributions R_e and L_e can be calculated using an infinite series.

The earth wires cannot be entirely eliminated from the series impedance matrices in the present study since the impedance matrix, given in terms of the differential operator p as $Z = R + L \cdot p$, has an inverse whose elements are, generally, high degree polynomials in (p). It is only in special cases, when these polynomials can be reduced, that the elimination of the earth wires may be achieved without undue complication. Single frequency analysis, when p may be replaced by jw, and lossless analysis are examples of such cases.

Therefore the equivalent circuit of a typical transmission line segment, and the corresponding inductance and capacitance matrices, are shown in Fig. A2.1.

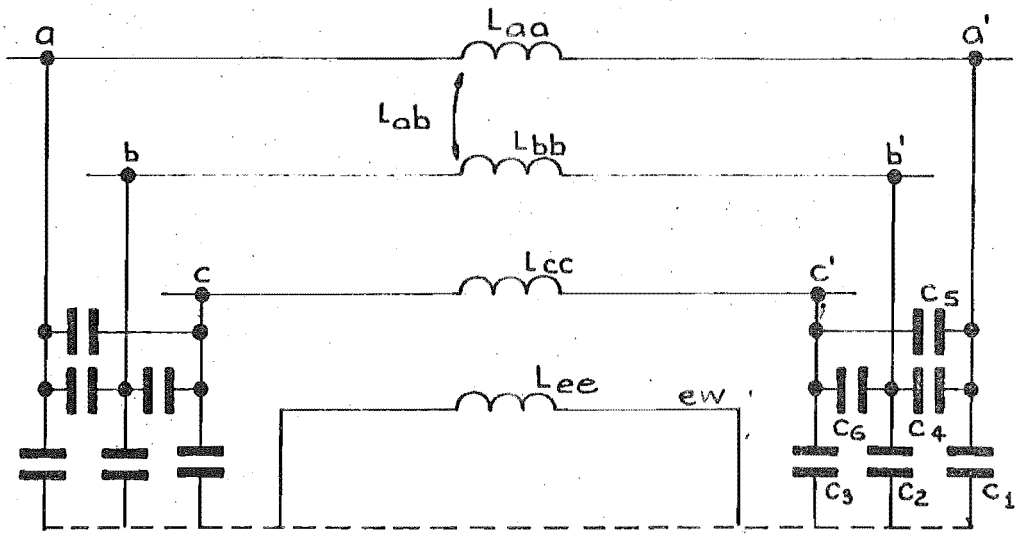

(a) Equivalent pi-segment model

L_{aa}	L_{ab}	L_{ac}	L_{ae}
L_{ba}	L_{bb}	L_{bc}	L_{be}
L_{ca}	L_{cb}	L_{cc}	L_{ce}
L_{ea}	L_{eb}	L_{ec}	L_{ee}

(b) Inductance matrix

	a'	b'	c'
a'	C_{aa}	C_{ab}	C_{ac}
b'	C_{ba}	C_{bb}	C_{bc}
c'	C_{ca}	C_{cb}	C_{cc}

(c) Capacitance matrix

Fig. A2.1 Transmission Line representation (typical pi-section)

The elements of the capacitance matrix are related to the equivalent circuit by, typically,

$$C_{aa} = C_1 + C_4 + C_5$$

and

$$C_{ab} = - C_4$$

APPENDIX A3

STATE VARIABLE EQUATION SET

Applying the principles of Section 2.4.5 to the equations detailed in Section 2.4.3 yields:

$$\psi_1 = L_1 I_1 \quad \ldots (A3.1)$$

$$Q_\alpha = C_\alpha V_\alpha \quad \ldots (A3.2)$$

$$V_\beta = -R_\beta (K_{\beta 1} I_1 + K_{\beta r} R_r^{-1} K_{r\alpha}^t V_\alpha) \quad \ldots (A3.3)$$

$$V_\gamma = -L_\gamma K_{\gamma 1} L_1^{-1} (E_1 - R_1 I_1 - pL_1 \cdot I_1 + K_{1\alpha}^t V_\alpha + K_{1\beta}^t V_\beta) \quad \ldots (A3.4)$$

$$I_r = R_r^{-1} (K_{r\alpha}^t V_\alpha + K_{r\beta}^t V_\beta) \quad \ldots (A3.5)$$

$$p\psi_1 = E_1 - R_1 I_1 + K_{1\alpha}^t V_\alpha + K_{1\beta}^t V_\beta + K_{1\gamma}^t V_\gamma \quad \ldots (A3.6)$$

$$pQ_\alpha = -K_{\alpha 1} I_1 - K_{\alpha r} I_r \quad \ldots (A3.7)$$

where the L and C matrices are reactance and susceptance matrices respectively, and derivatives are performed with respect to an angular frame of reference, i.e. $d/d\theta$.

APPENDIX A4

FORMULATION FOR VARIABLE TOPOLOGY

The inductive subnetwork is now defined to contain $(l + k)$ inductive branches; the k branches denoting branches involved in a convertor representation, and the l branches denoting all inductive branches external to the convertor. An inductive branch between the two inductive subnetworks will be specified as a k branch so that the connection matrix $K_{l\delta}{}^{t}$ is null. Therefore δ nodes will have only inductive branches within a convertor subnetwork (k branches) connected to it, whereas γ nodes have any external inductive (l) branches or an extremity of a convertor subnetwork connected to it. Therefore:

$$K_{kn}{}^{t} = [K_{k\alpha}{}^{t}\ K_{k\beta}{}^{t}\ K_{k\gamma}{}^{t}\ K_{k\delta}{}^{t}] \qquad \ldots (A4.1)$$

and $K_{l\delta}{}^{t}$, $K_{r\delta}{}^{t}$, $K_{c\delta}{}^{t}$ are all null.

Because of the nature of the convertor subnetwork, it may be assumed that it contains no e.m.f. sources, or time variant inductances (i.e. $pL_k = 0$). Applying partitioning to Kirchhoff's current law, yields:

$$K_{\delta k} I_k = 0$$

$$\text{or} \quad K_{\delta k} pI_k = 0 \qquad \ldots (A4.2)$$

$$K_{\gamma k} I_k + K_{\gamma l} I_l = 0 \qquad \ldots (A4.3)$$

$$K_{\beta k} I_k + K_{\beta l} I_l + K_{\beta r} I_r = 0 \qquad \ldots (A4.4)$$

$$K_{\alpha k} I_k + K_{\alpha l} I_l + K_{\alpha r} I_r + K_{\alpha c} I_c = 0 \qquad \ldots (A4.5)$$

The k branch voltage equations may be written in a diakoptical form as

$$pI_k = L_k^{-1}(-R_kI_k + K_{k\alpha}{}^tV_\alpha + K_{k\beta}{}^tV_\beta + K_{k\gamma}{}^tV_\gamma + K_{k\delta}{}^tV_\delta) \quad \ldots (A4.6)$$

along with the following equations from Section 2.4.3

$$pI_l = L_l^{-1}(E_l - R_lI_l - pL_l \cdot I_l + K_{l\alpha}{}^tV_\alpha + K_{l\beta}{}^tV_\beta + K_{l\gamma}{}^tV_\gamma) \quad \ldots (A4.7)$$

$$I_r = R_r^{-1}(K_{r\alpha}{}^t V_\alpha + K_{r\beta}{}^t V_\beta) \quad \ldots (A4.8)$$

$$pV_\alpha = C_\alpha^{-1} K_{\alpha c} I_c \quad \ldots (A4.9)$$

where from equation (A4.5)

$$J_\alpha = K_{\alpha c} I_c = -K_{\alpha l}I_l - K_{\alpha k}I_k - K_{\alpha r}I_r \quad \ldots (A4.10)$$

This equation set now has three dependent variables V_β, V_γ and V_δ which can be evaluated directly. Premultiplying equation (A4.8) by $K_{\beta r}$, yields

$$V_\beta = -R_\beta (K_{\beta r}R_r^{-1}K_{r\alpha}{}^tV_\alpha + K_{\beta l}I_l + K_{\beta k}I_k) \quad \ldots (A4.11)$$

Using equation (A4.2) and multiplying equation (A4.6) by $K_{\delta k}$, yields

$$0 = K_{\delta k}L_k^{-1}(-R_kI_k + K_{k\alpha}{}^tV_\alpha + K_{k\beta}{}^tV_\beta + K_{k\gamma}{}^tV_\gamma + K_{k\delta}{}^tV_\delta) \quad \ldots (A4.12)$$

Then defining

$$L_\delta = (K_{\delta k}L_k^{-1}K_{k\delta}{}^t)^{-1} \quad \ldots (A4.13)$$

yields

$$V_\delta = -L_\delta K_{\delta k}L_k^{-1}(-R_kI_k + K_{k\alpha}{}^tV_\alpha + K_{k\beta}{}^tV_\beta + K_{k\gamma}{}^tV_\gamma) \quad \ldots (A4.14)$$

Differentiation of equation (A4.3) yields

$$K_{\delta k}\, pI_k + K_{\delta l}\, pI_l = 0 \qquad \ldots \text{(A4.15)}$$

Substituting equations (A4.6) and (A4.7) yields

$$K_{\delta k}L_k^{-1}\,(-R_kI_k + K_{k\alpha}{}^tV_\alpha + K_{k\beta}{}^tV_\beta + K_{k\gamma}{}^tV_\gamma + K_{k\delta}{}^tV_\delta)$$
$$+ K_{\gamma l}I_l^{-1}(E_l - R_lI_l - pL_l\cdot I_l + K_{l\alpha}{}^tV_\alpha + K_{l\beta}{}^tV_\beta + K_{l\gamma}{}^tV_\gamma) = 0 \qquad \ldots \text{(A4.16)}$$

or

$$V_\gamma = -L_\varepsilon \Big[K_{\gamma k}L_k^{-1}(-R_kI_k + K_{k\alpha}{}^tV_\alpha + K_{k\beta}{}^tV_\beta + K_{k\delta}{}^tV_\delta)$$
$$+ K_{\gamma l}I_l^{-1}(E_l - R_lI_l - pL_l\cdot I_l + K_{l\alpha}{}^tV_\alpha + K_{l\beta}{}^tV_\beta)\Big] \qquad \ldots \text{(A4.17)}$$

where

$$L_\varepsilon = (K_{\gamma k}L_k^{-1}K_{k\gamma}{}^t + K_{\gamma l}L_l^{-1}K_{l\gamma}{}^t)^{-1} \qquad \ldots \text{(A4.18)}$$

which is not affected by topology changes, but is, in general, not sparse. Inspection of equations (A4.14) and (A4.17) indicates that they are two inter-dependent equations for the two vectors V_γ and V_δ. To solve for these two vectors would require an iterative process, but the associated computational burden would be prohibitive. However, in a practical interconnected a.c./d.c. power system, the only interface between convertor and non-convertor inductive subnetworks occurs at the convertor transformer's a.c. terminals. The usual practice is to have a.c. harmonic filters, including a high pass, connected on the a.c. side, which would by definition create a β node at this busbar. Alternatively the connection of an a.c. line or static capacitors will define it as an α node. Thus if

the restriction $K_{\gamma k} = 0$ is applied, the computational problem is removed without imposing any real system representation restrictions. In the rare case of the convertor busbar being a γ node the formulation without δ nodes may be used i.e. equations (A3.1) - (A3.7), since this would be more economic than using an iterative process to solve V_γ and V_δ as above.

By applying this network restriction, i.e. $K_{\gamma k}$ null, to the above equations, one obtains a direct solution viz.

$$V_\delta = -L_\delta K_{\delta k} L_k^{-1} (-R_k I_k + K_{k\alpha}^t V_\alpha + K_{k\beta}^t V_\beta) \quad \ldots (A4.19)$$

and

$$V_\gamma = -L_\gamma K_{\gamma 1} L_1^{-1} (E_1 - R_1 I_1 - pL_1 \cdot I_1 + K_{1\alpha}^t V_\alpha + K_{1\beta}^t V_\beta) \quad \ldots (A4.20)$$

With the state variables as defined in Section 2.4.5, the equation set for a variable topology formulation will then be as set out in equations (2.38) - (2.47).

APPENDIX A5

DESIGNATION OF CONVERTOR NODES

All convertor configurations assume that one end of the bridge combination is earthed and the other connected to the smoothing reactor. Hence, only two nodes are explicitly defined in 6-pulse operation to simulate valve switching, with a further node needed to represent the neutral of the transformer secondary in a star bridge. Five nodes altogether are needed to simulate 12-pulse operation, of which one is shared between the two bridges and another represents the neutral of the star-connected secondary. The allocation of new δ-nodes to a new set of convertor data, assuming that m such nodes have already been defined, is shown in Table A5.1 where it is assumed the convertor is nominally a rectifier. For a nominal invertor, the δ_t and δ_b designations are reversed.

Table A5.1 Convertor Node Designations

Type of convertor		neutral	δ_t	δ_m	δ_b	δ-range	
						min	max
6-pulse STAR		m+1	m+2	m+3	0	m+1	m+3
6-pulse DELTA		-	m+1	m+2	0	m+1	m+2
12-pulse	STAR	m+1	m+2	m+3	m+4	m+1	m+5
	DELTA	-	m+4	m+5	0	m+1	m+5

Table A5.1 indicates that a fixed structure is used in representing the variation in topology caused by valve switchings. This implies that, during commutations for instance, redundant nodes are retained to the detriment of computation efficiency. However, the dynamic re-ordering and relocation of data, which would otherwise be required, is avoided by adopting the fixed structure. The convertor bridge, on the other hand, should under normal conditions be in a non-commutating state, which requires all the nodes defined for the greater part of the time. In some special cases, explicitly the non-commutating arm short circuit and the open circuit condition, the number of nodes defined above is insufficient to deal with the configuration in the direct manner used in the others. Action is taken in these special cases to free one of the redundant nodes and use it in representing the relevant condition. This approach was preferred, since specification of extra nodes to deal with this situation, whilst easier, would increase computation time.

As an example, consider when two phases simultaneously have no conducting valves, so that both are set to δ_m, as in Mode C (see Appendix A7). In this case, the smoothing reactor bridge terminal (d1 or d2 in Fig. 2.4(b)) is set to the opposite side of the bridge, thus describing the short circuit. Similarly, to describe an open circuit condition, action is taken to connect the smoothing reactor bridge terminal to the other end of the reactor. This latter case is permissible since the smoothing reactor normally has no mutual coupling with any other inductive element in the

network. Moreover, if the third phase is also assigned to the node which normally corresponds to the smoothing reactor bridge end, a similar change can be carried out for that phase. This process leaves a free node to which one of the two open phases may be assigned, thereby establishing the independence of these two phases.

The relation between a bridge's designated nodes and the transformer secondary terminals is thus generally defined by the mode of operation. As an example consider Mode A, the non-commutating mode. Referring to Fig. 2.4(b), if valve v_1 is ON, then a is set to δ_t and if valve v_4 is ON, then a is set to δ_b, otherwise, if both v_1 and v_4 are OFF, a is set to δ_m. When the process is repeated for b and c, all bridge nodes (a, b, c, d1 and d2) will have been assigned to the set of δ-nodes defined as in Table A5.1.

APPENDIX A6

FORMATION OF NON-COMMUTATING NODAL MATRIX L_δ(NC)

By assuming equal leakage reactances (see Section 2.5.2) this matrix may be written by inspection using the nodal specifications as detailed in Appendix A5. The results are indicated in Fig. A6.1 for:

(a) star-star bridge

(b) star-delta bridge

(c) 12 pulse convertor bridge.

The inductance x_d, representing the smoothing reactor, is then connected between m + 1 and 0 for a 6 pulse delta convertor or between m + 2 and 0 for 6 pulse star and 12 pulse convertors using the method detailed in Appendix A7.

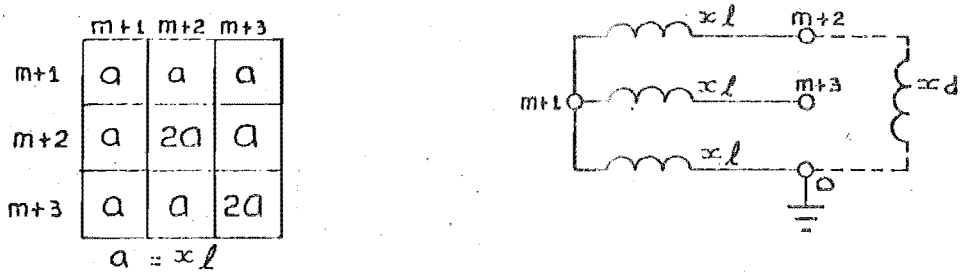

(a) Star

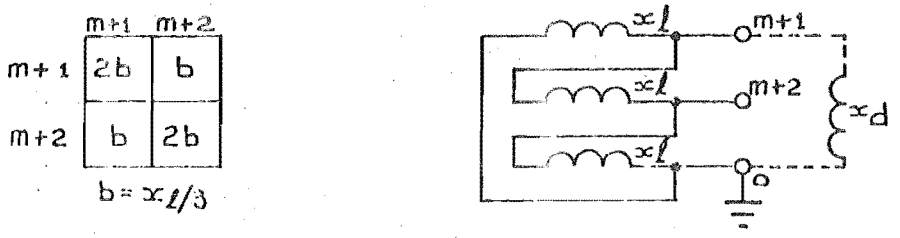

(b) Delta

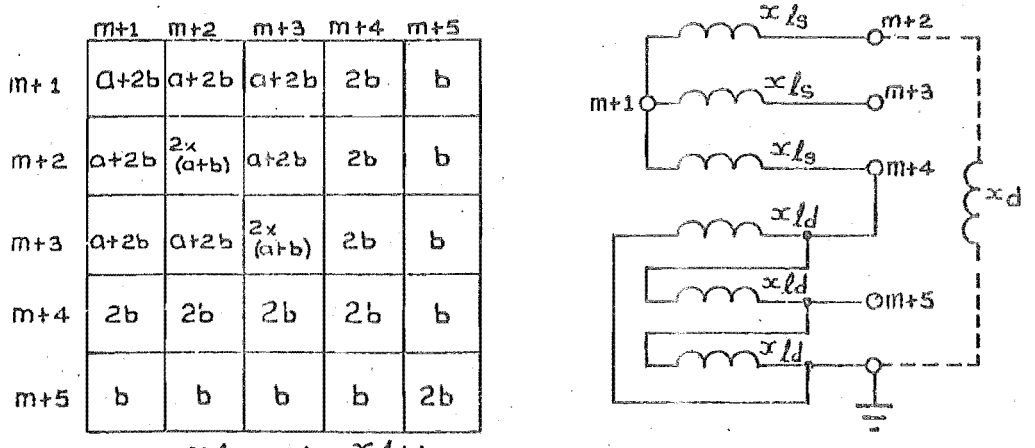

(c) 12-pulse

Fig. A6.1 Non-Commutating Nodal Matrices

APPENDIX A7

FORMATION OF ACTUAL NODAL MATRIX L_δ

Using the non-commutating nodal matrix $L_\delta(NC)$ as a basis, each of the other modes of operation are simulated by a process which is illustrated here for the normal commutating mode (Mode B), with the commutation process taking place in the top half of the bridge, e.g. valves v1, v2 and v3 conduct. A zero inductance link, representing an extra valve conducting in comparison with the "basic" mode, is then inserted between δ_t and δ_m according to the following process.

When an additional link of inductance (x) is connected between nodes i and j in the network, $L_\delta(NC)$ is modified to the new matrix L_δ whose general element (L_{pq}') is given, in terms of the elements of $L_\delta(NC)$, by

$$L_{pq}' = L_{pq} - (L_{pi} - L_{pj})\,(L_{iq} - L_{jq})\,/\,S \quad \ldots \quad (A7.1)$$

where

$$S = L_{ii} + L_{jj} - L_{ij} - L_{ji} + x \,.$$

One of the nodes i and j may be external to the δ-network, in which case the corresponding elements in equation (A7.1) will be zero. Conducting valves are represented by adding a link of zero inductance, and the removal of an existing branch is represented by adding a link of negative inductance equal in magnitude to that of the removed branch and connected in parallel with it. In the latter case, if the branch to be removed provides the only path from one part

of the network to the external system or to the common reference point, that part of the network will become isolated. This condition is indicated by a vanishing denominator (S), and it must be avoided.

The above treatment is quite general and applies equally well to all modes of operation. In general then, mode B is formed by connecting a zero inductance link between δ_m and either δ_t or δ_b, depending on where the commutation process is taking place. The commutating short circuit condition (mode D1) is also easily represented by connecting a single zero inductance link between δ_t and δ_b. The three phase short-circuit (mode E1) is represented by connecting a zero inductance between δ_m and δ_b, and another between δ_t and δ_b.

However, in the non-commutating d.c. short-circuit mode (Mode C), due to the limited number of δ-nodes available, special action is taken to represent the condition. With 6-pulse operation the smoothing reactor is removed from its normal δ-node and connected to the common reference point. This action frees a node to which one of the two non-conducting arms may be assigned.

Twelve pulse convertors can be more complicated, depending on which of the two bridges is in mode C. If the short circuit is in the star bridge, the reactor is removed from its normal δ-node and connected to the node shared between the two bridges (m + 4 in Table A5.1), as shown in Fig. A7.1(a). If, however, the delta bridge is in mode C then all the branches in the star bridge that are connected to (m + 4) are disconnected from this node

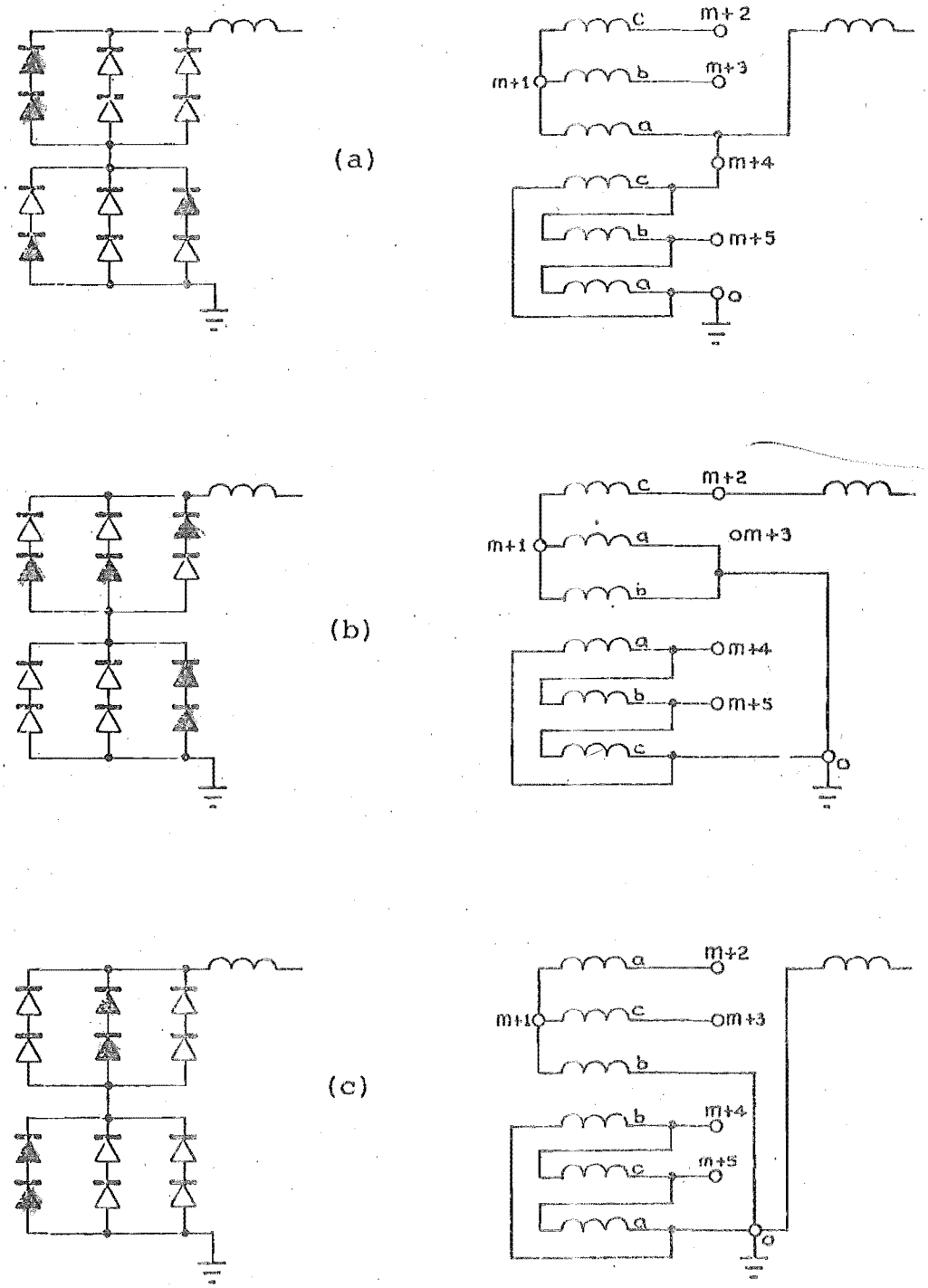

Fig. A7.1 Non-commutating arm short circuit in 12 pulse convertors

and connected to the common reference point. The branches switched over are effectively connected in parallel and the program lumps them together and, therefore, one removal and connection process is required. Fig. A7.1(b) shows this condition with the star bridge in a commutating state on the shared-node side. Finally, if both bridges are in mode C, the smoothing reactor and one transformer branch in the star bridge are both disconnected from their normal δ-nodes and connected to the common reference point as shown in Fig. A7.1(c).

To represent the convertor when it is in a non-conducting mode, i.e. the current path is interrupted, the modification of L_δ required is to remove the smoothing reactor from its normal δ-node and to connect it to an extra δ-node (δ_x) whose voltage is set equal to the d.c. line voltage. This frees a node which can be assigned to any of the transformer secondary terminals. The extra node δ_x is not represented in L_δ and, therefore, the structure of the convertor network is unchanged by its definition. The condition arrived at describes a true open circuit on the smoothing reactor side of the convertor.

APPENDIX A8

FORMATION OF CONVERTOR CONNECTION MATRIX $K_{\delta k}$

Since the connections of transformer secondary windings and the d.c. smoothing reactor are permanently fixed to a, b, c, d1 and d2 (Fig. 2.4(b)), by using the nodal assignment detailed in Appendix A5, one may obtain the convertor incidence matrix $K_{\delta k}$ for the specific combination of conducting valves.

Fig. A8.1 shows, as an example, a 12 pulse convertor in which the Δ-bridge is undergoing commutation. The convertor δ-nodes are assigned to the bridge and transformer terminal nodes, according to the combination of conducting valves given, as shown in Fig. A8.1(b). The permanent branch list shown in Fig. A8.1(c) is transformed to the working list, defined in terms of δ-nodes shown in Fig. A8.1(d). Finally the δ-k incidence matrix, shown in Fig. A8.1(e) is derived from the working branch list. The process is limited to the bridge nodes, and the external connections of the convertor network, established permanently at input, are indicated by zero entries.

(a)

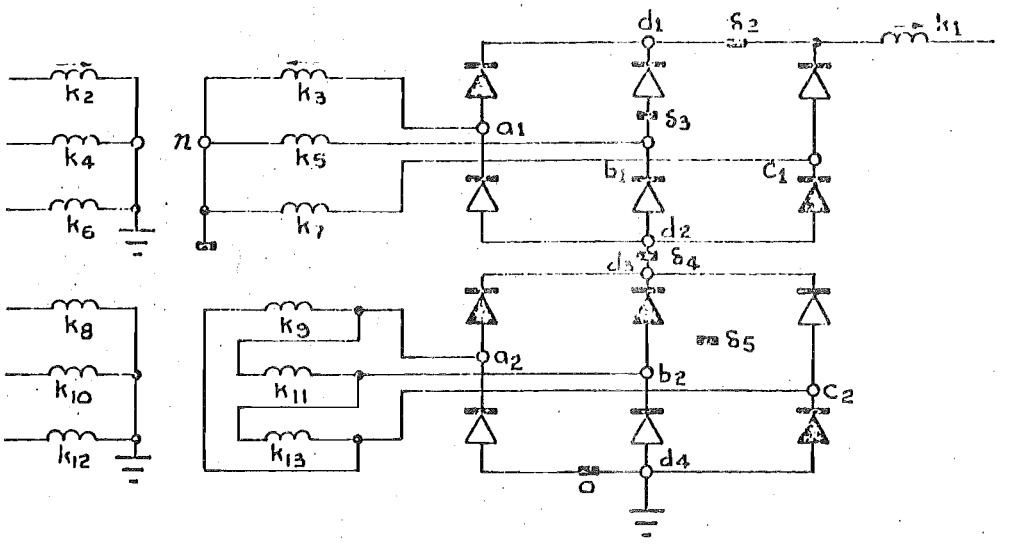

(b)

Bridge nodes	n	a_1	b_1	c_1	d_1	d_2	a_2	b_2	c_2	d_3	d_4
δ – nodes	δ_1	δ_2	δ_3	δ_4	δ_2	δ_4	δ_4	δ_4	0	δ_4	0

(c)

branch	from	to
k_1	d_1	0
k_2	0	0
k_3	a_1	n
k_4	0	0
k_5	b_1	n
k_6	0	0
k_7	c_1	n
k_8	0	0
k_9	a_2	c_2
k_{10}	0	0
k_{11}	b_2	a_2
k_{12}	0	0
k_{13}	c_2	b_2

(d)

branch	from	to
k_1	δ_2	0
k_2	0	0
k_3	δ_2	δ_1
k_4	0	0
k_5	δ_3	δ_1
k_6	0	0
k_7	δ_4	δ_1
k_8	0	0
k_9	δ_4	0
k_{10}	0	0
k_{11}	δ_4	δ_4
k_{12}	0	0
k_{13}	0	δ_4

(e)

$K_{\delta k}$	$-k_3$	$-k_5$	$-k_7$	k_1	k_3	k_5	k_7	k_9	$-k_{13}$
	1	2	3	4	5	6	7	8	9
$L_{\delta k}$	1	4	6	7	10	10			

Fig. A8.1 Formation of δ-k Incidence Matrix

APPENDIX A9

DATA SET FOR AC AND DC FAULT STUDIES

A9.1 N.Z. AC/DC SYSTEM

The data set on the following pages represents the N.Z. 220 kV power system consisting of two asynchronous systems (viz. N.I. and S.I.) and their HVDC link interconnection. The steady state busbar data was obtained from an a.c./d.c. load flow, and the branch, synchronous machine, shunt loads and d.c. link information was obtained from New Zealand Electricity. The parameters are calculated using the p.u. bases normally used for single phase power system studies.

This data set formed the input to the a.c./d.c. transient stability programme used to obtain a reduced representation for the a.c. system(s). The representation used in the dynamic analysis is depicted in Fig. A9.1 where the dotted lines encircle the Thevenin Equivalent information obtained from the transient stability programme. All other plant in Fig. A9.1 is explicitly modelled by the dynamic programme.

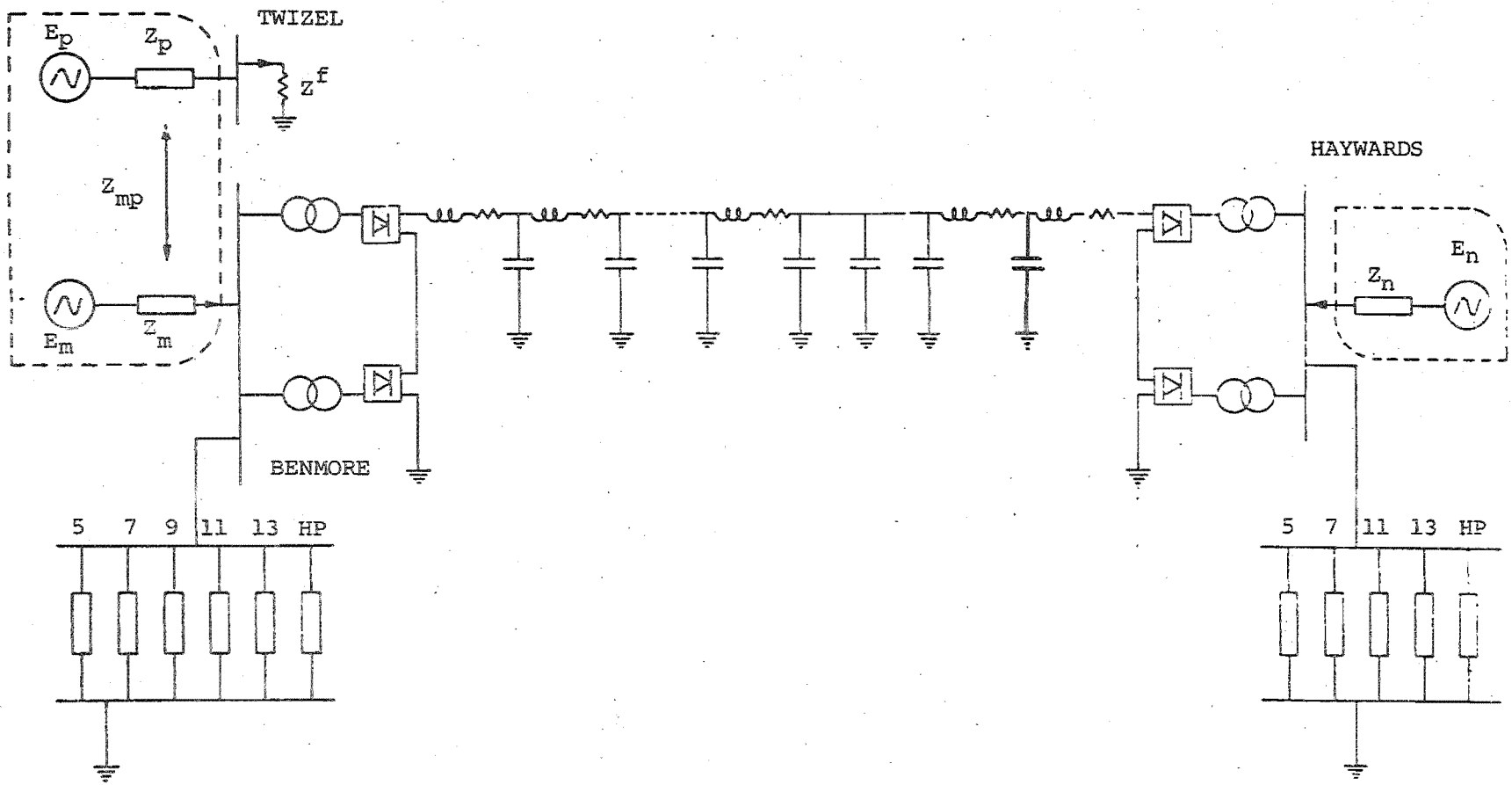

Fig. A9.1 Dynamic Analysis Representation of N.Z. System

ELECTRICAL POWER-SYSTEM TRANSIENT-STABILITY STUDY

DEPARTMENT OF ELECTRICAL ENGINEERING - UNIVERSITY OF CANTERBURY
CHRISTCHURCH, NEW ZEALAND.

15/05/80

SYSTEM NO. 5

NZ 220KV SYSTEM
63 BUSBARS,92 LINES,24 MACHINES
LOAD FLOW INITIAL CONDITIONS

SYSTEM FREQUENCY = 50.0 HERTZ
M.V.A. BASE = 100.0 M.V.A.

NO SYNCHRONOUS MACHINE CONTROLLER DATA INPUT
NO INDUCTION MOTOR DATA INPUT

STEADY-STATE SYSTEM DATA

BUSBAR DATA INPUT

BUSBAR	VOLTAGE	ANGLE	GEN MW	GEN MVAR	LOAD MW	LOAD MVAR
AVIEMORE--11	1.04000	12.8670	220.00000	-1.70000	0.00000	0.00000
AVIEMORE-220	1.04200	7.6590	0.00000	0.00000	0.00000	0.00000
BENMORE---16	1.02500	8.1430	540.00000	92.51000	0.00000	0.00000
BENMORE---DC	1.02500	8.1430	0.00000	0.00000	0.00000	0.00000
BENMORE--220	1.04000	7.4020	0.00000	0.00000	0.00000	0.00000
BROMLEY--220	1.00100	-9.8410	0.00000	0.00000	129.60000	38.30000
HALFWAYBU220	1.02600	-3.7230	0.00000	0.00000	95.30000	40.40000
INVERCARG220	1.00800	-7.7490	0.00000	0.00000	183.20000	20.00000
ISLINGTON220	1.00500	-10.5180	0.00000	159.45000	504.10000	124.30000
KIKIWA---220	1.00400	-24.0660	0.00000	0.00000	59.20000	9.20000
LIVINGSTN220	1.03800	3.6920	0.00000	0.00000	0.00000	0.00000
MANAPOURI-14	1.06000	0.9230	400.00000	91.33000	0.00000	0.00000
MANAPOURI220	1.04300	-2.9890	0.00000	0.00000	0.00000	0.00000
OHAU-A---11	1.05000	9.8630	214.00000	11.92000	0.00000	0.00000
OHAU-A---220	1.04500	6.0600	0.00000	0.00000	0.00000	0.00000
OHAU-B---11	1.04900	9.6920	175.00000	9.25000	0.00000	0.00000
OHAU-B---220	1.04400	5.8090	0.00000	0.00000	0.00000	0.00000
OHAU-C---11	1.05000	9.8880	175.00000	10.56000	0.00000	0.00000
OHAU-C---220	1.04500	6.0110	0.00000	0.00000	0.00000	0.00000
ROXBURGH--11	1.05500	0.0000	82.80000	36.52000	0.00000	0.00000
ROXBURGH-220	1.04300	-1.3630	0.00000	0.00000	0.00000	0.00000
SOUTHDON-220	1.02700	-3.5900	0.00000	0.00000	34.20000	12.70000
STOKE---220	1.01000	-25.4830	0.00000	0.00000	53.20000	-20.26000
TEKAPOAB--11	1.04600	8.3050	160.00000	5.96000	0.00000	0.00000
TEKAPOAB-220	1.04200	5.3590	0.00000	0.00000	0.00000	0.00000
TIWAI----220	1.00000	8.6200	0.00000	0.00000	420.00000	157.42000
TWIZEL---220	1.04400	5.6880	0.00000	0.00000	0.00000	0.00000
WAITAKI---11	1.05200	9.8010	70.00000	9.52000	0.00000	0.00000
WAITAKI--220	1.04200	7.0500	0.00000	0.00000	0.00000	0.00000
AHATIATIA-11	1.03200	29.8880	70.00000	2.23000	0.00000	0.00000
AHATIATIA220	1.03200	29.8880	0.00000	0.00000	0.00000	0.00000
ATIAMURI--11	1.05000	30.0720	50.00000	13.08000	0.00000	0.00000
ATIAMURI-220	1.05000	30.0720	0.00000	0.00000	0.00000	0.00000
BRUNSWICK220	1.03600	4.7880	0.00000	0.00000	0.00000	0.00000
BUNTMORE220	1.02500	2.8260	0.00000	0.00000	66.90000	16.80000
EDGECUMBE220	1.00400	21.2020	0.00000	0.00000	135.50000	11.70000
HAMILTON--11	1.04000	0.0320	150.00000	6.33000	0.00000	0.00000
HAMILTON-220	1.04000	-8.1580	0.00000	0.00000	120.00000	40.00000
HAYWARDS-220	0.98000	-4.2490	0.00000	183.12000	716.60000	73.54000
HAYWARDS--DC	0.98000	-4.2490	0.00000	0.00000	0.00000	0.00000
HENDERSON220	0.99200	-15.0880	0.00000	0.00000	160.00000	40.00000
MARKETAI--11	1.06500	-1.0558	210.00000	75.55000	0.00000	0.00000
MARKETAI-220	1.04500	-3.6670	0.00000	0.00000	0.00000	0.00000
MARSDEN--11	1.07000	-7.2260	150.00000	67.46000	0.00000	0.00000
MARSDEN--220	1.03300	-11.5320	0.00000	0.00000	0.00000	0.00000
NEWPLYMTH-11	1.06500	12.0480	400.00000	103.66000	0.00000	0.00000
NEWPLYMTH220	1.05000	8.9780	0.00000	0.00000	200.00000	100.00000
OHAKURI--11	1.03300	33.7990	170.00000	8.64000	0.00000	0.00000
OHAKURI--220	1.03300	27.3440	0.00000	0.00000	0.00000	0.00000
OTAHUHU--11	1.02500	-11.1000	200.00000	106.92000	0.00000	0.00000
OTAHUHU--220	0.98800	-14.9900	0.00000	0.00000	500.00000	100.00000
PENROSE--220	0.98200	-15.6890	0.00000	0.00000	300.00000	90.00000
STRATFORD220	1.04900	7.6730	0.00000	0.00000	0.00000	0.00000
TAKUKEWA220	1.03700	27.4690	0.00000	0.00000	0.00000	0.00000
TOKAANU--11	1.06000	3.0300	180.00000	27.95000	0.00000	0.00000
TOKAANU--220	1.04800	-1.1380	0.00000	0.00000	2.50000	0.80000
WAIPAPA--11	1.06100	-0.2240	40.00000	8.74000	0.00000	0.00000
WAIPAPA--220	1.04600	-3.4660	0.00000	0.00000	0.00000	0.00000
WAIRAKEI--11	1.03000	31.1760	140.00000	2.14000	0.00000	0.00000
WAIRAKEI-220	1.02900	26.3300	0.00000	0.00000	19.20000	6.30000
WHIRINAKI-11	1.03000	28.2860	160.00000	20.26000	0.00000	0.00000
WHIRINAKI220	1.02300	25.5600	0.00000	0.00000	200.00000	50.00000
WHAKAMARU-11	1.05500	0.0000	91.30000	13.93000	0.00000	0.00000
WHAKAMARU220	1.04000	-4.1630	0.00000	0.00000	0.00000	0.00000

BRANCH DATA INPUT

SENDING BUSBAR	RECEIVING BUSBAR	RESISTANCE P.U.	REACTANCE P.U.	SUSCEPTANCE P.U.	TAP P.C.
BENMORE---16	BENMORE---DC	0.00001	0.00001	0.00000	0.00
HAYWARDS--DC	HAYWARDS-220	0.00001	0.00001	0.00000	0.00
AVIEMORE-220	BENMORE--220	0.00325	0.01509	0.02304	0.00
AVIEMORE-220	AVIEMORE--11	0.00150	0.04470	0.00000	0.00
AVIEMORE-220	BENMORE--220	0.00330	0.01530	0.02298	0.00
AVIEMORE-220	WAITAKI--220	0.00153	0.00723	0.01062	0.00
BENMORE--220	TWIZEL---220	0.00429	0.02430	0.08201	0.00
BENMORE--220	BENMORE---16	0.00095	0.03300	0.00000	0.00
BROMLEY--220	ISLINGTON220	0.00203	0.01051	0.05364	0.00
BROMLEY--220	TWIZEL---220	0.01714	0.13490	0.45460	0.00
HALFWAYBU220	ROXBURGH-220	0.00768	0.06592	0.19082	0.00
HALFWAYBU220	SOUTHDUN-220	0.00175	0.01010	0.01665	0.00
INVERCARG220	MANAPOURI220	0.01338	0.09178	0.25996	0.00
INVERCARG220	MANAPOURI220	0.01338	0.09178	0.25996	0.00
INVERCARG220	ROXBURGH-220	0.01880	0.11223	0.17208	0.00
INVERCARG220	ROXBURGH-220	0.01915	0.11252	0.17814	0.00
INVERCARG220	TIWAI----220	0.00226	0.01456	0.04596	0.00
INVERCARG220	TIWAI----220	0.00226	0.01456	0.04596	0.00
ISLINGTON220	KIKIWA---220	0.03326	0.20030	0.30182	0.00
ISLINGTON220	LIVINGSTN220	0.03230	0.17662	0.35841	0.00
ISLINGTON220	TEKAPO-B-220	0.02112	0.14576	0.36973	0.00
ISLINGTON220	TWIZEL---220	0.01630	0.13037	0.44180	0.00
KIKIWA---220	STOKE----220	0.00762	0.04370	0.07278	0.00
LIVINGSTN220	ROXBURGH-220	0.02649	0.12351	0.18426	0.00
LIVINGSTN220	WAITAKI--220	0.00588	0.02787	0.04092	0.00
MANAPOURI220	TIWAI----220	0.01549	0.10734	0.29780	0.00
MANAPOURI220	TIWAI----220	0.01549	0.10734	0.29780	0.00
MANAPOURI220	MANAPOURI-14	0.00068	0.01902	0.00000	0.00
OHAU-A---220	TWIZEL---220	0.00115	0.00662	0.00109	0.00
OHAU-A---220	TWIZEL---220	0.00115	0.00662	0.00109	0.00
OHAU-A---220	OHAU-A----11	0.00170	0.03410	0.00000	0.00
OHAU-B---220	TWIZEL---220	0.00024	0.00179	0.00057	0.00
OHAU-B---220	TWIZEL---220	0.00024	0.00179	0.00057	0.00
OHAU-B---220	OHAU-C---220	0.00064	0.00477	0.00152	0.00
OHAU-B---220	OHAU-B----11	0.00210	0.04250	0.00000	0.00
OHAU-C---220	OHAU-C----11	0.00210	0.04250	0.00000	0.00
OHAU-C---220	TWIZEL---220	0.00085	0.00656	0.00209	0.00
ROXBURGH-220	SOUTHDUN-220	0.00849	0.07059	0.19654	0.00
ROXBURGH-220	TWIZEL---220	0.01590	0.13710	0.43180	0.00
ROXBURGH-220	TWIZEL---220	0.01590	0.13710	0.43180	0.00
ROXBURGH-220	ROXBURGH--11	0.00160	0.03230	0.00000	0.00
TWIZEL---220	TEKAPO-B-220	0.00230	0.01554	0.04860	0.00
TEKAPO-B--11	TEKAPO-B-220	0.00190	0.03510	0.00000	0.00
WAITAKI---11	WAITAKI--220	0.00668	0.07605	0.00000	0.00
ARATIATIA220	WAIRAKEI-220	0.00060	0.00340	0.00532	0.00
ATIAMURI--220	OHAKURI--220	0.00120	0.00570	0.00832	0.00
ATIAMURI--220	TARUKENGA220	0.00650	0.03750	0.06152	0.00
ATIAMURI--220	TARUKENGA220	0.00650	0.03750	0.06152	0.00
BRUNSWICK220	BUNTHORPE220	0.00460	0.03790	0.11985	0.00
BRUNSWICK220	BUNTHORPE220	0.00460	0.03790	0.11985	0.00
BRUNSWICK220	STRATFORD220	0.01450	0.08470	0.13470	0.00
BRUNSWICK220	STRATFORD220	0.01440	0.08330	0.13565	0.00
BRUNSWICK220	STRATFORD220	0.01440	0.08330	0.13565	0.00
BUNTHORPE220	HAYWARDS-220	0.02210	0.10490	0.15180	0.00
BUNTHORPE220	HAYWARDS-220	0.02210	0.10490	0.15180	0.00
BUNTHORPE220	TOKAANU--220	0.02900	0.13800	0.20000	0.00
BUNTHORPE220	TOKAANU--220	0.02900	0.13800	0.20000	0.00
BUNTHORPE220	WAIRAKEI-220	0.03120	0.18440	0.28490	0.00
EDGECUMBE220	OHAKURI--220	0.01390	0.08250	0.12750	0.00
HAMILTON-220	OTAHUHU--220	0.01040	0.06960	0.19960	0.00
HAMILTON-220	WHAKAMARU220	0.00860	0.05130	0.17320	0.00
HENDERSON220	MARSDEN--220	0.01490	0.09240	0.17560	0.00
HENDERSON220	MARSDEN--220	0.01490	0.09240	0.17560	0.00
HENDERSON220	OTAHUHU--220	0.00220	0.01880	0.05767	0.00
HENDERSON220	OTAHUHU--220	0.00220	0.01880	0.05767	0.00
MARAETAI-220	WAIPAPA--220	0.00210	0.01000	0.01441	0.00
MARAETAI-220	WHAKAMARU220	0.00170	0.00810	0.01171	0.00
MARAETAI-220	WHAKAMARU220	0.00170	0.00810	0.01171	0.00
NEWPLYMTH220	STRATFORD220	0.00300	0.02500	0.07886	0.00
NEWPLYMTH220	STRATFORD220	0.00300	0.02500	0.07886	0.00
OHAKURI--220	WAIRAKEI-220	0.00490	0.02350	0.03396	0.00
OTAHUHU--220	PENROSE--220	0.00140	0.00830	0.01282	0.00
OTAHUHU--220	PENROSE--220	0.00140	0.00830	0.01282	0.00
OTAHUHU--220	WHAKAMARU220	0.03550	0.16850	0.24390	0.00
OTAHUHU--220	WHAKAMARU220	0.01780	0.11710	0.34860	0.00
OTAHUHU--220	WHAKAMARU220	0.01780	0.11710	0.34860	0.00
TOKAANU--220	WHAKAMARU220	0.01300	0.06300	0.09200	0.00
TOKAANU--220	WHAKAMARU220	0.01300	0.06300	0.09200	0.00
TOKAANU--220	WHAKAMARU220	0.01300	0.06300	0.09200	0.00
WAIRAKEI-220	WHIRINAKI220	0.00880	0.07300	0.23060	0.00
WAIRAKEI-220	WHIRINAKI220	0.00880	0.07300	0.23060	0.00
ARATIATIA-11	ARATIATIA220	0.00340	0.09090	0.00000	0.00
ATIAMURI--11	ATIAMURI-220	0.00680	0.10010	0.00000	0.00
HAMILTON--11	HAMILTON-220	0.02420	0.10070	0.00000	0.00
MARAETAI--11	MARAETAI-220	0.00180	0.02480	0.00000	0.00
MARSDEN---11	MARSDEN--220	0.00280	0.05660	0.00000	0.00
NEWPLYMTH-11	NEWPLYMTH220	0.00050	0.01510	0.00000	0.00
OHAKURI---11	OHAKURI--220	0.00440	0.07130	0.00000	0.00
OTAHUHU---11	OTAHUHU--220	0.00140	0.03510	0.00000	0.00
TOKAANU---11	TOKAANU--220	0.00150	0.04510	0.00000	0.00
WAIPAPA---11	WAIPAPA--220	0.00840	0.15880	0.00000	0.00
WAIRAKEI--11	WAIRAKEI-220	0.00230	0.06400	0.00000	0.00
WHIRINAKI-11	WHIRINAKI220	0.00150	0.03150	0.00000	0.00
WHAKAMARU-11	WHAKAMARU220	0.00690	0.08830	0.00000	0.00

SHUNT IMPEDANCE DENOTED BY - *

SYNCHRONOUS MACHINE DATA

M/C PARAMETERS

BUSBAR NAME	MACHINE NO	MODEL	DATA MVA BASE	INERT. CONST. MWSKVA	REACTANCES (P.U.) TRANSIENT D-AXIS	TRANSIENT Q-AXIS	SYNCHRONOUS D-AXIS	SYNCHRONOUS Q-AXIS	SUB-TRANSIENT D-AXIS	SUB-TRANSIENT Q-AXIS	MUT-UAL	ARM. RESIST (P.U.)	O/C TCS (SECS) TRANSIENT D-AXIS	TRANSIENT Q-AXIS	SUB-TRANSIENT D-AXIS	SUB-TRANSIENT Q-AXIS	SATN. FACT.	RTR. TYPE
AVIEMORE---11	1	A	100.00	6.838	0.0990	0.0990	0.2990	0.2990	0.0660	0.0660	0.000	0.0018	4.07	0.054	0.0530	0.0530	0.000	SAL
BENMORE---16	1	A	100.00	16.506	0.0390	0.0390	0.1900	0.1900	0.0290	0.0290	0.000	0.0003	6.00	0.080	0.0800	0.0800	0.000	SAL
ISLINGTON220	1	A	100.00	1.082	0.3350	0.3350	0.3350	0.3350	0.3350	0.3350	0.000	0.0047	99.99	99.999	0.0000	0.0000	0.000	-
MANAPOURI-14	1	A	100.00	24.540	0.0390	0.0390	0.1510	0.1510	0.0240	0.0240	0.000	0.0005	6.00	0.080	0.0800	0.0800	0.000	SAL
OHAU-A----11	1	A	100.00	6.751	0.0940	0.0940	0.4110	0.4110	0.0470	0.0470	0.000	0.0015	5.00	0.043	0.0430	0.0430	0.000	SAL
OHAU-B----11	1	A	100.00	7.421	0.0920	0.0920	0.4810	0.4810	0.0550	0.0550	0.000	0.0016	5.00	0.043	0.0430	0.0430	0.000	SAL
OHAU-C----11	1	A	100.00	7.421	0.0920	0.0920	0.4810	0.4810	0.0550	0.0550	0.000	0.0016	5.00	0.043	0.0430	0.0430	0.000	SAL
ROXBURGH--11	1	A	100.00	7.950	0.0860	0.0860	0.4500	0.4500	0.0520	0.0520	0.000	0.0017	7.16	0.055	0.0550	0.0550	0.000	SAL
TEKAPO-B--11	1	A	100.00	9.770	0.0990	0.0990	0.4909	0.4909	0.0760	0.0760	0.000	0.0011	6.68	0.013	0.0130	0.0130	0.000	SAL
WAITAKI----11	1	A	100.00	9.715	0.1900	0.1900	0.5000	0.5000	0.1540	0.1540	0.000	0.0056	3.94	0.044	0.0440	0.0440	0.000	SAL
ARATIATIA--11	1	A	100.00	3.062	0.2400	0.2400	0.9400	0.9400	0.1800	0.1800	0.000	0.0076	5.00	0.050	0.0500	0.0500	0.000	SAL
ATIAMURI---11	1	A	100.00	3.060	0.2350	0.2350	0.9100	0.9100	0.1690	0.1690	0.000	0.0070	5.00	0.050	0.0500	0.0500	0.000	SAL
MAMILTON---11	1	A	100.00	16.650	0.1240	0.1240	0.4560	0.4560	0.1070	0.1070	0.000	0.0016	5.00	0.050	0.0500	0.0500	0.000	SAL
MAYWARDS-220	1	A	100.00	0.288	0.0520	0.0520	0.3440	0.3440	0.0250	0.0250	0.000	0.0006	5.00	0.050	0.0500	0.0500	0.000	SAL
MARAETAI---11	1	A	100.00	11.850	0.0650	0.0650	0.2700	0.2700	0.0430	0.0430	0.000	0.0065	5.00	0.050	0.0500	0.0500	0.000	SAL
MANSDEN----11	1	A	100.00	14.400	0.0630	0.0630	0.4830	0.4830	0.0530	0.0530	0.000	0.0005	6.90	0.050	0.0500	0.0500	0.000	SAL
NEWPLYMTH--11	1	A	100.00	20.050	0.0380	0.0380	0.2620	0.2620	0.0220	0.0220	0.000	0.0002	6.70	0.050	0.0500	0.0500	0.000	SAL
OHAKURI----11	1	A	100.00	9.035	0.1850	0.1850	0.6830	0.6830	0.1290	0.1290	0.000	0.0039	5.00	0.050	0.0500	0.0500	0.000	SAL
OTAHUHU----11	1	A	100.00	15.480	0.0520	0.0520	0.3490	0.3490	0.0120	0.0120	0.000	0.0010	8.50	0.075	0.0750	0.0750	0.000	SAL
TOKAANU----11	1	A	100.00	6.520	0.1090	0.1090	0.3290	0.3290	0.0730	0.0730	0.000	0.0020	5.00	0.060	0.0600	0.0600	0.000	SAL
WAIPAPA----11	1	A	100.00	4.527	0.4400	0.4400	1.5700	1.5700	0.3170	0.3170	0.000	0.0055	5.00	0.050	0.0500	0.0500	0.000	SAL
WAIRAKEI---11	1	A	100.00	8.4683	0.1120	0.1120	0.5800	0.5800	0.0728	0.0728	0.000	0.0050	5.00	0.050	0.0500	0.0500	0.000	SAL
WHIRINAKI--11	1	A	100.00	7.520	0.0580	0.0580	0.4730	0.4730	0.0337	0.0337	0.000	0.0050	5.00	0.050	0.0500	0.0500	0.000	SAL
WHAKAMARU--11	1	A	100.00	2.590	0.2250	0.2250	0.8550	0.8550	0.1530	0.1530	0.000	0.0038	5.04	0.059	0.0590	0.0590	0.000	SAL

M/C LOADINGS

BUSBAR NAME	M/C NO.	M/C POWER CUTPUT MW	MVAR	DAMPING FACTOR	
AVIEMORE---11	1	220.00000	-1.70000	0.00	
BENMORE---16	1	540.00000	92.51000	0.00	
ISLINGTON220	1	0.00000	159.43000	0.00	
MANAPOURI-14	1	400.00000	91.33000	0.00	
OHAU-A----11	1	214.00000	11.92000	0.00	
OHAU-B----11	1	175.00000	9.25000	0.00	
OHAU-C----11	1	175.00000	10.56000	0.00	
ROXBURGH--11	1	82.80000	36.52000	0.00	
TEKAPO-B--11	1	160.00000	5.90000	0.00	
WAITAKI----11	1	70.00000	9.52000	0.00	
ARATIATIA-11	1	70.00000	2.23000	0.00	A
ATIAMURI---11	1	50.00000	13.08000	0.00	A
MAMILTON---11	1	150.00000	6.33000	0.00	A
MAYWARDS-220	1	0.00000	183.12000	0.00	A
MARAETAI---11	1	210.00000	75.55000	0.00	A
MANSDEN----11	1	150.00000	67.40000	0.00	A
NEWPLYMTH--11	1	400.00000	103.80000	0.00	A
OHAKURI----11	1	170.00000	8.64000	0.00	A
OTAHUHU----11	1	200.00000	106.92000	0.00	A
TOKAANU----11	1	180.00000	27.95000	0.00	A
WAIPAPA----11	1	40.00000	8.74000	0.00	A
WAIRAKEI---11	1	140.00000	2.14000	0.00	A
WHIRINAKI--11	1	180.00000	20.26000	0.00	A
WHAKAMARU--11	1	91.30000	13.93000	0.00	A

M/C USING ALTERNATIVE REF. M/C DENOTED BY = A

DC LINK PARAMETERS

BUS NAME	ANGLE LIMITS MAX	MIN	SERIES BRIDGES	VOLTAGE BASE(KV)	CURRENT MARGIN(A)	LINE RESIS (OHMS)	REACTANCE(PU) COM	TRAN	FILTER	TAP %
BENMORE---DC	90.00	3.00	12.00	420.00	0.00	25.560	0.02243	0.02243	0.492609	0.000
MAYWARDS--DC	90.00	18.00	12.00	420.00	120.00	25.560	0.01905	0.01905	1.033250	0.000

SHUNT LOADS

BUSBAR NAME	MEGAWATTS	MEGAVARS	NON-IMPEDANCE TYPE LOAD (PC) VARYING WITH V P	Q	FIXED P	Q
BROMLEY--220	129.60000	38.30000	0.	0.	0.	0.
HALFWAYBU220	95.30000	40.40000	0.	0.	0.	0.
INVERCARG220	183.20000	20.00000	0.	0.	0.	0.
ISLINGTON220	504.10000	124.30000	0.	0.	0.	0.
KIKIWA---220	59.20000	9.20000	0.	0.	0.	0.
SOUTHDUN--220	34.20000	12.90000	0.	0.	0.	0.
STOKE----220	53.20000	-20.26000	0.	0.	0.	0.
TIWAI----220	420.00000	157.42000	0.	0.	0.	0.
BUNTHORPE220	66.90000	16.80000	0.	0.	0.	0.
EDGECUMBE220	135.50000	11.70000	0.	0.	0.	0.
HAMILTON-220	120.00000	20.00000	0.	0.	0.	0.
HAYWARDS-220	716.60000	73.54000	0.	0.	0.	0.
HENDERSON220	160.00000	40.00000	0.	0.	0.	0.
NEWPLYMTH220	200.00000	100.00000	0.	0.	0.	0.
OTAHUHU--220	500.00000	100.00000	0.	0.	0.	0.
PENROSE--220	300.00000	90.00000	0.	0.	0.	0.
TOKAANU--220	2.50000	0.80000	0.	0.	0.	0.
WAIRAKEI-220	19.20000	6.30000	0.	0.	0.	0.
WHIRINAKI220	200.00000	50.00000	0.	0.	0.	0.

NOTE - ANY NON-ESSENTIAL PARAMETERS MISSING FROM THE INPUT DATA HAVE BEEN ASSIGNED APPROPRIATE VALUES IN THE CALCULATION PROCESS, AS SHOWN ABOVE. A VALUE INDICATED AS A SERIES OF 9S IS ACTUALLY VERY LARGE.

A9.2 P.U. SYSTEMS OF DYNAMIC ANALYSIS PROGRAMMES

The p.u. system is based on fundamental, r.m.s. voltages and currents in the a.c. system. These are used for quantities in both the a.c. and d.c. parts of the power system.

Let V_B and I_B denote the base voltage (in kV) and current (in kA) respectively, and ω_o the base frequency (rads/sec).

Then base impedance

$$Z_B = V_B / \sqrt{3} I_B \ \Omega \qquad \text{for a.c. system parameters}$$

and $$Z_B = V_B / I_B \ \Omega \qquad \text{for d.c. system parameters,}$$

and base power

$$S_B = \sqrt{3} V_B \ I_B \qquad \text{MVA throughout the system.}$$

P.U. quantities throughout the system are then defined by

$$V_{pu} = V(kV) / V_B$$

$$I_{pu} = I(kA) / I_B$$

$$R_{pu} = R(\Omega) / R_B$$

$$X_{pu} = L(H) \ \omega_o / Z_B$$

$$B_{pu} = C(F) \ \omega_o \ Z_B$$

and in p.u.

$$S_{ac} = V_{ac} \ I_{ac}$$

$$S_{dc} = V_{dc} \ I_{dc} / \sqrt{3}$$

Table A9.1 gives the values used for the N.Z. power system to implement this p.u. system. The p.u. values for inductance and capacitance refer to reactance and susceptance respectively, as defined above.

Table A9.1 Dynamic Analysis P.U. System

	a.c. side	d.c. side
1. Base quantities		
voltage, kV	220	210
current, kA	0.2643	0.27493
power, MVA	100	100
impedance, Ω	484	763.834
frequency, Hz	50	50
2. Typical values		
resistance, 1Ω	0.002066	0.001309
inductance, 1mH	0.000649	0.000411
capacitance, 1μF	0.152053	0.239966

A9.3 N.Z. HVDC CONVERTOR TRANSFORMERS

Whereas the transient stability programme uses a single bridge convertor representation, in order to correctly identify 12 pulse operation the dynamic analysis uses a double bridge convertor representation. The equivalent leakage reactances are depicted in Table A9.2.

Table A9.2 N.Z. HVDC Convertor Transformer Data

X_{1a} (p.u.)	Transient Stability Base System, Single Bridge Convertor	Transient Stability Base System, Double Bridge Convertor	Dynamic Analysis Base System, Double Bridge Convertor
S.I.	0.02243	0.04486	0.02590
N.I.	0.01905	0.03810	0.021997

The equivalent transformer matrices, based on 1% magnetizing admittance, are therefore:

$$[L_t]_{SI\lambda} = \begin{bmatrix} 100. & 99.98705 \\ 99.98705 & 100. \end{bmatrix}$$

$$[L_t]_{SI\Delta} = \begin{bmatrix} 100. & 173.1827 \\ 173.1827 & 300. \end{bmatrix}$$

$$[L_t]_{NI\lambda} = \begin{bmatrix} 100. & 99.989 \\ 99.989 & 100. \end{bmatrix}$$

$$[L_t]_{NI\Delta} = \begin{bmatrix} 100. & 173.186 \\ 173.186 & 300. \end{bmatrix}$$

A9.4 N.Z. AC HARMONIC FILTERS

The S.I. d.c. link terminal has a.c. harmonic filters tuned to harmonic orders 5, 7, 9, 11 and 13 with a high pass filter tuned to approximately the 17th harmonic. The N.I. terminal has the same configuration, except that no 9th order filter is installed. The data (Robinson 1966) for the filters, converted to the required base, are depicted below.

Table A9,3 S.I. Filter Data (p.u.)

	Filter Order				
Element	5	7	9	11	13
C	0.36621	0.23703	0.14340	0.27495	0.19081
L	0.10909	0.08578	0.08328	0.02998	0.03123
R	0.01092	0.01204	0.01485	0.00660	0.00809

Table A9.4 N.I. Filter Data (p.u.)

	Filter Order			
Element	5	7	11	13
C	0.30682	0.23571	0.40295	0.23308
L	0.12966	0.08619	0.02039	0.02526
R	0.01303	0.01212	0.00451	0.00661

The high pass filters were of the configuration depicted in Fig. 2.2(b) and the data for this set is detailed in Table A9.5.

Table A9.5 High Pass Filter Data (p.u.)

	r	L	C	R
S.I.	0.00001	0.00500	0.53331	0.11929
N.I.	0.00001	0.00378	0.49907	0.08708

A9.5 N.Z. HVDC TRANSMISSION LINK

The data for the N.Z. HVDC link, described in Section 4.2.4 and depicted in Fig. 4.2, was obtained from New Zealand Electricity. The total bipole line resistance of 25.56Ω in the steady state data was made up (at rated current) from:

(i) Overhead line 10.95Ω per pole

(ii) Cable resistance 1.51Ω per pole

(iii) Smoothing reactor 0.32Ω per pole.

The four smoothing reactors each had an inductance value of 0.8H, and the Submarine Cable (per pole) had a

capacitance of 0.333 μF/km which is a total capacitance of approximately 13.3331 μF. The series inductance used for the overhead line was 1.33 mH/km, and the shunt capacitance used was 0.012 μF/km.

The d.c. line representation for a.c. and d.c. faults was different, so the p.u. quantities used are indicated in Figs 4.3 and 5.2 respectively.

A9.6 THEVENIN EQUIVALENT REPRESENTATION OF AC SYSTEMS

Fig. A9.1 illustrates the basic equivalent used for the studies in Chapters 4 and 5. The data for the elements explicitly represented has been discussed above. The information contained within the dotted lines pertains to the Thevenin Equivalent representation. Fig. A9.1 actually depicts the representation for an a.c. fault in the S.I. system of impedance Z^f. Obviously, a fault in the N.I. would result in the interrelated equivalents being at that end. For the case of a d.c. fault, the a.c. system at both ends reduces to the representation illustrated at the invertor end in Fig. A9.1. An indication of the numerical values of the Thevenin Equivalents is provided in Table A9.6, using the dynamic analysis programme data base for the case of a 3 phase fault at Twizel in the S.I. system (case 321).

Table A9.6 Thevenin Equivalents' Data (p.u.)

	Rectifier	Invertor	Fault	"Mutual"
$\|E\|$ $\angle E$	1.06936 12.335^o	0.98965 7.746^o	1.05448 5.117^o	
Z	0.00055 +j.01413	0.00575 +j.01759	0.00155 +j.01066	0.00039 +j.00347

APPENDIX A10

DETAILED GENERATOR MODEL STUDIES DATA

A10.1 CONVERSION OF P.U. DATA

The generator data set obtained for a detailed generator model based on the Kingsnorth machines (Campos Barros 1976), used a p.u. system based on phase-neutral voltages and single phase power as follows:

Generator rating	588 MVA
Rated Stator Voltage	23.5 kV
Rated Field Current	2.03 kA

The p.u. system used by Campos Barros had the following base quantities, where subscripts sB and rB denote stator and rotor base quantities respectively.

S_{sB} = 392 MVA S_{rB} = 392 MVA

V_{sB} = 19.1877 kV V_{rB} = 285.6 kV

I_{sB} = 20.4298 kA I_{rB} = 1.3725 kA

Z_{sB} = 0.9392 Ω Z_{rB} = 208.08 Ω

Z_{srB} = 13.98 Ω

Using this information, the p.u. quantities of Campos Barros were converted into real values and then changed into p.u. values suitable for representation in the dynamic programme. This second conversion was based on the following base system.

S_{sB} = 588 MVA S_{rB} = 588 MVA

V_{sB} = 23.5 kV V_{rB} = 10 kV

I_{sB} = 14.446 kA I_{rB} = 58.8 kA

Z_{sB} = 0.9392 Ω Z_{rB} = 0.17007 Ω

Z_{srB} = 0.39966 Ω

A10.2 DATA FOR PQ LOAD MODEL

The synchronous machine was modelled using the data in Table A10.1. The load transformer was assumed to have a leakage reactance of 0.02 p.u. From this, and a nominal terminal voltage r.m.s. value, the steady state conditions were calculated in the absence of the excitation current as a first approximation (case 0195). The load impedance and transformer matrix were determined so as to approximate a convertor plant to be investigated (see Appendix A10.4), and using quasi-steady state approximations, the firing angle of the exciter was calculated as follows.

Given a field current I_{fd}, then the firing angle α_e may be approximated (Kimbark 1971) by

$$\alpha_e = \cos^{-1}\left((V_{fd} + 3X_c I_{fd}/\pi)/1.3505\right)$$

where X_c is the commutation reactance based on the excitation transformer's leakage reactance and the transient reactance (0.31 p.u.) of the generator. Using this information, the excitation line current may be included in the calculations of Section 3.2.1.2 to obtain more exact values for I_{fd} and θ_o (case 1195).

Table A10.1 Generator Data

	p.u. (Campos Barros)	Real Quantity	p.u. (Heffernan)
1. Stator-Stator			
Stator Self Inductance $L_{aa} = L_{bb} = L_{cc}$	1.99	5.95 mH	1.99
Stator Mutual Inductance $L_{ab} = L_{bc} = L_{ac}$	0.915	2.735 mH	0.915
Stator 2nd Harmonic Inductance (Self and Mutual)	0.05	0.15 mH	0.05
Armature Resistance $R_a = R_b = R_c$	0.0015	0.00141Ω	0.0015
2. Stator-Rotor			
Stator-field Inductance $L_{afd} = L_{bfd} = L_{cfd}$	1.88	83.66 mH	65.3142
Stator-d damper Inductance $L_{akd} = L_{bkd} = L_{ckd}$	1.88	83.66 mH	65.3142
Stator-q damper Inductance $L_{akq} = L_{bkq} = L_{ckq}$	1.78	79.21 mH	61.84
3. Rotor-Rotor			
Field Inductance L_{fd}	1.99	1.3181 H	2401.8561
d-axis damper Inductance L_{kd}	1.892	1.253 H	2283.5672
q-axis damper Inductance L_{kq}	1.792	1.687 H	2162.4129
Field-d damper Inductance L_{fkd}	1.88	1.245 H	2269.0840
Rotor Field Resistance R_{fd}	0.0014	0.2913Ω	1.69897
Rotor damper Resistances $R_{kd} = R_{kq}$	0.0063	1.311Ω	7.60441

A10.3 TRANSFORMER MAGNETIZING CURRENT CALCULATIONS

Using the calculated generator terminal voltage phase angle relationships, estimates of the transformer magnetizing currents (both exciter and load) were obtained as follows. The instantaneous magnitude of transformer magnetizing current at time zero is approximately

$$i_m = Y_m V_g \sin \theta_g$$

for a cosinusoidal voltage waveform.

Since the secondary currents in both exciter and load transformer circuits are known (in the first case being controlled by the valve states), it is possible to recalculate the instantaneous primary currents for each transformer using

$$i_1 = - (i_2 - i_m)$$

Then by Kirchhoff's current law the instantaneous stator currents can be calculated. These more exact instantaneous currents were then used in the study case number 2195.

A10.4 DATA FOR (UN)CONTROLLED RECTIFIER LOAD

A single pole-double bridge d.c. link was modelled with the following parameters, based on the Kingsnorth scheme (Campos Barros 1976):

$$P_{dr}^{sp} = 425 \text{ MW}$$
$$V_{di}^{sp} = 100 \text{ kV}$$
$$R_{dc} = 0.652 \Omega$$
$$L_d = 0.47 \text{ H}$$

and the following d.c. base quantities:

$$S_B = 588 \text{ MVA}$$

$$V_{B_{dc}} = 47 \text{ kV}$$

$$I_{B_{dc}} = 12.51 \text{ kA}$$

$$Z_{B_{dc}} = 3.7568\,\Omega$$

The controlled bridge was assumed to have an initial firing angle of 15°, compared to the effective 0° delay angle of the diode rectifier scheme. As a result, different values for the generator states were obtained but essentially they were similar to those calculated for a PQ load model above. The invertor end was represented by a variable e.m.f. at the end of a simple series resistance d.c. line. Normal convertor representation was used for the rectifier unit.

APPENDIX A11

Fault studies in a.c. systems interconnected by h.v. d.c. links

J. Arrillaga, M.Sc. Tech., Ph.D., C.Eng., F.I.E.E., M.D. Heffernan, B.E., M.E., C.B. Lake, B.E., M.E., and C.P. Arnold, M.Sc., Ph.D., C.Eng., M.I.E.E.

Indexing terms: *D.C. power transmission, Electrical faults, Modelling, Power convertors, Power systems, Relay protection, Switchgear*

Abstract: Steady state and dynamic models of high voltage direct current transmission links, suitable for the analysis of a.c./d.c. power systems under fault conditions, are described. The New Zealand a.c./d.c. system is used to test the models with balanced and unbalanced faults. The results are used to discuss the extent of their applicability and, particularly, the scope of the dynamic simulation in the design of switchgear, protective systems and convertor controls.

1 Introduction

Different analytical models are needed to predict the effects of power system faults depending on the specific information required. Steady-state power frequency studies are commonly carried out for the calculation of circuit-breaker ratings and transient stability levels; they normally involve the complete power system and use linear circuit analysis to obtain information at particular instants of time.

Dynamic studies are also carried out to obtain information of transient current and voltage waveforms, following the inception of a fault, or its clearance, for the purpose of dynamic testing of switchgear and protective relays. They usually require more detailed representation, but do not normally involve explicit modelling of the complete system.

The highly nonlinear behaviour of h.v. d.c. convertors cannot be simulated by conventional a.c. fault algorithms, and their effect is often neglected, without proper justification, for the sake of analytical simplicity. However, the power ratings of h.v. d.c. convertors are too large to be ignored, and their speed of controllability has a profound effect on the system behaviour during and immediately after the fault. Moreover, a.c. system disturbances will influence the type and characteristics of the d.c. controls to be used with each particular scheme.

It is the purpose of this paper to describe the integration of h.v. d.c. transmission links into both steady state and dynamic models, and to discuss the extent of their applicability to the analyses of power systems under fault conditions.

2 Nodal system analysis

The steady-state prefault nodal voltages of an a.c./d.c. power system can be described by the following matrix equation:

$$[V] = [Z][I] + [Z][J] \tag{1}$$

where

- $[Z]$ is the busbar impedance matrix
- $[I]$ is a vector of nodal injected currents owing to a.c. generators
- $[J]$ is a vector of nodal current injected by the d.c. terminals

Paper 476C, first received 31st July and in revised form 9th October 1979

Dr, Arrillaga and Dr. Arnold are with the University of Canterbury, Christchurch, New Zealand, and Mr. Heffernan and Mr. Lake are with New Zealand Electricity, Christchurch, New Zealand

A 3-phase fault can be represented by a current I^f flowing out of the faulted busbar p and the d.c. link requires a new set of injected currents $[J^f]$.

From the matrix eqn. 1 the following expressions are extracted for the nodal voltages at the convertors and fault busbars (Fig. 1):

$$V_m^f = V_m + Z_{mm}(I_m^f + J_m^f) + Z_{mn}(I_n^f + J_n^f) - Z_{mp}I^f \tag{2}$$

$$V_n^f = V_n + Z_{nm}(I_m^f + J_m^f) + Z_{nn}(I_n^f + J_n^f) - Z_{np}I^f \tag{3}$$

$$V_p^f = Z^f I^f = V_p + Z_{pm}(I_m^f + J_m^f) + Z_{pn}(I_n^f + J_n^f) - Z_{pp}I^f \tag{4}$$

where Z^f is the fault impedance and V_m, V_n, V_p are the prefault voltages in the absence of d.c. transmission.

3 Dynamic model

The time-variant nature of the current and voltage waveforms in an interconnected a.c./d.c. system which is under fault conditions can only be predicted generally by dynamic analysis of the interconnected system components. There is no need to subdivide the system into a.c. and d.c. plant components in the dynamic model, provided that the variable topology caused by the switching sequences of the convertor plant is followed by the computer model.

A state-variable technique with diakoptical handling of the frequent convertor topological changes has been recently described.[1]

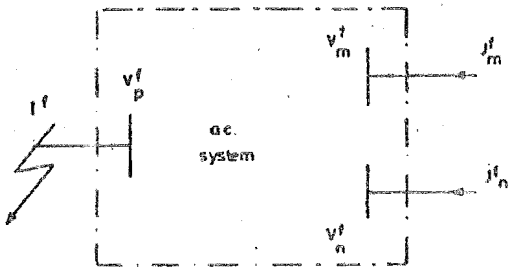

Fig. 1 *Current injections from convertors and fault busbars*

The state-space equations to be solved are:

$$p(\omega\psi_l) = E_l - R_l I_l + K^t_{l\alpha} V_\alpha + K^t_{l\beta} V_\beta + K^t_{l\gamma} V_\gamma \quad (5)$$

$$p(\omega\psi_k) = -R_k I_k + K^t_{k\alpha} V_\alpha + K^t_{k\beta} V_\beta + K^t_{k\delta} V_\delta \quad (6)$$

$$p(\omega Q_\alpha) = -K_{\alpha l} I_l - K_{\alpha k} I_k - K_{\alpha r} I_r \quad (7)$$

where ψ_l (flux linkages $I_l L_l$), ψ_k (flux linkages $I_k L_k$) and Q_α (capacitor charge $C_\alpha V_\alpha$) are the state variables, and

- I = branch current vector
- V = nodal voltage vector
- R, L and C = respectively, resistance, inductance and capacitance matrices
- K^t_{ql} = branch (q) to node (i) incidence matrix
- α = nodes with at least one capacitive branch
- β = nodes with at least one resistive branch but no capacitive branches
- γ = nodes with only inductive branches
- δ = convertor nodes with only inductive branches
- r = resistive branches
- l = inductive branches
- k = convertor inductive branches

The differential eqns. 5–7 are solved for each integration step, starting from given initial conditions and using an implicit integration procedure.

Machines are represented by their e.m.f. behind an appropriate reactance, based on the Thévenin equivalent. The model permits varying such reactance, starting with the subtransient and changing into the transient as the study progresses. These parameter changes are implemented by altering the values of E_l and L_l in eqn. 5. The dynamic programme also provides an alternative representation of the machine by its full transient equations.

Convector transformers are represented by the coupled-circuit model. In purely a.c. systems the recovery voltage is often strongly influenced by the transformer magnetising current, particularly when switching is involved. The convertor transformers, however, are kept in service during the a.c. fault conditions, with the d.c. regulators trying to maintain constant current throughout the fault, and the problem of magnetising inrush currents does not occur under these operating conditions. However, the presence of overvoltages during recovery is bound to cause some transformer saturation with further waveform deterioration. This effect requires further investigation and the present model can be easily adapted for the purpose.

3.1 *Process of establishing fault condition*

In the first place the 3-phase real and imaginary terms of the branch impedances of the steady state eqn. 1 describing the system are transferred to the topological matrices R_l and L_l, respectively. The state-space model (eqns. 5–7) can then be solved for the prefault condition to obtain realistic initial conditions at the instant of fault occurrence. This is necessary to go from the sine-wave conditions, determined by the load-flow analysis, to the distorted wave condition inherent in practical convertor operation, which can only be determined by dynamic simulation. The prefault dynamic study is carried out until such a time as the waveforms of the system are adequately stable at the operating point determined by the initial steady-state analysis.

To facilitate the application of a particular fault, the topology constraints require that a fault branch is previously established in the branch list. For the initial conditions, this branch impedance is given a high numerical value such that I^f is effectively zero. When the time is reached for fault application, alteration of the fault impedance to the required value provides the appropriate faulted network.

4 Steady state model

Whenever a reasonably steady state d.c. condition can be expected prior to the instant of fault clearance, the complexity of the dynamic model can be avoided in the calculation of fault current levels. In each case, however, the applicability of a steady-state model can only be assessed by comparison with the results of the dynamic simulation.

The steady-state integration of the d.c. transmission link is not straightforward, because conventional short-circuit models only include fixed load impedances whereas the equivalent impedance of an h.v. d.c. convertor terminal is voltage dependent and cannot be set in advance.

In the nodal analysis described in Section 2 the d.c. link is represented by injected currents at the convertor terminals. With the d.c. link on constant current control the magnitude of the steady-state current injections J_m and J_n is fixed, i.e.

$$J^f_n = J^f_m = K_2 I^{sp}_d$$

where I^{sp}_d is the specified constant-current value, but their respective phase angles (ω_m and ω_n) will depend on the terminal voltages and d.c. link operating conditions.

Eight variables are involved in the fault study, i.e. V_m/ϕ_m, V_n/ϕ_n, ω_m, ω_n, α_m, δ_n, when the fault current is eliminated from eqns. 2–4. This results in four a.c. equations, i.e. the real and imaginary parts of

$$V^f_m = \{Z_{mm} - Z_{mp}(Z_{pp} + Z^f)^{-1} Z_{pm}\} I^f_m + \{Z_{mn} - Z_{mp}(Z_{pp} + Z^f)^{-1} Z_{pn}\} I^f_n + \{V_m - Z_{mp}(Z_{pp} + Z^f)^{-1} V_p\} \quad (8)$$

$$V^f_n = \{Z_{nm} - Z_{np}(Z_{pp} + Z^f)^{-1} Z_{pm}\} I^f_m + \{Z_{nn} - Z_{np}(Z_{pp} + Z^f)^{-1} Z_{pn}\} I^f_n + \{V_n - Z_{np}(Z_{pp} + Z^f)^{-1} V_p\} \quad (9)$$

The remaining four equations involving the eight variables are obtained from the a.c./d.c. relationships described in the Appendix (Section 9), i.e.

$$K_1 V_m(\cos\alpha_m - \cos(\phi_m - \omega_m)) - K_2 X_m I^{sp}_d = 0 \quad (10)$$

$$K_1 V_n(\cos\delta_n - \cos(\phi_n - \omega_n)) - K_2 X_n I^{sp}_d = 0 \quad (11)$$

$$K_1 V_m \cos\alpha_m - K_1 V_n \cos\delta_n + (K_2 X_n - K_2 X_m - R_f) I^{sp}_d = 0 \quad (12)$$

$$\cos\delta_n - \cos\delta^{sp}_n = 0 \quad \text{or} \quad \cos\alpha_m - \cos\alpha^{sp}_m = 0 \quad (13\text{–}14)$$

The real and imaginary parts of eqns. 8 and 9, together with eqns. 10–14, can be solved by the Newton-Raphson algorithm,[2] using reasonable starting values of the variables as obtained from a preliminary load flow. When convergence is achieved, a final check is needed to ensure that the commutation angle of the convertor bridges is below 60°, the limit of normal convertor operation.

It must be emphasised, however, that the applicability of these equations is subject to convertor controllability fol-

lowing the disturbance, i.e. the attainment of normal switching sequences and constant current control by the fault clearing time.

5 Test system and results

The New Zealand power transmission scheme is used as a test system. It consists of two separate 220 kV a.c. networks of comparable capacity containing 21 busbars in the North Island and 19 busbars in the South Island, which are interconnected by a ± 250 kV h.v. d.c. transmission link. The d.c. link includes both long overhead line and submarine cable.

The studies carried out were primarily concerned with the fault and immediate postfault periods. Extensions of the study periods to investigate system stability are possible but computationally expensive.

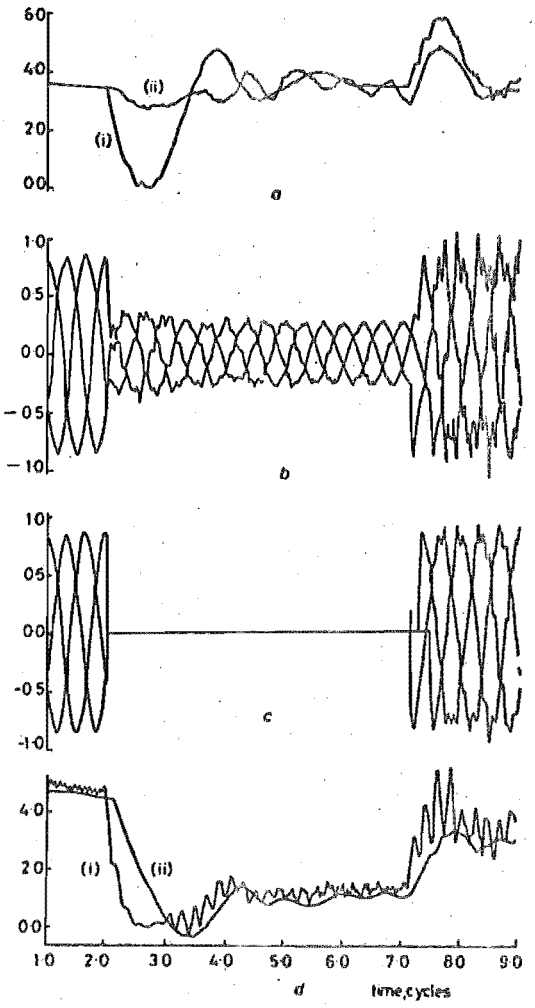

Fig. 2 *Effect of a 3-phase short-circuit on the rectifier side of the system*

a Direct current waveforms
(i) rectifier end
(ii) invertor end
b Alternating voltage waveforms at the rectifier busbar
c Alternating voltage waveforms at the faulted busbar
d Direct power waveforms
(i) rectifier end
(ii) invertor end

The following a.c. faults, balanced and unbalanced, were simulated with the South Island station rectifying and the North Island inverting:

(i) a 3-phase fault in the South Island resulting in a reduction of the rectifier alternating voltage to approximately 30% of the prefault value

(ii) as in (i) except that the fault is applied in the North Island, thus reducing the invertor alternating voltage to about 30% of the prefault value

(iii) a 3-phase fault in the North Island, close to the convertor station

(iv) as in (iii) but with a single-phase fault

No attempt was made to optimise the h.v. d.c. link controller constants independently for each fault condition under dynamic simulation, but rather a set was used which gave a fast yet sufficiently damped and stable response to all a.c. fault conditions tested. A typical fault clearing time of 100 ms (5 cycles) was used in all the test examples.

(i) The dynamic response of the a.c/d.c. system prior to, during, and after the short circuit is illustrated by the waveforms shown in Fig. 2. The waveform in Fig. 2*a* shows the large direct-current variation which occurs for about two cycles following the abrupt alternating voltage changes, i.e. subsequent to fault occurrence (between cycles 2 and 4) and after fault clearance (cycles 7 to 9). Corresponding changes in alternating current take place during those periods, and, owing to the relatively slow response of the harmonic filters, very large alternating current waveform distortion occurs. This in turn causes considerable alternating voltage waveform distortion at the convertor terminals (Fig. 2*b*) and at the faulted busbar (Fig 2*c*). Fig. 2*d* shows the d.c. power variation during the fault. The a.c. disturbance produces no consequential convertor maloperation, and after about 80 ms (cycle 6) the d.c. controllers are able to keep the current levels (waveform Fig. 2*a*) very close to the specified settings.

Steady-state solutions with the d.c. link operating and blocked (after the disturbance) were also carried out and a comparison of results at the instant of fault clearance is made in Table 1. It is apparent from the Table that, for this particular fault and location, the steady-state models provide adequate information for the fault current. The presence of the d.c. link is shown to reduce the current slightly at the point of the fault, and increase it elsewhere.

(ii) When a similar a.c. fault is placed at the invertor end, the disturbance is sufficient to cause repeated commutation failures at the invertor bridges, producing a large direct current peak of about 300% 15 ms after fault inception. These convertor disturbances cause extensive current fluctuation (Fig. 3*a*), and thus the control angles and current magnitudes at the fault clearing time can not be accurately predicted with the steady-state model. For instance the steady-state prediction of fault level for a 5-cycle clearance is 40% higher than the value obtained from the dynamic simulation.

The current control action during the disturbance causes substantial alternating current and voltage fluctuation and harmonic distortion at both ends of the d.c. link. By way of illustration, the rectifier end voltage waveforms of Fig. 3*b* show a voltage peak of over 150% during the fault. The faulted busbar voltage waveforms following fault clearance are illustrated in Fig. 3*c*.

(iii) A low impedance fault is applied at the invertor a.c. busbar reducing its voltage level to less than 10% of the nominal. The immediate effect is a commutation failure in

Table 1: Comparative results for case (i) at the fault clearance instant

	Dynamic	Steady state with d.c. link	Steady state with d.c. link blocked
α degree	9·5	5·0	not applicable
δ degree	68·7	73·8	not applicable
E_R	0·35	0·33/6·8	0·41/16·76
I^R, kA	13·6	13·8	14·5
Close generator current, kA	—	2·2	2·0
Distant generator current, kA	—	1·4	1·2

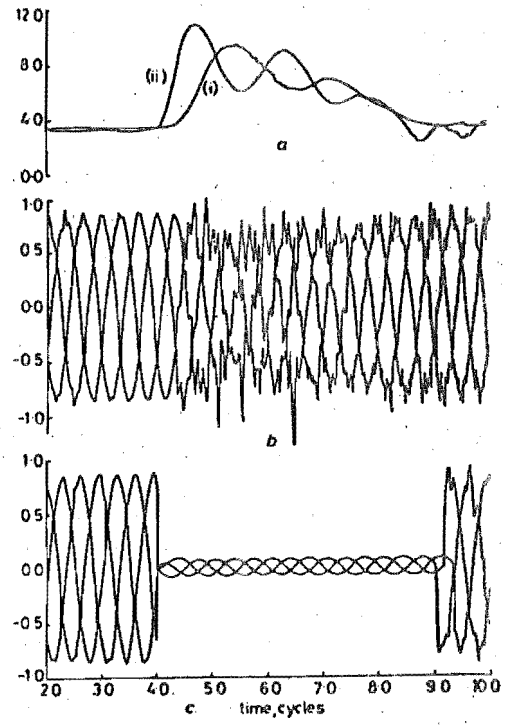

Fig. 3 *Effect of a 3-phase short circuit on the invertor side of the system*

a Direct current waveforms
(i) rectifier end
(ii) invertor end
b Alternating voltage waveforms at the 'healthy' (rectifier) end of the link
c Alternative voltage waveforms at the faulted busbar

each of the invertor bridges, with subsequent failures and continuous d.c. short circuit. The direct voltage variation of Fig. 4*a* illustrates this effect, and clearly for this fault there is no alternative to the dynamic simulation model.

The d.c. waveforms illustrated in Fig. 4*b* show a rapid rise owing to the invertor d.c. short circuit. This results in correspondingly large variations in the convertor alternating currents with peaks of 3 and 4 times normal load values at, respectively, the rectifier and invertor ends. The rectifier end current waveforms (Fig. 4*c*) are again very distorted and unbalanced.

After 5 cycles the direct currents are close to the normal settings, but the control angles are close to 90°. Therefore the convertor currents are almost purely reactive and cause large voltage regulation at both ends of the link.

The recovery voltages, owing to the proximity of the fault, are greatly affected by the convertor behaviour. For instance, Fig. 4*d* shows that one of the phases experiences a peak of 135% on fault clearance.

(iv) A low impedance fault is now applied to one phase only. The collapse of one phase causes an immediate reduction of the invertor direct voltage and a sharp increase of direct current that results in a series of commutation failures. The initial response of the d.c. link is thus very similar to case (iii), and again can only be assessed by the dynamic model.

The direct currents and invertor side alternating voltage waveforms are illustrated in Fig. 5. The voltage unbalance

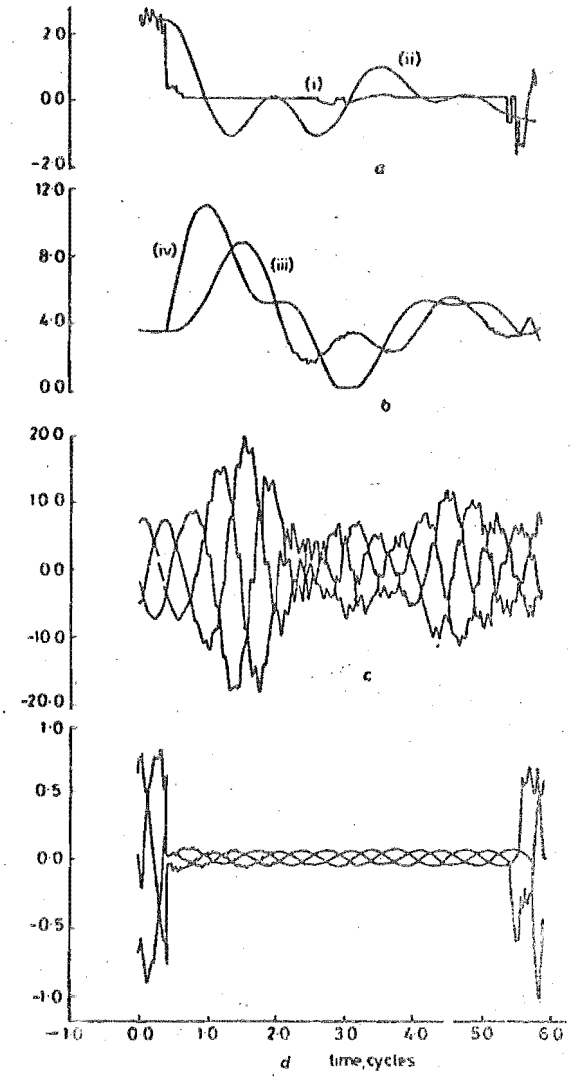

Fig. 4 *Effect of a 3-phase short circuit close to the invertor busbar*

a Direct voltage waveforms
(i) convertor terminals
(ii) d.c. line
b Direct current waveforms
(iii) rectifier end
(iv) invertor end
c Alternating current waveforms at the 'healthy' (rectifier) end
d Alternating voltage waveforms at the faulted busbar

produces two extended commutation overlaps per cycle. This effect produces a continuous variation of the firing angle (particularly under symmetrical firing control) and causes d.c. fluctuation (especially at the invertor). Moreover the two convertor ends operate with angles close to 90° during the fault, and these two effects result in considerable voltage unbalance, regulation and distortion of the two healthy phases (Fig. 5*b*).

Although some commutation failures still occur after 80 ms (cycle 5 in the Figure), their effect on the direct current level is small owing to the reduced direct voltage present.

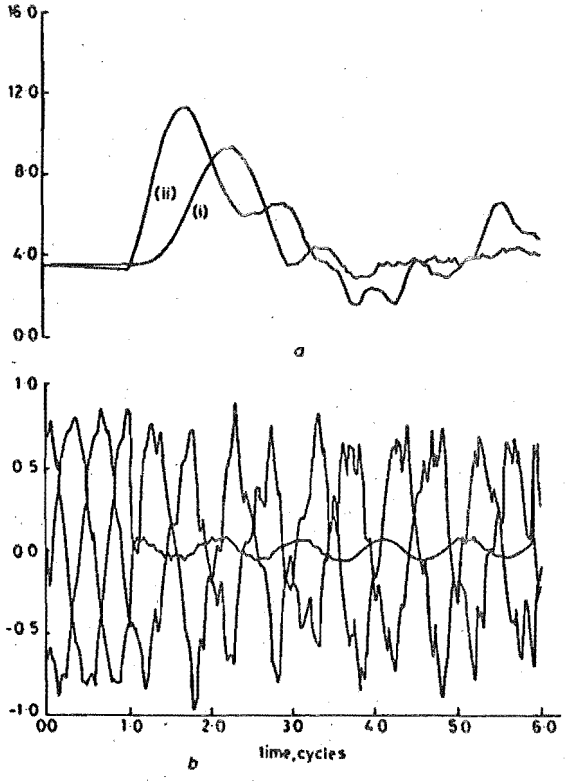

Fig. 5 *Effect of a single-phase-to-earth short circuit close to the invertor bus*
a Direct current waveforms
(i) rectifier end
(ii) invertor end
b Alternating voltage waveforms at the faulted busbar

6 Conclusions

A dynamic model of general applicability has been described to predict the effect of various a.c. faults in a.c./d.c./a.c. power systems. While no specific conclusions are drawn regarding the effect of the d.c. link, it is evident that the current and voltage levels and waveforms are greatly influenced by the transient behaviour of the harmonic filters and convertor controls. Information on waveform distortion, transient voltage peaks, recovery voltages and the effect of internal convertor faults is essential to the reliable performance of switchgear and protective systems, and can only be accurately predicted by dynamic simulation

With the prospective use of faster fault discrimination schemes[3] it should be possible to use the control characteristics best suited to each particular fault. The dynamic model constitutes an essential tool in the design of such controls.

A steady-state iterative model has also been developed for the calculation of alternating fault currents at the fault-clearing instant. Comparison with the dynamic simulation results has shown good agreement for symmetrical a.c. faults sufficiently distant from the convertor terminals to allow normal convertor operation. However, 3-phase faults close to the convertor terminals cause repeated commutation failures, and the steady-state formulation cannot be relied upon for the calculation of fault levels.

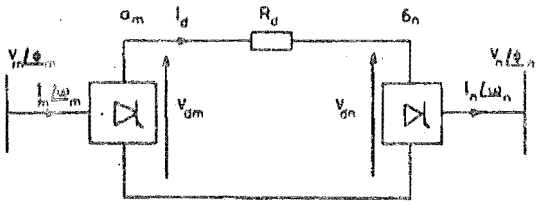

Fig. 6 *Basic model of d.c. link interconnecting nodes m and n*

7 Acknowledgments

The authors wish to express their gratitude to Mr. P.W. Blakeley, General Manager of New Zealand Electricity, and to the staff of the Computer Centre of the University of Canterbury for their help. Their thanks are also extended to A. Brameller, K. Wong and J.G. Campos Barros for their participation in the initial stages of this work.

8 References

1 ARRILLAGA, J., AL-KHASHALI, H.J., and CAMPOS BARROS, J.G.: 'General formulation for dynamic studies in power systems including static convertors', *Proc. IEE*, 1977, 124, (11), pp. 1047–1052
2 RALSTON, A.: 'A first course in numerical analysis' (McGraw-Hill, 1965)
3 ARRILLAGA, J., and GALANOS, G.: 'Fault detection scheme for a direct digital control of a.c.-d.c. interconnections.' *Proc. IEE*, 1970, 117, (4), pp. 785–793
4 ADAMSON, C., and HINGORANI, N.G.: 'High-voltage direct current power transmission' (Garraway Press, 1960)

9 Appendix

A.C./D.C. formulation

With reference to the schematic diagram of Fig. 6, and subject to the assumptions normally made in steady-state analysis,[4] the following a.c./d.c. equations apply:

$$V_{dm} = K_1 V_m \cos \alpha_m - K_2 X_m I_d$$

$$V_{dn} = K_1 V_n \cos \delta_n - K_2 X_n I_d$$

$$V_{dm} = R_d I_d + V_{dn}$$

$$I_m = I_n = K_1 I_d^{sp}$$

$$V_{dm} = K_1 V_m \cos (\phi_m - \omega_m)$$

$$V_{dn} = K_1 V_n \cos (\phi_n - \omega_n)$$

$$\cos \delta_n = \cos \delta_n^{sp}$$

if the fault is electrically closer to the invertor end or

$$\cos \alpha_m = \cos \alpha_m^{sp}$$

if the fault is closer to the rectifer end.

APPENDIX A12

80 SM 675-9

RECOVERY FROM TEMPORARY H.V.D.C. LINE FAULTS

M. D. Heffernan,
New Zealand Electricity

J. Arrillaga,
University of Canterbury (N.Z.)

K. S. Turner,
Student Mem., IEEE
New Zealand Electricity

C. P. Arnold, Mem, IEEE
University of Canterbury (N.Z.)

Abstract - Modelling techniques are described to simulate the behaviour of a.c./d.c. systems following temporary d.c. line short-circuits. The basic tools employed are a small step dynamic simulation and a multi-machine transient stability programme. Test results are shown to illustrate the speed of recovery from a d.c. short-circuit. The effects of fast fault detection, fault development and line re-energization controls are also discussed.

INTRODUCTION

Most transmission line short-circuits are of a temporary nature (e.g. insulator flashovers caused by lightning) and automatic recovery with only temporary interruption is possible. In the case of d.c. transmission, however, the absence of circuit-breakers precludes the normal a.c. transmission solution of temporary switching and auto-reclosing.

Large sustained fault currents will be prevented by normal constant current control at both convertors which act to maintain a nett voltage difference across the link. In the steady state then, the fault current will be limited to the difference between the convertors' current settings, i.e. to the current margin. To eliminate this residual fault current, the rectifier is temporarily driven into inversion. The duration of this emergency control and of the subsequent return to normal power transmission are important for stability considerations.

The subject of h.v.d.c. line faults has been discussed in several papers, each concentrating on a particular aspect of the disturbance, i.e. the effect of the d.c. configuration[1] [2], the maximum expected fault level [3] and the dynamic behaviour of the convertor plant [4]. However, these models are not suitable to analyse the overall fault behaviour from its detection to final recovery. A more general approach with varying degrees of system representation depending on the information required is described in the paper. The proposed model is based on two programmes recently developed to integrate d.c. links with a.c. power systems, viz. small step transient simulation [5] and multi-machine transient stability [6].

The New Zealand h.v.d.c. link is used as a test system to investigate the effect of various system parameters and control characteristics on the detection, current extinction, line re-energisation and final power recovery following the occurrence of a d.c. line fault.

MODEL REQUIREMENTS

A zero fault resistance at the rectifier terminals will provide the most severe d.c. line fault in terms of overcurrent peak. The largest current peak is often calculated [3] using a quasi-steady state d.c. representation with an infinite a.c. system behind commutation reactance.

However, such a model yields pessimistic current peaks as it cannot accurately represent the actual timing of the valve firings in relation to the fault occurrence, or the subsequent effects of rapid control action associated with normal or protective action. It is also totally inadequate to assess the subsequent behaviour of a.c./d.c. interconnections for the following reasons.

- The current increase caused by the fault will produce transient harmonic current imbalance between convertor filters and the a.c. system which will always result in a.c. waveform distortion for an a.c. system with finite short circuit capacity.
- The a.c. voltage source will change with time in phase and magnitude.
- The fault current variation will cause corresponding a.c. voltage regulation in the system impedance.

Thus a more accurate simulation is needed including the a.c. system, filters, d.c. system parameters and effect of convertor controls to assess the effect of voltage regulation, commutation and waveform distortion. A state variable approach has been developed by one of the authors [5] and is used as the basis for the d.c. fault modelling. However the voltage source variation can only be assessed with the help of a transient stability model.

A.C. System

The a.c. system forms an oscillatory circuit with the a.c. harmonic filters which in general will have some natural frequencies of low order. A disturbance may excite these natural frequencies giving rise to large waveform distortion which in turn interacts with the convertor controls. The complexity of the a.c. system model depends on the availability of information. In the absence of more detailed information a reasonably accurate representation has been suggested [7] for the lower harmonics in the form of a modified Thevenin equivalent with a series-parallel combination of resistance and inductance, the parameters of which are calculated to give a constant impedance angle over the low range of frequencies. Looking from the convertor terminals, see figure 1, the a.c. system includes the convertor transformer and the Thevenin equivalent of the a.c. system in parallel with the a.c. harmonic filters. However for this equivalent to be a realistic representation of the a.c. network it must include all the associated generator effects, i.e. must be time-variant under disturbed conditions.

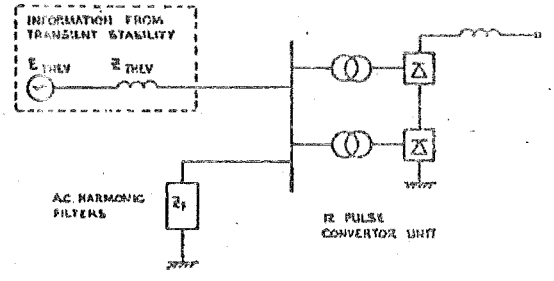

Fig 1 REPRESENTATION OF EACH CONVERTOR AND ASSOCIATED A.C. SYSTEM.

80 SM 675-9 A paper recommended and approved by the IEEE Transmission & Distribution Committee of the IEEE Power Engineering Society for presentation at the IEEE PES Summer Meeting, Minneapolis, Minnesota, July 13-18, 1980. Manuscript submitted January 10, 1980; made available for printing June 6, 1980.

The behaviour of the Thevenin source depends on the short circuit ratio (s.c.r.) of the a.c. system and in general will need updating at regular intervals during the dynamic simulation of the faulted circuit. A transient stability study is required for this purpose.

At each integration step of the transient stability analysis the d.c. network is represented as a given steady state model [6] and an iterative solution is carried out to obtain the Thevenin equivalent of the a.c. network.

Details of the formulation required for time variant network equivalents are given in the Appendix. To illustrate the interaction between the a.c. sources and d.c. transmission, simulation of a total loss of d.c. power after 2 cycles and subsequent resumption of full power transmission after 18 cycles in the N.Z. system produced the results illustrated in figure 2.

D.C. System

Once the rectifier current reduces to zero the only source of fault current is the energy stored in the d.c. line and the rate of decay of this current is determined by an oscillatory RLC circuit consisting of the smoothing reactors, line L and C parameters and the resistances of the line, earth path and arc.

The line parameters vary from scheme to scheme and the natural frequency of oscillation ranges between 10 and 60 Hz.

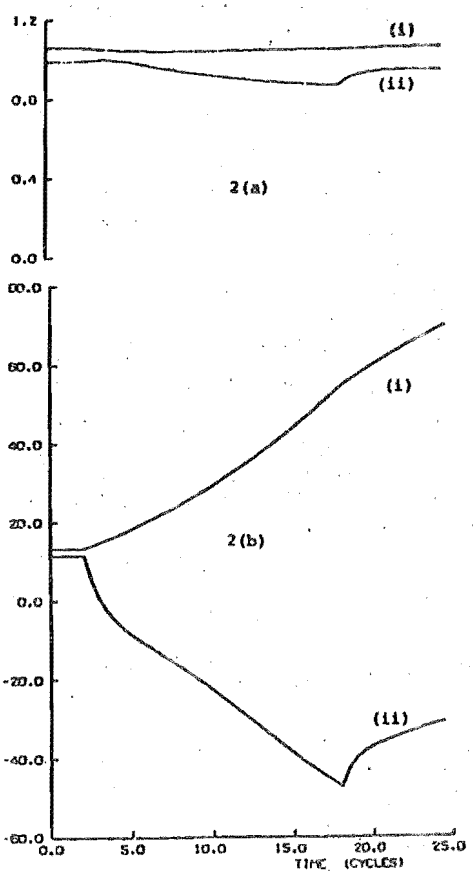

Fig. 2. Time variant Thevenin equivalents
(a) RMS voltage magnitude variation
(b) Phase angle (degrees) variation
(i) Rectifier end
(ii) Invertor end

In power frequency related studies requiring mainly the behaviour of the d.c. link at the two terminals and the fault point, it is sufficiently accurate to model the line by a number of π equivalents, depending on distance, and including the smoothing reactors. The behaviour of the smoothing reactors is reasonably linear for currents up to two or three times the rated value and their presence limits considerably the magnitude and rate of rise of current.

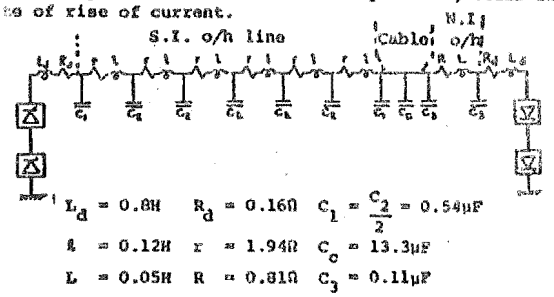

$L_d = 0.8H \quad R_d = 0.16\Omega \quad C_1 = \frac{C_2}{2} = 0.54\mu F$

$L = 0.12H \quad r = 1.94\Omega \quad C_c = 13.3\mu F$

$L = 0.05H \quad R = 0.81\Omega \quad C_3 = 0.11\mu F$

Fig. 3. D.C. line representation of the New Zealand system.

Figure 3 illustrates half of the equivalent circuit of a 4 bridge bipolar scheme representing the New Zealand d.c. link, which consists of 530 km of over head line (South Island), 40 km of submarine cable (Cook Strait) and 37 km of over head line (North Island).

If a bipole to ground fault is to be investigated the same equivalent can be used by doubling the series and halving the shunt parameters. However single pole faults in a bipole system require explicit representation of each pole. The fault is represented by a shunt resistive element.

FAULT CHARACTERISTICS

Arc Extinction

With a naturally oscillating current waveform there will be several instances at which the arc may extinguish. However, the arc will continue to conduct current until the voltage impressed across the still ionised arc path has insufficient peak amplitude to sustain further arc current.

To establish the behaviour of the arc, Kohler [8] carried out tests for a zero-resistance fault immediately adjacent to the smoothing reactor. The results indicated that the arc voltage drop for arc lengths of 0.4 to 2.0 metres has an average value of 2kV/m.

Kohler measured the deionization time from the instant when the arc current falls below 1A and concluded that 20-50 ms is sufficient to prevent arc reignition on convertor restart. However he used a test system with much lower rating than the system under investigation here. Therefore the more conservative Uhlmann's specification of 100msecs [9] as a safe deionization period was accepted for the purpose of this work.

Fault Resistance

Fault studies carried out on the assumption of a dead short circuit are unrealistic. The fault resistance will at least include the magnitude of the tower footing resistance (typically up to 20 Ω) [1] and the arc resistance which is dependent on the instantaneous fault current, since the arc voltage drop is constant (typically 4kV for sustained insulator flashover).

In the computer model the effect of fault (including arc) resistance is simulated by inserting the appropriate resistive element into the branch list. When the peak arc voltage falls below the arc sustain level of 2 kV/metre, current is extinguished at a current zero. The fault resistance is then increased to effectively infinity, since no current flows to earth, and deionization begins.

After the deionization period, the arc path is

assumed to be completely deionized. The fault is then removed by deleting the corresponding element from the branch list.

The value of fault resistance affects quite dramatically the time required for arc extinction. Two extreme cases showing the effect of fault resistance are illustrated in figures 4(a) and (b). These results are obtained using the d.c. line of figure 3 in isolation, with the state of the d.c. line at rectifier turn off time as initial condition.

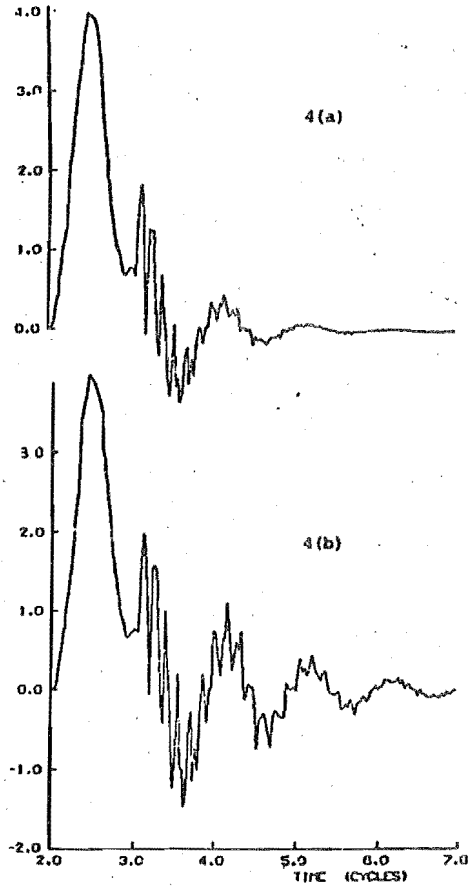

Figure 4. Effect of earth resistance on fault current.
(a) 100 ohms
(b) 20 ohms

FAULT DETECTION

The voltage and current gradients of the travelling waves set up by the fault provide the basis for fast fault detection and discrimination. Their polarity with respect to the line voltage holds sufficient information to identify bipolar and monopolar faults as well as the poles involved. A monopolar fault could induce overvoltage on the healthy pole due to mutual coupling [1].

Fault location and line characteristics affect the overvoltage magnitude at the terminals, but convertor controls have practically no effect on the first wave reflections at the terminals, which in general involve the peak overvoltages.

In the case of a line fault, the rate of fall of voltage at the rectifier terminals is higher than it is for convertor or a.c. system faults, since in the latter case there is much more inductance in the circuit. However, with high resistance ground faults close to the invertor end of a long line, information based exclusively on voltage magnitude and rate of change may not be sufficiently reliable.

Detection based on current comparison at both ends of the link is also unreliable and requires signal transmission. The current gradient provides more reliable information and can easily be obtained from an instrument transformer.

For fast d.c. line fault discrimination it is better to use the weighted sum of the direct voltage (V_{dc}) and current (I_{dc}) gradients [10], i.e.

$$\epsilon = K_1 \, p \, V_{dc} + K_2 \, p \, I_{dc}$$

which is directly related to the travelling waves initiated by the fault and contains information of fault type and location. If the d.c. line is represented by two poles each pole will require this detection. With the state variable formulation referred to above, the fault detection equation is more conveniently expressed in terms of the state variables ψ_ℓ (flux linkage) and Q_α (capacitor charge), where ℓ indicates smoothing reactor and α convertor line-side termination, i.e.

$$\epsilon = K_1 \, pQ_\alpha + K_2 \, p\psi_\ell$$

By suitable choice of K_1 and K_2, restraints may be put on ϵ to prevent a monopolar fault being detected as a fault on the healthy pole of a bipolar system due to mutual coupling action.

Although the above considerations have been made in relation to the rectifier-end, the invertor end should be equipped with a similar detection scheme (but with different settings) to ensure fast arc extinction.

An indication of the relative detection times for the two convertor ends is shown in figure 5. These results are obtained from dynamic simulation of bipolar-ground fault (R_f=50Ω) at the rectifier end of the line of figure 3. An indication of the travelling wave initiated by the fault and of the natural frequency of the d.c. line can also be obtained from the results in figure 5.

FAULT DEVELOPMENT CONTROL

On detection of a d.c. line fault the rectifier firing angle α_r is delayed into the inverting region (say α_r=120° to 135°) to speed up the rectifier current collapse and is kept at that value until arc extinction and deionization have been completed. Similarly, to ensure that the invertor end maintains its correct line voltage polarity, it is necessary to limit the invertor firing angle advance (e.g. $\alpha_i > 100°$). However, the presence of a large capacitance due to the cable can create large overswings and polarity reversal of the d.c. line voltage at the invertor end. These overswings may also result in additional fault current due to charging current flow on the d.c. line. This voltage swing can be avoided if the normal invertor constant current control is overriden and the invertor is kept operating on minimum extinction angle control (i.e. on full inversion). This policy also improves the restarting procedure discussed below.

RESTARTING PROCEDURE

On completion of the deionization period the restart procedure can begin in order to restore normal voltage and prefault power. If re-energization at full voltage is not acceptable (e.g. due to wet or dirty insulators), then a lower voltage may be used by bypassing one or more of the bridges.

A starting order is needed to release the emergency control systems of the convertors during the fault. The restart time required will depend on the properties of the d.c. line and the convertor controls. Instantaneous restart will normally produce serious oscillations at the natural frequency of the line, with large overshoots which may cause the arc to restrike and/or put

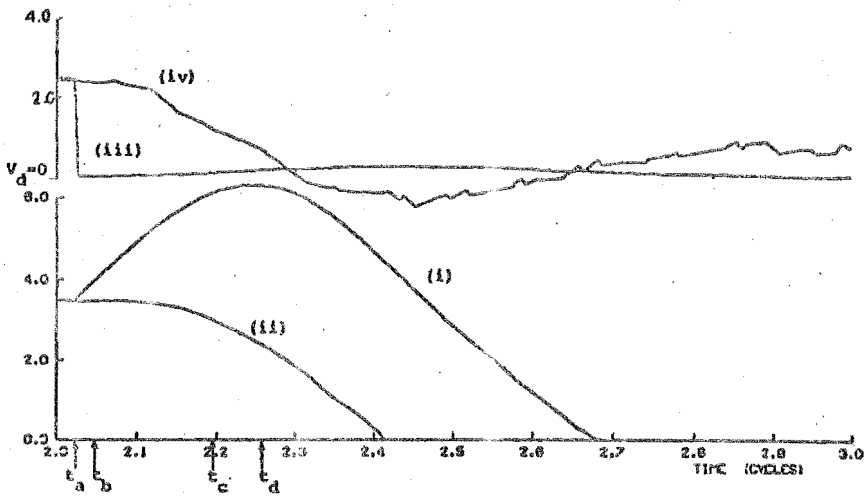

Fig. 5. Indication of relative detection times

t_a	= fault ON	(i)	Rectifier direct current
t_b	= rectifier detection	(ii)	Inverter direct current
t_c	= rectifier retard effective	(iii)	Rectifier line side direct voltage (fault voltage)
t_d	= invertor detection	(iv)	Invertor line side direct voltage

additional stress on the transmission plant. The time constant of the d.c. line (approximately 25 ms in the case of figure 3) will give an indication of the rate of response which may be acceptable.

Some methods use a linear increase of the convertor reference setting, while maintaining sufficient current margin between the sending and receiving ends. A typical performance, using linear ramping, is illustrated in figure 6. In this case the firing angle advance was limited to 15° per firing, so that nominal voltages were achieved within one cycle. The response, although rapid, is unacceptable.

A better performance is exhibited by overriding conventional current control and using an exponential function to recharge the d.c. line. Following completion of the deionization period, the rectifier firing angle is stepped from 125° to 90° over one firing instant. Subsequent firing action is controlled by the following restart function

$$\alpha_r = \alpha_o + (90-\alpha_o)e^{-k.\Delta\theta}$$

where α_o is the control angle which will give nominal line voltage, $\Delta\theta$ is the elapsed time since the beginning of restart control action (i.e. from when α=90°) and k is a constant controlling the rate of response. Throughout the recharge period, the invertor continues operating under extinction angle control (i.e. $\delta_i=\delta_o$).

Figure 7 illustrates the variation of α_r with time for various values of k with α_o=10°. With critical damping of the exponential recharge function, the ideal minimal overshoot of d.c. line voltage can be approached

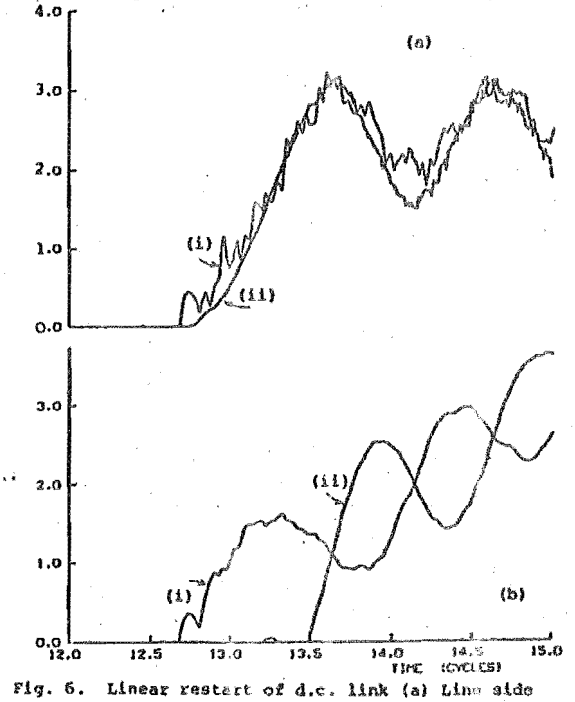

Fig. 6. Linear restart of d.c. link (a) Line side direct voltages
(i) Rectifier end (b) Direct currents
(ii) Invertor end

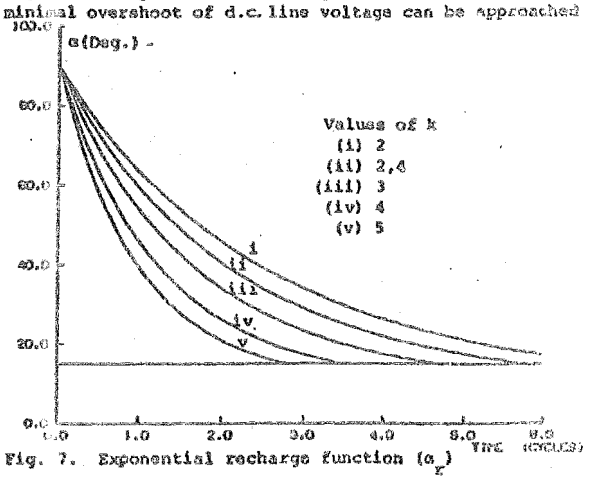

Fig. 7. Exponential recharge function (α_r)

This is done by selecting k so that the rectifier no load voltage reaches 63% of its nominal (α_o) value when $\Delta\theta$ equals the d.c. line time constant. A reasonably well damped d.c. line response is then obtained over the recharge period.

OVERALL TEST RESULTS

Data from the New Zealand a.c./d.c./a.c. power system is used to discuss the overall performance of the system following a bipole-ground fault. The equivalent circuit used for the d.c. system is illustrated in Figure 3 where a monopolar equivalent is used.

It is assumed that, prior to fault occurrence the convertors operate with their nominal firing angles.

A non zero-resistance fault located on the line side, and adjacent to the smoothing reactor, is assumed to occur immediately after a valve firing, i.e. with a delay of 30° (for 12-pulse operation) before any control action can be implemented.

A flow chart indicating the coordination of the special control functions implemented in the overall control behaviour during a d.c. disturbance is indicated in figure 8.

Typical results of the simulated performance of d.c. voltage, current and power at each end of the link are shown in figures 9(a)-(c).

The fault is applied after 2 cycles of (normal) dynamic simulation, i.e. at cycle 2, and the arc is extinguished at cycle 7. The deionization period will then extend up to cycle 12. At this point d.c. line re-charge control starts. A control constant of k=2.4 is used and the results in figure 9 show a small amount of overshoot of the d.c. line voltages. Moreover, the d.c. fault produces no consequential convertor disturbances.

The a.c. terminal voltages experience some waveform

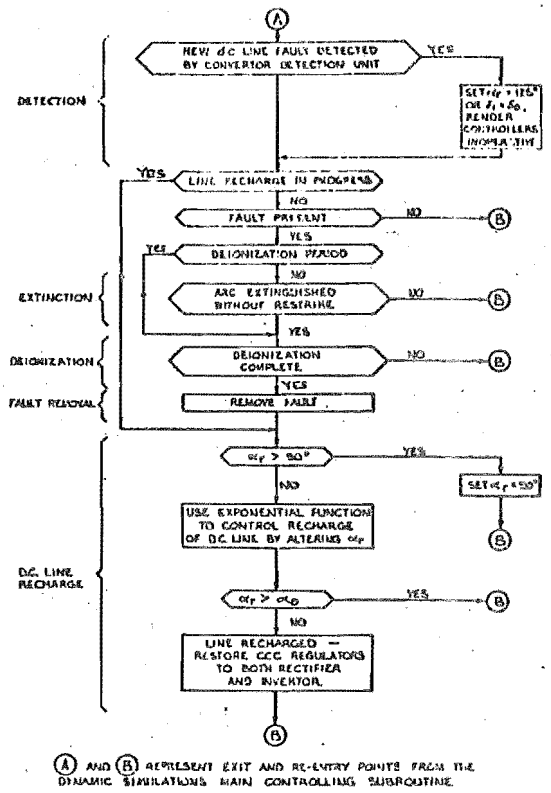

Fig. 8. Flow chart of coordination of special control functions

distortion during periods of substantial control angle change (cycles 2-4 and 14-20) due to the relatively slow response of the harmonic filters. The greatest distortion occurs on power resumption especially at the rectifier and which experiences larger control angle fluctuations.

The d.c. line recharges in about 80 ms (figure 9(c)), during which time very little d.c. power transmission occurs. When the d.c. line is fully recharged to nominal voltage at the correct polarity (cycle 16), conditions are conducive to resumption of normal power transfer. At this time the control angles are $\alpha_r = 15°$ and $\delta_i = \delta_o$, and the rectifier can return to constant current control whilst the invertor continues on extinction angle control. Figure 9(c) shows that full d.c. power is restored within a further 50 ms with subsequent deviations of less than 10% about the nominal values at the invertor end.

During the dynamic simulation the Thevenin source at the invertor end experiences voltage drops of up to 12% of the pre-fault value which shows the importance of modelling the generator response.

CONCLUSIONS

The main factors influencing the duration of the interruption following a d.c. line short-circuit have been investigated. It has been shown that a small-step dynamic simulation programme is essential to keep track of the energy states of the system with varying convertor topology. Moreover the behaviour of the generating sources following the disturbance cannot be ignored; this is updated at regular intervals by means of a multimachine transient stability study.

Test results indicate that system recovery from d.c. line faults is generally better than from a.c. faults, and that the response can be greatly improved by means of faster detection schemes, fault development control and line re-energization control. In the New Zealand scheme, even with very low fault resistances, an upper interruption limit of 300 ms is found to be realistic. However, minimum outage time does not always provide the optimum response in terms of system stability and it is suggested that re-energisation control should include information of generator swings.

ACKNOWLEDGEMENTS

The authors wish to express their gratitude to the General Manager of New Zealand Electricity, Mr. K. D. McCool and to the staff of the Electrical Engineering Department and Computer Centre of the University of Canterbury for their help. Their thanks are also extended to Dr. A. Erinmez of the C.E.G.B. for his participation in the initial stages of this work.

REFERENCES

[1] Hingorani, N. G. "Transient Overvoltage on a Bipolar HVDC Overhead Line caused by D.C. Line Faults", IEEE Transactions on Power Apparatus and Systems, Vol. PAS89, No. 4, April 1970, pp. 592-610.

[2] Kimbark, E. W. "Transient Overvoltages caused by Monopolar Ground Fault on Bipolar D.C. Line: Theory and Simulation", ibid, pp. 584-592.

[3] Peterson, H. A., Phadke, A. G., and Reitan, D. K. "Transients in EHVDC Power Systems: Park I - Rectifier Fault Currents", Ibid Vol. PAS 88, No. 7, July 1969, pp. 981-989.

[4] Reeve, J. and Kapoor, S. C. "Dynamic Fault Analysis for HVDC Systems with A.C. System Representation", ibid Vol. PAS 91, No. 2, Feb. 1972, pp. 688-696.

[5] Arrillaga, J., Al Khashali, H.J. and Campos Barros, J. G. "General Formulation for Dynamic Studies in Power Systems including Static Convertors" Proceedings IEE, Vol. 124, No. 11, November 1977, p.p. 1047-1052.

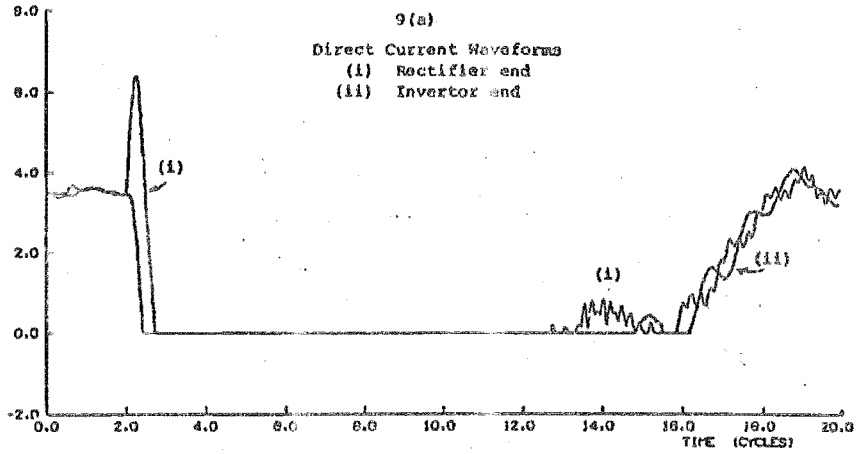

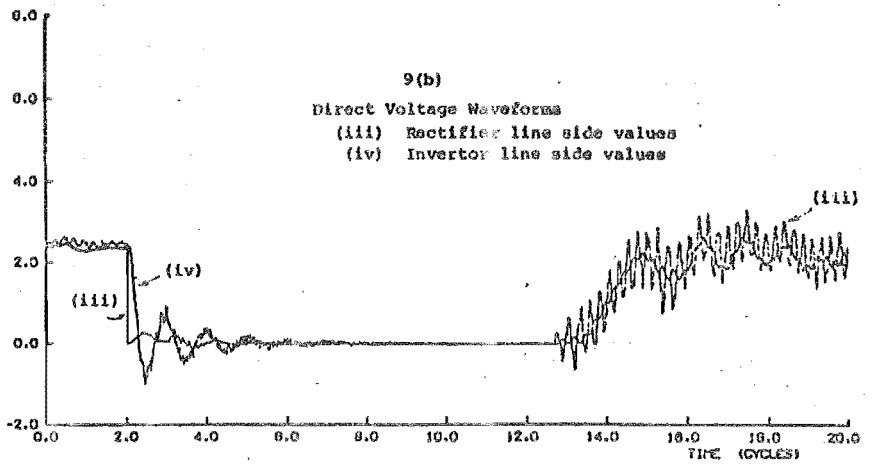

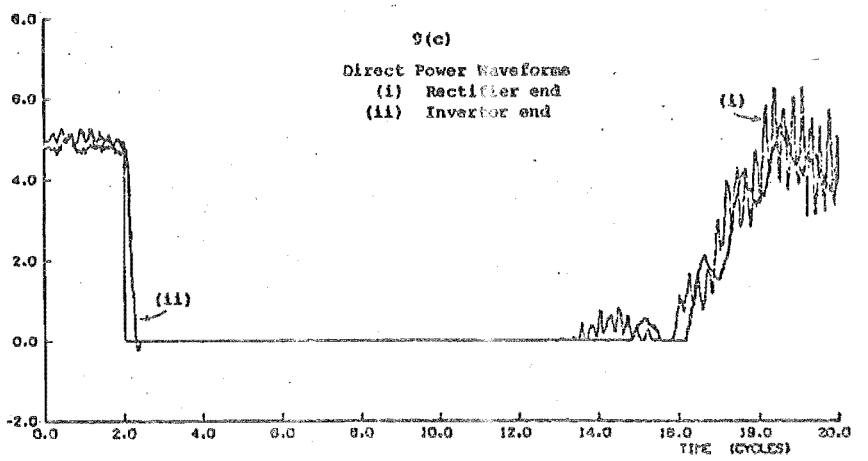

Fig. 9. Effect of a rectifier end d.c. line fault.

[6] Arnold, C. P., Turner, K. S. and Arrillaga, J. "Modelling Rectifier Loads for a Multi-machine Transient Stability Programme", Paper F79 662-8 presented at the IEEE PES Summer Meeting, Vancouver, July 15-20 1979.

[7] Bowles, J. P. "A.C. System and Transformer Representation for HVDC Transmission Studies", Trans. IEEE, PAS 89, No. 7, 1970, pp. 1603-1607.

[8] Kohler, A. "Earth Fault Clearing on an HVDC Transmission Line, with Special Consideration of the Properties of the D.C. Arc in Free Air", IEEE Transactions on Power Apparatus and Systems, Vol. PAS 86, No. 3, March 1967, pp. 298-304.

[9] Uhlmann, E. "Power Transmission by Direct Current" (Book), Springer-Verlag, 1975.

[10] Erinmez, A. "Direct Digital Control of HVDC Links", Ph.D. Thesis, University of Manchester, 1971.

APPENDIX:
INCORPORATION OF TIME VARIANT NETWORK EQUIVALENTS

In the presence of multibridge h.v.d.c. convertors, the simulation of waveform dynamics requires a very small integration step (of the order of 0.1 ms). On the other hand the transient stability programme, used to determine the generators' response during disturbances, provides reliable information with integration steps of 10 ms, i.e. one for every 100 dynamic simulation steps.

In the transient stability programme, the gradual changes of a.c. system parameters from the subtransient to the transient, as obtained from the generator response, are used to update the injected currents at the terminals of each generator. The updated current injections yield a new Thevenin source voltage, while the Thevenin impedance remains constant.

The r.m.s. magnitude (E) and phase angle (θ) of each Thevenin voltage at times t_j and t_{j+1} as calculated by the transient stability study are stored in a data file. The rates of change of these Thevenin voltages over each time step of the transient stability study are small enough to allow a linear interpolation to find an appropriate equivalent at each time step of the dynamic simulation, i.e. at time t_x

$$E_x = E_j + (E_{j+1} - E_j) * \Delta t$$

$$\theta_x = \theta_j + (\theta_{j+1} - \theta_j) * \Delta t$$

where

$$\Delta t = (t_x - t_j)/(t_{j+1} - t_j)$$

and

$$t_j < t_x < t_{j+1}$$

The dynamic simulation then calculates instantaneous phase values for each Thevenin equivalent source voltage at t_x from these quantities by

$$E_i = E_x \cos(\theta_x + \omega t + \xi_{oi})$$

for i = a,b,c.

Careful alignment of the transient stability data file with the dynamic simulation is necessary to correctly identify fault application and removal times. An initial solution at t=0 by the transient stability programme which yields information in the form of a load flow provides the initial Thevenin equivalents. To shorten the establishment of pre-fault initial conditions the reference angle at the inverter is adjusted so that the run begins within a commutation - free period. Thus all future invertor and reference angles obtained from the transient stability data file must be similarly adjusted.

Fault application initiates the process of obtaining the time variant Thevenin equivalents from the transient stability data file, as described above.

To correctly match fault clearance times, which are indicated in the dynamic simulation by resumption of power transfer, the transient stability programme may need to be rerun, using the correct fault removal times, to provide the appropriate Thevenin equivalent. In this transient stability run, the d.c. link power may be ramped (at 10 ms intervals) up to full load at a predetermined rate, or simply stepped from no load to full load in one 10 ms period, depending on the response time of the test system.